Charged Aerosol Detector Performance Evaluation and Development of Optimization Strategies for the Analysis of Amino Acids

Dissertation zur Erlangung des naturwissenschaftlichen Doktorgrades der Julius-Maximilians-Universität Würzburg

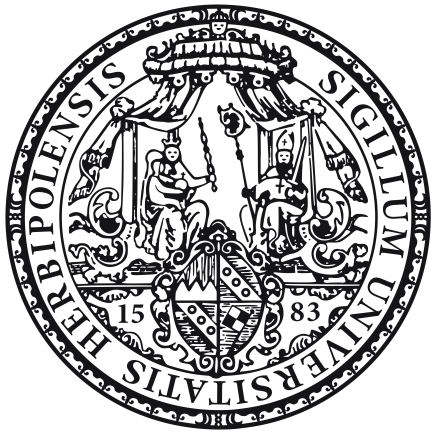

vorgelegt von
Ruben Pawellek
aus Marktheidenfeld

Würzburg 2021

Charged Aerosol Detector Performance Evaluation and Development of Optimization Strategies for the Analysis of Amino Acids

Dissertation zur Erlangung des naturwissenschaftlichen Doktorgrades der Julius-Maximilians-Universität Würzburg

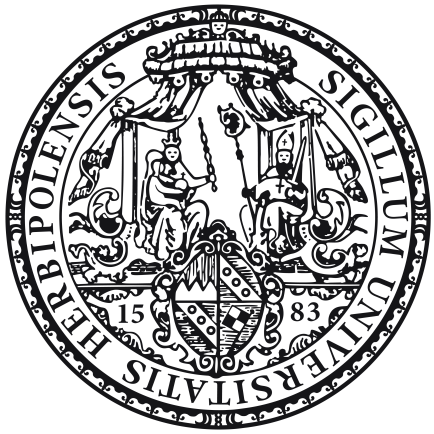

vorgelegt von
Ruben Pawellek
aus Marktheidenfeld

Würzburg 2021

Eingereicht bei der Fakultät für Chemie und Pharmazie am

_____

Gutachter der Dissertation

1. Gutachter: _____

2. Gutachter: _____

Prüfer des öffentlichen Promotionskolloquiums

1. Prüfer: _____

2. Prüfer: _____

3. Prüfer: _____

Tag des öffentlichen Promotionskolloquiums

_____

Doktorurkunde ausgehändigt am

_____

"A certain type of perfection can only be realized through a limitless accumulation of the imperfect."

Haruki Murakami, Kafka On The Shore.

Meiner Familie

Danksagung

Die vorliegende Arbeit entstand am Institut für Pharmazie und Lebensmittelchemie der Julius-Maximilians-Universität Würzburg auf Anregung und unter Anleitung von

Frau Prof. Dr. Ulrike Holzgrabe

Ich möchte mich an dieser Stelle für die freundliche Aufnahme in den Arbeitskreis, das in mich gesetzte Vertrauen, die Unterstützung in allen Phasen der Promotion und die Möglichkeit zum selbstständigen und eigenverantwortlichen Verfassen der Dissertation bedanken.

Herzlichen Dank auch an alle Kolleginnen und Kollegen des AK Holzgrabe für ihre Hilfsbereitschaft und die angenehme Zeit auf und neben der Arbeit:

Adrian, Alex, Anja, Antonio, Christiane, Christine E., Christine H., Cristian, Curd, Daniela, Emilie, Flo, Jens, Jonas U., Jonas W., Joseph, Joshi, Klaus, Laura, Lina, Liling, Lu, Lukas, Markus, Mohamed, Nelson, Niclas, Nic, Nina, Patrick, Paul, Rasmus, Sebastian, Sylvia, Theresa, sowie auch Frau Ebner, Frau Möhler und Frau Weidinger.

Weiterer Dank gilt den Kooperationspartnern von Thermo Fisher Scientific für die stets unkomplizierte und produktive Zusammenarbeit:

Dr. Paul Gamache, Dr. Frank Steiner, Dr. Tibor Müllner, Dr. Katherine Lovejoy, Dr. Benjamin Eggart, Dr. Susanne Fabel und Sylvia Grosse.

Ich danke Prof. Dr. Oliver Scherf-Clavel für seine Hilfe bei analytischen Fragestellungen.

Danke auch an die Assistenten des 1. und 2. Semesters für die unterhaltsame und reibungslose Praktikumsbetreuung.

“Hvala” an die serbischen Kolleginnen Jovana, Nevena und Ana für die erfolgreiche Kooperation.

Danke Max für den gemeinsamen Weg vom Studium bis zur Promotion.

Table of contents

List of abbreviations

AAA	amino acid analyzer
ACN	acetonitrile
Ala	L-alanine
ANN	artificial neural network
API	active pharmaceutical ingredient
Asn	L-asparagine
Asp	L-aspartic acid
BCAA	branched-chain amino acid
CAD	charged aerosol detector
CCD	central composite design
CE	capillary electrophoresis
CNLSD	condensation nucleation light scattering detector
Cys	L-cysteine
DoE	design of experiments
EDQM	European Directorate for the Quality of Medicines & HealthCare
ELSD	evaporative light scattering detector
EtOH	ethanol
FA	formic acid
FAME	fatty acid methyl ester
FFD	fractional factorial design
FIA	flow injection analysis
FID	flame ionization detector
GBT	gradient boosted trees
GC	gas chromatography
Glu	L-glutamic acid
Gly	glycine
GMP	good manufacturing practice

HFBA	heptafluorobutyric acid
HILIC	hydrophilic interaction chromatography
HPLC	high performance liquid chromatography
ICH	International Conference on Harmonisation of Technical Requirements for Registration of Pharmaceuticals for Human Use
ID	internal diameter
IEX/IEC	ion exchange
Ile	L-isoleucine
IPC	ion pair chromatography
Leu	L-leucine
LOD	limit of detection
LOQ	limit of quantitation
MeOH	methanol
Met	L-methionine
MLA	machine learning algorithm
MMC	mixed-mode chromatography
MS	mass spectrometry
MTBE	tert-butyl methyl ether
MW	molecular weight
NFPA	nonafluoropentanoic acid
NP	normal phase
PEG	polyethylene glycol
PFCA	perfluorinated carboxylic acid
PFPA	pentafluoropropionic acid
PFV	power function value
Ph. Eur.	European Pharmacopoeia
Phe	L-phenylalanine
Pro	L-proline
QSPR	quantitative structure-property relationship

R^2	coefficient of determination
REML	restricted maximum likelihood analysis
RI	refractive index
RMSE	root mean squared error
RP	reversed-phase
RPC	reversed-phase chromatography
RSD	relative standard deviation
RSM	response surface methodology
S/N	signal-to-noise ratio
Sar	sarcosine
SCX	strong cation exchange
Ser	L-serine
SMD	Sauter mean diameter
ß-Ala	beta-alanine
TDFHA	tridecafluoroheptanoic acid
TFA	trifluoroacetic acid
Tyr	L-tyrosine
UHPLC	ultra high performance liquid chromatography
USP	United States Pharmacopoeia
UV	ultraviolet
UV/VIS	ultraviolet/visible
Val	L-valine

1. Introduction

Pharmaceutical analysis is of utmost importance for the quality control in the pharmaceutical industry, since it comprises the qualitative and quantitative assessment of drug substances and drug products [1]. Among the analytical techniques available, high performance liquid chromatography (HPLC) [2, 3] stands out due to its high efficiency and robustness. Thus, HPLC is predominantly employed for the impurity analysis of drugs in the regulated environment [2, 4], e.g. pharmacopoeial procedures. The vast majority of the compendial methods in the European Pharmacopoeia (Ph. Eur.) [5] and the United States Pharmacopoeia (USP) [6] utilize HPLC coupled to a UV/VIS detector for the detection and quantitation of the impurities in active pharmaceutical ingredients (APIs). HPLC-UV is well suited for routine analysis purposes [7, 8] considering its broad linear range, the adequate sensitivity, and the convenient handling. However, the detection technique may suffer from poor sensitivity toward analytes without a decent chromophore. In addition, the sensitivity is highly dependent on the physico-chemical properties of the analyte, e.g. the respective molar extinction coefficient [9, 10].

Techniques with a more universal detection scope may offer a solution to the limitations of UV/VIS as their response is almost independent of the analyte properties and roughly uniform at constant experimental conditions, though they all have their own specific drawbacks [8]. Besides the refractive index (RI) detector [11] and the mass spectrometer (MS) [12], the aerosol-based evaporative light scattering (ELS) [13] and condensation nucleation light scattering (CNLS) [14] detectors provide a quasi-universal response for nonvolatile analytes. The most recent representative of the aerosol-based detectors is the charged aerosol detector (CAD) [15, 16]. The older CAD models, however, suffer from less sensitivity and a limited linearity. The current models can, to some extent, provide an improvement in case of proper adjustment of the instrumental settings. Moreover, the hyphenation of UV-CAD techniques further extends the detection scope which enables the analysis of challenging impurity profiles in one single chromatographic run.

The aim of this thesis is to evaluate the performance characteristics of the latest CAD model. Based on the obtained results, optimization strategies were developed which can serve as basis for the development of sensitive, robust, and straightforward methods for the impurity analysis of challenging amino acids and their derivatives for an intended compendial application.

1.1. Charged aerosol detection

Charged aerosol detection is a universal detection technique for quantitative analysis employed in liquid chromatography [17]. Since its commercial introduction in 2005 [18], the technology and instrumentation has evolved resulting in the implementation of a heated evaporation tube and a power function algorithm for signal linearization. The detection process is depicted in Fig. 1.

In brief, the solute containing column effluent is nebulized by a nitrogen stream to form a primary aerosol (1). The aerosol then passes an impactor, where droplets above a specific d_{cut} are directed to the waste upon impaction, while the remaining droplets form the secondary aerosol, which enters an evaporation tube (2). The aerosol droplets are spray-dried to form a residue consisting of the nonvolatile analyte and mobile phase impurity particles (3). A separate nitrogen stream is ionized by corona discharge and collides with the opposing stream of residue particles in a mixing chamber, thereby transferring positive charge to the latter (4). Subsequent to the removal of excess charge by an ion trap, the particles charge is measured by a sensitive electrometer (5).

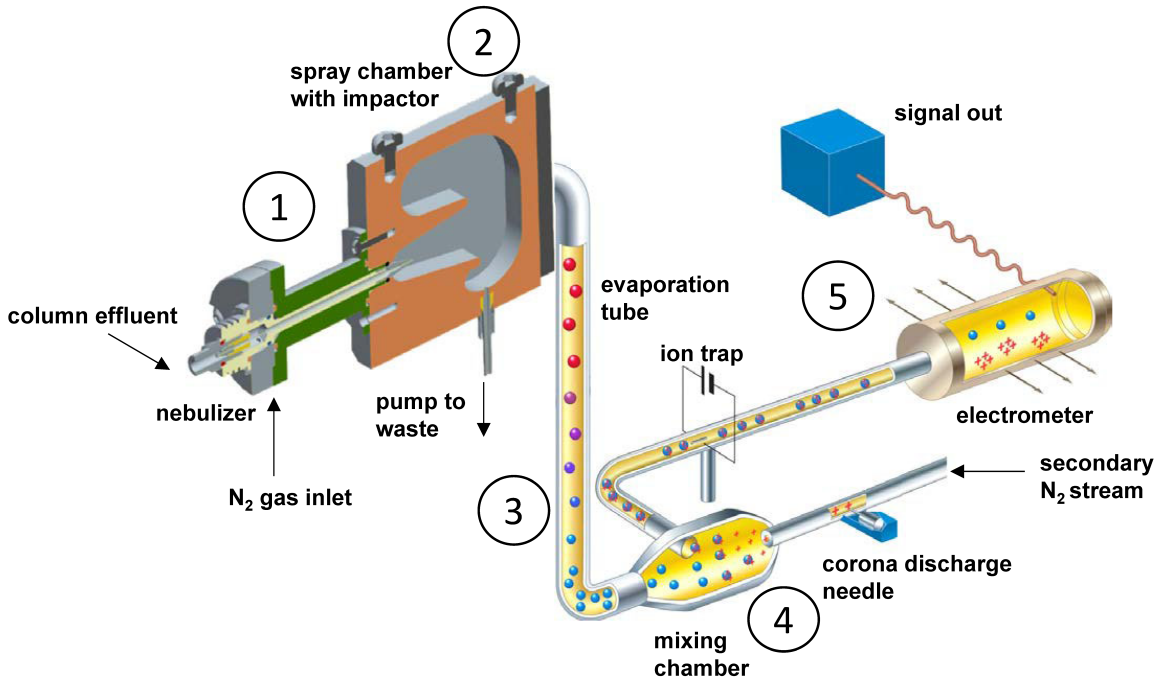

Figure 1. Detection scheme of the Vanquish CAD. Modified with permission from [19].

CAD has been employed to solve analytical challenges in various application areas, e.g. the quality control of drugs [20], the analysis of lipids [21] and carbohydrates [22], and the assessment of natural products [23]. A comprehensive overview of the CAD applications areas is provided in Ref. [17].

1.2. Performance characteristics of the CAD

1.2.1. Uniformity

Uniformity refers to a steady response/amount relationship for different analytes in the following context. Consequently, the signal of a detector with truly uniform response would be independent of the chemical structure or physicochemical properties of an analyte [24]. Uniform response is highly desirable for impurity profiling applications when the impurities are quantified relative to a single calibrator or when unknown impurities are to be determined [17, 25]. The response uniformity of the common aerosol-based detectors, which are often referred to as mass-dependent detectors [26, 27], is mainly affected by solvent gradients, analyte volatility and salt formation, analyte density, and the particle material of the residue [17].

The processes leading to the formation of residue particles are basically the same for all evaporative aerosol-based detectors [28, 29]. The initial diameter of a spherical droplet in the primary aerosol after nebulization (Sauter mean diameter, SMD) is described by the Nukiyama-Tanasawa [17, 30] equation:

$$\mathrm{SMD} = \frac{585\sigma^{0.5}}{(v_g - v_l)\rho^{0.5}} + 597\left[\frac{\eta}{(\sigma\rho)^{0.5}}\right]^{0.45} \times \left(1000 \times \frac{Q_l}{Q_g}\right)^{1.5} \qquad \text{Eq. (I)}$$

where σ is the surface tension, ρ is the density, and η the dynamic viscosity of the effluent. The liquid flow rate of the effluent is represented by Q_l whereas the gas flow rate is Q_g. The axial liquid and gas velocities, v_l and v_g, are defined by the respective flow rates and the nebulizer specifications. Since droplets above a specific d_{cut} are removed to the waste upon impaction of the primary aerosol, it follows that the effluent composition is crucial for the formation of analyte particles and thus response. Organic solvents such as acetonitrile exhibit lower viscosities and surface tensions compared to aqueous solvent, consequently they produce droplets of smaller size according to Eq. 1. Moreover, highly organic droplets are more susceptible to pre-impactor evaporation, which is also beneficial for the aerosol transport as droplets above d_{cut} are not removed by impaction when their size is previously reduced [17]. Due to the more efficient nebulization and aerosol transport processes for organic solvents, a higher proportion of the analyte enters the evaporation tube leading to an increased response, e.g. when an aqueous-organic gradient is applied.

The relationship between the diameter d_p of a dried residue particle and the analyte concentration C is nonlinear according to Eq. II [29, 31]:

$$d_p = d_d \left(\frac{C}{\rho_p}\right)^{1/3} \quad \text{Eq. (II)}$$

where d_d is the diameter of the initial primary aerosol droplet and ρ_p is the density of the analyte. It should be mentioned that both C and ρ_p may include nonvolatile impurities, which also contribute to the dried particle size [29]. The nonlinear relationship evident from Eq. II directly affects the aerosol-based detectors performance as will be further discussed in paragraph 1.2.3. From Eq. 2 it follows that the size of the dried particle and, thus, the response is also dependent on the density of the analyte [32, 33].

The decisive step in the detection process, which differs among the aerosol-based detectors and results in a more uniform CAD response, is the measurement of the dried particles. Charging of the dried aerosol particles by unipolar diffusion processes is almost independent on the residue particle material, e.g. the analyte properties [17, 18, 27, 34, 35], while the light scattering detection mechanisms of the ELSD [13, 36, 37] and the CNLSD [38] are more influenced by specific analyte characteristics, e.g. the refractive index. Consequently, a superior uniformity of response of the CAD has been demonstrated in numerous studies [39- 46] (Fig. 2).

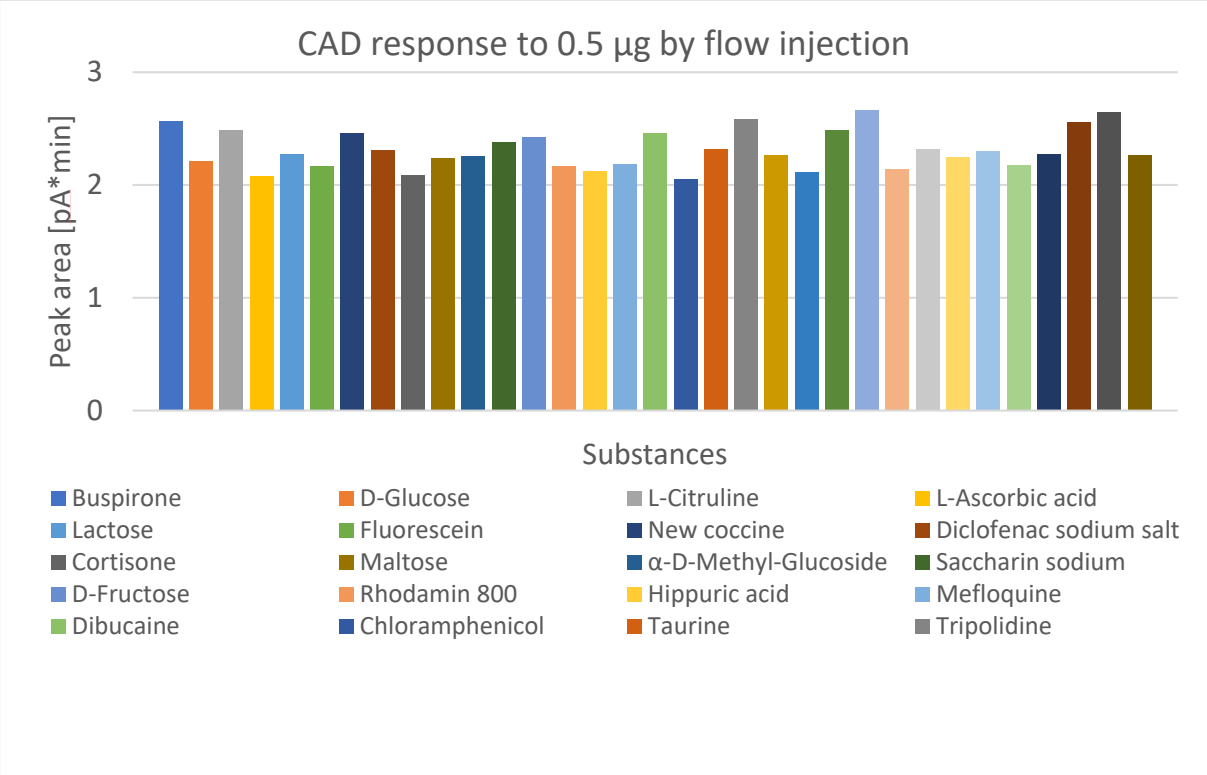

Figure 2. Uniform CAD response obtained by flow injection analysis for diverse nonvolatile compounds. Reprinted with permission from [24].

In general, the volatility of an analyte is the most influential characteristic toward the CAD responsiveness [18, 27]. Although the volatility of a compound can be estimated by its vapor pressure or boiling point, there are no distinct boundaries between nonvolatile and semivolatile compounds; therefore, the classification requires experimental verification. While the salt formation of mobile phase additives with ionized nonvolatile analytes can negatively affect the response uniformity due to an increased response of the latter [47], the same effect improves the sensitivity for semivolatile analytes [48]. Low molecular mass mobile phase additives produce a more uniform response compared to higher mass additives [47, 49].

Several approaches exist to address a nonuniform CAD response. The most common approach to obtain a uniform response in gradient elution mode is the application of a gradient compensation technique [27, 50-54]. A second pump delivers an inverse gradient to the separation gradient resulting in a constant mobile phase composition, which significantly improves the uniformity of response. Different approaches aimed at establishing a CAD response model accounting for experimental variables and molecular properties of the analytes in order to predict the CAD response for varying conditions. Hutchinson et al. [34] constructed a three-dimensional model relating the CAD response to the analyte concentration and the mobile phase composition. The model allows, with some limitations, the quantitation of unknown nonvolatile analytes without using calibration standards. Robinson et al. [33] correlated the estimated relative surface area of the dried analyte particles to the CAD response instead of the injected mass, thereby improving the error of quantification for 50 compounds with varying properties. The suggested surface area dependent response of the CAD is in accordance with the detection principle of the CAD [20] and further supported by incorporation of a molecular descriptor into a QSPR model [55], which could adequately predict the CAD response of aminoglycoside antibiotics and sugars. A comprehensive QSPR model relating the CAD response to the molecular descriptors of diverse compound classes would be highly desirable. Machine learning algorithms are beneficial tools for the establishment of these rather complex models and are likely to be employed more frequently in the future.

1.2.2. Sensitivity

The comparison of the aerosol-based detectors sensitivity has been the subject to numerous studies. In most cases, the CAD provided lower sensitivity limits than the ELSD [25, 39, 41, 42, 56-59]. Few studies compared the CAD's sensitivity to the CNLSD, with divergent results [28, 29, 48, 60, 61]. However, the comparison studies were performed with the legacy cross-flow design CAD models providing lower sensitivity compared to the recent concentric design models [17].

As it is the case for all universal detectors, the mobile phase composition is a crucial factor for the sensitivity of a method. Besides the aforementioned response dependency on aqueous-organic gradients, the purity of the mobile phase is a highly contributing factor toward sensitivity [17, 62-64], e.g. the concentration of present nonvolatile and semivolatile impurities. This also includes the applied mobile phase additives [26, 65], which need to be sufficiently volatile and of high purity.

With the Corona Veo charged aerosol detector model introduced in 2015, the temperature of the evaporation tube can be adjusted. The evaporation temperature setting has a direct impact on the response of the analyte as well on the background noise of the CAD (Fig. 3). The optimal evaporation temperature is obtained for the best compromise of both, which depends on the analyte's volatility and on the nature and concentration of the present mobile phase impurities. Thus, the optimal setting requires experimental verification because the response of the analytes is not always predictable solely based on their physicochemical properties [17, 33]. Figures 3a. and 3b. illustrate the influence of the evaporation temperature on the CAD performance for two general cases.

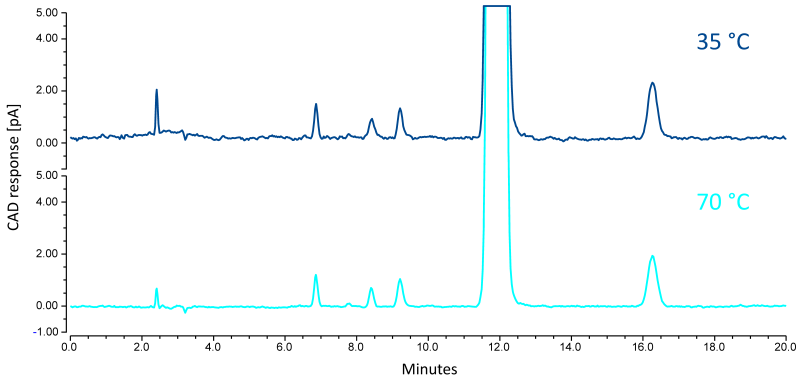

Figure 3a. Influence of an elevated evaporation temperature (70 °C) on the response of nonvolatile analytes and on the the background noise.

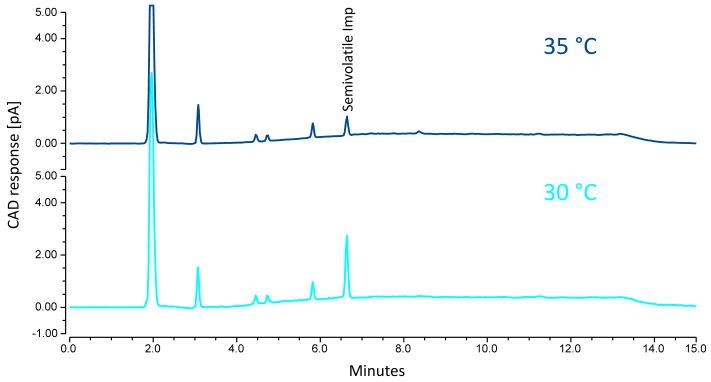

Figure 3b. Influence of a low evaporation temperature (30 °C) on the response of a semivolatile analyte.

A good practice is to choose the lowest evaporation temperature possible that still produces the required sensitivity [17], since a more uniform response is obtained here in most cases. In contrast, many compound classes behave as semivolatiles at elevated evaporation temperatures [47]. However, polar nonvolatile analytes often produce a constant response even at elevated temperatures, thus their signal-to-noise ratio (S/N) can be improved by increasing the evaporation temperature.

1.2.3. Linearity

Due to its principle of detection, the CAD's response is inherently nonlinear, analogously to the other aerosol-based detectors. Two processes are predominantly contributing to the observed nonlinear response [17]. As described previously, the concentration of the nonvolatile residue after evaporation is proportional to the cubic root of the dried particle diameter (Eq. II). The second process with a substantial impact on the shape of the response curve is the charging of the dried residue particles. The mean charge per particle transferred by unipolar diffusion processes depends on the particle diameter d [16, 66-68] and is proportional to $d^{1.133}$ for d>9 nm, while the exponent is $d^{2.25}$ for d<9 nm.

The shape of the response curve can be described by Eq. III [17]:

$$A = a(m_{inj})^b \qquad \text{Eq. (III)}$$

where *A* is the peak area, *a* is sensitivity coefficient, m_{inj} the injected mass, and *b* a power law exponent derived from the two subprocesses described above. The *a* and *b* variables depend on the analyte properties and the experimental conditions. For *b*=1, a linear response is observed, whereas *b*>1 indicates supralinear response and *b*<1 sublinear response, respectively. It should be noted that the CAD response is often quasi-linear over concentration ranges up to two orders of magnitude [69-74], while a nonlinear response is observed for broader concentration ranges. Compared to the ELSD, the CAD's power law exponent *b* deviates less from 1 due to the higher influence of the light scattering mechanisms (mean charge per particle proportional to ~d^2-d^6) involved in the particle measurement of the ELSD [13, 75].

A common linearization approach [34, 39, 76, 77] is the double-logarithmic transformation of Eq. III resulting in Eq. IV:

$$\log(A) = b \times \log\left(m_{inj}\right) + \log(a) \qquad \text{Eq. (IV)}$$

where the power law *b* becomes the slope of the response curve and the coefficient *a* becomes the y-intercept. The double logarithmic transformation and other mathematical fitting options share one drawback. They require the subsequent manipulation of original calibration data which can be an issue in GMP regulated environment [78].

A relatively new linearization approach makes use of the built-in power function value (PFV) setting of the recent CAD models [79]. The PFV is basically a correction factor to the power law exponent *b* of Eq. III [17], which directly alters the signal output of the CAD to improve the detector's linearity in the desired range. Since this approach does not require a subsequent manipulation of data, it is of relevance for the regulated environment. Consequently, an increasing number of publications relies on the PFV optimization [44, 51, 52, 78, 80-84] to compensate the nonlinear CAD response.

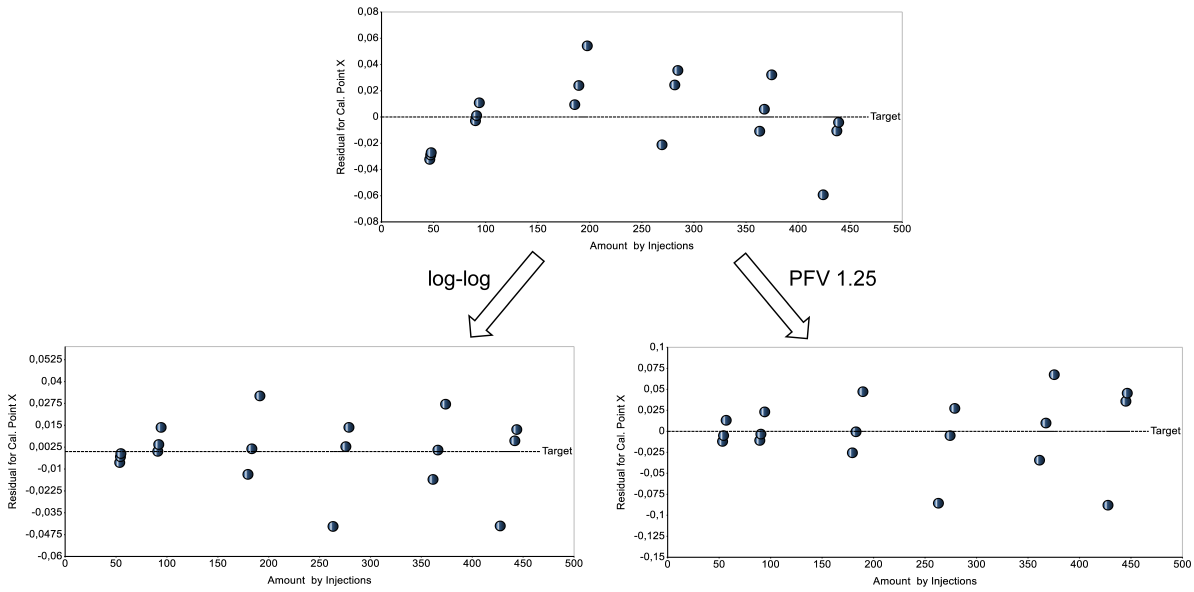

Figure 4. A nonlinear response of an analyte as indicated by the trend in the residual plot can be linearized either applying a double logarithmic transformation or a PFV of 1.25.

1.3. Liquid chromatography techniques for the separation of small polar compounds

High-performance liquid chromatography using a reversed-phase column (RP-HPLC) is a robust and powerful separation technique for a wide variety of compound types [85]. However, the technique only weakly retains small hydrophilic compounds in most cases [86]. Additionally, numerous small polar compounds, e.g. amino acids and sugars, do not possess a suitable chromophore for the routinely applied UV detection. Pre-column [87-89] and post-column [90-92] derivatization techniques can help to overcome the separation issues and improve the detectability of weakly-chromophoric compounds by introduction of an UV- or fluorescence responsive group, however, they share several drawbacks such as unwanted side products of the derivatization reaction [93] and blindness to compounds without derivatizable group.

Ion pair chromatography (IPC), mixed-mode chromatography (MMC), and hydrophilic interaction chromatography (HILIC) represent more straightforward alternatives to the derivatization methods and will be described in more detail in the following also regarding their impact on the CAD performance. It should be mentioned that they usually comprise vastly different proportions of organic modifier and mobile phase additives, especially for IPC. Characteristic parameters of the separation techniques and their assumed influence on the CAD performance are illustrated in Table 1.

Table 1. IPC, MMC, and HILIC characteristics and their assumed impact on the CAD response (+) and background current (*).

Characteristic	Parameter	IPC	MMC	HILIC
mobile phase composition[a]	organic percentage	low[b] (+)	low-high (+−+++)	high (+++)
	mobile phase additives	volatile ion-pairing reagents (***)	volatile buffers/ pH modifiers (*)	volatile buffers/ pH modifiers (*)
stationary phase	column material	RP columns, e.g. C18	bimodal/trimodal functionalized columns, e.g. RP/IEX	polar columns, e.g. silica-based amino/amide/diol columns
	column bleed	low (*)	low-high (*−***)	high (***)
MS compatibility		low	high	high
sample solvent		aqueous/organic	aqueous/organic	≥ 50% organic
selected CAD applications		amino acid analysis [69, 94, 95], gentamicin [96], streptomycin [97]	carbocisteine [98], aspartate [77], methionine and arginine [99]	amino acid analysis [100, 101], glucosamine [73], apramycin [57], gabapentin [102]

[a] When used with CAD.

[b] With respect to the other separation techniques.

1.3.1. IPC

In IPC, the retention of ionized compounds on RP columns is increased by using ion-pairing reagents of opposite charge to form ion pairs. The structure of an ion-pairing reagent contains a lipophilic group, which interacts with the stationary phase and an ionizable moiety for the interaction with the analyte. Since multiple mechanisms contribute to the observed retention, the discussed theoretical retention models tend to be rather sophisticated [103, 104]. Key aspects of simplified models include the dynamic modification of the surface of the RP column by adsorption of the ion-pairing reagent, thereby creating ion exchange sites, the formation of neutral ion pairs able to partition into the hydrophobic stationary phase, and a combination of

both mechanisms [103]. IPC comes along with some drawbacks. RP columns used with ion-pairing reagents should be dedicated to IPC applications due to the potential irreversible adsorption of the applied reagent. Further consequences of the adsorption mechanism are the relatively slow column equilibration [105, 106] and the time-consuming re-equilibration in methods with gradient elution. Perfluorinated carboxylic acids (PFCAs), which are widely employed as ion-pairing reagents, are environmentally persistent [107] and potentially toxic [108].

The preferred mobile phase for IPC is a water-rich eluent, because analyte retention decreases with increasing proportion of the organic modifier [103]. Thus, a lower CAD response is to be expected compared to highly organic mobile phases [109]. Furthermore, the salt formation of the applied ion-pairing reagent with the analyte as well with present mobile phase impurities has a direct impact on the analyte signal [47] and the background noise [24], respectively. With CAD, volatile ion-pairing reagents are required, i.e. PFCAs [94, 95, 97] for basic analytes and substituted alkylamines [48, 110, 111] for acidic analytes.

1.3.2. MMC

Some IPC related shortcomings can be avoided by using MMC instead. In MMC, the employed stationary phases are functionalized to have multiple retention mechanisms [112], e.g. RP and ion exchange (IEC). They can be classified [113] in accordance with the respective retention modes into RPC/HILIC, RPC/IEC, HILIC/IEC, and others, e.g. with a ternary retention mode. As different interactions contribute to the retention of the analytes, the simultaneous analysis of charged and neutral compounds becomes feasible without the usage of ion-pairing reagents. A wide variety of columns with diverse column chemistries and unique selectivities are commercially available [114]. The mobile phase composition is a more critical factor compared to RPC, because the type and the proportion of the organic modifier, the type of the mobile phase additive, the pH, and the ionic strength have a substantial impact on the chromatographic performance and retention of the analytes due to the concurrent separation mechanisms [115]. It was demonstrated [116] that the loading capacity for ionized bases is higher for MMC columns compared to RPC columns, which is of particular importance for impurity profiling methods, where concentrated samples have to be injected. However, the method development is less straightforward compared to RPC due to the multiple interactions involved between the analytes and the multimodal stationary phase, which requires a greater extent of optimization of the chromatographic conditions [114]. Moreover, the MMC columns lack of standardization due to the proprietary functionalization procedures, which means that even columns with identical functionalities from different manufacturers might not provide a comparable selectivity. However, some MMC columns are listed in the USP [6].

Since MMC columns can be operated in the RPC mode as well as in the HILIC mode [114], the organic proportion in the mobile phase, and thus the CAD response, varies in dependence of the elution mode and the applied mobile phase additive. Typically, the mobile phases comprise a buffer or acidic modifier. However, the use of long chain ion-pairing reagents is not necessary due to the additional retention mode. Thus, the impact of the mobile phase additive on the analyte signal and the background noise of the CAD is presumably less pronounced compared to IPC. Column bleed is a relevant factor for the development of MMC-CAD methods in particular when a HILIC retention mode is involved [117].

1.3.3. HILIC

HILIC comprises polar stationary phases and highly organic mobile phases. It can be characterized as the chromatographic technique using a normal phase (NP) stationary phase, e.g. bare silica, neutral polar chemical bonded (amino, amide, diol, etc.), ion exchange, and zwitterionic stationary phases, in combination with a RP mobile phase, containing more than 50% organic solvent in water [86]. According to present theory, retention in HILIC is mainly caused by partitioning of the analytes between the acetonitrile-rich mobile phase and a water-enriched layer adsorbed onto the hydrophilic stationary phase. Electrostatic interaction and hydrogen bonding effects may also play a role [118, 119]. While the initial method development was solely based on univariate approaches [120], chemometric-assisted method development including quantitative structure-retention relationship models and computer-aided column classification could further facilitate the application of HILIC [121]. HILIC is well-suited for the separation of small polar compounds [122]; thus, it represents an alternative to IPC with a complementary selectivity. An increased sample loading capacity for HILIC compared to RPC has been reported [123]. Similar to MMC, the standardization of HILIC columns is not as far advanced as for RPC. However, HILIC columns are also listed in the USP [6]. A prerequisite for satisfactory chromatographic performance in HILIC is the solubility of the sample in highly organic diluent. For impurity profiling purposes, where the injection of highly concentrated samples of the main substance is inevitable, this represents a serious limitation.

Due to the highly organic mobile phases employed in HILIC, the CAD response is significantly increased compared to the RPC conditions [109]. Volatile buffers such as ammonium formate and ammonium acetate are typically applied as mobile phase additives. The mobile phase requirements are identical to those of a mass spectrometer, enabling a straightforward method transfer of a HILIC-CAD method to MS. A HILIC-associated issue with an impact on the CAD performance is column bleed. As universal detector, the CAD is sensitive towards nonvolatile mobile phase impurities which may arise from dissolution of silica-based HILIC columns [124]. Consequently, significant levels of column bleed have been reported for several HILIC-CAD

applications [102, 125, 126]. Polymer-based [127] as well as coated silica [128] stationary phases show significantly less column bleed and might thus provide a solution.

1.4. Hyphenated detection techniques with CAD

The CAD is often referred to as universal detector, however, this holds true only for nonvolatile compounds. Thus, the hyphenation of detection techniques can be a great asset to extend the detection scope and to obtain complementary and comprehensive information on the challenging impurity profile of APIs. One promising strategy for the impurity profiling of drugs is the hyphenation of CAD and MS, which can easily be done, as the detectors share the same mobile phase requirements. Due to their destructive detection principle, flow splitting of the column effluent [129] or the usage of separate HPLC systems [101] is required. While the CAD's almost uniform response for nonvolatile analytes allows the quantitation of unknown impurities without using a reference standard, the hyphenated MS detection provides structural information on unknown compounds [97, 130-132].

In case of well-known impurity profiles and for routine analysis purposes, hyphenation of UV-CAD is sufficient to benefit from the complementary detection techniques when dealing with a set of physico-chemical diverse analytes, e.g. volatile and weakly chromophoric impurities (Fig. 5). Hyphenation can easily be achieved by connecting the outlet of the non-destructive UV detector to the CAD and represents a robust and straightforward application. Thus, there is an increasing number of publications where UV-CAD [71, 133-137] was employed for a comprehensive analysis. UV-CAD coupled to HPLC analysis has also been introduced into the Ph. Eur. for the test of related substances of the drug vigabatrin [138]. However, the mobile phase composition is a crucial factor for the development of sensitive methods with hyphenated detection because the CAD is limited to volatile mobile phases, while the UV detector requires non-absorbing organic modifiers and mobile phase additives.

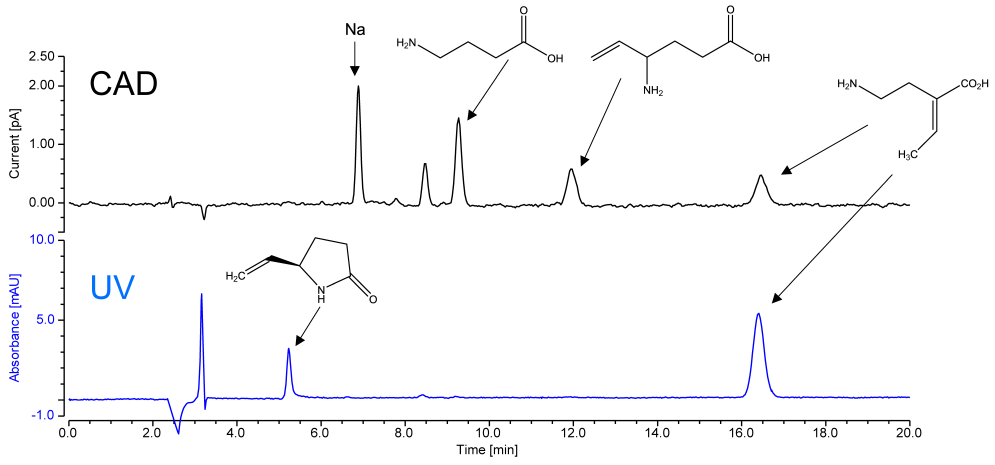

Figure 5. Comprehensive impurity profiling of non-chromophoric and volatile compounds by hyphenated UV-CAD techniques. Here, the impurity profiling of vigabatrin is displayed.

1.5. Challenges in the analysis of amino acids and related compounds

There are two main challenges in the analysis of amino acids and their derivatives using HPLC. One challenge is the separation of these small polar compounds. Due to their zwitterionic properties (pK_{COOH} ~2, pK_{amino} ~9) they are permanently charged in aqueous solution; thus, RPC is not feasible in most cases. For impurity profiling purposes, potential impurities, e.g. organic acids, must be considered as well. The previously discussed IPC, MMC, and HILIC techniques are viable options. However, the selection of the most appropriate separation technique depends on the individual impurity profile of the API and on its physicochemical properties. Although HILIC is perfectly suited for the separation of small polar analytes, it is limited to applications where a concentrated solution of the API is soluble in highly organic (>50%, v/v) solvent. MMC columns with RP/SCX functionalities are a good choice for the separation of amino acids, however, they lack separation power towards organic acids without basic moiety. In IPC methods, the retention and selectivity must be optimized by the selection of the applied ion-pairing reagent(s). Consequently, the initial method development requires extensive experimentation, e.g. the screening of diverse separation techniques and column chemistries.

Besides the challenging separation of the amino acids and their possible impurities, the coverage of the entire impurity profile in one single chromatographic run is not easily accomplished as well. Most of the amino acids do not possess an UV absorbing structural feature with the carboxylic moiety being the sole weak chromophore at short wavelength UV (<210 nm). In contrast, the CAD provides a reliable and sensitive detection of the nonvolatile amino acids. However, the impurity profile of the respective amino acid may not only contain weakly chromophoric compounds, but also volatile impurities not accessible with CAD. In this case, hyphenated UV-CAD can be employed to expand the detection scope.

In this thesis, RPC, IPC, MMC, and HILIC methods for the impurity profiling of amino acids and their derivatives were elaborated (Table 2). The separation techniques were coupled to CAD or UV-CAD where appropriate.

Table 2. Selected compounds for the development and validation of impurity profiling methods.

Compound	Structure	logD[a] (pH 5.5)	Impurity profile[b]	Analysis method
L-aspartic acid	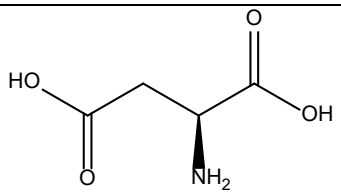	−4.30	semivolatile and weakly-chromophoric	IPC-UV-CAD
gabapentin	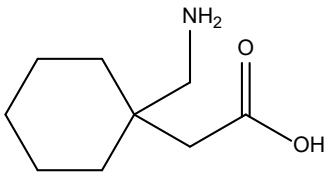	−1.45	volatile, semivolatile, and weakly-chromophoric	RPC-UV-CAD
glycine	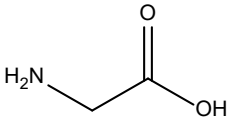	−3.20	volatile and weakly-chromophoric	IPC-UV-CAD
L-valine	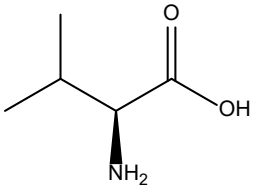	−2.16	weakly-chromophoric	HILIC-CAD
vigabatrin	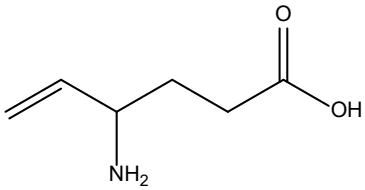	−2.74	volatile and weakly-chromophoric	MMC-UV-CAD

[a] Predicted by ACD labs software version 2020.2.0 (ACD Labs, Toronto, Canada).

[b] With respect to the Ph. Eur. 10 [5].

1.6. References

[1] S. Ahuja, S. Scypinski, Handbook of modern pharmaceutical analysis, Academic press, 2001.

[2] S. Ahuja, M. Dong, Handbook of pharmaceutical analysis by HPLC, Elsevier, 2005.

[3] Y. Kazakevich, R. LoBrutto, HPLC for pharmaceutical scientists, Wiley Online Library, 2007.

[4] S. Görög, The changing face of pharmaceutical analysis, TrAC 26(1) (2007) 12-17.

[5] Council of Europe, European Pharmacopeia Online 10.5, EDQM, Strasbourg, France, 2021.

[6] United States Pharmacopeia, USP 38 NF 33, The United States Pharmacopeial Convention, Rockville, MD, USA, 2015.

[7] M.R. Siddiqui, Z.A. AlOthman, N. Rahman, Analytical techniques in pharmaceutical analysis: A review, Arab. J. Chem. 10 (2017) S1409-S1421.

[8] K. Zhang, K.L. Kurita, C. Venkatramani, D. Russell, Seeking universal detectors for analytical characterizations, J. Pharm. Biomed. Anal. 162 (2019) 192-204.

[9] S. Gorog, Ultraviolet-visible spectrophotometry in pharmaceutical analysis, CRC press, 2018.

[10] M. Swartz, HPLC detectors: a brief review, J. Liq. Chromatogr. Relat. Technol. 33(9-12) (2010) 1130-1150.

[11] J.L. Chávez-Servín, A.I. Castellote, M.C. López-Sabater, Analysis of mono-and disaccharides in milk-based formulae by high-performance liquid chromatography with refractive index detection, J. Chromatogr. A 1043(2) (2004) 211-215.

[12] E. De Hoffmann, Mass spectrometry, Kirk-Othmer Encyclopedia of Chemical Technology (2000).

[13] T.H. Mourey, L.E. Oppenheimer, Principles of operation of an evaporative light-scattering detector for liquid chromatography, Anal. Chem. 56(13) (1984) 2427-2434.

[14] L.B. Allen, J.A. Koropchak, Condensation nucleation light scattering: a new approach to development of high-sensitivity, universal detectors for separations, Anal. Chem. 65(6) (1993) 841-844.

[15] R.W. Dixon, D.S. Peterson, Development and testing of a detection method for liquid chromatography based on aerosol charging, Anal. Chem. 74(13) (2002) 2930-2937.

[16] A. Medved, F. Dorman, S. Kaufman, A. Pöcher, A new corona-based charger for aerosol particles, J. Aerosol Sci. 31 (2000) S616-S617.

[17] P.H. Gamache, Charged Aerosol Detection for Liquid Chromatography and Related Separation Techniques, John Wiley & Sons, 2017.

[18] P.H. Gamache, R.S. McCarthy, S.M. Freeto, D.J. Asa, M.J. Woodcock, K. Laws, R.O. Cole, HPLC analysis of nonvolatile analytes using charged aerosol detection, Lc Gc Europe 18(6) (2005) 345.

[19] B. Bailey, Expanding Your High Performance Liquid Chromatography and Ultra High Performance Liquid Chromatography Capabilities with Universal Detection: Shedding Light on Compounds That Lack a Chromophore, Pittcon Conference & Expo 2014.

[20] K. Schilling, U. Holzgrabe, Recent applications of the Charged Aerosol Detector for liquid chromatography in drug quality control, J. Chromatogr. A 1619 (2020) 460911.

[21] M.R. Infantes-Garcia, S. Verkempinck, J. Guevara-Zambrano, M. Hendrickx, T. Grauwet, Development and validation of a rapid method to quantify neutral lipids by NP-HPLC-charged aerosol detector, J. Food Compos. Anal. 102 (2021) 104022.

[22] D. Hu, B. Han, C. Chen, N. Chen, B. Zhu, J. Zhao, S. Li, Determination of seven oligosaccharides and sucrose in Pseudostellaria heterophylla by pressurized liquid extraction and ultra-high performance liquid chromatography with charged aerosol detector and tandem mass spectrometry, J. Chromatogr. A 1609 (2020) 460441.

[23] H. Jiang, W. Zhang, J. Yang, G. Xue, S. Su, C. Li, Q. Wang, W. Guo, H. Xu, Miniaturized solid-phase extraction using a mesoporous molecular sieve SBA-15 as sorbent for the determination of triterpenoid saponins from Pulsatilla chinensis by ultrahigh-performance liquid chromatography-charged aerosol detection, J. Pharm. Biomed. Anal. 194 (2021) 113810.

[24] M. Menz, B. Eggart, K. Lovejoy, I. Acworth, P. Gamache, F. Steiner, Charged aerosol detection - factors affecting uniform analyte response, Thermo Scientific (2018). https://assets.thermofisher.com/TFS-Assets/CMD/Technical-Notes/tn-72806-uhplc-charged-aerosol-detection-tn72806-en.pdf. (Accessed 07.06.2021).

[25] S. Almeling, D. Ilko, U. Holzgrabe, Charged aerosol detection in pharmaceutical analysis, J. Pharm. Biomed. Anal. 69 (2012) 50-63.

[26] T. Vehovec, A. Obreza, Review of operating principle and applications of the charged aerosol detector, J. Chromatogr. A 1217(10) (2010) 1549-1556.

[27] T. Gorecki, F. Lynen, R. Szucs, P. Sandra, Universal response in liquid chromatography using charged aerosol detection, Anal. Chem. 78(9) (2006) 3186-3192.

[28] R.D. Cohen, Y. Liu, 1 Advances in Aerosol, Adv. Chromatogr. 52 (2014) 1.

[29] L.-E. Magnusson, D.S. Risley, J.A. Koropchak, Aerosol-based detectors for liquid chromatography, J. Chromatogr. A 1421 (2015) 68-81.

[30] S. Nukiyama, An Experiment on the Atomization of Liquid by means of an Air Stream (1), J. Soc. Mech. Eng., Japan 4 (1938) 128-135.

[31] J.A. Koropchak, L.-E. Magnusson, M. Heybroek, M. Anisimov, S. Sadain, X. Yang, Fundamental aspects of aerosol-based light-scattering detectors for separations, Adv. Chromatogr. 40 (1999) 275-314.

[32] S. Matsuyama, Y. Orihara, S. Kinugasa, H. Ohtani, Effects of densities of brominated flame retardants on the detection response for HPLC analysis with a corona-charged aerosol detector, Anal. Sci. 31(2) (2015) 61-65.

[33] M.W. Robinson, A.P. Hill, S.A. Readshaw, J.C. Hollerton, R.J. Upton, S.M. Lynn, S.C. Besley, B.J. Boughtflower, Use of calculated physicochemical properties to enhance quantitative response when using charged aerosol detection, Anal. Chem. 89(3) (2017) 1772-1777.

[34] J.P. Hutchinson, J. Li, W. Farrell, E. Groeber, R. Szucs, G. Dicinoski, P.R. Haddad, Universal response model for a corona charged aerosol detector, J. Chromatogr. A 1217(47) (2010) 7418-7427.

[35] J.P. Hutchinson, T. Remenyi, P. Nesterenko, W. Farrell, E. Groeber, R. Szucs, G. Dicinoski, P.R. Haddad, Investigation of polar organic solvents compatible with Corona Charged Aerosol Detection and their use for the determination of sugars by hydrophilic interaction liquid chromatography, Anal. Chim. Acta 750 (2012) 199-206.

[36] M. Righezza, G. Guiochon, Effects of the nature of the solvent and solutes on the response of a light-scattering detector, J. Liq. Chromatogr. 11(9-10) (1988) 1967-2004.

[37] L.E. Oppenheimer, T.H. Mourey, Examination of the concentration response of evaporative light-scattering mass detectors, J. Chromatogr. A 323(2) (1985) 297-304.

[38] J. Koropchak, C. Heenan, L. Allen, Direct comparison of evaporative light-scattering and condensation nucleation light-scattering detection for liquid chromatography, J. Chromatogr. A 736(1-2) (1996) 11-19.

[39] N. Vervoort, D. Daemen, G. Török, Performance evaluation of evaporative light scattering detection and charged aerosol detection in reversed phase liquid chromatography, J. Chromatogr. A 1189(1-2) (2008) 92-100.

[40] D. Kou, G. Manius, S. Zhan, H.P. Chokshi, Size exclusion chromatography with Corona charged aerosol detector for the analysis of polyethylene glycol polymer, J. Chromatogr. A 1216(28) (2009) 5424-5428.

[41] K. Takahashi, S. Kinugasa, M. Senda, K. Kimizuka, K. Fukushima, T. Matsumoto, Y. Shibata, J. Christensen, Quantitative comparison of a corona-charged aerosol detector and an evaporative light-scattering detector for the analysis of a synthetic polymer by supercritical fluid chromatography, J. Chromatogr. A 1193(1-2) (2008) 151-155.

[42] J. Shaodong, W.J. Lee, J.W. Ee, J.H. Park, S.W. Kwon, J. Lee, Comparison of ultraviolet detection, evaporative light scattering detection and charged aerosol detection methods for liquid-chromatographic determination of anti-diabetic drugs, J. Pharm. Biomed. Anal. 51(4) (2010) 973-978.

[43] C. Merle, C. Laugel, P. Chaminade, A. Baillet-Guffroy, Quantitative study of the stratum corneum lipid classes by normal phase liquid chromatography: comparison between two universal detectors, J. Liq. Chromatogr. Relat. Technol. 33(5) (2010) 629-644.

[44] G. Liu, B. Zhu, X. Ren, J. Wang, Universal response method for the quantitative analysis of multi-components in josamycin and midecamycin using liquid chromatography coupled with charged aerosol detector, J. Pharm. Biomed. Anal. 192 (2021) 113679.

[45] P. Lezana, M. García-Mayoral, B. Lamothe, M. Pena-Abaurrea, Comprehensive ethoxymer characterization of complex alcohol ethoxy sulphate products by mixed-mode high-performance liquid chromatography coupled to charged aerosol detection, J. Chromatogr. A 1639 (2021) 461927.

[46] J. Wang, G. Liu, B. Zhu, L. Tang, Universal quantification method of degradation impurities in 16-membered macrolides using HPLC-CAD and study on source of the impurities, J. Pharm. Biomed. Anal. 184 (2020) 113170.

[47] J.J. Russell, J.C. Heaton, T. Underwood, R. Boughtflower, D.V. McCalley, Performance of charged aerosol detection with hydrophilic interaction chromatography, J. Chromatogr. A 1405 (2015) 72-84.

[48] R.D. Cohen, Y. Liu, X. Gong, Analysis of volatile bases by high performance liquid chromatography with aerosol-based detection, J. Chromatogr. A 1229 (2012) 172-179.

[49] I. Sinclair, R. Gallagher, Charged aerosol detection: factors for consideration in its use as a generic quantitative detector, Chromatogr. Today 1(3) (2008) 5-9.

[50] B. Behrens, M. Baune, J. Jungkeit, T. Tiso, L.M. Blank, H. Hayen, High performance liquid chromatography-charged aerosol detection applying an inverse gradient for quantification of rhamnolipid biosurfactants, J. Chromatogr. A 1455 (2016) 125-132.

[51] M. Eckardt, M. Kubicova, T.J. Simat, Universal response quantification approach using a Corona Charged Aerosol Detector (CAD)–Application on linear and cyclic oligomers extractable from polycondensate plastics polyesters, polyamides and polyarylsulfones, J. Chromatogr. A 1572 (2018) 187-202.

[52] P. Lucci, S. Moret, F. Buchini, G. Ferlat, L. Conte, Improved analysis of olive oils triacylglycerols by UHPLC-charged aerosol detection, J. Food Compos. Anal. 66 (2018) 230-236.

[53] M. Lísa, F. Lynen, M. Holčapek, P. Sandra, Quantitation of triacylglycerols from plant oils using charged aerosol detection with gradient compensation, J. Chromatogr. A 1176(1-2) (2007) 135-142.

[54] T.R. Baker, B.T. Regg, A multi-detector chromatographic approach for characterization and quantitation of botanical constituents to enable in silico safety assessments, Anal. Bioanal. Chem. 410(21) (2018) 5143-5154.

[55] K. Schilling, J. Krmar, N. Maljurić, R. Pawellek, A. Protić, U. Holzgrabe, Quantitative structure-property relationship modeling of polar analytes lacking UV chromophores to charged aerosol detector response, Anal. Bioanal. Chem. 411(13) (2019) 2945-2959.

[56] H.Y. Eom, S.-Y. Park, M.K. Kim, J.H. Suh, H. Yeom, J.W. Min, U. Kim, J. Lee, J.-R. Youm, S.B. Han, Comparison between evaporative light scattering detection and charged aerosol detection for the analysis of saikosaponins, J. Chromatogr. A 1217(26) (2010) 4347-4354.

[57] Z. Long, Z. Guo, I.N. Acworth, X. Liu, Y. Jin, X. Liu, L. Liu, L. Liang, A non-derivative method for the quantitative analysis of isosteroidal alkaloids from Fritillaria by high performance liquid chromatography combined with charged aerosol detection, Talanta 151 (2016) 239-244.

[58] I. Marquez-Sillero, S. Cardenas, M. Valcarcel, Comparison of two evaporative universal detectors for the determination of sugars in food samples by liquid chromatography, Microchem. J. 110 (2013) 629-635.

[59] J. Liu, M. Ronk, K. Fujimori, H. Lee, Y. Nashed-Samuel, Analysis of Silicone Oil in Prefilled Syringes and Biopharmaceutical Drug Products Using High-Performance Liquid Chromatography, AAPS PharmSciTech 22(2) (2021) 1-9.

[60] J.P. Hutchinson, J. Li, W. Farrell, E. Groeber, R. Szucs, G. Dicinoski, P.R. Haddad, Comparison of the response of four aerosol detectors used with ultra high pressure liquid chromatography, J. Chromatogr. A 1218(12) (2011) 1646-1655.

[61] J.M. Cintrón, D.S. Risley, Hydrophilic interaction chromatography with aerosol-based detectors (ELSD, CAD, NQAD) for polar compounds lacking a UV chromophore in an intravenous formulation, J. Pharm. Biomed. Anal. 78 (2013) 14-18.

[62] M. Plante, B. Bailey, F, Kusinitz, I. Acworth, Effect of Mobile Phase Quality on Analytical Performance of Corona Charged Aerosol Detectors, Thermo Scientific (2016). https://assets.thermofisher.com/TFS-Assets/CMD/Application-Notes/TN-159-LC-CAD-Mobile-Phase-TN71390-EN.pdf. (Accessed 07.06.2021).

[63] R.A. Moreau, The analysis of lipids via HPLC with a charged aerosol detector, Lipids 41(7) (2006) 727-734.

[64] M. Ligor, S. Studzińska, A. Horna, B. Buszewski, Corona-charged aerosol detection: an analytical approach, Crit. Rev. Anal. Chem. 43(2) (2013) 64-78.

[65] A. Błażewicz, Z. Fijałek, M. Warowna-Grześkiewicz, M. Jadach, Determination of atracurium, cisatracurium and mivacurium with their impurities in pharmaceutical preparations by liquid chromatography with charged aerosol detection, J. Chromatogr. A 1217(8) (2010) 1266-1272.

[66] H. Jung, D.B. Kittelson, Characterization of aerosol surface instruments in transition regime, Aerosol Sci. Tech. 39(9) (2005) 902-911.

[67] K.-S. Woo, D.-R. Chen, D.Y. Pui, W.E. Wilson, Use of continuous measurements of integral aerosol parameters to estimate particle surface area, Aerosol Sci. Tech. 34(1) (2001) 57-65.

[68] L. Li, D.-R. Chen, P.-J. Tsai, Use of an electrical aerosol detector (EAD) for nanoparticle size distribution measurement, J. Nanoparticle Res. 11(1) (2009) 111-120.

[69] U. Holzgrabe, C.-J. Nap, S. Almeling, Control of impurities in l-aspartic acid and l-alanine by high-performance liquid chromatography coupled with a corona charged aerosol detector, J. Chromatogr. A 1217(3) (2010) 294-301.

[70] L. Nováková, D. Solichová, P. Solich, Hydrophilic interaction liquid chromatography–charged aerosol detection as a straightforward solution for simultaneous analysis of ascorbic acid and dehydroascorbic acid, J. Chromatogr. A 1216(21) (2009) 4574-4581.

[71] P. Sun, X. Wang, L. Alquier, C.A. Maryanoff, Determination of relative response factors of impurities in paclitaxel with high performance liquid chromatography equipped with ultraviolet and charged aerosol detectors, J. Chromatogr. A 1177(1) (2008) 87-91.

[72] F. Weber, L. Rahnfeld, P. Luciani, Analytical profiling and stability evaluation of liposomal drug delivery systems: A rapid UHPLC-CAD-based approach for phospholipids in research and quality control, Talanta 220 (2020) 121320.

[73] C. Asthana, G.M. Peterson, M.D. Shastri, R.P. Patel, A novel and sensitive HILIC-CAD method for glucosamine quantification in plasma and its application to a human pharmacokinetic study, J. Pharm. Biomed. Anal. 178 (2020) 112954.

[74] H. Wang, S. Song, M. Shao, Y. Gao, C. Yang, Y. Li, W. Wang, Y. He, P. Li, Determination of bisphenol analogues in food-contact plastics using diode array detector, charged aerosol detector and evaporative light-scattering detector, Ecotox. environ. saf. 186 (2019) 109778.

[75] G. Guiochon, A. Moysan, C. Holley, Influence of various parameters on the response factors of the evaporative light scattering detector for a number of non-volatile compounds, J. Liq. Chromatogr.11(12) (1988) 2547-2570.

[76] R. Ghosh, P. Kline, HPLC with charged aerosol detector (CAD) as a quality control platform for analysis of carbohydrate polymers, BMC Res. Notes 12(1) (2019) 1-7.

[77] P. Li, W. Sun, L. Zuo, Z. Zhu, T. Zhao, R. Wang, M. Zhu, X. Leng, X. Qiu, L. Bai, Fast simultaneous determination of main components and impurity sodium ion in PAMA injection by mixed-mode chromatography, J. Pharm. Biomed. Anal. 161 (2018) 407-413.

[78] I.A.H. Ahmad, A. Blasko, J. Tam, N. Variankaval, H.M. Halsey, R. Hartman, E.L. Regalado, Revealing the inner workings of the power function algorithm in Charged Aerosol Detection: A simple and effective approach to optimizing power function value for quantitative analysis, J. Chromatogr. A 1603 (2019) 1-7.

[79] T. Muellner, I. Acworth, P. Gamache, Getting the most out of your charged aerosol detector, Thermo Scientific (2021). https://manuals.plus/m/400cde2a775fdbbf9328d2dfacf9f8f0196cd19a147097355253d37053912510.pdf. (Accessed 07.06.2021).

[80] A. Soliven, I.A.H. Ahmad, J. Tam, N. Kadrichu, P. Challoner, R. Markovich, A. Blasko, A simplified guide for charged aerosol detection of non-chromophoric compounds—Analytical method development and validation for the HPLC assay of aerosol particle size distribution for amikacin, J. Pharm. Biomed. Anal. 143 (2017) 68-76.

[81] J. Tam, I.A.H. Ahmad, A. Blasko, A four parameter optimization and troubleshooting of a RPLC–charged aerosol detection stability indicating method for determination of S-lysophosphatidylcholines in a phospholipid formulation, J. Pharm. Biomed. Anal. 155 (2018) 288-297.

[82] Y. He, P. Brown, M.R.B. Piatchek, J.A. Carroll, M.T. Jones, On-line coupling of hydrophobic interaction column with reverse phase column-charged aerosol detector/mass spectrometer to characterize polysorbates in therapeutic protein formulations, J. Chromatogr. A 1586 (2019) 72-81.

[83] I.A.H. Ahmad, A. Blasko, H. Wang, T. Lu, I. Mangion, E.L. Regalado, Charged aerosol detection in early and late-stage pharmaceutical development: selection of regressionmodels at optimum power function value, J. Chromatogr. A 1641 (2021) 461997.

[84] H. Takeda, M. Takahashi, T. Hara, Y. Izumi, T. Bamba, Improved quantitation of lipid classes using supercritical fluid chromatography with a charged aerosol detector, J. Lipid Res. 60(8) (2019) 1465-1474.

[85] J. Kirkland, Development of some stationary phases for reversed-phase HPLC, J. Chromatogr. A 1060(1-2) (2004) 9-21.

[86] P. Jandera, Stationary and mobile phases in hydrophilic interaction chromatography: a review, Anal. Chim. Acta 692(1-2) (2011) 1-25.

[87] F. Antoine, C. Wei, R. Littell, M. Marshall, HPLC method for analysis of free amino acids in fish using o-phthaldialdehyde precolumn derivatization, J. Agric. Food Chem. 47(12) (1999) 5100-5107.

[88] P. Fürst, L. Pollack, T. Graser, H. Godel, P. Stehle, Appraisal of four pre-column derivatization methods for the high-performance liquid chromatographic determination of free amino acids in biological materials, J. Chromatogr. A 499 (1990) 557-569.

[89] J. Dai, Y. Wu, S.-w. Chen, S. Zhu, H.-p. Yin, M. Wang, J. Tang, Sugar compositional determination of polysaccharides from Dunaliella salina by modified RP-HPLC method of precolumn derivatization with 1-phenyl-3-methyl-5-pyrazolone, Carbohydr. Polym. 82(3) (2010) 629-635.

[90] G. Morovján, P. Csokan, L. Nemeth-Konda, HPLC determination of colistin and aminoglycoside antibiotics in feeds by post-column derivatization and fluorescence detection, Chromatographia 48(1-2) (1998) 32-36.

[91] A. Andersson, A. Isaksson, L. Brattström, B. Hultberg, Homocysteine and other thiols determined in plasma by HPLC and thiol-specific postcolumn derivatization, Clin. Chem. 39(8) (1993) 1590-1597.

[92] A. Yamatodani, H. Fukuda, H. Wada, T. Iwaeda, T. Watanabe, High-performance liquid chromatographic determination of plasma and brain histamine without previous purification of biological samples: cation-exchange chromatography coupled with post-column derivatization fluorometry, J. Chromatogr. B 344 (1985) 115-123.

[93] O. Wahl, U. Holzgrabe, Amino acid analysis for pharmacopoeial purposes, Talanta 154 (2016) 150-163.

[94] S. Furota, N.O. Ogawa, Y. Takano, T. Yoshimura, N. Ohkouchi, Quantitative analysis of underivatized amino acids in the sub-to several-nanomolar range by ion-pair HPLC using a corona-charged aerosol detector (HPLC–CAD), J. Chromatogr. B 1095 (2018) 191-197.

[95] X. Qiu, L. Zuo, S. Sun, X. Zhao, S. Xu, Z. Zhu, T. Zhao, Z. Sun, J. Yao, G. Shan, Impurity profiling of Compound Amino Acid Injection (6AA) using ion-pair high performance liquid chromatography coupled with corona-charged aerosol detection and high resolution mass spectrometry, J. Pharm. Biomed. Anal. (2021) 114099.

[96] A. Joseph, A. Rustum, Development and validation of a RP-HPLC method for the determination of gentamicin sulfate and its related substances in a pharmaceutical cream using a short pentafluorophenyl column and a charged aerosol detector, J. Pharm. Biomed. Anal. 51(3) (2010) 521-531.

[97] U. Holzgrabe, C.-J. Nap, N. Kunz, S. Almeling, Identification and control of impurities in streptomycin sulfate by high-performance liquid chromatography coupled with mass detection and corona charged-aerosol detection, J. Pharm. Biomed. Anal. 56(2) (2011) 271-279.

[98] O. Wahl, U. Holzgrabe, Impurity profiling of carbocisteine by HPLC-CAD, qNMR and UV/vis spectroscopy, J. Pharm. Biomed. Anal. 95 (2014) 1-10.

[99] S. Chin, X.X. Lin, B. Santarra, J.A. Gruenhagen, P. Yehl, T. Chen, Multiplexed small molecule impurity monitoring in antibody-based therapeutics by mixed-mode chromatography paired with charged aerosol detection, J. Pharm. Biomed. Anal. 197 (2021) 113952.

[100] A. Socia, J.P. Foley, Direct determination of amino acids by hydrophilic interaction liquid chromatography with charged aerosol detection, J. Chromatogr. A 1446 (2016) 41-49.

[101] S. Schiesel, M. Lämmerhofer, W. Lindner, Comprehensive impurity profiling of nutritional infusion solutions by multidimensional off-line reversed-phase liquid chromatography× hydrophilic interaction chromatography–ion trap mass-spectrometry and charged aerosol detection with universal calibration, J. Chromatogr. A 1259 (2012) 100-110.

[102] S. Jia, J.H. Park, J. Lee, S.W. Kwon, Comparison of two aerosol-based detectors for the analysis of gabapentin in pharmaceutical formulations by hydrophilic interaction chromatography, Talanta 85(5) (2011) 2301-2306.

[103] T. Cecchi, Ion pairing chromatography, Crit. Rev. Anal. Chem. 38(3) (2008) 161-213.

[104] T. Cecchi, Theoretical models of ion pair chromatography: a close up of recent literature production, J. Liq. Chromatogr. Relat. Technol. 38(3) (2015) 404-414.

[105] K. Petritis, P. Chaimbault, C. Elfakir, M. Dreux, Ion-pair reversed-phase liquid chromatography for determination of polar underivatized amino acids using perfluorinated carboxylic acids as ion pairing agent, J. Chromatogr. A 833(2) (1999) 147-155.

[106] S. Lamotte, S. Kromidas, F. Steiner, Comparison and selection of modern HPLC columns, The HPLC Expert: Possibilities and Limitations of Modern High Performance Liquid Chromatography (2016).

[107] C.R. Powley, S.W. George, T.W. Ryan, R.C. Buck, Matrix effect-free analytical methods for determination of perfluorinated carboxylic acids in environmental matrixes, Anal. Chem. 77(19) (2005) 6353-6358.

[108] T. Buhrke, A. Kibellus, A. Lampen, In vitro toxicological characterization of perfluorinated carboxylic acids with different carbon chain lengths, Toxicol. Lett. 218(2) (2013) 97-104.

[109] C.R. Mitchell, Y. Bao, N.J. Benz, S. Zhang, Comparison of the sensitivity of evaporative universal detectors and LC/MS in the HILIC and the reversed-phase HPLC modes, J. Chromatogr. B 877(32) (2009) 4133-4139.

[110] Y. Cong, Y.-B. Zhou, J. Chen, Y.-M. Zeng, J.-H. Wang, Alkaloid profiling of crude and processed Veratrum nigrum L. through simultaneous determination of ten steroidal alkaloids by HPLC–ELSD, J. Pharm. Biomed. Anal. 48(3) (2008) 573-578.

[111] L. Imbert, R. Ramos, D. Libong, S. Abreu, P. Loiseau, P. Chaminade, Identification of phospholipid species affected by miltefosine action in Leishmania donovani cultures using LC-ELSD, LC-ESI/MS, and multivariate data analysis, Anal. Bioanal. Chem. 402(3) (2012) 1169-1182.

[112] Y. Yang, X. Geng, Mixed-mode chromatography and its applications to biopolymers, J. Chromatogr. A 1218(49) (2011) 8813-8825.

[113] L. Zhang, Q. Dai, X. Qiao, C. Yu, X. Qin, H. Yan, Mixed-mode chromatographic stationary phases: recent advancements and its applications for high-performance liquid chromatography, TrAC 82 (2016) 143-163.

[114] K. Zhang, X. Liu, Mixed-mode chromatography in pharmaceutical and biopharmaceutical applications, J. Pharm. Biomed. Anal. 128 (2016) 73-88.

[115] R. Nogueira, M. Lämmerhofer, W. Lindner, Alternative high-performance liquid chromatographic peptide separation and purification concept using a new mixed-mode reversed-phase/weak anion-exchange type stationary phase, J. Chromatogr. A 1089(1-2) (2005) 158-169.

[116] N.H. Davies, M.R. Euerby, D.V. McCalley, A study of retention and overloading of basic compounds with mixed-mode reversed-phase/cation-exchange columns in high performance liquid chromatography, J. Chromatogr. A 1138(1-2) (2007) 65-72.

[117] K. Zhang, L. Dai, N.P. Chetwyn, Simultaneous determination of positive and negative pharmaceutical counterions using mixed-mode chromatography coupled with charged aerosol detector, J. Chromatogr. A 1217(37) (2010) 5776-5784.

[118] B. Buszewski, S. Noga, Hydrophilic interaction liquid chromatography (HILIC)—a powerful separation technique, Anal. Bioanal. Chem. 402(1) (2012) 231-247.

[119] P. Hemström, K. Irgum, Hydrophilic interaction chromatography, J. Sep. Sci. 29(12) (2006) 1784-1821.

[120] B. Dejaegher, D. Mangelings, Y. Vander Heyden, Method development for HILIC assays, J. Sep. Sci. 31(9) (2008) 1438-1448.

[121] M. Taraji, P.R. Haddad, R.I. Amos, M. Talebi, R. Szucs, J.W. Dolan, C.A. Pohl, Chemometric-assisted method development in hydrophilic interaction liquid chromatography: a review, Anal. Chim. Acta 1000 (2018) 20-40.

[122] B. Dejaegher, Y. Vander Heyden, HILIC methods in pharmaceutical analysis, J. Sep. Sci. 33(6-7) (2010) 698-715.

[123] N. Gray, J. Heaton, A. Musenga, D.A. Cowan, R.S. Plumb, N.W. Smith, Comparison of reversed-phase and hydrophilic interaction liquid chromatography for the quantification of ephedrines using medium-resolution accurate mass spectrometry, J. Chromatogr. A 1289 (2013) 37-46.

[124] T. Teutenberg, J. Tuerk, M. Holzhauser, T. Kiffmeyer, Evaluation of column bleed by using an ultraviolet and a charged aerosol detector coupled to a high-temperature liquid chromatographic system, J. Chromatogr. A 1119(1-2) (2006) 197-201.

[125] Z. Huang, M. Richards, Y. Zha, R. Francis, R. Lozano, J. Ruan, Determination of inorganic pharmaceutical counterions using hydrophilic interaction chromatography coupled with a Corona® CAD detector, J. Pharm. Biomed. Anal. 50(5) (2009) 809-814.

[126] G. Kiełbowicz, P. Micek, C. Wawrzeńczyk, A new liquid chromatography method with charge aerosol detector (CAD) for the determination of phospholipid classes. Application to milk phospholipids, Talanta 105 (2013) 28-33.

[127] S. Li, Z. Li, F. Zhang, H. Geng, B. Yang, A polymer-based zwitterionic stationary phase for hydrophilic interaction chromatography, Talanta 216 (2020) 120927.

[128] K. Qian, Z. Yang, F. Zhang, B. Yang, P.K. Dasgupta, Low-bleed silica-based stationary phase for hydrophilic interaction liquid chromatography, Anal. Chem. 90(15) (2018) 8750-8755.

[129] M.G. Hvizd, B. Bailey, C. Crafts, M. Plante, I. Acworth, Simple separation and detection techniques for the analysis of carbohydrates, Thermo Scientific (2011). https://assets.thermofisher.com/TFS-Assets/CMD/posters/110521-PO-IC-Carbohydrates-21Nov2011-LPN2954-01.pdf. (Accessed 07.06.2021).

[130] K. Scholz, M. Seyfried, O. Brumhard, L.M. Blank, T. Tiso, H. Hayen, Comprehensive liamocin biosurfactants analysis by reversed phase liquid chromatography coupled to mass spectrometric and charged-aerosol detection, J. Chromatogr. A 1627 (2020) 461404.

[131] K. Zhang, Y. Li, M. Tsang, N.P. Chetwyn, Analysis of pharmaceutical impurities using multi-heartcutting 2D LC coupled with UV-charged aerosol MS detection, J. Sep. Sci. 36(18) (2013) 2986-2992.

[132] K. Stypulkowska, A. Blazewicz, Z. Fijalek, M. Warowna-Grzeskiewicz, K. Srebrzynska, Determination of neomycin and related substances in pharmaceutical preparations by reversed-phase high performance liquid chromatography with mass spectrometry and charged aerosol detection, J. Pharm. Biomed. Anal. 76 (2013) 207-214.

[133] A.G. Pereira, F.B. D'Avila, P.C.L. Ferreira, M.G. Holler, R.P. Limberguer, P.E. Froehlich, Method Development and Validation for Determination of Cocaine, its Main Metabolites and Pyrolytic Products by HPLC–UV–CAD, Chromatographia 79(3-4) (2016) 179-187.

[134] C.-E. Zhang, L.-J. Liang, X.-H. Yu, H. Wu, P.-f. Tu, Z.-J. Ma, K.-J. Zhao, Quality assessment of Astragali Radix from different production areas by simultaneous determination of thirteen major compounds using tandem UV/charged aerosol detector, J. Pharm. Biomed. Anal. 165 (2019) 233-241.

[135] O. Wahl, J. Cleynhens, A.M. Verbruggen, U. Holzgrabe, Impurity profiling of N, N′-ethylenebis-l-cysteine diethyl ester (Bicisate), J. Pharm. Biomed. Anal. 150 (2018) 132-136.

[136] A. Socia, Y. Liu, Y. Zhao, A. Abend, W.P. Wuelfing, Development of an ultra-high-performance liquid chromatography-charged aerosol detection/UV method for the quantitation of linear polyethylenimines in oligonucleotide polyplexes, J. Sep. Sci. 43(20) (2020) 3876-3884.

[137] M. Eckardt, M. Kubicova, D. Tong, T.J. Simat, Determination of color developers replacing bisphenol A in thermal paper receipts using diode array and Corona charged aerosol detection—A German market analysis 2018/2019, J. Chromatogr. A 1609 (2020) 460437.

[138] Council of Europe, European Pharmacopeia Online 10.5, EDQM, Strasbourg, France, 2021, Monograph no. 2305. https://pheur.edqm.eu/app/10-5/content/10-5/2305E.htm. (Accessed 14.01.2021).

2. Aim of the thesis

As a relatively new detection technique in liquid chromatography, charged aerosol detection is still evolving, which is reflected by the implementation of additional instrumental settings and the increasing use of CAD in hyphenated detection setups. Independently, novel chromatographic techniques for the separation of small polar molecules such as MMC and HILIC have been established over the last decade. The present doctoral thesis aimed at combining both developments for an optimized analysis of the challenging amino acids and their derivatives. It can be divided into two main objectives, which are of fundamental and applied nature, respectively, and build on one another.

The first main objective aimed at exploring the basic detector capabilities and their potential optimization. As fundamental aspects of the CAD technique, the performance characteristics uniformity, sensitivity, and linearity were evaluated and optimized considering the influence of the recently introduced CAD settings evaporation temperature and power function value (PFV). Another essential research topic was the systematic comparison of the impact of diverse chromatographic separation techniques accompanied by their individual mobile phase compositions on the CAD performance. Additionally, the applicability of hyphenated UV-CAD was investigated.

The second main objective was the development of CAD methods for the impurity profiling of amino acids and amino acid-like APIs suited for a compendial application. Optimization procedures derived from the previously conducted performance evaluation served as basis for the method development to achieve the required sensitivity and linearity. The methods should represent more selective and straightforward alternatives to the derivatization and multi-method approaches of the Ph. Eur. Each method was validated with respect to ICH guideline Q2(R1) to meet the compendial requirements.

The main objectives can be subdivided into the following projects:

- Uniformity: Investigation of significant chromatographic and molecular features towards the observed nonuniform CAD response for fatty acids ranging from C12 to C18 and accurate prediction of the CAD response by a machine learning approach; Evaluation of the influence of the CAD's evaporation temperature setting on the response uniformity for fatty acids (C12 to C18) representing semivolatile and nonvolatile compounds.
- Sensitivity: Performance evaluation of IPC and HILIC coupled to the CAD by a response surface methodology approach and comparison of the sensitivity of IPC and HILIC methods for the impurity profiling of branched-chain amino acids; Studies on the

influence of the evaporation temperature setting and the filter constant setting on the response and limits of quantitation of semivolatile fatty acids.

- Linearity: Comparison of double logarithmic transformation and experimental power function optimization as linearization procedures for the CAD response of fatty acids; Comparison of empirical and mathematical power function optimization strategies for the linearization of the CAD response for gabapentin and its impurities.
- Hyphenation of UV-CAD: Studies on the influence of the mobile phase composition on the hyphenated detection for the impurity analysis of vigabatrin.
- Development and validation of a method for the impurity analysis of gabapentin by RPC-UV-CAD.
- Development of a generic method for the impurity analysis of branched-chain amino acids by IPC-CAD and HILIC-CAD, respectively, and validation of the HILIC method for L-valine.
- Development and validation of a method for the impurity analysis of vigabatrin by MMC-UV-CAD.
- Development and validation of methods for the impurity analysis of L-aspartic acid and glycine by IPC-UV-CAD, respectively.

3. Results

3.1. Influence of Charged Aerosol Detector instrument settings on the ultra-high-performance liquid chromatography analysis of fatty acids in polysorbate 80

Klaus Schilling[1], Ruben Pawellek[1], Katherine Lovejoy, Tibor Muellner, Ulrike Holzgrabe

[1]These authors contributed equally to this work.

Reprinted with permission from J. Chromatogr. A 2018, 1576, 58-66.

Abstract

The analysis of polysorbate 80 is a challenge because all components lack a chromophore. Here, an ultra-high-performance liquid chromatography system equipped with a charged aerosol detector (UHPLC-CAD) was used to study the effect of systematic variation of the CAD settings, namely evaporation temperature, filter constant and power function value (PFV), on the detector response of fatty acid standards and manufacturing batches of polysorbate. Evaporation temperature and filter constant strongly affect the detection limits described by signal-to-noise (S/N) ratios. Although evaporation temperature can be increased to improve signal to noise ratios, analyte volatility at higher temperatures is an important limiting factor. The PFV was found to be a strong tool for optimizing response linearity, but the optimal PFV differed depending on analyte volatility. Because PFV optimization required some additional measurement time and because double-logarithmic transformation at the default PFV of 1.0 yielded satisfying universal results with less measurement time over a range of two orders of magnitude for every homologue fatty acid from C14 to C18, use of the log-log transformation is the favored linearization strategy. Possible optimization procedures for semi volatile substances are presented. Overall, this new UHPLC method offers improved detection limits, as well as time savings of over 75% and eluent savings of more than 40% compared to the previously published HPLC-CAD method for polysorbate analysis.

1. Introduction

Fatty acids play an important role in the pharmaceutical and cosmetic field as excipients [1]. They are present in various diverse substance classes as emulsifiers [2]. Polysorbates are esterified with a sorbitan backbone together with polyethylene glycols (PEGs) [3]. Furthermore, esters of fatty acids with fatty alcohols yield waxes and esters of fatty acids with glycerin form triglycerides which, as well as the free fatty acids themselves, are commonly used in dermatological formulations [4].

An in-depth comparison of currently applied methods for the analysis of fatty acids was given by Wu et al. [5], elaborating on advantages and disadvantages of the respective methods. Due to their physicochemical properties, fatty acids are mainly assessed by means of gas chromatography (GC) after derivatization with methanol to fatty acid methyl esters (FAMEs) [6, 7] as also described in the Ph. Eur. [8]. The most common approach involves a flame ionization detector (FID), whereas GC-mass-spectrometry (MS) can be used for more selective and sensitive analysis [9]. Analytical methods such as capillary electrophoresis (CE) with indirect UV detection [10] or tedious pre-column derivatization with e.g. naphthoyl chloride and coupling to HPLC [11] have been described but rarely used. More recently, near-infrared spectroscopy [12] and NMR [13-15] as non-destructive methods of analysis have been reported; however, model establishment for NIR is tedious and both methods lack sensitivity [5]. HPLC-MS methods are accessible without derivatization procedures [16], yet are very costly [5].

Furthermore, aerosol-based detection methods utilizing either evaporative light scattering detection (ELSD) or charged aerosol detection (CAD) combined with HPLC have been reported [5, 17-20]. They are rather easy-to-use, cheap in comparison to MS analytics and not dependent on chromophores. The aerosol based detection of CAD and ELSD relies on nebulization of the effluent which, by evaporation of the solvent, forms particles [21]. These particles are then detected by measuring electrical charge that was transferred to the particles by a nitrogen stream passing a corona needle in case of the CAD. Alternatively, in case of the ELSD, the particles pass a light beam and the combined angular light-scattering in the detection flow path is analyzed. Thus, analytes do not need to possess a chromophore – as it is the case for fatty acids – but only need to be sufficiently non-volatile in order to ensure acceptable signals [21]. The ELSD is known to be inferior when it comes to dynamic range, sensitivity and signal irregularities when highly concentrated samples have to be used [22] as is the case for impurity profiling. This leaves the CAD as the more reliable and more suitable of the two quasi-universal aerosol detectors because it possesses a greater linear and dynamic range [23, 24]. Ilko et al. [25] presented a HPLC-CAD method for the analysis of free fatty acids

in polysorbate 80 batches after liquid-liquid extraction and for the fatty acid composition after hydrolysis and liquid-liquid extraction.

To the best of our knowledge, no UHPLC-CAD method benefiting from the time and eluent saving and the capabilities of modern CAD detection for fatty acids has been established. Interestingly, although the semi-volatile character of the fatty acids significantly affects the detector signal, no systematic study of the settings of CAD parameters and their impact on the signal intensity of these homologues has been undertaken. The UHPLC method development is described shortly and a focus on the systematic evaluation of CAD settings is presented in this article.

2. Experimental

2.1. Chemicals and reagents

Octanoic acid, decanoic acid, lauric acid, myristic acid, palmitic acid, petroselinic acid, oleic acid, linoleic acid, alpha-linolenic acid, stearic acid, HPLC grade acetonitrile, potassium hydroxide, *tert*.-butyl methyl ether (MTBE), HPLC grade methanol, HPLC grade 50% formic acid and 100% formic acid were purchased from Sigma-Aldrich Chemie GmbH (Steinheim, Germany). Margaric acid was purchased from VWR international (Darmstadt, Germany). All chemicals used were of analytical grade unless otherwise stated. Ultrapure water was produced by a water purification system from Merck Millipore (Schwalbach, Germany) specified at a resistivity of 18.2 MΩ-cm. The polysorbate batches were from NOF (Tokyo, Japan), Kolb (Hedingen, Switzerland), Merck (Darmstadt, Germany) and Croda (East Yorkshire, UK). The batch coding does not necessarily match with the presented manufacturer order.

2.2. Apparatus

The UHPLC-CAD experiments were performed on a Thermo Scientific™ Vanquish™ Flex modular chromatographic system consisting of a binary flex pump with online degasser, a thermostatted split sampler, a thermostatted column compartment with integrated pre-heater, a variable wavelength detector and a Vanquish Horizon charged aerosol detector (Thermo Fisher Scientific, Germering, Germany). The charged aerosol detector was supplied with nitrogen gas from an ESA nitrogen generator (Thermo Fisher Scientific, Germering, Germany) connected to the in-house compressed air system. The instrument was controlled and runs were processed using the Chromeleon® Data System Version 7.2.6 software program (Thermo Fisher Scientific).

2.3. Chromatographic procedure

A core-shell octadecylsilyl (C18) Kinetex column (100 x 2.1 mm i.d., with a particle size of 2.6 µm and pore size of 100 Å) (Phenomenex, Aschaffenburg, Germany) was used as stationary phase. The chromatographic system was operated using gradient elution at a column compartment temperature of 25 °C ran in still air mode. Mobile phase A consisted of an aqueous 0.05% (v/v) formic acid solution, whereas mobile phase B was acetonitrile with addition of 0.05% (v/v) formic acid.

The final gradient runs at a flow rate of 1.5 mL/min and utilizes 75% B from 0 to 0.8 min, linearly increases to 85% B within 1.7 min and holds at 85% B for 0.5 min, followed by a re-equilibration with a gradient to 75% B within 0.5 min and a 1 min hold, resulting in a total run time of 4.5 min. The injection volume was 10 µL.

Detection was performed by means of the Vanquish® CAD with the evaporation temperature set to 30 °C, a power function value of 1.0, a filter constant of 1 s, a data collection rate of 10 Hz and a gas inlet pressure of 56.4 psi unless specified otherwise.

2.4. Preparation of solutions

The stock solutions for the respective fatty acids were prepared by exactly weighing 10.0 mg of the fatty acid and dissolving in 10.0 mL of methanol. These stock solutions were stored in a freezer at -20 °C and diluted with a mixture of acetonitrile 75% and water 25% (v/v) to the appropriate concentration on a daily basis. The procedures for the preparation of the sample solutions were adopted from Ilko et al. [25] who modified a saponification process from Hu et al. [26] and a liquid-liquid extraction from Matyash et al. [27].

2.4.1. Preparation of the sample solutions for the determination of the fatty acid composition in batches of polysorbate 80

15.0 mg of the polysorbate was exactly weighed and dissolved in 1 M potassium hydroxide solution containing 10% (v/v) methanol and made up to 10.0 mL. Saponification was achieved after incubation at 40 °C for a minimum of 6 hours.

50 µL of 100% formic acid was added to 250 µL of the solution after saponification in a glass centrifuge tube (VWR International, Darmstadt, Germany). After addition of 500 µL of MTBE the mixture was vortexed and centrifuged at 2700 rpm (EBA 20 centrifuge, Hettich, Tuttlingen, Germany) for 5 min. The entire organic phase was collected in a vial, dried under a gentle nitrogen gas stream and the residue reconstituted in 1000 µL of a mixture of acetonitrile 75%/water 25% (v/v).

Quantitative analysis of the fatty acid composition was performed using external standards and double logarithmic calibration curves for each individual fatty acid.

2.4.2. Preparation of the sample and reference solutions for the determination of the free fatty acids in batches of polysorbate 80

100.0 mg of the polysorbate was exactly weighed in a 10.0 mL volumetric flask. After addition of 500 µL of the 1 mg/mL methanolic margaric acid stock solution as internal standard, the analyte was dissolved and made up to 10.0 mL with water. The internal standard is added in a concentration of about 0.5% (m/m). The exact concentration of the internal standard needs to be calculated referring to the sample weight.

100 µL of 100% formic acid was added to 1000 µL of the polysorbate and internal standard solution in a glass centrifuge tube. After addition of 1000 µL of MTBE the mixture was vortexed and centrifuged at 2700 rpm for 45 min. 500 µL of the organic phase was collected, dried under a gentle nitrogen gas stream and the residue reconstituted in 500 µL of a mixture of acetonitrile 75%/water 25% (v/v).

The reference solution consisted of margaric acid and oleic acid at a concentration of 50 µg/mL each. It was obtained by diluting the respective stock solutions with a mixture of acetonitrile 75%/water 25% (v/v). For the evaluation of the free fatty acids, the peak area ratio of this reference solution was determined and used in the batch analysis with the internal standard.

3. Results and discussion

3.1. UHPLC method optimization

The initial LC method employing a conventional HPLC instrument reported by Ilko et al. [25] used a core-shell octadecylsilyl (C18) Kinetex (Phenomenex, Aschaffenburg, Germany) column in the dimensions 100 x 3.0 mm with 2.6 µm particles. The mobile phase flow-rate was set at 0.6 mL/min and a gradient method with a run time of 15 min consisting of an initial hold at 75% B for 5 min and a linear 10 min gradient step to 85% B was applied. Mobile phase A was aqueous 0.05% (v/v) formic acid, while mobile phase B consisted of acetonitrile with addition of 0.05% (v/v) formic acid.

To keep the column’s selectivity and chemistry as close as possible to the original method, a Kinetex C18 column, was chosen for the method optimization to UHPLC as well. The standard Kinetex columns (i.d. 3.0 mm) are stable up to a backpressure of 600 bar, whereas the columns with an internal diameter of 2.1 mm are stable up to a backpressure of 1000 bar and thus suitable for UHPLC applications. Hence, a 100 x 2.1 mm column of the same chemistry and particle size was chosen.

Since the smaller diameter column and the UHPLC system are capable of withstanding higher backpressure, it was the ultimate goal to save time and eluent consumption after the optimization. Because all column parameters aside from the i.d. are the same for both columns,

their correlation in column volume can be narrowed down to the formula shown in equation 1 [8]:

$$Ratio_{V_c} = (\frac{ID_1}{ID_2})^2 \quad (1)$$

V_C : column volume; *ID* : internal diameter

Using the resulting factor of 2, the mobile phases and percentage gradient levels were initially used according to Ilko et al. [25] as mentioned at the beginning of this section. In order to evaluate which flow-rate would be the most appropriate, flow-rates between 0.6 and 1.5 mL/min were screened. A mixture of the main fatty acid, namely oleic acid, and the internal standard, namely margaric acid, was used. Additionally, a batch of polysorbate 80 was analyzed for its free fatty acids. The initial method screening was performed with the default CAD settings of 35 °C evaporation temperature, a power function value (PFV) of 1.0 and a filter constant of 1 s. Upon method development, variations in the gradient steps and levels were examined as well. Since a decrease of mobile phase B to 70% resulted in a slightly better separation but inferior signal intensities, increased analysis time and increased backpressure, a gradient of initial 75% of mobile phase B up to 85% was considered more appropriate.

Figure S1 illustrates the chromatograms of the reference solution containing 50 µg/mL of oleic acid (65-88% purity) and margaric acid in addition to the impurities of linoleic acid, palmitic acid, petroselinic acid and stearic acid at different flow rates. The injection volume was maintained to be 10 µL since no indicators of overloading of the column occurred.

The final optimized method utilized a flow-rate of 1.5 mL/min with an initial hold at 75% B for 0.8 min and a linear gradient to 85% B within 1.7 min. Resulting in a separation time lower than 3 minutes, with no backpressure problems. Reequilibration starting with 85% B for 0.5 min, back to 75% B in 0.5 min, followed by 1 min of 75% B was found to be sufficient, resulting in a total run time of 4.5 min compared to the 19 min of the HPLC method when reequilibration is also considered. The time reduction of over 75% and an eluent consumption reduction of more than 40% compared to the HPLC method of Ilko et al. [25] underlines the superiority of the UHPLC method.

The optimized CAD parameters used in batch analysis were: 30 °C evaporation temperature, a power function value of 1.0, a gas inlet pressure of 56.4 psi, a filter constant of 1 s and a data collection rate of 10 Hz. Double logarithmic transformation was applied to the calibration curves of the fatty acids. The optimization of the CAD instrument settings is presented in detail in section 3.2. Example chromatograms of a batch analysis with regard to its fatty acid composition and of injections near the LOQ are presented in Figure 1.

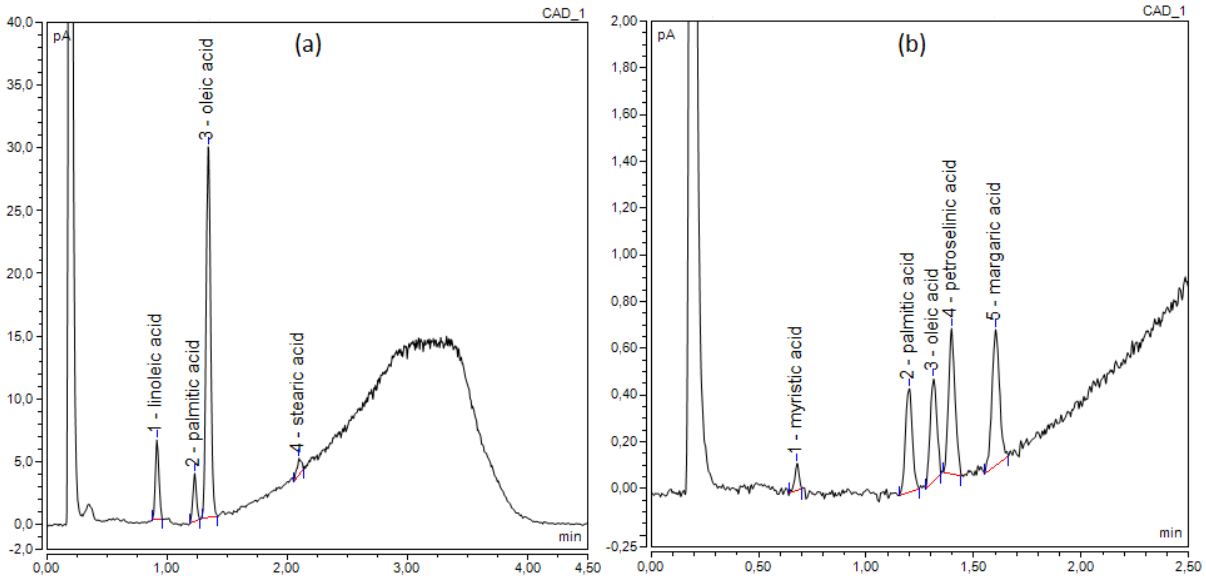

Fig. 1. (a) Chromatogram of the fatty acid composition of batch D1. Linoleic acid, palmitic and stearic acid are present besides the main component oleic acid. Percentage contents (% m/m) are listed in Table 3, for chromatographic conditions: see section 2.3.; (b) Chromatogram of 5 ng on column of myristic acid, palmitic acid, oleic acid, petroselinic acid and margaric acid for LOQ determination. Linoleic acid and stearic acid were injected separately (chromatograms not shown), for chromatographic conditions: see section 2.3.

3.2. Evaluation of CAD parameters for the detection of fatty acids

Since CAD detection is based on the formation of analyte particles, non-volatility is crucial for the response of a substance [29]. Fatty acids show different volatilities depending on the chain length. The main fatty acid present in polysorbate 80 is oleic acid ($C_{18:1}$) together with others ranging from C_{14} (myristic acid) to C_{18} (stearic acid). To include a broader range of fatty acids and to evaluate the CADs limits in this mobile phase composition, a selection of shorter chain length fatty acids was added. The fatty acids from C_8 to C_{18} were chosen in an initial screening at the default CAD settings of 35 °C evaporation temperature, a PFV of 1.0 and a filter constant of 1 s at a concentration of 50 µg/mL. No peaks due to caprylic acid and capric acid could be detected using these conditions. Only fatty acids of C_{12} or longer are sufficiently non-volatile to give a measurable detector response at lower concentration levels. Additionally, fatty acids shorter than C_{12} are not well retained. Because of these two factors, this method is most applicable for analysis of C_{12} (lauric acid) and longer fatty acids.

3.2.1. Evaluation of evaporation temperature based on sensitivity

The evaporation temperature setting controls the temperature of the thermostatted evaporation tube in which, ideally, the mobile phase is quickly and completely evaporated. After eluent evaporation, the condensed phase analyte particles that remain undergo unipolar diffusion charging and produce a signal in the form of a current. The evaporation temperature setting

controls the relative solute partitioning between gas and condensed phases and is therefore of utmost importance for detection selectivity [30]. Whereas the evaporation tube temperature of the 2005 ESA Corona CAD cannot vary from ambient temperature, the evaporation tube temperature of the CAD used here can set anywhere between ambient temperature and 100 °C. Since particle formation is based on the volatility, a higher temperature generally leads to a decrease of the signal intensity for semivolatile substances [31]. Figure 2 shows the correlation of peak height and the variation of evaporation temperature settings exemplarily for the series of saturated fatty acids and for the non-saturated $C_{18:1}$ oleic acid for evaporation temperature settings between 25 °C and 50 °C. As expected, the signals decrease substantially upon raising the evaporation temperature. Temperatures higher than 50 °C do not give analyzable results, especially for the more volatile shorter chain length fatty acids.

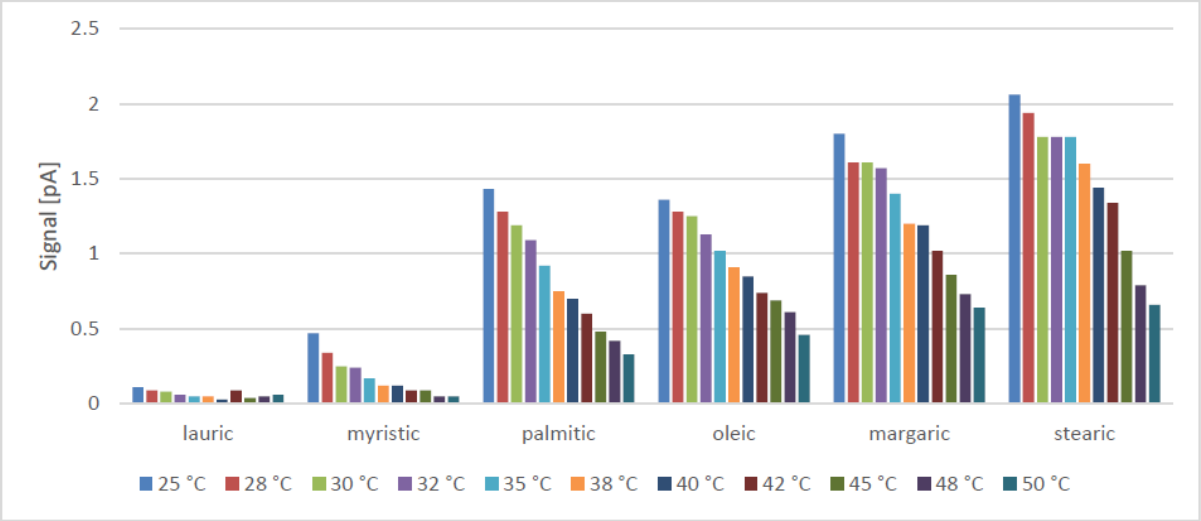

Fig. 2. Peak height at different evaporation temperatures of injections of 10 ng on column of the respective fatty acid; for chromatographic parameters see section 2.3.

For non-volatile analytes, the signal is depending on the size distribution of the dried aerosols. While this size distribution does vary with the cube root of the particle density, this effect is only minor in nature. In conjunction with the unipolar charging process which is virtually independent from the analytes` physicochemical properties the charged aerosol detector shows a highly similar response for all analytes. This behavior is often referred to as uniformity of response [29]. This is in contrast to ELSD, where a significant influence on the materials' properties, like density, refractive index, absorption and fluorescence have been suggested and verified by experiments [32]. The mobile phase composition on the other hand has been found to have a severe impact on the generated aerosol, thus the uniformity of response can only be observed when the mobile phase composition entering the detector is constant, i.e. during isocratic elution or by utilizing an inverse gradient setup. With the non-compensated gradient elution described here, we expect an increased signal for later eluting peaks, as the signal intensity increases with higher acetonitrile content in acetonitrile-water mixtures. Even

with this consideration, the significantly reduced signal intensity for the shorter chain length lauric and myristic acid is more than would be expected due to the varying acetonitrile content and confirms that they possess a significantly higher volatility than the longer fatty acids.

One may suggest that increasing the evaporation temperature does not bring any positive effects, but the opposite is the case. Sensitivity can be improved drastically by optimization. Detection limits as per definition of the ICH guidelines [28] are usually assessed through the S/N approach. The baseline noise mainly depends on the mass concentration of nonvolatile and semivolatile impurities in the effluent, which can be minimized by using ultra-pure solvents and additives but cannot be completely eliminated. If the impurities have a higher volatility than the analytes of interest, a modest increase in temperature can shift the ratio of analyte amount vs. impurities in the condensed phase and thus improve the observed S/N ratios. Lowest detection limits are therefore obtained at the best compromise between decreasing baseline noise and maintaining sufficient analyte signal.

Figure 3 shows the correlation of the S/N-ratios for the same data shown in Figure 2 representatively for myristic acid as a saturated short fatty acid (C_{14}), margaric acid as a saturated long fatty acid (C_{17}) and oleic acid as an unsaturated long fatty acid ($C_{18:1}$). A maximum of S/N ratio could be identified at 30 °C for most of the analytes when injected at low level concentrations that are slightly above the LOQs of the original method.

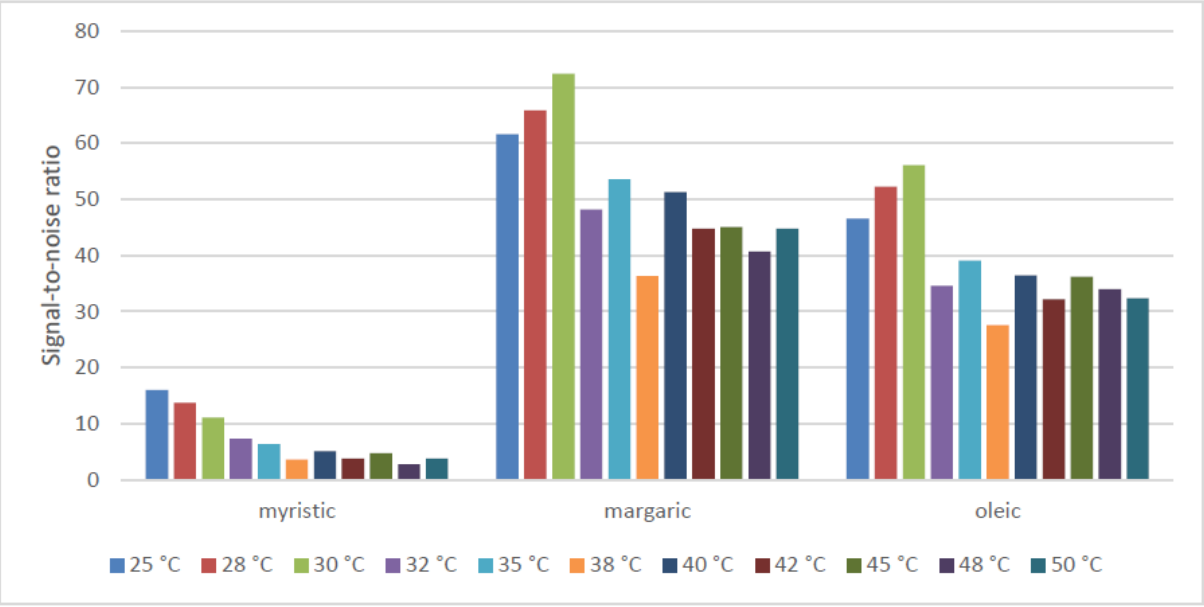

Fig. 3. S/N ratios at different evaporation temperatures of injections of 10 ng on column of the respective fatty acid; for chromatographic parameters see section 2.3.

The experimental LOQs were determined using the S/N approach according to the ICH guideline [28] and injecting 1 ng, 5 ng and 10 ng on column. Table 1 displays the comparison of the LOQs obtained with the original HPLC method coupled to the “older” CAD [25] with the

UHPLC method. The superiority of detection for every analyte with the exception of the most volatile, myristic acid, using the CAD parameter optimized UHPLC-method can be clearly seen. RSD values calculated for 5 ng on column injections (n = 4) ranged from 0.84 to 1.82 %, except for myristic acid (9.17 %) where 5 ng on column is below its LOQ. The superiority of the LOQ for myristic acid in the previous method can be traced down to the ambient evaporation temperature of the older CAD used. Myristic acid showed improved S/N-ratios at lower temperatures in our measurements as well (see Figure 3).

Table 1. LOQs of the transferred UHPLC-CAD method with optimized evaporation temperature at 30 °C compared to the HPLC method with the old CAD of Ilko et al. [25].

Analyte	LOQ [ng on column] of [25] using HPLC-CAD	LOQ [ng on column] of optimized UHPLC-CAD
Myristic acid ($C_{14}H_{28}O_2$)	6.1	8.1
Palmitic acid ($C_{16}H_{32}O_2$)	4.0	2.2
Stearic acid ($C_{18}H_{36}O_2$)	3.4	1.3
Linoleic acid ($C_{18}H_{32}O_2$)	3.0	1.8
Oleic acid ($C_{18}H_{34}O_2$)	3.9	2.1
Petroselinic acid ($C_{18}H_{34}O_2$)	3.2	1.4

3.2.2. Evaluation of sensitivity in dependence on filter constant setting

The filter constant has significant impact on the baseline noise and thus on the detection limits of a method. It is applied to the output current of the detector and affects the collection of the raw data and the data collection rate. Generally, a higher filter constant results in smoothed baseline, whereas a lower filter constant does not remove a lot or any baseline noise at all [33].

This was confirmed by examining injections of 10 ng on column of a mixture of myristic acid, palmitic acid, oleic acid, petroselinic acid and margaric acid at different filter constant settings of 0.1 seconds (s), 1 s, 3.6 s, 5 s and 10 s with an evaporation temperature of 30, 35 and 40 °C. An evaluation of the S/N-ratios for an evaporation temperature of 30 °C is shown in Figure 4. The trend was also analogous for the other evaporation temperatures (data not shown).

Although these plain data show a significant baseline smoothing resulting from an increased filter constant and a tremendous gain in S/N-ratio obtained, it was no option to choose this filter setting from chromatographic point of view due to the loss of resolution by peak broadening effects. This makes the enormous S/N-ratio obtained with the higher filter constants less appealing when the separation efficiency is taken into consideration. Thus, a filter constant of 1 s was chosen because best resolution was achieved.

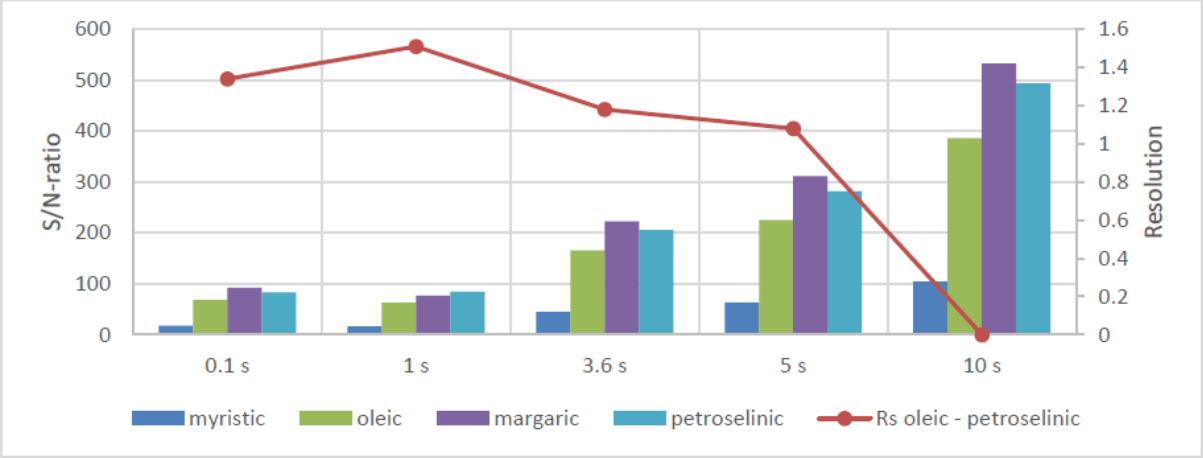

Fig. 4. S/N ratios and resolution of the critical peak pair oleic acid - petroselinic acid, 10 ng on column of the mixture of the fatty acids at varied filter settings; for chromatographic parameters see section 2.3.

3.2.3. Evaluation of power function value

Similar to all aerosol-based detectors, the CAD is a non-linear detector and response can be described by a power law function equation [34] as shown in equation 2:

$$A = a(m_{inj})^b \quad (2)$$

A linear response can be observed when b equals 1.0 and the sensitivity coefficient *a* then is the slope of the ratio of peak area/mass injected. With b > 1, the shape of the response curve is supralinear. Sublinear response is indicated by b < 1. Although CAD response is typically quasi-linear over about two orders of magnitude [34], it is advisable to have a closer look at the curve fit, especially for the lower calibration levels. By itself, a coefficient of determination close to 1 does not necessarily indicate good linearity over the whole range investigated [35]. In order to extend the quasi-linear dynamic range of the detector, newer CAD instruments allow for an alteration of the power function value in the range of 0.7-2.0, which affects signal output.

To evaluate the optimal power function value for each analyte, calibration curves were established covering concentration levels of 1 µg/mL, 25 µg/mL, 50 µg/mL, 75 µg/mL and 100 µg/mL at power function values ranging from 0.8 to 1.6. All measurements were performed at 30 °C, 35 °C and 40 °C evaporation temperature. The R^2-values were established by means of linear regression (Table 2, values for evaporation temperature of 30 °C). Double logarithmic transformation was performed at the default PFV of 1.0. For a better estimation of linearity, the response factor (peak area/mass injected) was plotted against the respective concentration level (Fig. 5, shown for the example of palmitic acid). Response linearity is represented by the slope of the resulting regression line. The optimal power function value would then have a slope of zero [36]. The obtained regression lines either show a negative slope indicating

sublinear response, or a positive slope indicating supralinear response. The optimal power function value of the examined levels was determined by comparing the relative standard deviation of the response factors of each analyte for every power function as shown in Figure 6. The lowest RSD indicates the best linearity of response [36].

Table 2. Coefficients of determination obtained at 30 °C evaporation temperature; PFV 1.0 with lg-lg transformation was used for batch testing.

Analyte/ PFV	myristic acid	palmitic acid	margaric acid	stearic acid	oleic acid	petrosel-inic acid	linoleic acid	alpha-linolenic acid
0.8	0.9999	0.9909	0.9891	0.9994	0.9876	0.9836	0.9994	0.9994
0.9	0.9605	0.9935	0.9897	0.9883	0.9891	0.9861	0.9873	0.9955
1.0	0.9981	0.9972	0.9947	0.9914	0.9937	0.9922	0.9929	0.9988
1.1	0.997	0.999	0.9977	0.9979	0.9996	0.9973	0.9978	0.9975
1.2	0.9938	0.9983	0.9994	0.9993	0.9993	0.9991	0.9994	0.9985
1.3	0.9902	0.9983	0.9994	0.9996	0.9992	0.9999	0.9997	0.9942
1.4	0.9804	0.995	0.9976	0.9979	0.9981	0.9994	0.9985	0.9936
1.5	0.9782	0.9928	0.9947	0.9921	0.9953	0.9976	0.9949	0.9876
1.6	0.9664	0.9878	0.9921	0.9906	0.9914	0.9949	0.9919	0.9843
1.0 lg-lg	0.9998	0.9998	0.9995	0.9993	0.9994	0.9993	0.9995	0.9995

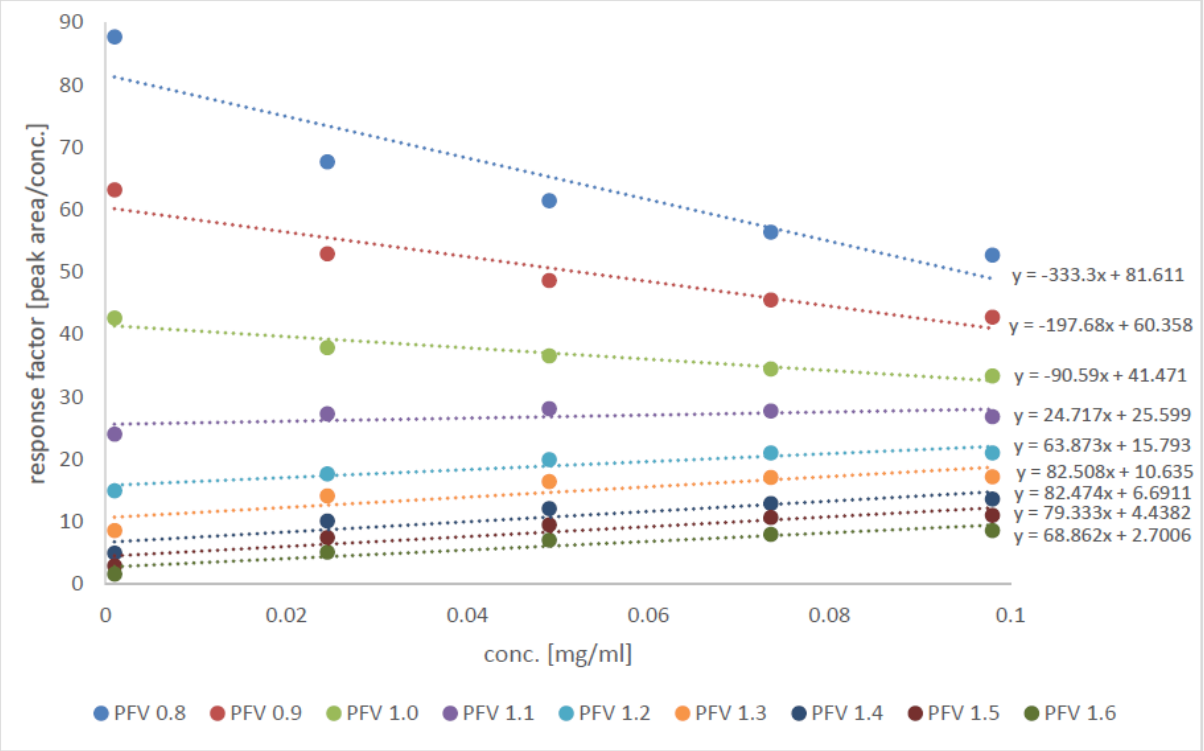

Fig. 5. Response factor versus analyte concentration plot for palmitic acid exemplarily at 30 °C evaporation temperature for power function values 0.8-1.6.

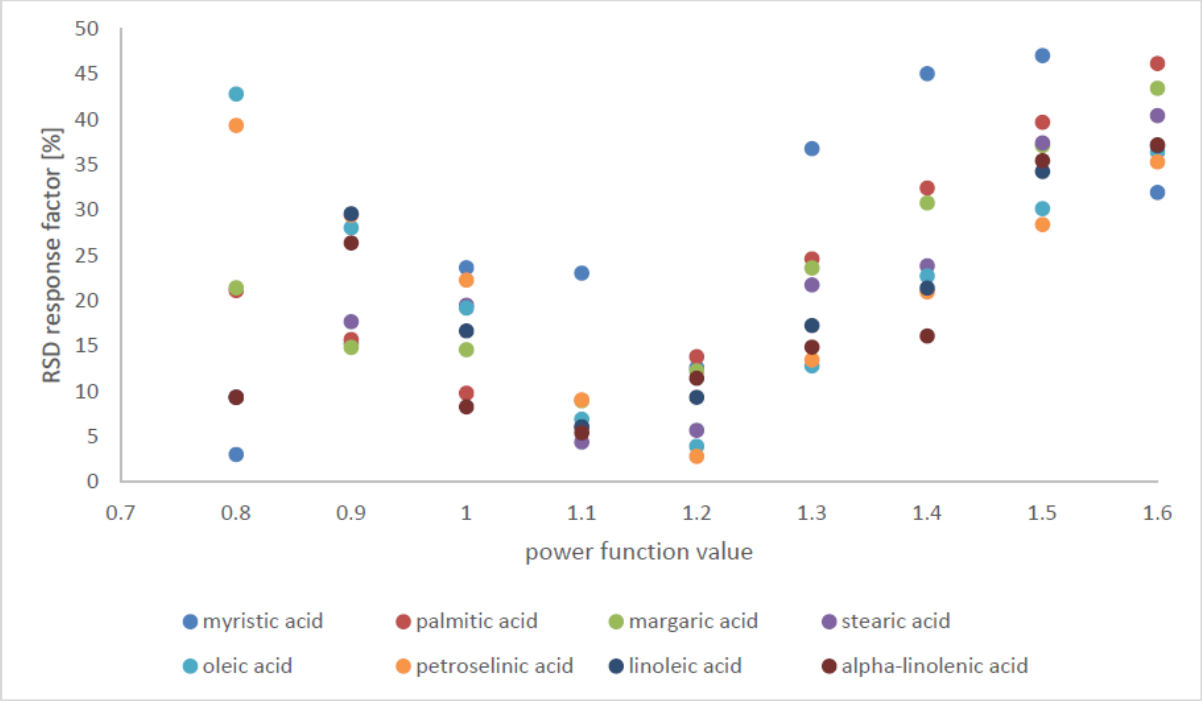

Fig. 6. RSD of the response factors [%] at evaporation temperature 30 °C (n=5).

The same experiments were performed at evaporation temperatures of 35 and 40 °C and used to assess power function values ranging from 0.8 to 1.6 in steps of 0.1 units (Supplementary material: Fig S2). The optimal power function value was then determined for each analyte as described above.

After identifying a suitable power function value, different evaporation temperatures were evaluated. The evaluation was equivalent to the determination of the optimal power function value. Response factor versus concentration plots were obtained for evaporation temperatures of 30 °C, 35 °C and 40 °C at the same PFV. The optimal evaporation temperature for a given PFV was determined by comparison of the slopes of the regression lines as well as of the relative standard deviations of the corresponding response factors (Figure 7, restricted to five analytes for better readability). With exception of myristic acid, all fatty acids followed the same trend. Although the optimal power function value slightly differed for each analyte, a PFV of 1.1 turned out to be beneficial in terms of linearity of response and coefficient of determination compared to the standard value of 1.0 (see Fig. 6).

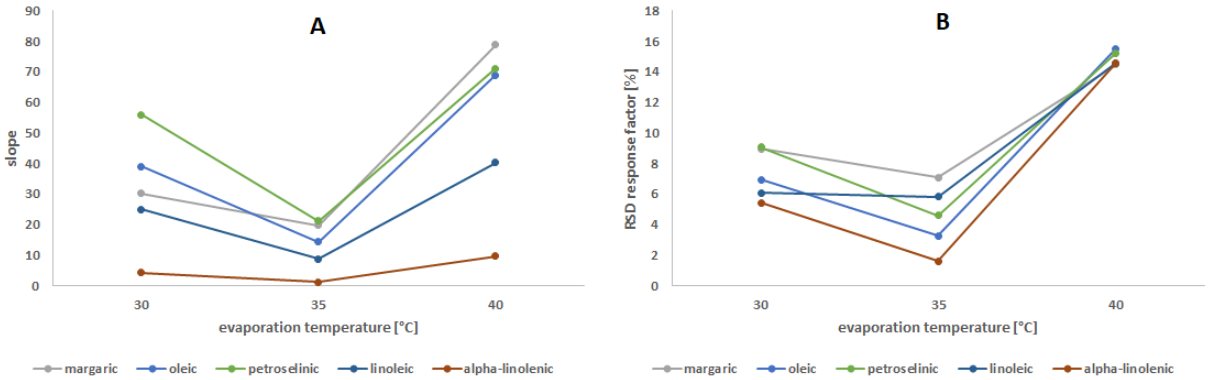

Fig. 7. A: Slope of the response factors versus evaporation temperature plot for PFV 1.1; B: RSD of the response factors versus evaporation temperature plot for PFV 1.1 (n = 5).

Of note, myristic acid, the most volatile fatty acid, did not follow that trend. Being a rather volatile compound, the best results are expected at a PFV <1.0 [37]. In accordance with this, optimal results for this analyte were found at a PFV of 0.8. For all fatty acids, response linearity at 30 °C and 35 °C was similar when maintaining a PFV of 1.1 (median RSD 5.21 % to 6.50 %), whereas response linearity at 40 °C and a PFV of 1.1 was not optimal (median RSD 15.37 %). For partially volatile analytes such as the fatty acids, it can therefore be concluded that an optimal PFV determined at a given temperature is no longer valid when evaporation temperature is changed (Figure 7).

An alternative to using the power function value is a double logarithmic transformation of the calibration curve. The quality of the linear fit for every analyte, expressed as the coefficient of determination achieved by the double logarithmic transformation, was $R^2 > 0.999$. Furthermore, the obtained residuals for the calibration levels showed very satisfying results, even at low concentrations (Supplementary material: Fig S3), whereas residuals, especially at the lowest concentrations, varied drastically with changes in PFV. This shows that, for a multiple analyte mixture, it can be sufficient to use the default PFV of 1.0 and log-log transformation to achieve a linear fit of the response, rather than to apply a more complex fitting model.

In many cases the application's goal is to obtain satisfactory and low LOQs. Thus, for partially volatile analytes, it seems most appropriate to evaluate the optimal evaporation temperature before determining the best power function value to receive an appropriate fit. This conclusion arises from the facts that evaporation temperature strongly affects sensitivity (Fig. 3) and that the ideal PFV changes when altering evaporation temperature (Fig. 7). This is in contrast to the common approach of determining PFV before evaporation temperature for non-volatiles [34].

3.3. Validation and application of the optimized method

3.3.1. Method validation

The method was validated with regard to ICH guideline Q2(R1) [28]. Hereby, specificity, linearity and range, accuracy, precision, limit of quantitation (LOQ) and robustness were assessed.

Specificity could be demonstrated by individual analysis and analysis of mixtures of reference standards of all possible sample compounds. Separation of the fatty acids from each other was achieved and the extraction procedure did not interfere with any peaks needed for quantitation as confirmed with the analysis of blank extractions.

Linearity was shown by establishing calibration curves over a range of two orders of magnitude at concentration levels of 1, 25, 50, 75 and 100 µg/ml covering the estimated analyte amount of the sample. Application of linear regression after double logarithmic transformation of concentration and peak area resulted in coefficients of determination (R^2) higher than 0.999 for each analyte over the investigated range (Table 2).

For demonstration of *accuracy*, recovery rates were calculated at 1, 25 and 100 µg/mL concentration levels for each fatty acid standard (n = 3) using calibration curves. Quantification was done by linear regression after double logarithmic transformation of concentration and peak area. The mean recoveries were satisfactory with values ranging from 94.3 to 107.1 %.

Precision was assessed by injections of fatty acid standards in triplicate at concentration levels of 1, 25 and 100 µg/mL. RSD values ranging from 0.07 to 2.52 % were obtained indicating good precision with exception of the 1 µg/ml level of myristic acid showing an increased RSD of 6.61 %. Since myristic acid was not present in the current investigation and the method was still capable of meeting the requirements set by the Ph. Eur. (limit of 5 %), this was accepted.

LOQs of the fatty acids were determined with respect to the S/N approach according to ICH guideline Q2(R1) [28]. A S/N ratio of 10, derived from analyte signal compared to a blank, was hereby defined as the LOQ. For linear extrapolation, standard solutions at 0.1, 0.5 and 1.0 µg/mL concentration level were used. Ranging from 1.3 to 8.1 ng on column (Table 1), the LOQs were significantly affected by the chain length of the fatty acid as further elaborated in section 3.2.

Robustness in terms of CAD parameter settings could be evaluated with regard to the systematic variations of the method optimization procedure and is elaborated in-depth in section 3.2., here especially evaporation temperature was found to be critical. Chromatographic robustness in general was evaluated for the following variations: column temperature ± 2.5 °C, initial percentage of mobile phase B ± 1 %, final percentage of mobile

phase B ± 1 % and flow rate ± 0.06 mL/min. Robustness is sufficient with recovery rates ranging from 96 to 102 % for all substances with exception of myristic acid having recovery rates between 103 and 110 % (Supplementary material: Table S1) which was acceptable due to its absence within the current batch analysis (Table 3). Separation was maintained for all examined variations.

3.3.2. Polysorbate 80 batch analysis

16 batches of polysorbate 80 analyzed by Ilko et al. [25] were subjected to analysis applying the optimized UHPLC method. The findings indicate sufficient stability of polysorbate 80 when stored at room temperature for four years with only rare exposure to light (Table 3).

Table 3. Percentage (% m/m) content of fatty acids in polysorbate 80 batches, average of n=2 extractions shown with standard error; n/a= error not available because only n=1 was evaluated. Values in brackets indicate the percentage change after four years of storage.

	Alpha-linolenic acid	Myristic acid	Palmito-leic acid	Linoleic acid	Palmitic acid	Oleic acid	Petrose-linic acid	Stearic acid	Free fatty acids
A1	-	-	- (-0.8)	16.5±0.25 (+9.9)	4.9±0.16 (-0.5)	75.8±0.74 (-9.4)	1.5±0.02 (+0.7)	1.4±0.35 (+0.2)	0.7±0.02 (+0.1)
A2	-	-	- (-0.8)	19.2±0.06 (+9.6)	4.8±0.09 (-0.6)	72.7±0.33 (-9.2)	1.8±0.00 (+0.6)	1.6±0.30 (+0.2)	0.8±0.07 (+0.2)
A3	-	-	- (-0.8)	18.7±0.54 (+8.6)	4.4±0.08 (-1.4)	74.4±0.77 (-6.2)	1.7±0.09 (+0.7)	0.9±0.05 (-0.8)	0.8 n/a (-0.4)
A4	-	-	- (-0.8)	14.9±0.81 (+8.1)	4.2±0.12 (-1.6)	78.4±0.58 (-5.7)	1.7±0.05 (+0.5)	0.8±0.07 (-0.8)	1.1 n/a (+0.5)
B1	-	-	-	-	- (-0.8)	100±0.00 (+3.3)	-	- (-0.4)	0.3±0.00 (+0.3)
B2	-	-	-	-	- (-1.0)	100±0.00 (+3.6)	-	- (-0.5)	0.2±0.00 (+0.2)
B3	-	-	- (-0.6)	-	- (-0.7)	100±0.00 (+4.7)	-	- (-0.4)	0.1±0.03 (+0.1)
C1	-	-	- (-0.5)	15.7±0.02 (+6.3)	9.4±0.12 (-2.8)	72.7±0.11 (-1.3)	1.0±0.21 (-)	1.1±0.04 (-1.6)	0.4±0.00 (-0.3)
C2	-	-	- (-0.7)	15.2±0.26 (+8.1)	9.5±0.23 (-1.1)	72.3±0.41 (-5.7)	1.0±0.01 (+0.1)	2.0±0.06 (-0.9)	0.4±0.01 (-)
C3	-	-	-	16.0±0.19 (+5.3)	11.4± 0.07 (-3.2)	67.2±0.14 (-0.6)	3.3±0.06 (+0.7)	2.0±0.03 (-1.6)	0.3 n/a (-)
D1	-	- (-0.2)	-	17.4±0.88 (+6.1)	6.5±0.31 (-1.8)	75.1±0.73 (-2.6)	- (-0.3)	1.0±0.46 (1.0)	0.5±0.06 (+0.1)
D2	-	- (-0.1)	-	16.9±0.22 (+5.3)	6.2±0.37 (-1.3)	75.5±0.49 (-2.7)	- (-0.3)	1.4±0.10 (-0.5)	0.4±0.00 (+0.1)
D3	-	-	-	18.5±0.07 (+6.7)	6.0±0.02 (-1.4)	74.4±0.10 (-3.7)	- (-0.3)	1.1±0.04 (-0.9)	0.4±0.01 (+0.1)
E1	-	-	-	10.0±0.15 (+8.9)	1.6±0.01 (-0.9)	85.4±0.03 (-7.0)	1.6±0.08 (+0.4)	1.4±0.19 (-1.3)	0.1±0.01 (+0.1)
E2	-	-	-	8.5±0.13 (+8.5)	2.1±0.10 (-0.9)	86.1±0.12 (-6.1)	1.6±0.18 (+0.6)	1.6±0.10 (-1.5)	0.1±0.00 (+0.1)
E3	-	-	-	-	3.4±0.05 (-1.0)	93.9±0.25 (+1.6)	0.8±0.25 (-0.2)	1.9±0.23 (-0.9)	0.8±0.05 (+0.8)

Of note, the analysis of the *fatty acid composition* revealed an increase in linoleic acid for all batches except for the ones of manufacturer B and batch E3. Since linoleic acid is a double unsaturated fatty acid that can originate from oxidation of oleic acid, oxidative degradation during storage can be suggested because the increase in linoleic acid occurred upon a decrease of oleic acid content only. Batch E3 was stored in a brown glass bottle, which should prevent photo oxidation. Consequently, no formation of linoleic acid was observed in this batch, supporting the suggested degradation pathway.

Only three batches, namely A2, A3 and D3, were no longer within the specifications of the European Pharmacopoeia (Ph. Eur.) due to an excessive content of linoleic acid greater than 18 % (m/m).

4. Conclusion

An UHPLC method for the analysis of polysorbate 80 was successfully optimized for use with the newest generation CAD resulting in time savings of over 75% and eluent consumption savings of more than 40%, respectively, while achieving superior LOQs when compared to a former method run on a conventional HPLC-CAD system. Moreover, the dependence of detector response on CAD settings was assessed in a systematic approach for a series of homologous fatty acids ranging from C_{14} to C_{18}. It could be verified that the evaporation temperature of the detector has a significant impact on sensitivity. Furthermore, S/N ratios can be optimized by the choice of an appropriate evaporation temperature. Modern CAD detectors allow for the use of an integrated power function value which was evaluated here. Use of the power function value can drastically improve linearity of response, especially at the lower levels of the calibration curve. However, a double-logarithmic transformation proved to be superior and less time consuming for the investigated two order concentration range of rather volatile analytes. It was shown that linearity of response and limit of quantification vary greatly with different PFV and evaporation temperature settings. Thus, these two parameters should be chosen and optimized based on an application's individual goal and depending on volatility of the analytes.

Conflict of interest statement

The Thermo Fisher Scientific Vanquish™ UHPLC System was generously provided by Thermo Fisher Scientific for this cooperation.

Acknowledgements

Special thanks are due to Christiane Theiss and her assistance with her expert knowledge of fatty acids and their properties as well as Oliver Wahl (both University of Wuerzburg) for insightful discussions and advice, as well as Paul Gamache (Thermo Fisher Scientific, Chelmsford, Massachusetts, USA) and Frank Steiner (Thermo Fisher Scientific, Germering, Germany) for project coordination and crucial ideas, reviews and discussions

Supplementary material

Table S1. Robustness of the UHPLC method. Percentage recovery rates of a 100 µg/mL solution for different chromatographic variations.

	No variation	Temperature (°C)		Flow rate (ml/min)		% Mobile Phase B at start		% Mobile Phase B at end	
		22.5	27.5	1.44	1.56	74	76	84	86
% Recovery									
Alpha-linolenic	100	99	99	101	96	98	98	100	98
Myristic	100	108	109	110	103	104	105	107	110
Linoleic	100	100	101	102	98	102	98	99	100
Palmitic	100	99	97	102	96	98	97	96	96
Oleic	100	99	96	98	96	100	98	99	99
Petroselinic	100	101	97	99	96	96	96	98	98
Stearic	100	100	99	98	97	99	100	97	97

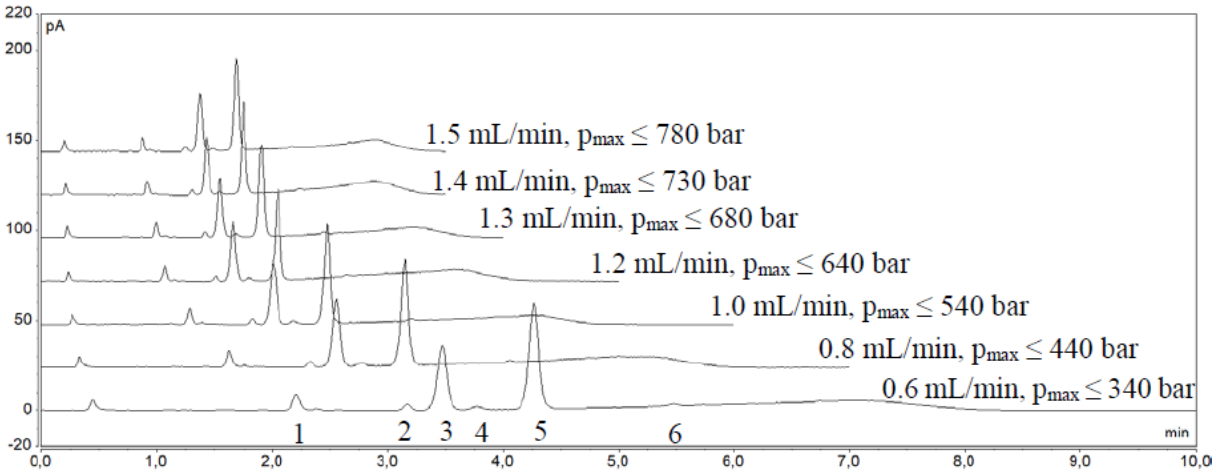

Fig. S1. Chromatograms and resulting maximum backpressure for variation of flow rate while adjusting hold and gradient time by the ratio of flow rates; 10 µL injection of a 50 µg/mL oleic acid (65 88% purity) and margaric acid solution; elution order: 1: linoleic acid, 2: palmitic acid, 3: oleic acid, 4: petroselinic acid, 5: margaric acid, 6: stearic acid.

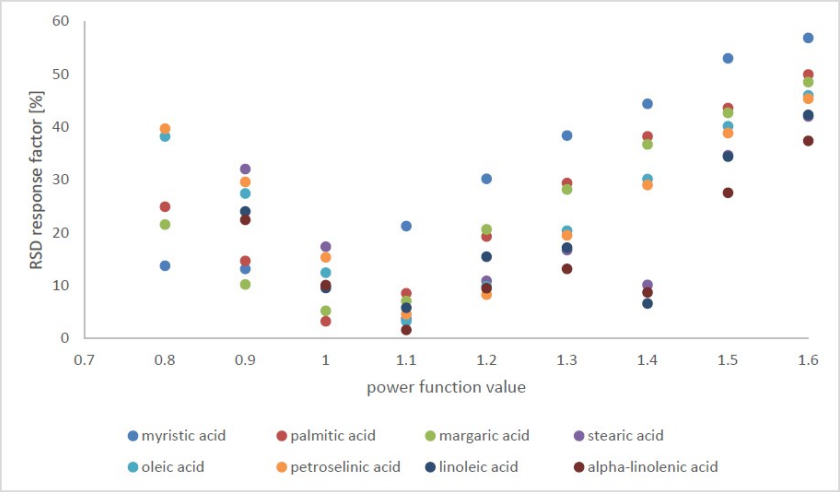

Fig. S2. RSD of the response factors [%] for PFV 0.8 to 1.6 at evaporation temperature 35 °C (n = 5).

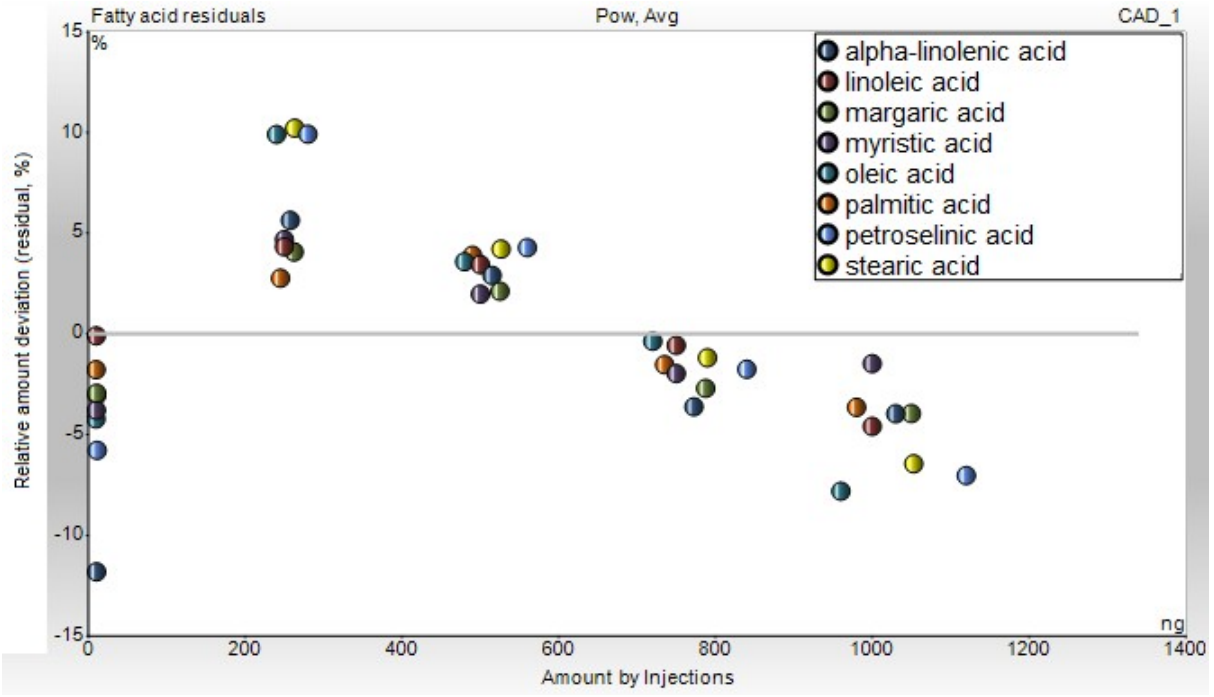

Fig. S3. Residual plot of the relative amount deviation for each calibration level for lg-lg transformation at 30 °C evaporation temperature and a PFV of 1.0 (n = 5).

References

[1] A.C. Rustan, C.A. Drevon, Fatty acids: structures and properties. Encyclopedia of Life Sciences, 2005: John Wiley & Sons.

[2] A. Tomlinson, B.I. Demeule, B. Lin, S. Yadav, Polysorbate 20 degradation in biopharmaceutical formulations: quantification of free fatty acids, characterization of particulates, and insights into the degradation mechanism. Mol pharm, 2015. 12(11): p. 3805-3815.

[3] S. Fekete, K. Ganzler,J. Fekete, Fast and sensitive determination of Polysorbate 80 in solutions containing proteins. J. Pharm. Biomed. Anal., 2010. 52(5): p. 672-679.

[4] G. Eccleston, Functions of mixed emulsifiers and emulsifying waxes in dermatological lotions and creams. Colloid Surface A, 1997. 123: p. 169-182.

[5] Z. Wu, Q. Zhang, N. Li, Y. Pu, B. Wang, T. Zhang, Comparison of critical methods developed for fatty acid analysis: a review. J. Sep. Sci., 2017. 40(1): p. 288-298.

[6] M. Collomb, U. Bütikofer, R. Sieber, B. Jeangros, J.O. Bosset, Composition of fatty acids in cow's milk fat produced in the lowlands, mountains and highlands of Switzerland using high-resolution gas chromatography. Int Dairy J, 2002. 12(8): p. 649-659.

[7] T. Seppänen-Laakso, I. Laakso, R. Hiltunen, Analysis of fatty acids by gas chromatography, and its relevance to research on health and nutrition. Anal. Chim. Acta, 2002. 465(1-2): p. 39-62.

[8] European Directorate for the Quality of Medicine and Healthcare, European Pharmacopoeia Online 9.5, Monograph No. 01848. 2018. Available from: http://online6.edqm.eu/ep905/, Access Date: April 3rd, 2018.

[9] D. Kloos, H. Lingeman, O. Mayboroda, A. Deelder, W.M.A. Niessen, M. Giera, Analysis of biologically-active, endogenous carboxylic acids based on chromatography-mass spectrometry. TrAC, Trends Anal. Chem., 2014. 61: p. 17-28.

[10] E. Drange,E. Lundanes, Determination of long-chained fatty acids using non-aqueous capillary electrophoresis and indirect UV detection. J. Chromatogr. A, 1997. 771(1-2): p. 301-309.

[11] S.-H. Chen,Y.-J. Chuang, Analysis of fatty acids by column liquid chromatography. Anal. Chim. Acta, 2002. 465(1-2): p. 145-155.

[12] W. Liu, Z.-Z. Wang, J.-P. Qing, H.-J. Li, W. Xiao, Classification and quantification analysis of peach kernel from different origins with near-infrared diffuse reflection spectroscopy. Pharmacogn. mag., 2014. 10(40): p. 441.

[13] G. Knothe, J.A. Kenar, Determination of the fatty acid profile by 1H-NMR spectroscopy. Eur. J. Lipid Sci. Technol., 2004. 106(2): p. 88-96.

[14] C. Skiera, P. Steliopoulos, T. Kuballa, B. Diehl, et al., Determination of free fatty acids in pharmaceutical lipids by 1H NMR and comparison with the classical acid value. J. Pharm. Biomed. Anal., 2014. 93: p. 43-50.

[15] C. Skiera, P. Steliopoulos, T. Kuballa, U. Holzgrabe, B. Diehl, Determination of free fatty acids in edible oils by 1H NMR spectroscopy. Lipid Technol., 2012. 24(12): p. 279-281.

[16] D. Perret, A. Gentili, S. Marchese, M. Sergi, et al., Determination of free fatty acids in chocolate by liquid chromatography with tandem mass spectrometry. Rapid Commun. Mass Spectrom., 2004. 18(17): p. 1989-1994.

[17] J. Zhao, S. Li, F. Yang, P. Li, Y.T. Wang, Simultaneous determination of saponins and fatty acids in Ziziphus jujuba (Suanzaoren) by high performance liquid chromatography-evaporative light scattering detection and pressurized liquid extraction. J. Chromatogr. A, 2006. 1108(2): p. 188-194.

[18] L.M. Nair, J.O. Werling, Aerosol based detectors for the investigation of phospholipid hydrolysis in a pharmaceutical suspension formulation. J. Pharm. Biomed. Anal., 2009. 49(1): p. 95-99.

[19] M. Plante, B. Bailey, I. Acworth, The use of charged aerosol detection with HPLC for the measurement of lipids, in Lipidomics. 2009, Springer. p. 469-482.

[20] E. Bravi, G. Perretti, L. Montanari, Fatty acids by high-performance liquid chromatography and evaporative light-scattering detector. J. Chromatogr. A, 2006. 1134(1-2): p. 210-214.

[21] N. Vervoort, D. Daemen, G. Török, Performance evaluation of evaporative light scattering detection and charged aerosol detection in reversed phase liquid chromatography. J. Chromatogr. A, 2008. 1189(1-2): p. 92-100.

[22] S. Almeling, U. Holzgrabe, Use of evaporative light scattering detection for the quality control of drug substances: Influence of different liquid chromatographic and evaporative light scattering detector parameters on the appearance of spike peaks. J. Chromatogr. A, 2010. 1217(14): p. 2163-2170.

[23] S. Almeling, D. Ilko, U. Holzgrabe, Charged aerosol detection in pharmaceutical analysis. J. Pharm. Biomed. Anal., 2012. 69: p. 50-63.

[24] T. Vehovec,A. Obreza, Review of operating principle and applications of the charged aerosol detector. J. Chromatogr. A, 2010. 1217(10): p. 1549-1556.

[25] D. Ilko, A. Braun, O. Germershaus, L. Meinel, U. Holzgrabe, Fatty acid composition analysis in polysorbate 80 with high performance liquid chromatography coupled to charged aerosol detection. Eur J Pharm Biopharm, 2015. 94: p. 569-574.

[26] M. Hu, M. Niculescu, X. Zhang, A. Hui, High-performance liquid chromatographic determination of polysorbate 80 in pharmaceutical suspensions. J. Chromatogr. A, 2003. 984(2): p. 233-236.

[27] V. Matyash, G. Liebisch, T.V. Kurzchalia, A. Shevchenko, D. Schwudke, Lipid extraction by methyl-tert-butyl ether for high-throughput lipidomics. J. Lipid Res., 2008. 49(5): p. 1137-1146.

[28] International Conference on Harmonisation of Technical Requirements for Registration of Pharmaceuticals for Human Use, Validation of analytical procedures: text and methodology Q2(R1)2005. Available from: https://www.ich.org/fileadmin/Public_Web_Site/ICH_Products/Guidelines/Quality/Q2_R1/Step4/Q2_R1__Guideline.pdf, Access Date: April 3rd 2018.

[29] T. Gorecki, F. Lynen, R. Szucs, P. Sandra, Universal response in liquid chromatography using charged aerosol detection. Anal. Chem., 2006. 78(9): p. 3186-3192.

[30] J.P. Hutchinson, J. Li, W. Farrell, E. Groeber, R. Stucs, G. Dicinoski, P.R. Haddad, Comparison of the response of four aerosol detectors used with ultra high pressure liquid chromatography. J. Chromatogr. A, 2011. 1218(12): p. 1646-1655.

[31] A.G. Osborn, D.R. Douslin, Vapor-pressure relations for 15 hydrocarbons. J. Chem. Eng. Data, 1974. 19(2): p. 114-117.

[32] S. Lane, B. Boughtflower, I. Mutton, C. Paterson, D. Farrant, N. Taylor, Z. Blaxill, C. Carmody, P. Borman, Toward single-calibrant quantification in HPLC. A comparison of three detection strategies: evaporative light scattering, chemiluminescent nitrogen, and proton NMR. Analytical chemistry, 2005. 77(14): p. 4354-4365.

[33] M. Plante, B. Bailey, P. Gamache, I. Acworth, Guidelines for Method Transfer and Optimizaion of the Corona Veo Charged Aerosol Detector. 2016. Available from: https://assets.thermofisher.com/TFS-Assets/CMD/posters/PN-64690-CAD-Method-Transfer-Guidelines-Corona-Veo-Pittcon2016-PN64690-EN.pdf, Access Date: April 3rd, 2018.

[34] P.H. Gamache, Charged aerosol detection for liquid chromatography and related separation techniques. 2017: John Wiley & Sons.

[35] M.M. Kiser, J.W. Dolan, Selecting the best curve fit. LC GC NORTH AMERICA, 2004. 22(2): p. 112-117.

[36] A. Soliven, I.A.H. Ahmad, J. Tam, N. Kadrichu, P. Challoner, R. Markovich, A. Blasko, A simplified guide for charged aerosol detection of non-chromophoric compounds—Analytical method development and validation for the HPLC assay of aerosol particle size distribution for amikacin. J. Pharm. Biomed. Anal., 2017. 143: p. 68-76.

[37] B. Bailey, P. Gamache, I. Acworth, Guidelines for method transfer and optimization—from earlier model Corona detectors to Corona Veo and Vanquish charged aerosol detectors. 2017. Available from: https://assets.thermofisher.com/TFS-Assets/CMD/Technical-Notes/tn-71290-cad-method-transfer-tn71290-en.pdf, Access Date: April 3rd, 2018

3.2. Charged Aerosol Detector response modeling for fatty acids based on experimental settings and molecular features: a machine learning approach

Ruben Pawellek[1], Jovana Krmar[1], Adrian Leistner, Nevena Djajić, Biljana Otašević, Ana Protić, Ulrike Holzgrabe

[1]These authors contributed equally to this work.

Manuscript accepted for publication in J. Cheminformatics.

Abstract

The charged aerosol detector (CAD) is the latest representative of aerosol-based detectors that generate a response independent of the analytes' chemical structure. This study was aimed at accurately predicting the CAD response of homologous fatty acids under varying experimental conditions. Fatty acids from C12 to C18 were used as model substances due to semivolatile characterics that caused non-uniform CAD behaviour.

Considering both experimental conditions and moleculardescriptors, a mixed Quantitative Structure-Property Relationship (QSPR) modeling was performed using Gradient Boosted Trees (GBT). The ensemble of 10 decisions trees (learning rate set at 0.55, the maximal depth set at 5, and the sample rate set at 1.0) was able to explain approximately 99% (Q^2: 0.987, RMSE: 0.051) of the observed variance in CAD responses. Validation using an external test compound confirmed the high predictive ability of the model established (R^2: 0.990, RMSEP: 0.050). With respect to the intrinsic attribute selection strategy, GBT used almost all independent variables during model building. Finally, it attributed the highest importance to the power function value, the flow rate of the mobile phase, evaporation temperature, the content of the organic solvent in the mobile phase and the molecular descriptors such as molecular weight (MW), Radial Distribution Function - 080/weighted by mass (RDF080m) and average coefficient of the last eigenvector from distance/detour matrix (Ve2_D/Dt).

The identification of the factors most relevant to the CAD responsiveness has contributed to a better understanding of the underlying mechanisms of signal generation. An increased CAD response that was obtained for acetone as organic modifier demonstrated its potential to replace the more expensive and environmentally harmful acetonitrile.

1. Introduction

Among the various detectors used in high-performance liquid chromatography (HPLC), the UV detector is frequently referred to as the workhorse, being predominantly employed for quality control purposes and routine analysis. Though characterized by high a sensitivity, a broad linear dynamic range, and a user-friendly application, the prerequisite for the usage of the detector is the existence of UV absorbing structural features of the analytes known as chromophores, such as aromatic ring systems or conjugated double bonds. Thus, the detector suffers from poor sensitivity toward analytes lacking suitable chromophores like fatty acids and sugars. This shortcoming can be addressed by using universal detection techniques instead, e.g. aerosol-based detection techniques [1]. The most recent aerosol-based detector, the charged aerosol detector (CAD), stands out in terms of response uniformity due to its unique principle of detection. In contrast to the other aerosol-based detectors, the analyte particles obtained from evaporation of aerosol droplets that were previously generated by nebulization of the mobile phase, are charged by diffusion processes independent of the particle characteristics [2]. In comparison, the refractive index and thus the analyte characteristics comprising the dried particle is critical for the measurement of the light dispersion in evaporative light scattering detection (ELSD). This difference results in higher uniformity in CAD response compared to ELSD [3,4]. Condensation nucleation light scattering detection (CNLSD) dependence on particle characteristics is even more pronounced, further reducing response uniformity [5,3]. However, the response of the CAD is not truly uniform, as a mobile phase gradient, the analyte volatility, salt formation, and the analyte density also have an impact on signal generation [2]. Thus, the molecular properties of the analytes as well as the chromatographic conditions must be considered when developing methods to achieve uniform response of the analytes. Several approaches have been reported aimed at generating uniform CAD response, including the application of inverse gradient programs [6] and the establishment of models describing the influence of experimental parameters [7]. However, there is little evidence on the predominant analyte-related and experimental factors influencing CAD response when investigating a set of structurally similar analytes of varying volatility.

In this study, a homologous series of chromophore-deficient fatty acids (Fig. 1) was selected to evaluate the influence of experimental parameters and molecular properties on the CAD response. Despite their similar structure, the molecular properties of the fatty acids, e.g. the volatility, vary as a function of chain length (Fig. 1). Thus, a comprehensive model accurately describing the influence of the chain length of the fatty acids on the CAD signal would contribute to a better understanding of the underlying mechanisms of signal generation. Such a mathematical tool could reliably estimate the most significant molecular characteristics contributing to the higher CAD responsiveness. To enable drawing valid conclusion on the influence of the experimental and molecular parameters on CAD response of the selected fatty

acids, a Mixed Quantitative Structure-Property Relationship (QSPR) approach was applied. The QSPR model was built with the aid of a Gradient Boosted Trees (GBT) machine learning algorithm (MLA). GBT algorithms combine predictors in a sophisticated manner that can reveal complex patterns that other techniques may miss. GBT utilizes boosting as a technique of building predictive models of elevated complexity that can be superior to other MLAs such as Artificial Neural Networks (ANNs) that were used in similar QSPR studies [8]. Thus, a mixed GBT-QSPR model was employed to accurately describe the influence of experimental parameters and molecular properties on the CAD response. The most significant factors were then evaluated comparing their individual impact on the CAD response. Special emphasis was placed on the environmentally friendly alternatives, acetone and ethanol (EtOH), to the more commonly used organic solvents acetonitrile (ACN) and methanol (MeOH). By validating the effectiveness of green solvents, CAD's potential to be employed in green chromatography [9] could be demonstrated.

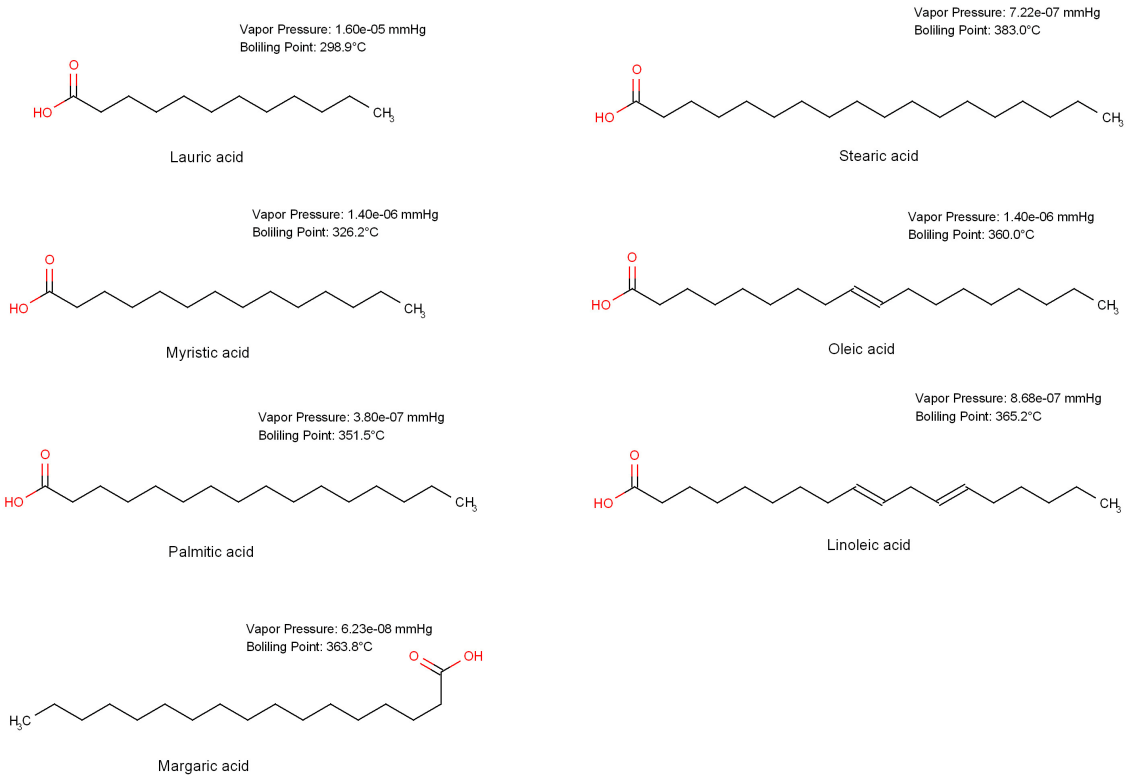

Fig. 1. Structural formulas of the seven fatty acids utilized as model substances, with the corresponding vapor pressure and boiling point values.

2. Materials and methods

2.1. Chemicals and reagents

Lauric acid (98%), linoleic acid (≥ 99%), margaric acid (≥ 98%), myristic acid (≥ 99%), oleic acid (≥ 99%), palmitic acid (≥ 99%), and stearic acid (≥ 98.5%) as well as formic acid (98-

100%), HPLC plus grade acetone, HPLC gradient grade acetonitrile (ACN), HPLC grade ethanol (EtOH), and HPLC gradient grade methanol (MeOH) were purchased from Sigma Aldrich (Steinheim, Germany). Ultra-pure deionized (DI) water was delivered by a Milli-Q® system (Merck, Darmstadt, Germany).

2.2. Instrumentation

The experiments were performed on a Thermo Scientific Vanquish™ Flex modular chromatographic system (Thermo Fisher Scientific, Germering, Germany) consisting of a binary pump with online degasser, a thermostatted split sampler, a thermostatted column compartment with passive pre-heater, and a variable wavelength detector in-line with a Vanquish™ Horizon CAD. The CAD was supplied with nitrogen gas from an ESA nitrogen generator (Thermo Fisher Scientific) connected to the in-house compressed air system. The HPLC instrument was controlled and runs were processed using the Chromeleon® Data System Version 7.2.6 software program (Thermo Fisher Scientific).

2.3. Preparation of solutions

Stock solutions of the fatty acid standards were prepared by accurately weighing 5.0 mg of the respective fatty acid and dissolving in acetone, ACN, EtOH, and MeOH, respectively. The stock solutions were diluted to a concentration of 50 µg/mL with a mixture of DI water and organic solvent in proportions equivalent to the mobile phase composition used according to the experimental plan in each case (Table S1, hosted by figshare [10]).

2.4. Flow injection analysis (FIA)

The outlet capillary of the Vanquish™ sytem's injection valve was linked to the inlet capillary of the UV detector by a connector (Viper™ union, Thermo Fisher Scientific) to perform the FIA at sufficient back pressure. Isocratic runs with a runtime of 2 min, an injection volume of 10 µl, and flow rates of 0.5 mL/min, 1.0 mL/min, and 1.5 mL/min, respectively, were carried out. The temperature of the column chamber was held constant at 25 °C, while the mobile phase consisted of 0.1% (v/v) formic acid in DI water and 0.1% (v/v) formic acid in either acetone, ACN, MeOH, or EtOH in various proportions (75%, 82.5%, 90% (v/v) organic solvent) according to the experimental plan (Table S1, hosted by figshare [10]. Prior to each new run, the system was equilibrated for 5 min at the upcoming mobile phase conditions. When switching the organic solvent, the system was flushed for at least 30 min at the upcoming mobile phase conditions until a stable baseline was obtained. CAD was employed for the detection of the fatty acids with the instrumental settings evaporation temperature (24 °C, 36 °C, 48 °C) and power function value (PFV) (0.8, 1.2, 1.6) being altered according to the experimental plan (Table S1 [10]), whereas the filter constant was maintained at 1.0 s.

2.5. Selection of the experimental variables and their design levels

To evaluate the influence of various experimental parameters on the CAD response, screening experiments by FIA based on a 2^{5-1} fractional factorial design (FFD) were performed. The selected factors and their corresponding ranges were as follows: the organic solvent's content in the mobile phase (70% – 90%, v/v), the flow rate of the mobile phase (0.5 mL/min – 1.5 mL/min), the evaporation temperature (24 ℃ – 48 ℃), the PFV (0.8 – 1.6), and the filter constant (1 s – 5 s). The FIA experiments were conducted with four different organic solvents, namely ACN, MeOH, acetone and EtOH. In order to estimate the experimental error, 4 additional runs at the central point of the experimental domain were included in the FFD plan. With lauric acid, palmitic acid, and stearic acid representing the low, medium, and high levels of the set of analytes investigated, 20 experiments with 4 different solvents were performed in a randomized order for each fatty acid. The significance of the examined factors' influence was assessed using Student's t-tests and Pareto diagrams.

Response surface methodology (RSM) was subsequently employed for the thorough description of the experimental domain. The selection of parameters investigated with their respective ranges was based on the results of the screening phase, except for the content of the organic solvents. Their low levels were increased from 70% to 75% v/v, respectively, due to the insufficient solubility of stearic acid in higher aqueous proportion. The statistically significant factors derived from the screening experiments were varied according to the experimental plan created by Central Composite Design (CCD). Within the experimental plan, the type of the organic solvent used was coded by assigning the numbers 1-4 to ACN, MeOH, acetone and EtOH, respectively. The plan of the CCD is depicted in Table S1 of the Supplemental Material [10]. The filter constant was maintained at 1 s, since it did not significantly influence the CAD response. The RSM experiments were carried out in random order. The magnitude of the CAD response was studied as the system's response.

Design-Expert 7.0.0. (Stat-Ease, Inc., Minneapolis, USA) was used to construct the 2^{5-1} FFD and the CCD experimental plans.

2.6. Computation of the molecular descriptors

The chemical structures of lauric acid, myristic acid, palmitic acid, margaric acid, stearic acid, oleic acid, and linoleic acid were sketched in ChemDraw Ultra 8.0 software (PerkinElmer, Massachusetts, USA). Each structure was subjected to geometry optimization using the semi-empirical MOPAC/PM3 method in Chem 3D® Ultra 8.0 (Cambridge Soft Corporation, Cambridge, USA). The compounds' conformations with the minimum energy were used to calculate physico-chemical, topological, geometrical, and spatial structural descriptors in Dragon 6.0.7. software (Talete srl, Milano, Italy). To prevent potential correlation issues,

descriptors that were strongly correlated to the other descriptors (using a correlation coefficient $|r| > 0.90$), descriptors with constant values (RSD <5%), i.e. descriptors that were not available for all analytes were excluded. After this step, the set of several thousand descriptors originally calculated was reduced to 60 molecular descriptors.

2.7. Exploratory analyses

Basic statistics (mean, min, max, etc.) of each feature are described in Table S2 of the Supplemental Material. The range (max - min) for the experimental factors was chosen to ensure the satisfactory CAD response of the tested compounds. Due to the DoE approach used and symmetrical placement of -1 and +1 levels around nominal (0) level, the mean and median were exactly the same for these attributes. As for other attributes (molecular descriptors), descriptive statistics was determined by the structure of the analytes. For instance, the higher representation of C18 than C12-C13 fatty acids in the dataset caused the MW descriptor to have a greater median than the mean. In the same way, other reported statistics was as expected. Also, no missing data were observed.

2.8. Calculation of the skewness coefficients

Skewness coefficients were obtained from the SKEW function in Excel 2010 (Microsoft Office, Redmond, Washington, USA). By the means of the SKEW function, skewness G_1 of sample S containing n number of random variables x is estimated as follows (Eq. 1):

$$G_1 = \frac{n}{(n-1)(n-2)} \sum \left(\frac{x_i - \bar{x}}{s}\right)^3 \quad (1)$$

In Eq. 1, s is the standard deviation of a data set S, while $\bar{x}$ is the mean. It should be applied only if n >2. The skewness coefficients were calculated separately for the training and the test data.

2.9. GBT algorithm

Decision tree (DT) is a machine learning algorithm that splits a feature space by which objects are described, into several different and mutually excluded subspaces by a recursive partitioning method [11,12]. It is usual accompanied by a tree-like diagram that displays different outcomes from a series of decisions. Among the available range of techniques utilized for real-world data, DT is favored for its easiness of interpretation and elegant ability to work with missing values [13-15]. Additionally, DT is capable of dealing with extensive datasets and neglecting redundant descriptors, which makes it quite useful in QSPR model building [16].

On the other hand, DTs are characterized as weak learners. Additionally, even a slight change within the training set could lead to a major change in the algorithm topology, making DTs unstable classifiers. Therefore, a concept of building additive tree structures based on

ensemble learning has been adopted [16,17]. Ensembles that probably achieve better predictive performance than individual constituent (base) algorithms are typically generated by using boosting and bagging techniques. GBT utilize boosting as a technique of building predictive models of elevated complexity. Boosting is regarded as one of the most powerful ideas introduced in the last few decades within the machine learning domain [18]. Within particular concept, the individual (base) algorithms are combined in a sequence in order to provide a solution to a demanding computational problem. Prevention of mutual correlations between trees, induced by the engagement of the same training set, is managed using certain "penalties". These penalties, by repeatedly modifying original data, put emphasis on the errors made by the previous algorithms and, consequently, facilitate the process of learning for the currently added tree. At each step, the model employs the algorithm that best fits the current residuals. This process is usually repeated many times. During each step, parameters of existing trees are kept unchanged, giving rise to so-called stage-wise additive modeling. The purpose of this approach is to reduce the risk of overfitting.

In order to detect the residuals, a loss function is used. GBT sequentially combines DTs in way that each new added instance minimizes arbitrarily chosen, differentiable loss functions in descent gradient fashion. In terms of mathematical principles, GBT model can be presented using Eq. 2:

$$f_i(x) = f_{i-1}(x) + \nu w_i G_i(x); \quad 0 < \nu \leq 1 \tag{2}$$

In the Eq. 2 $fi(x)$ and $f_{i-1}(x)$ are models constructed at iteration i and $i-1$, respectively. The term denoted as w_i represents weight ("penalty") while ν is a regularization parameter – shrinkage or learning rate. The lower the learning rate, the slower the model learns. At the same time, it achieves better performance in terms of accuracy. However, if the learning rate is low, more trees are needed to be included in the ensemble. Engagement of too many trees indicates a high risk of overfitting. The identification of $G_i(x)$ required to be added to the model is the primary optimization problem.

2.10. Predictive modeling workflow

A QSPR modeling workflow was created using the Rapidminer Studio 9.1.000 (RapidMiner, Boston, MA, USA) software. The data related to margaric acid were excluded from the primary set and used as external test set. The remaining data were divided into 10 subsets of equal size by the Cross Validation Operator. This is a nested Operator that has two subprocesses. Inside the first subprocess of the Cross Validation Operator, the GBT algorithm was trained on 9 of the 10 subsets. The trained model was then applied in the second subprocess where its performance was measured. The omitted subset was used as an input of the testing stage. This procedure was repeated 10 times, so that each subset was used one time as a test set.

The overall model's performance was estimated by averaging the results (cross-validation correlation coefficient, Q^2 and root mean squared error, RMSE) from 10 iterations. The subsets used in the Cross Validation procedure were made by shuffled sampling.

After being trained and tested, the GBT-based QSPR model was applied to the external validation test set of the margaric acid data using the Apply model operator. The actual predictive power of a given model was quantified in terms of root mean squared error of prediction (RMSEP) and R^2. The RMSEP and R^2 estimates were obtained from the Performance operator. The detailed Rapidminer workflow is available as part of the supplementary material.The optimal performance of the model was achieved by grid tuning of hyperparameters, namely the learning rate (0.1 - 1.0, 30 steps); maximum depth (5-10, 6 steps) and sample rate (0.1 - 1, 9 steps). The number of decision trees (4-20, 9 steps) was adjusted by a trial-and-error approach. The number of trees was chosen to prevent overfitting. All hyperparmaters were adjusted to reduce the RMSEP.

3. Results and disscussion

3.1. Selection of the fatty acids investigated

The uniform response of the CAD for non-volatile analytes has been demonstrated in multiple studies [19,7,20]. Thus, the selection of semi-volatile and non-volatile fatty acids that are structural homologues but differ significantly in their response was essential to develop a model that could accurately predict the CAD response based on a mixed model including the response-determining molecular descriptors. Previous studies on the CAD response of fatty acids revealed a pronounced decline in the response of myristic acid (C14) compared to its structural homologue palmitic acid (C16) [21]. With respect to this preliminary observation, fatty acids ranging from lauric acid (C12) to stearic acid (C18) were selected as test substances due to their estimated differences in CAD response. The differences in response were evident when comparing the average response values obtained for each fatty acid from the CCD based FIA runs as depicted in Table S1 [10]. Going from lauric acid (C12) to stearic acid (C18), the CAD response increased with the chain length of the fatty acids (Fig. 2).

Interestingly, a pronounced decline in response could be observed between myristic acid (C14) and palmitic acid (C16), while the response for fatty acids >C16 did not significantly increase. Thus, fatty acids <C16 can be considered as semi-volatile compounds. These results strongly indicated the need for a mixed model as was employed here to include the molecular properties of the fatty acids in the modeling of the CAD response.

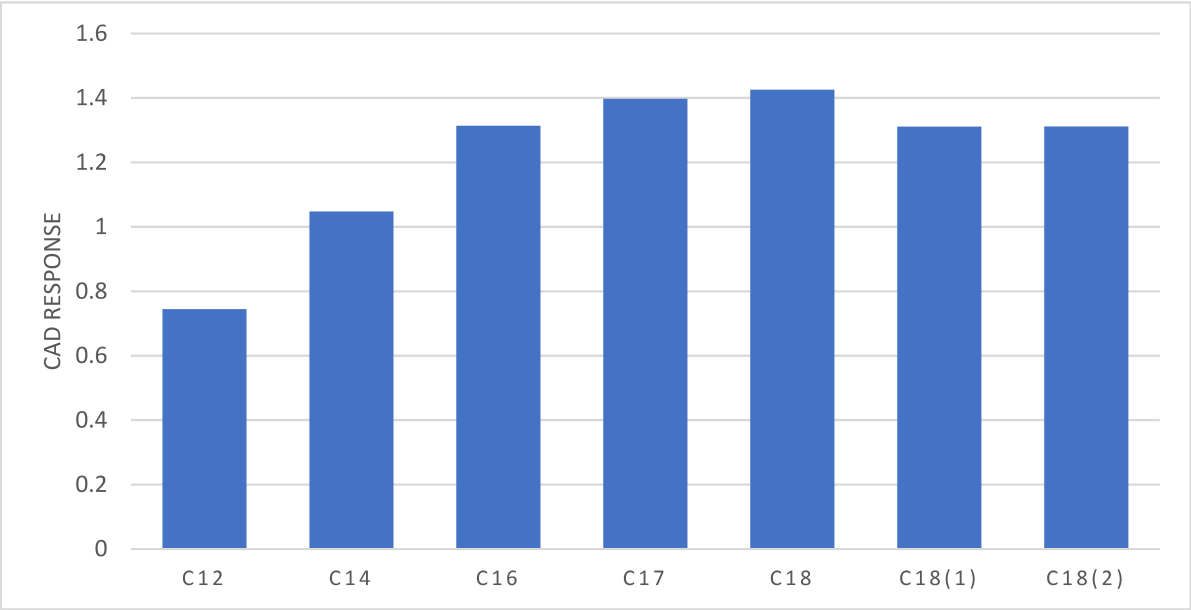

Fig. 2. Average CAD response for the fatty acids investigated obtained from FIA. The fatty acids are coded with their respective number of C-atoms. The degree of unsaturation is indicated in brackets where applicable.

3.2. DoE assisted development of the QSPR dataset

Design of experiments (DoE) is used to test versatile hypotheses in efficient manner. Within the DoE concept, independent variables (factors) are systematically varied in order to draw conclusion about factors' influences toward the target response [22]. In this study, DoE was utilized with a two-fold purpose. To examine the impact of the five pre-selected experimental factors and their possible interactions on the response of interest using DoE, it was necessary to conduct 32 (2^5) screening experiments. However, with the general goal of preserving all possible resources in the first phase, it was decided to fractionalize the experimental plan. Application of FFD allowed valid conclusions to be drawn with only 16 experiments per 4 different organic solvents. In the screening stage, the CAD responses were measured for three fatty acids (lauric acid, palmitic acid, and stearic acid). In accordance with their structural characteristics, lauric, palmitic and stearic acid were the representatives of the tested compounds. Therefore, in dependence of the fatty acid's chain length, estimated CAD responses could be at low, medium, or high level. According to the applied tests, the most significant experimental parameters toward CAD response were the type of the organic solvent, its proportion in the mobile phase, the flow rate of the mobile phase, the evaporation temperature, and the PFV.

The usage of 2^{5-1} FFD enabled a preliminary assessment of the QSPR model's performance that was subsequently conducted. Namely, if no screening has been carried out and an insignificant experimental variable (filter constant) had been included in the model

development, the GBT algorithm would have been loaded with identical cases in the training phase. The use of identical cases (that is, examples that differ in the values of insignificant factor) in the learning stage would likely lead to an overestimation of the QSPR model's predictive ability.

In the following CCD experiments, the examined levels of significant factors were retained from the screening stage along with the obligatory addition of a central level. As an exception, the low value of the organic solvents' volume fraction was increased from 70% to 75% (v/v) due to the precipitation of stearic acid at 70% MeOH (v/v) proportion. The insignificant parameter filter constant was maintained at 1 s since it was associated with the lowest background noise. The CCD experiments were carried out in random order to minimize the effects of uncontrollable variables.

Significant factors and a combination of their values according to CCD are incorporated in Table S1 [10], together with the results of the experiments.

3.3. Distribution of the outcome variable

Prior to the statistical analysis, the distribution of the experimentally obtained CAD responses was examined. Therefore, the skewness coefficient of the distribution was calculated in accordance with Eq. 1. In numerical terms, the skewness of a normal distribution is approximately zero. If the given coefficient is less than -1 or more than +1, the distribution is highly skewed, while the distribution is moderately skewed if the coefficient is between -1 and -1/2 or between +1/2 and +1. Positive coefficients indicate positive skewness and vice versa [23,24].

From the machine learning perspective, a highly skewed distribution could impair the predictive performance of the models developed. This claim finds its support in the fact that machine learning algorithms try to minimize the prediction error by learning to predict the response in the densest region of endpoints. As an implication of this concept, it is less likely that these algorithms will successfully predict the response of those endpoints that do not reside in the densest area. The usual strategy for addressing this issue is the transformation of the skewed variable, that is, the application of the same function to each of its values [25].

Here, the target variable showed a highly skewed distribution with a skewness coefficient of +1.8 calculated from Eq. 1 (Fig. S1a of the Supplemental Material). Common transformations applied to positively skewed data include logarithmic, square-root, and cube-root transformation [25-29]. Given how logarithmic, square-root, and cube-root transformed data displayed a skew of -0.70, 0.79, and 0.36, respectively, it was decided to use the latter transformation in the QSPR model construction. Fig. S1b of the Supplemental Material shows the distribution of the target response after applying the cube root transformation to each value.

3.4. QSPR modeling

The aim of this study was to develop a QSPR model that could predict the CAD response of fatty acids showing different volatility in a certain experimental domain with satisfying accuracy. In addition, the identification of the most important experimental and response-determining structural features would contribute to a comprehensive and mechanistic understanding of signal generation.

The QSPR model was built by linking the molecular descriptors computed for 6 fatty acids representing semi-volatile and non-volatile compounds to their CAD responses via GBT. The responses were measured under 25 different experimental conditions for each of the four organic solvents. As stated in section 3.3, the output values were transformed using the cube-root (see Table S1 [10]) to remove the skewness from the experimental data.

To demonstrate the validity of the applied modeling approach, a conventional QSPR model and a RSM model that solely linked the experimental parameters to the transformed CAD responses were developed simultaneously. The competing models, however, showed poor predictive performance compared to established mixed QSPR model. These results supported the assumption that the CAD response depends on both the experimental parameters and the molecular properties of the tested compounds. Hence, only the inclusion of both independent variables in the model provided a large rate of explained variance as well as enough observations that could be used in the process of training a machine-learning algorithm [30,8].

However, before any model can be used in practice, the reliability of its application must be confirmed by different validation procedures [31]. In this study, the GBT-based mixed model was validated via 10-fold cross-validation and, in addition, by an external validation set. The predictive ability of the developed QSPR relationships was evaluated using data related to margaric acid, which were not employed in the model generation. The test analyte was chosen with respect to its structural properties at the intermediate level of the fatty acids investigated and due to its similar distribution of CAD responses compared to the training set. The obtained responses for margaric acid were also included in Table S1 [10].

GBT was used as model building technique due to beneficial intrinsic attribute selection strategy and a pronounced ability to predict a target value that was close to the true response value for the given observations. The GBT-based QSPR model with the learning rate set at 0.55, the maximal depth set at 5, and the sample rate set at 1.0, showed satisfactory performance in terms of low RMSE, i.e. RMSEP and high Q^2, i.e. R^2 values. By using the significant experimental parameters and descriptors listed in section 3.5., the ensemble of 10 DTs was capable to explain approximately 99% (Q^2: 0.987, RMSE: 0.051) of the observed variance in CAD responses. Low RMSE values of 0.050 and high R^2 values of 0.990 for the

external validation set suggested the high predictive ability of the model developed. The consistency of the 10-fold CV with the external validation results clearly indicated that no overfitting occurred in the learning stage. The performance statistics are summarized in Table S3 of the Supplemental Material.

Considering that the QSPR model development involved cube-root transformed output data, it was decided to examine whether the model's performance was retained for the back transformed response values. In this regard, the correlation between the measured and the predicted CAD responses for the validation data set is visualized and presented in Fig. 3a. It can be noticed that there are few endpoints (with values of CAD response between 6 and 14) that have been poorly predicted by the GBT-QSPR model. It is possible that an estimation error occurred due to the utilized set of attributes. In other words, a different set of input variables might be able to better distinguish responses within the given range. It is equally probable that GBT did not show the best adaptation to the generated data and that some other machine learning algorithms could more accurately learn the patterns contained in the experimental results. Nonetheless, a comprehensive analysis of the observed phenomenon is going to be the subject of prospective studies.

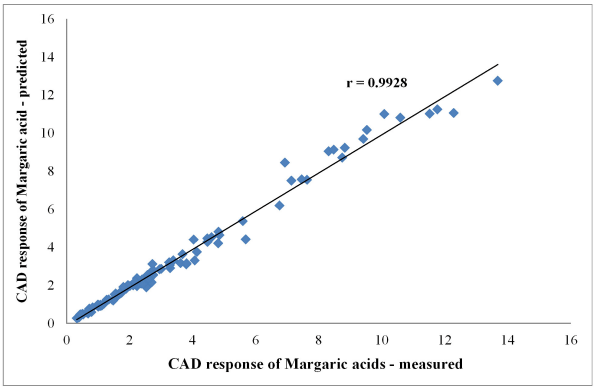

a

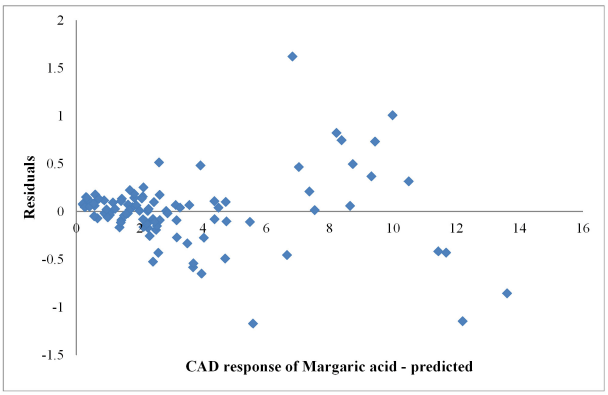

b

Fig. 3a. Regression plot of the optimized GBT-QSPR model. **Fig. 3b.** Residual plot of the optimized GBT-QSPR model.

To provide a more detailed discussion on the predictive performance of the developed model, the residuals of GBT regression were visually inspected. The residual plot (Fig. 3b) shows the distribution of overestimated and underestimated CAD responses. Ideally, all residuals should be small; this would indicate reasonable underlying assumptions and appropriateness of the fitted model [32]. As can be seen, the predictions met this criterion for low CAD response values (up to 4). However, as the fitted values increase, the residuals tend to deviate more from the 0% error line. Due to the investigated ranges of experimental variables, and, consequently, a much smaller number of observations with larger values of CAD response, this result was somewhat expected.

3.5. Significant features

In general, the model developed by GBT found non-linear patterns of molecular descriptors and experimental parameters that predicted the CAD response of the fatty acids investigated relatively well. However, the provided accuracy came at the cost of low interpretability. In order to address this issue, the variable importance tool was used.

With the intrinsic strategy of attribute selection, the GBT algorithm makes use of all independent variables available while forming the model [33]. The attributes with the highest scaled importance were considered as most relevant toward the CAD response of the fatty acids investigated. The ten attributes (y-axis) with the highest scaled importance (x-axis) in descending order are shown in Fig. 4.

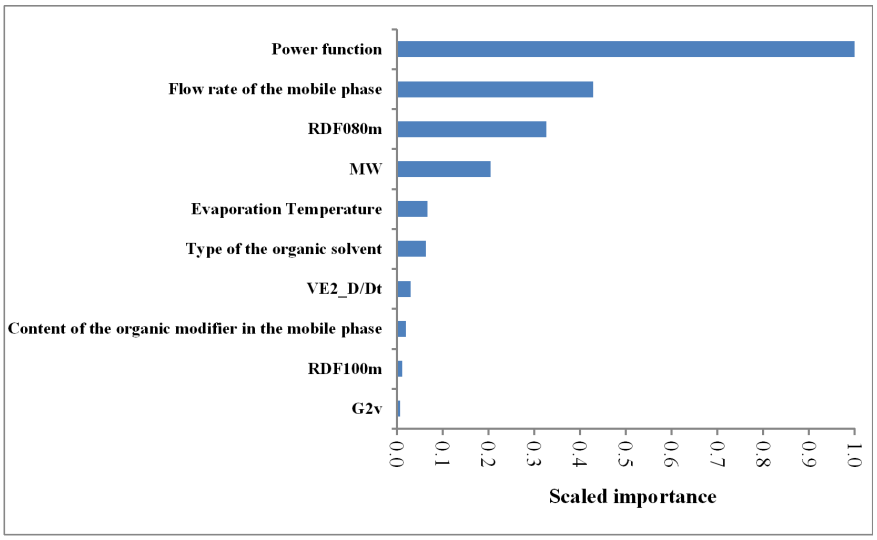

Fig. 4. The independent variables (y-axis) and their importance (x-axis) toward CAD response.

As it can be seen, GBT assigned great importance to the PFV, the flow rate of the mobile phase, and the molecular descriptors molecular weight (MW), Radial Distribution Function - 080 / weighted by mass (RDF080m) and average coefficient of the last eigenvector from distance/detour matrix (Ve2_D/Dt). It should be noted that the signal generation of the CAD

was also influenced by the CAD's evaporation temperature and the proportion of the organic solvent in the mobile phase, but to a much lesser extent. The impact of the significant factors on the CAD response is addressed thoroughly below, including graphical representations of the found patterns. The graphs provided are also part of a strategy to increase the interpretability of the GBT-based model.

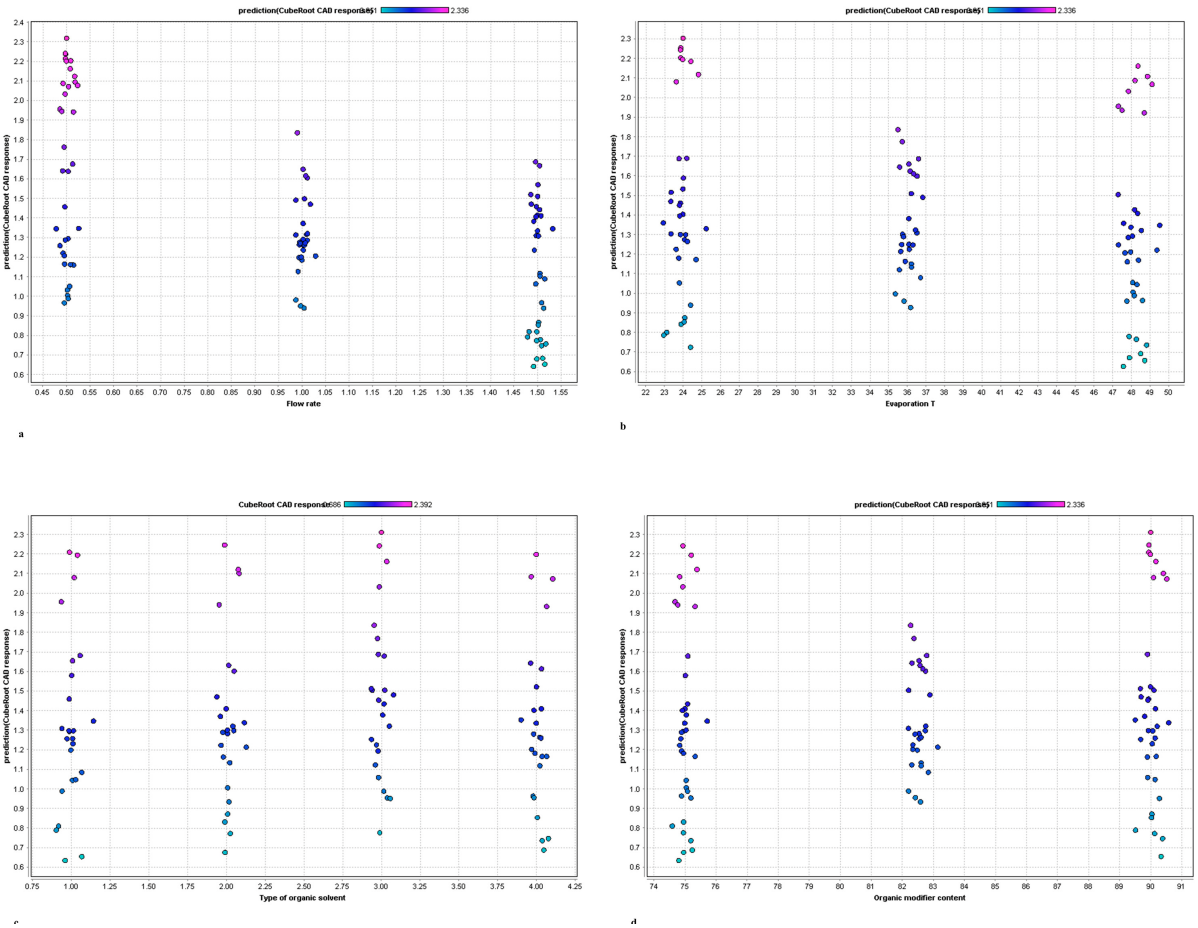

Fig. 5. Graphs showing the relationships between the predicted CAD response and a) flow rate b) evaporation temperature c) type of organic solvent: 1 – ACN; 2 – MeOH; 3 – Acetone; 4 – EtOH d) the content of organic solvent in the mobile phase (v/v).

The PFV setting raises the CAD's raw signal current to a specified power, thereby altering the signal output of the detector [34,35,2]. PFV other than the default value of 1.0 can be applied to improve the detector's linearity in the range of interest [2]. Therefore, its influence on the CAD's response is evident (Fig. S2 of the Supplemental Material), as the signal is directly modified by the respective PFV, which could be confirmed by its scaled importance value of 1.0. Thus, despite no additional information on the underlying mechanisms of signal generation was obtained here, the result supports the validity of the applied model. The influence of the flow rate being the most important among the chromatographic parameters toward CAD response was in line with the principle of function of the detector. Low mobile phase flow rates produce initial droplets of smaller size; thus, their evaporation is sped-up compared to larger

droplets, which is beneficial for the subsequent detection process [36,37]. Consequently, the CAD response of all fatty acids examined increased with flow rate reduction (Fig. 5a). Besides the two most influential parameters, the evaporation temperature, as one of the adjustable CAD settings, also had an impact on the CAD response. The evaporation temperature setting can be altered to adjust the selectivity of the detector toward a certain analyte dependent on its volatility [2]. Hence, low evaporation temperatures lead to a broader detection range due to the improved detection of semi-volatile analytes. The optimal evaporation temperature for a certain analyte requires experimental optimization, as the background noise of the CAD also changes with evaporation temperature due to enhanced evaporation of mobile phase impurities. However, at higher evaporation temperatures, analytes with semi-volatile characteristics, such as the short/medium chain fatty acids lauric acid and myristic acid, are expected to suffer a substantial loss of response [21]. Therefore, lower evaporation temperatures are contributing to enhanced CAD response for these fatty acids, and, consequently, could result in improved S/N (Fig. 5b).

Among the organic solvents commonly used with the CAD, ACN and MeOH are the predominantly applied solvents. The properties of the organic solvents applicable to the CAD, e.g. their low surface tension and viscosity, are beneficial for enhancing the detector's response due to the more efficient nebulization and aerosol transport processes compared to aqueous solvent [2]. In the current study, four different solvents were investigated, namely ACN, MeOH, acetone and EtOH. Fig. 5c illustrates that there were no remarkable differences toward CAD response obtained with the different solvents. However, slightly higher CAD responses were obtained with acetone in comparison to the remaining solvents. This observation is in accordance with the properties of the organic modifier, since acetone has the lowest viscosity and highest vapor pressure among the organic solvents investigated, which promotes efficient nebulization and evaporation. The use of inexpensive and environmental friendly acetone in experiments with CAD (instead of ACN) was previously suggested by Hutchinson et al. [38]. Apart from the response-enhancing properties of the solvent itself, the content of the organic solvent in the mobile phase also influences the magnitude of response generation. The organic solvent content in the mobile phase was varied in a rather small range from 75% to 90% (v/v) in our experiments due to solubility issues of some fatty acids at higher aqueous proportions. In addition, the separation of fatty acids is often achieved using mobile phases with high organic contents on C18 stationary phases [39,21]. The CAD response did not notably change with organic solvent content, which was somewhat expected. Slightly higher CAD responses were obtained with 90% (v/v) of organic solvent in the mobile phase (Fig. 5d), but the investigated range was too narrow for significant results. However, the influence of the organic content on CAD response has been evaluated in multiple studies and

can therefore be regarded as evident [38,40,37]. It must be kept in mind, that the variation of the organic content in the mobile phase is limited due to the separation of analytes.

A significant feature of the so-called universal detectors that justifies their use instead of the commonly applied UV detector, is the minor influence of the physicochemical properties of the analytes on the response. In fact, a relatively uniform response for non-volatile analytes has been demonstrated for the CAD in numerous studies [19,7,20]. However, there might be analyte-related properties influencing the CAD's response at constant experimental settings, such as the density of the compounds, their charge, the hydrogen bond donor capability [41], and the number of electronegative atoms [8]. Consistent with these assumptions, the results of the study performed indicate that there are indeed certain molecular properties influencing the CAD responsiveness.

Among the molecular properties that may have an impact on the response of aerosol-based detectors, the volatility of a compound, which is often characterized by its vapor pressure or boiling point, can be regarded as the most significant property toward detector responsiveness due to the mandatory evaporation step in the detection process of all aerosol-based detectors. The volatility of an analyte is strongly affected by its molecular weight [2]. Thus, the great importance attached to the MW descriptor by GBT is in accordance with the volatility requirements as stated above. However, there are no distinct limits determining the analyte as volatile, and, additionally, the volatility also depends on the experimental conditions, such as the CAD's evaporation temperature or the formation of less volatile salts with mobile phase additives [2]. While the response for analytes with low molecular weight tends to be decreased and non-uniform due to their relatively high volatility, the response for analytes with a molecular mass >300 Da can be regarded as independent of volatility and more uniform [42]. Fig. 6 confirms the positive correlation between molecular weight and CAD response, in case of the homologous fatty acids. As illustrated, the CAD response increases with chain length and thus molecular weight of the fatty acids.

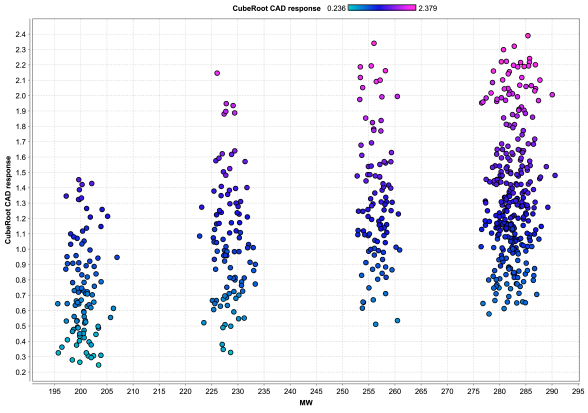

Fig. 6. Effect of the MW of the fatty acids investigated on the CAD response.

RDF080m, the most significant among the utilized descriptors, belongs to the class of Radial Distribution Function (RDF) molecular descriptors. It represents a three-dimensional mass distribution calculated at a radius of 8 Å from the center of a geometrical representation of the molecule. The high importance of this descriptor points out a high contribution of steric factors at the radius of 8 Å from the molecules' geometrical center to the observed response [43]. The different distance of the carboxyl groups from the geometrical center of the molecules investigated is most likely responsible for the distinct differences in CAD response corresponding to the chain length of the fatty acids. The respective distance of the carboxylic group from the geometric center of the fatty acids ranges from 4.77 to 10.52 Å. Stearic acid (C18) with a carboxyl group furthest from the geometric center showed the largest CAD response. It is followed by the response of margaric (C17, 9.36 Å) and palmitic acid (C16, 9.28 Å). The geometric center and its distance (Du) from the carboxyl group are shown exemplarily for myristic acid (C14) in Fig.7.

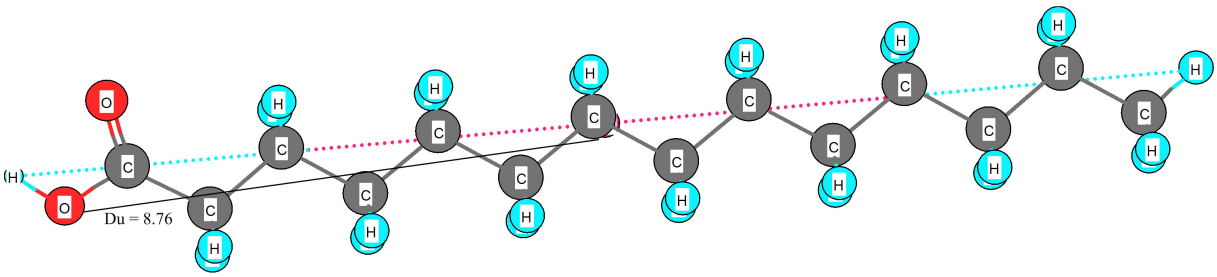

Fig. 7. Geometrical center of the 3D represented myristic acid.

Ve2_D/Dt is categorized as a 2D matrix-based molecular descriptor. Here, it specifically defines the average coefficient of the last eigenvector from a distance/detour matrix. Basically, it indicates that the topological distribution of molecular charge and mass might have some impact on CAD responsiveness [44]. This descriptor negatively affects the intensity of the CAD response, according to graph constructed via GBT (Fig. S3 of the Supplemental Material).

4. Conclusions

The influence of the molecular properties and experimental conditions on the observed CAD response was investigated for a homologous series of fatty acids of varying volatility using a GBT-QSPR approach. The applicability of the QSPR patterns was studied in a 5-dimensional experimental space, comprising PFV (0.8 – 1.6), evaporation temperature (24 ℃ – 48 ℃), flow rate of the mobile phase (0.5 mL/min – 1.5 mL/min), organic solvent (ACN, MeOH, EtOH, acetone), and content of organic solvent in the mobile phase (70% – 90%, v/v).

The reliability of the mixed QSPR model was confirmed by the 10-fold cross-validation and the external validation. The established pattern could explain 99% (Q^2: 0.987, RMSE: 0.051) of the observed variations in CAD responses despite the fatty acids' significant differences in volatility, and, thus, response. Low RMSEP values of 0.050 and high R^2 values of 0.990 for the external validation set confirmed that the developed model was capable to predict the CAD response for previously untested structural homologues with satisfying accuracy.

Though the CAD is often referred to as a detector producing a uniform response, the successfully established mixed model revealed the significance of MW, RDF080m and Ve2_D/Dt molecular descriptors toward the signal's magnitude. The joint importance of molecular weight and evaporation temperature highlighted the dependence of the CAD response on the volatility of the respective analyte. The high impact assigned to the RDF080m descriptor pointed out a significant contribution of steric factors to the generated response. Due to the importance of the Ve2_D/Dt descriptor, the different CAD response for the fatty acids can be partially assigned to versatile topological distribution of charge and mass.

The dependence of the CAD response on the operating conditions was once again confirmed. Thus, an advanced optimization of the corresponding parameters, such as evaporation temperature and flow rate, is highly recommended. Due to the slightly higher CAD responses obtained with acetone in comparison to the ACN, MeOH, and EtOH, its usage in CAD methods could be promising. However, as the elution strength and the background noise also differ among various organic modifiers, more detailed studies concentrated on method development are required to make valid conclusions.

Competing interests

The authors declare no competing interests.

Funding

This work was financially supported by the DAAD PPP Program for Project-Related Personal Exchange with Serbia (project title: Chemometrically supported study of Charged Aerosol Detector responsiveness in pharmaceutical analysis; project ID: 57514777), the Ministry of Education and Science of Germany, and the Ministry of Education and Science of the Republic of Serbia (451-03-68/2020-14/200161).

Acknowledgements

We would like to thank ThermoFisher Scientific (Germering, Germany) for supplying our group with the required instrumentation.

Supplementary material

Table S1. Data table for QSPR model building.

Table S1. is available through Ref [10].

Table S2. Basic statistics of employed features.

Feature/statistics	Min	Max	Mean	Median	First Quartile	Third Quartile
Organic modifier content	75.000	90.000	82.500	82.500	75.000	90.000
Flow rate	0.500	1.500	1.000	1.000	0.500	1.500
Evaporation T	24.000	48.000	36.000	36.000	24.000	48.000
Power f	0.800	1.600	1.200	1.200	0.800	1.600
MW	200.360	284.540	255.470	268.490	228.420	282.520
TIC4	146.692	245.668	191.741	178.274	160.547	240.989
VE2_D/Dt	0.107	0.136	0.118	0.115	0.115	0.117
VE2_B(m)	0.138	0.195	0.170	0.172	0.153	0.190
MATS5m	0.000	0.006	0.003	0.004	0.003	0.004
MATS4v	0.001	0.003	0.002	0.002	0.001	0.003
MATS5v	0.001	0.008	0.003	0.002	0.001	0.003
Eig15_EA(dm)	0.000	0.000	0.000	0.000	0.000	0.000
SPAN	8.800	10.667	9.858	10.087	8.945	10.559
DISPm	13.372	18.961	15.241	14.887	13.492	15.850
DISPv	5.442	7.588	6.923	7.112	6.773	7.510
TDB10m	0.090	0.115	0.106	0.109	0.101	0.114
TDB10v	0.128	0.163	0.151	0.156	0.140	0.162
RDF080m	0.014	1.040	0.498	0.543	0.015	0.832
RDF090m	1.021	3.291	2.285	2.392	1.647	2.970
RDF100m	2.979	7.255	5.352	5.848	3.014	7.166
RDF115m	0.740	2.490	1.476	1.451	0.934	1.788
Mor12u	-2.755	-1.421	-2.075	-2.139	-2.344	-1.653
Mor22u	0.885	1.131	1.021	1.023	0.931	1.131
Mor23u	-2.589	-2.060	-2.342	-2.328	-2.580	-2.170
Mor26u	0.359	0.530	0.467	0.478	0.440	0.514
Mor32u	-0.537	0.283	-0.123	-0.057	-0.486	0.116
Mor10m	0.342	0.749	0.535	0.515	0.489	0.602
Mor15m	-0.002	0.173	0.088	0.086	0.048	0.137
Mor24m	0.070	0.258	0.157	0.149	0.142	0.177
Mor29m	-0.219	-0.081	-0.139	-0.119	-0.202	-0.093
Mor04v	-0.135	1.475	0.490	0.416	0.224	0.546
Mor27v	0.256	0.557	0.480	0.533	0.450	0.554
Mor30v	-0.015	0.086	0.033	0.023	-0.001	0.083
Mor08p	0.014	0.176	0.113	0.132	0.076	0.147
Mor11s	0.312	1.379	0.818	0.758	0.562	1.139
Mor22s	2.261	2.773	2.558	2.566	2.448	2.735
Mor25s	0.673	2.052	1.169	1.101	0.854	1.234
Mor28s	-1.335	-0.925	-1.140	-1.128	-1.321	-1.002
Mor32s	-1.578	-0.438	-0.861	-0.811	-0.844	-0.684
G1m	0.147	0.160	0.153	0.153	0.148	0.159

Table S2. (continued)

G2m	0.169	0.211	0.184	0.181	0.174	0.188
E3m	0.022	0.159	0.075	0.073	0.023	0.104
G2v	0.157	0.200	0.180	0.187	0.163	0.188
G2e	0.156	0.199	0.182	0.182	0.174	0.198
E3e	0.362	0.641	0.480	0.474	0.382	0.549
G2p	0.167	0.310	0.203	0.182	0.174	0.200
G2s	0.148	0.245	0.196	0.203	0.155	0.220
Dv	0.305	0.380	0.337	0.332	0.317	0.357
Dp	0.320	0.387	0.360	0.372	0.335	0.376
Ds	0.472	0.596	0.545	0.548	0.512	0.593
H4u	2.153	3.326	2.717	2.646	2.506	3.023
HATS0v	0.038	0.055	0.047	0.046	0.044	0.052
HATS0p	0.049	0.063	0.056	0.056	0.055	0.060
HATS5p	0.074	0.096	0.084	0.084	0.079	0.086
R1u+	0.079	0.123	0.103	0.102	0.093	0.119
R3u+	0.046	0.061	0.052	0.051	0.048	0.055
R4u+	0.041	0.047	0.045	0.046	0.042	0.046
R5u+	0.022	0.030	0.026	0.027	0.024	0.028
R4m+	0.014	0.017	0.015	0.015	0.014	0.015
R1v+	0.045	0.052	0.049	0.048	0.047	0.052
R1e+	0.099	0.122	0.111	0.114	0.100	0.116
R3e+	0.043	0.063	0.052	0.053	0.049	0.054
R7e+	0.017	0.022	0.019	0.019	0.018	0.019
R1i+	0.116	0.148	0.136	0.140	0.127	0.144

Table S3. The results of 10-fold CV and external validation

	10-fold CV	External validation
RMSE	0.051	
Q^2	0.987	
RMSEP		0.050
R^2		0.990

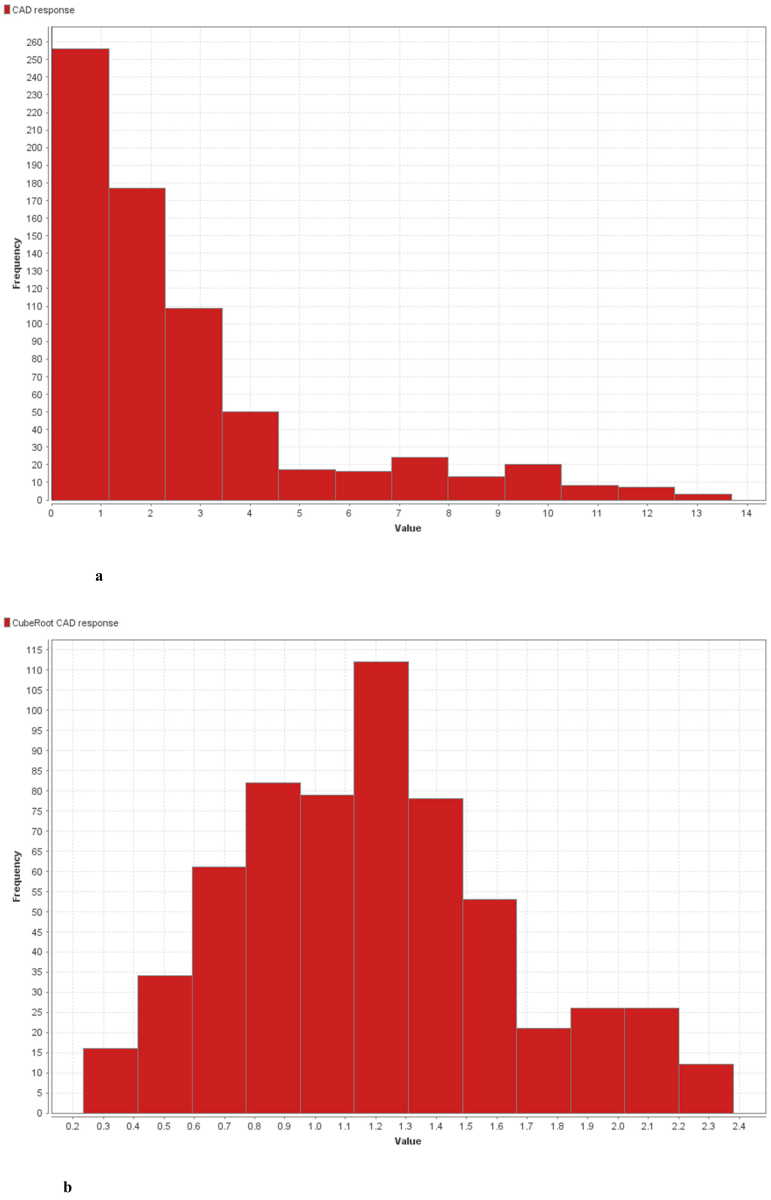

Fig. S1. Distribution of dependent variable a) before cube-root transformation b) after cube-root transformation.

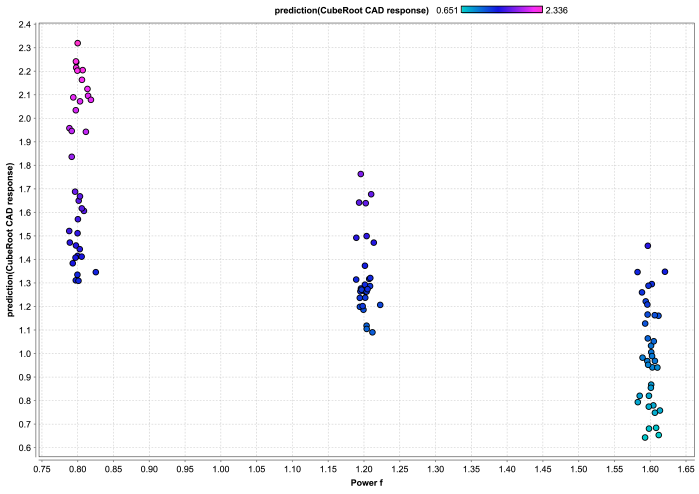

Fig. S2. Graph showing the relationships between the predicted CAD response and the PFV.

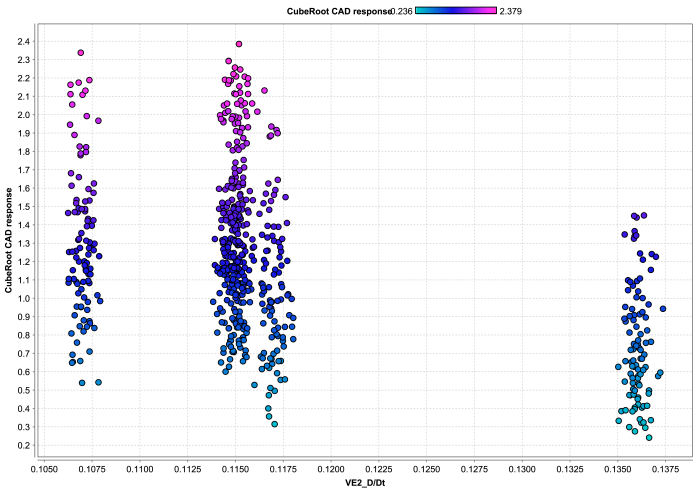

Fig. S3. Graph showing the relationships between the CAD response of fatty acids and the values of Ve2_D/Dt molecular descriptor.

References

[1] L.-E. Magnusson, D.S. Risley, J.A. Koropchak, Aerosol-based detectors for liquid chromatography, J. Chromatogr. A 1421 (2015) 68-81.

[2] P.H. Gamache, Charged aerosol detection for liquid chromatography and related separation techniques, John Wiley & Sons, 2017.

[3] J.P. Hutchinson, J. Li, W. Farrell, E. Groeber, R. Szucs, G. Dicinoski, P.R. Haddad, Comparison of the response of four aerosol detectors used with ultra high pressure liquid chromatography, J. Chromatogr. A 1218(12) (2011) 1646-1655.

[4] N. Vervoort, D. Daemen, G. Török, Performance evaluation of evaporative light scattering detection and charged aerosol detection in reversed phase liquid chromatography, J. Chromatogr. A 1189(1-2) (2008) 92-100.

[5] J. Koropchak, C. Heenan, L. Allen, Direct comparison of evaporative light-scattering and condensation nucleation light-scattering detection for liquid chromatography, J. Chromatogr. A 736(1-2) (1996) 11-19.

[6] T. Gorecki, F. Lynen, R. Szucs, P. Sandra, Universal response in liquid chromatography using charged aerosol detection, Anal. Chem. 78(9) (2006) 3186-3192.

[7] J.P. Hutchinson, J. Li, W. Farrell, E. Groeber, R. Szucs, G. Dicinoski, P.R. Haddad, Universal response model for a corona charged aerosol detector, J. Chromatogr. A 1217(47) (2010) 7418-7427.

[8] K. Schilling, J. Krmar, N. Maljurić, R. Pawellek, A. Protić, U. Holzgrabe, Quantitative structure-property relationship modeling of polar analytes lacking UV chromophores to charged aerosol detector response, Anal. Bioanal. Chem. 411(13) (2019) 2945-2959.

[9] J. Płotka, M. Tobiszewski, A.M. Sulej, M. Kupska, T. Górecki, J. Namieśnik, Green chromatography, J. Chromatogr. A 1307 (2013) 1-20.

[10] R. Pawellek et al., Pawellek_CAD response_ J Chem Inf_Table S1. figshare. Dataset. https://doi.org/10.6084/m9.figshare.14815857.v3.

[11] N. Goudarzi, D. Shahsavani, F. Emadi-Gandaghi, M.A. Chamjangali, Application of random forests method to predict the retention indices of some polycyclic aromatic hydrocarbons, J. Chromatogr. A 1333 (2014) 25-31.

[12] V.A. Dev, M.R. Eden, Gradient Boosted Decision Trees for Lithology Classification, Computer Aided Chemical Engineering, Elsevier, 2019, pp. 113-118.

[13] D.-S. Cao, Q.-S. Xu, Y.-Z. Liang, X. Chen, H.-D. Li, Automatic feature subset selection for decision tree-based ensemble methods in the prediction of bioactivity, Chemom. Intell. Lab. Syst. 103(2) (2010) 129-136.

[14] A.M. Mahmood, N. Satuluri, M.R. Kuppa, An Overview of recent and traditional decision tree classifiers in machine learning, Internat. J. Res. Rev. Ad Hoc Net 1(1) (2011) 2011.

[15] H. Sun, X. Hu, Attribute selection for decision tree learning with class constraint, Chemom. Intell. Lab. Syst. 163 (2017) 16-23.

[16] V. Svetnik, T. Wang, C. Tong, A. Liaw, R.P. Sheridan, Q. Song, Boosting: An ensemble learning tool for compound classification and QSAR modeling, J. Chem. Inf. Model. 45(3) (2005) 786-799.

[17] T. Hancock, R. Put, D. Coomans, Y. Vander Heyden, Y. Everingham, A performance comparison of modern statistical techniques for molecular descriptor selection and retention prediction in chromatographic QSRR studies, Chemom. Intell. Lab. Syst. 76(2) (2005) 185-196.

[18] T. Hastie, R. Tibshirani, J. Friedman, The elements of statistical learning: data mining, inference, and prediction, Springer Science & Business Media, 2009.

[19] P.H. Gamache, R.S. McCarthy, S.M. Freeto, D.J. Asa, M.J. Woodcock, K. Laws, R.O. Cole, HPLC analysis of nonvolatile analytes using charged aerosol detection, Lc Gc Europe 18(6) (2005) 345.

[20] M. Eckardt, M. Kubicova, T.J. Simat, Universal response quantification approach using a Corona Charged Aerosol Detector (CAD)–Application on linear and cyclic oligomers extractable from polycondensate plastics polyesters, polyamides and polyarylsulfones, J. Chromatogr. A 1572 (2018) 187-202.

[21] K. Schilling, R. Pawellek, K. Lovejoy, T. Muellner, U. Holzgrabe, Influence of charged aerosol detector instrument settings on the ultra-high-performance liquid chromatography analysis of fatty acids in polysorbate 80, J. Chromatogr. A 1576 (2018) 58-66.

[22] R. Leardi, Experimental design in chemistry: A tutorial, Anal. Chim. Acta 652(1-2) (2009) 161-172.

[23] B.C. Arnold, R.A. Groeneveld, Measuring skewness with respect to the mode, Am. Stat. 49(1) (1995) 34-38.

[24] M.C. Jones, Families of distributions arising from distributions of order statistics, Test 13(1) (2004) 1-43.

[25] S. Manikandan, Data transformation, J. Pharmacol. Pharmacother. 1(2) (2010) 126.

[26] D.J. Handelsman, Optimal power transformations for analysis of sperm concentration and other semen variables, J. Androl. 23(5) (2002) 629-634.

[27] A.G. O'Keeffe, G. Ambler, J.A. Barber, Sample size calculations based on a difference in medians for positively skewed outcomes in health care studies, BMC Med. Res. Methodol. 17(1) (2017) 1-11.

[28] J. Olivier, W.D. Johnson, G.D. Marshall, The logarithmic transformation and the geometric mean in reporting experimental IgE results: what are they and when and why to use them?, Ann. Allergy Asthma Immunol. 100(4) (2008) 333-337.

[29] N.J. Cox, Stata tip 96: Cube roots, Stata J. 11(1) (2011) 149-154.

[30] J. Čolović, M. Kalinić, A. Vemić, S. Erić, A. Malenović, Investigation into the phenomena affecting the retention behavior of basic analytes in chaotropic chromatography: Joint effects of the most relevant chromatographic factors and analytes' molecular properties, J. Chromatogr. A 1425 (2015) 150-157.

[31] I.Y. Joel, T.O. Adigun, O.O. Bankole, M.A. Iduze, T. AbelJack-Soala, O.G. ANI, E.O. Olapade, F.M. Dada, O.M. Adetiwa, B.E. Ofeniforo, Insights into features and lead optimization of novel type 1½ inhibitors of p38α mitogen-activated protein kinase using QSAR, quantum mechanics, bioisostere replacement and ADMET studies, Results in Chemistry 2 (2020) 100044.

[32] S.J. Haberman, The analysis of residuals in cross-classified tables, Biometrics (1973) 205-220.

[33] J. Krmar, M. Vukićević, A. Kovačević, A. Protić, M. Zečević, B. Otašević, Performance comparison of nonlinear and linear regression algorithms coupled with different attribute selection methods for quantitative structure-retention relationships modelling in micellar liquid chromatography, J. Chromatogr. A 1623 (2020) 461146.

[34] R. Pawellek, T. Muellner, P. Gamache, U. Holzgrabe, Power function setting in charged aerosol detection for the linearization of detector response–optimization strategies and their application, J. Chromatogr. A 1637 (2021) 461844.

[35] I.A.H. Ahmad, A. Blasko, J. Tam, N. Variankaval, H.M. Halsey, R. Hartman, E.L. Regalado, Revealing the inner workings of the power function algorithm in Charged Aerosol Detection: A simple and effective approach to optimizing power function value for quantitative analysis, J. Chromatogr. A 1603 (2019) 1-7.

[36] M. Ligor, S. Studzińska, A. Horna, B. Buszewski, Corona-charged aerosol detection: an analytical approach, Crit. Rev. Anal. Chem. 43(2) (2013) 64-78.

[37] T. Vehovec, A. Obreza, Review of operating principle and applications of the charged aerosol detector, J. Chromatogr. A 1217(10) (2010) 1549-1556.

[38] J.P. Hutchinson, T. Remenyi, P. Nesterenko, W. Farrell, E. Groeber, R. Szucs, G. Dicinoski, P.R. Haddad, Investigation of polar organic solvents compatible with Corona Charged Aerosol Detection and their use for the determination of sugars by hydrophilic interaction liquid chromatography, Anal. Chim. Acta 750 (2012) 199-206.

[39] V. Guarrasi, M. Mangione, V. Sanfratello, V. Martorana, D. Bulone, Quantification of underivatized fatty acids from vegetable oils by HPLC with UV detection, J. Chromatogr. Sci. 48(8) (2010) 663-668.

[40] J.J. Russell, J.C. Heaton, T. Underwood, R. Boughtflower, D.V. McCalley, Performance of charged aerosol detection with hydrophilic interaction chromatography, J. Chromatogr. A 1405 (2015) 72-84.

[41] M.W. Robinson, A.P. Hill, S.A. Readshaw, J.C. Hollerton, R.J. Upton, S.M. Lynn, S.C. Besley, B.J. Boughtflower, Use of calculated physicochemical properties to enhance quantitative response when using charged aerosol detection, Anal. Chem. 89(3) (2017) 1772-1777.

[42] I. Sinclair, R. Gallagher, Charged aerosol detection: factors for consideration in its use as a generic quantitative detector, Chromatogr. Today 1(3) (2008) 5-9.

[43] V. Dobričić, B. Marković, K. Nikolic, V. Savić, S. Vladimirov, O. Čudina, 17β-carboxamide steroids–in vitro prediction of human skin permeability and retention using PAMPA technique, Eur. J. Pharm. Sci. 52 (2014) 95-108.

[44] L. Yang, Y. Wang, W. Hao, J. Chang, Y. Pan, J. Li, H. Wang, Modeling pesticides toxicity to sheepshead minnow using QSAR, Ecotoxicol. Environ. Saf. 193 (2020) 110352.

3.3. Power function setting in charged aerosol detection for the linearization of detector response – optimization strategies and their application

Ruben Pawellek, Tibor Muellner, Paul Gamache, Ulrike Holzgrabe

Reprinted with permission from J. Chromatogr. A 2021, 1637, 461844.

Abstract

Charged aerosol detection (CAD) is a universal technique in liquid chromatography that is increasingly used for the quality control of drugs. Consequently, it has found its way into compendial monographs promoted by its simple and robust application. However, the response of CAD is inherently nonlinear due to its principle of function. Thus, easy and rapid linearization procedures, in particular regarding compendial applications, are highly desirable. One effective approach to linearize the detector's signal makes use of the built-in power function value (PFV) setting of the instrument. The PFV is basically a multiplication factor to the power law exponent of the equation describing the CAD's response, thereby altering the detector's signal output to optimize the quasi-linear range of the response curve. The experimental optimization of the PFV for a series of analytes is a time-consuming process, limiting the practicability of this approach.

Here, two independent approaches for the determination of the optimal PFV based on an empirical model and a mathematical transformation in each case, are evaluated. Both approaches can be utilized to predict the optimal PFV for each analyte solely based on the experimental results of a series of calibration standards obtained at a single PFV. The approaches were applied to the HPLC-UV-CAD impurity analysis of the drug gabapentin to improve the observed nonlinear response of the impurities in the range of interest. The predicted optimal PFV of both approaches were in good agreement with the experimentally obtained optimal PFV of the analytes. As a result, the accuracy of the method was significantly improved when using the optimal PFV (90 – 105% versus 81 – 115% recovery rate for quantitation by either single-point calibration or linear regression) for the majority of the analytes. The final method with a PFV adjusted to 1.30 was validated with respect to ICH guideline Q2(R1).

1. Introduction

The charged aerosol detector was commercially introduced in 2005 [1] as an alternative to other aerosol-based detection techniques in liquid chromatography, e.g. evaporative light scattering detection (ELSD) [2], or condensation nucleation light scattering detection (CNLSD) [3]. With its user-friendly application and a comparatively high reproducibility [4-7], the detector has increasingly found recognition in the field of pharmaceutical quality control [8-13], often replacing low sensitivity methods for the detection of non-chromophoric analytes (detection wavelength <200 nm). Consequently, the CAD has been introduced into the European Pharmacopoeia (Ph. Eur.) for the compendial related substances test of the drugs vigabatrine and topiramate [14, 15]. One drawback of the detection principle that is shared by all aerosol-based detectors, is the inherently nonlinear response. Since data integrity has become an essential element in the highly regulated environment of a quality control lab nowadays, the subsequent transformation of data for linearization purposes can be troublesome, or even prohibited. Thus, the calibration model that accurately describes the response–amount relationship of a certain analyte should preferentially be as simple as possible. A linear response–amount relationship is of particular importance when the quantitation of an analyte is done by means of relative quantitation procedures – as it holds true for the impurity analysis methods of the Ph. Eur. [16]. In many cases, the linearity of the CAD's response is sufficient over the range of interest, as the reported quasi-linear range of the detector has typically a magnitude of 10^2 [17]. However, there may be applications where the response is nonlinear even over a narrow range, especially at the lower end of the investigated mass range.

In particular, a nonlinear response was observed when developing an impurity analysis HPLC-UV-CAD method for the drug gabapentin (Table 1) over a concentration range from 0.03% to 0.24% with respect to the concentration of the main component. With the built-in power function value (PFV) setting of the recent model Vanquish™ Horizon CAD, there is an efficient way to linearize the response of the CAD so that no further data processing is required. The PFV is a correction factor that is applied to the exponent *b* of the equation describing the CAD's signal generation (Eq. 1) [17]. Linear response can be assumed when *b* = 1.0.

$$A = a(\mathrm{m_{inj}})^b \tag{1}$$

with *A* being the peak area, *a* being an analyte specific sensitivity coefficient, and $\mathrm{m_{inj}}$ is the injected mass. For *b* >1, a supralinear response is observed, whereas *b* <1 indicates sublinear response of the detector. Since the response of the recent CAD models is sublinear over almost their entire dynamic range [17], PFV >1 are usually applied to shift the response curve to more linear regions. However, there may be cases where a PFV <1 can be beneficial to linearize the response, e.g. semivolatile compounds that show supralinear response at the low mass range. The most evident approach to determine the optimal PFV for a particular analyte

is to conduct a series of linearity experiments at various PFV. The feasibility of this approach is albeit limited by its time-consuming execution and the inaccurate results when not investigating sufficiently narrow PFV ranges. Another approach for the optimization of the PFV is based on an empirically derived equation predicting the CAD's response at any PFV as proposed by Ahmad et al. [18] to linearize response for the antibiotic amikacin and the lysophosphatidylcholine 1-stearoyl-sn-glycero-3-phosphocholine, each of which were analyzed by different chromatographic methods. Assuming the general validity of the equation, the established constants can be used to estimate the response for any analyte at any PFV and any chromatographic method, enabling the subsequent evaluation of linearity. This approach is elucidated in more detail in section 3.1. Besides the aforementioned optimization strategies, there is also one based on a mathematical transformation. The CAD's signal can be subsequently modified by a feature of the Chromeleon™ software (Thermo Fisher Scientific), allowing for the interpretation of the linearity data at various PFV.

In this work, the two independent PFV optimization approaches described above were used to predict the optimal PFV for the impurities of gabapentin. The empirical approach of Ahmad et al. was validated on the most recent CAD model with data originated from a previously published method for the quantitation of fatty acids in polysorbate [19] and extended by its application to semivolatile analytes. Alternatively, the mathematical transformation approach was evaluated. The results of the two approaches were then compared to the experimentally obtained optimal PFV. To illustrate the benefit of an optimized PFV setting for the impurity analysis of gabapentin, the accuracy of a method with optimized PFV was compared to a method with a default PFV setting using either the compendial-favored single-point calibration or by linear regression for the quantitation of the impurities. The method containing the optimized PFV as indicated by both optimization approaches was validated with respect to ICH guideline Q2(R1) [20]. All compendial impurities [21] were separated and quantified in one chromatographic run using a C8 reversed phase column and UV-CAD detection.

Table 1. Impurity profile of gabapentin as depicted in the Ph. Eur. [21].

Gabapentin [1-(aminomethyl)cyclohexyl]acetic acid	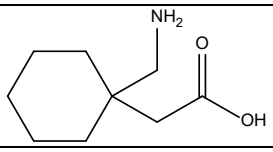
Impurity A (reaction product) 2-azaspiro[4.5]decan-3-one	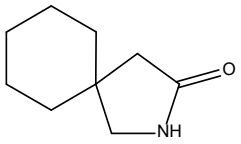
Impurity B (synthesis by-product) (1-cyanocyclohexyl)acetic acid	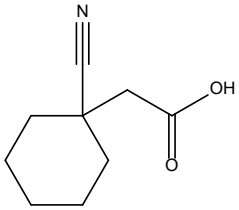
Impurity D (synthesis by-product) [1-[(3-oxo-2-azaspiro[4.5]dec-2- yl)methyl] cyclohexyl]-acetic acid	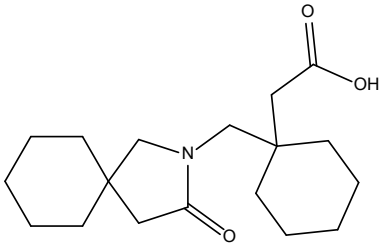
Impurity E (reaction product) 1-(carboxymethyl)cyclohexanecarboxylic acid	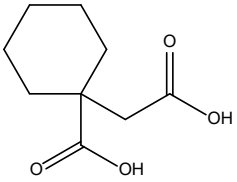
Impurity G (synthesis by-product) [1-(2-aminoethyl)cyclohexyl]acetic acid	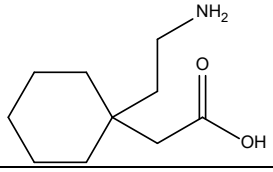

2. Experimental

2.1. Chemicals and reagents

Reference standards of the gabapentin impurities A, B, and D were obtained from the European Directorate for the Quality of Medicines & HealthCare (EDQM; Straßbourg, France), whereas the standards of the impurities E and G were purchased from Enamine (Riga, Latvia). The gabapentin samples were available from Polpharma (Warsaw, Poland), ammonium formate, formic acid, and the fatty acid standards from Sigma Aldrich (Steinheim, Germany). Ultra-pure deionized (DI) water was delivered by a Milli-Q® system (Merck, Darmstadt, Germany). HPLC grade acetonitrile (ACN) was supplied from Sigma Aldrich.

2.2. Apparatus

The HPLC experiments were performed on a Vanquish™ Flex modular chromatographic system (Thermo Fisher Scientific, Germering, Germany) consisting of a binary pump with online degasser, a thermostatted split sampler, a thermostatted column compartment with passive pre-heater, and a variable wavelength detector in-line with a Vanquish™ Horizon CAD. The CAD was supplied with nitrogen gas from an ESA nitrogen generator (Thermo Fisher Scientific) connected to the in-house compressed air system. The instrument was controlled and runs were processed using the Chromeleon® Chromatography Data System Version 7.2.6 software program (Thermo Fisher Scientific).

2.3. Chromatographic procedures

2.3.1. Fatty acid method [19]

For the fatty acid method, a flow rate of 0.8 mL/min, a column temperature of 25 °C (run in still air mode), and an injection volume of 10 µL were applied. The fatty acids were separated on a C18 coreshell Kinetex column (100 x 2.1 mm, 2.6 µm) (Phenomenex, Aschaffenburg, Germany) using gradient elution. Mobile phase A consisted of an aqueous 0.05% (v/v) formic acid solution, whereas mobile phase B was acetonitrile with addition of 0.05% (v/v) formic acid. The gradient program started at 75% B from 0 to 0.8 min, linearly increased to 85% B within 1.7 min and maintained at 85% B for 0.5 min, followed by a re-equilibration back to 75% B within 0.5 min and a 1 min hold, resulting in a total run time of 4.5 min. The fatty acids were detected by CAD using an evaporation temperature of 35 °C, a filter constant of 1 s, a data collection rate of 10 Hz, and various power function values ranging from 0.80 to 1.60.

2.3.2. Gabapentin method

The gabapentin method comprised a flow rate of 1.2 mL/min, a column temperature of 25 °C (run in still air mode), and an injection volume of 20 µL. The separation of gabapentin and its impurities was accomplished by a reversed phase C8 Agilent Zorbax-SB column (250 x 4.6 mm, 5 µm) (Waldbronn, Germany) using gradient elution. Mobile phase A consisted of 20 mM ammonium formate in DI water adjusted to pH 2.8 with formic acid. Mobile phase B contained a 20 mM ammonium formate buffer pH 2.8 in a mixture of 90% ACN and 10% DI water (v/v). The gradient program started with an isocratic step of 25% B for the first min, followed by a linear increase from 25% to 60% B in the next 4 min, a hold of 60% B from min 5 to 11, and a re-equilibration step between min 11 and 12 from 60% to 25% B and a 25% B hold for 3 min resulting in a total run time of 15 min. The detector settings for the CAD were as follows: evaporation temperature 30 °C, filter constant 5 s, data collection rate 10 Hz, and a power function value of 1.30. UV detection was performed with a data collection rate of 20 Hz and a detection wavelength of 210 nm.

2.4. Preparation of solutions

2.4.1. Standard solutions

Stock solutions of the fatty acid standards were prepared by weighing 10.0 mg of the fatty acid and dissolving in methanol. The stock solutions were stored in a freezer at −20 °C and diluted with a mixture of acetonitrile 75% and water 25% (v/v) to the appropriate concentration.
Stock solutions of the gabapentin impurity standards A, E, and G were prepared by weighing 1.0 mg of the impurity and dissolving in 10.0 mL DI water. The stock solutions were used as calibration or external standards and for spiking of the sample solutions by appropriate dilution with mobile phase A. They were stored at 8 °C. For the stock solutions of gabapentin impurities B and D, 1.0 mg of the respective impurity was weighed and dissolved in 10.0 mL methanol. The stock solution of impurity B was stored at -20 °C and at 8 °C in case of impurity D.

2.4.2. Sample solutions

The sample solutions were freshly prepared on a daily basis by weighing 80 mg of gabapentin and dissolving in 10.0 mL mobile phase A. The sample solutions were stable for at least one day at room temperature.

3. Processing of the calibration data

3.1. Empirical PFV optimization approach

This approach is based on Eq. 2 introduced by Ahmad et al. [18] that describes the PFV dependency of the CAD's response using a PFV correction constant, *y*, and another constant, *a*. The constants follow a trend with increasing PFV, which enables the prediction of the response of a particular analyte at any given PFV based on the peak area response obtained at PFV = 1.0.

$$(\text{area}_{\text{PFV}=x}) = a \times (\text{area}_{\text{PFV}=1})^{x+y} \quad (2)$$

with *a, y* being two PFV-dependent constants and *x* being a particular PFV. The *a* and *y* constants for an analyte can be modeled by the Excel add-in Microsoft Solver™. For this purpose, the Microsoft Solver™ settings were adjusted to minimize the difference between the observed experimental response factors (area/concentration) at a particular PFV and the calculated response factors obtained from the Eq. 2 with the PFV-dependent *a* and *y* constants for a series of calibration standards. An example of the Excel template used for the modeling is given in Table 2. The Solver parameters were set with the objective to minimize the average ($|\Delta RF|/\text{RF}_{\text{calculated}} \times 100$) across the calibration levels by altering two variable cells representing the *a* and *y* constants, respectively. The constants derived from the modeling were then applied to calculate the peak areas and, subsequently, the response factors for the calibration standards of the gabapentin impurities based on the peak areas obtained for the impurities at

PFV = 1.00. To assess the quality of fit for each PFV, the RSD of the resulting response factors across the investigated range was evaluated. Moreover, the residual plots and the coefficients of determination (R^2) obtained by linear regression of the predicted calibration points were examined to enable a meaningful comparison of the prediction results to the mathematical approach. Complete workflows from constant modeling to the prediction of the optimal PFV are illustrated in detail in the supplementary material.

Table 2. Example of the constant modeling by Microsoft Solver for myristic acid at PFV = 1.20 based on the response factors RF (concentration/peak area).

Concentration	Peak area (PFV=1.00)	Peak area (PFV=1.20)		RF (PFV=1.20)		$\frac{\lvert\Delta RF\rvert}{RF_{calc.}} \times 100$
	exp.[a]	exp.	calc.[b]	exp.	calc.	
0.01	0.007	0.002	0.002	0.22	0.21	5.06×10^{-5}
0.25	0.197	0.079	0.084	0.32	0.33	5.64
0.50	0.425	0.189	0.198	0.38	0.40	4.34
0.75	0.690	0.340	0.340	0.45	0.45	1.49×10^{-4}
1.00	0.936	0.498	0.478	0.50	0.48	4.23
						2.85[c]
	optimized constants	$a \rightarrow$	0.51			
		$y \rightarrow$	-0.082			

[a] Experimentally obtained value.

[b] Calculated value based on Eq. 2.

[c] The average of the $\frac{\lvert\Delta RF\rvert}{RF_{calc.}} \times 100$ across the concentration range.

3.2. Mathematical PFV optimization approach

For the mathematical PFV optimization approach, a feature of the proprietary Chromeleon™ software was used to transform the original calibration data of the gabapentin impurities obtained at PFV = 1.00. By this approach, the software creates a new signal channel where a certain power factor that corresponds to the PFV has already been applied to the original chromatogram (Fig. 1). The algorithm for the Chromeleon transformation is simply pA^{PF} where each data point within a chromatogram in pA units is raised to a user-selected power factor (PF). The resulting chromatogram is output to a new channel. Further details are provided in [22]. The applied power factor can be varied in increments of 0.05. The resulting chromatograms with transformed CAD signal were subsequently evaluated as calibration standards in terms of linearity. To assess the quality of fit at the respective applied power factor, the R^2 obtained by linear regression as well as the RSD of the response factors across the concentration range and the residual plots of the resulting calibration data points were examined as illustrated in section 4.1.2.2.

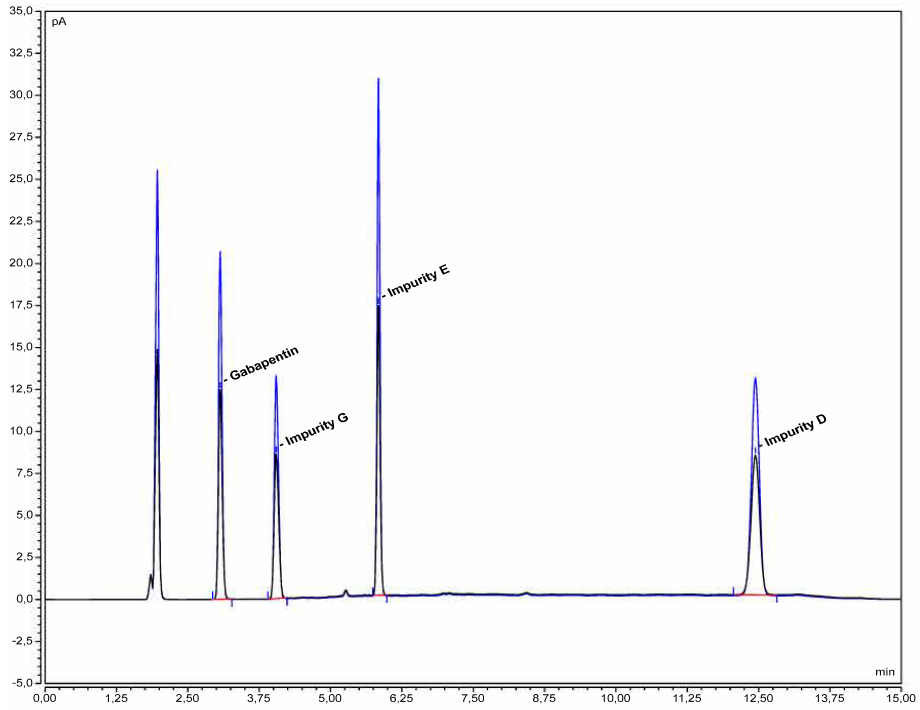

Fig. 1. Overlay of a chromatogram for a 0.1% solution of gabapentin and its nonvolatile impurities at PFV = 1.00 and the modified chromatogram after applying a power factor of 1.20 (blue trace). The PFV of impurity B was optimized separately due to its possible hydrolysis to impurity E.

4. Results and discussion

4.1. Gabapentin method development

4.1.1. Optimization of the chromatographic conditions other than PFV

The anticonvulsant gabapentin is a γ-aminobutyric acid derivative; therefore, it is weakly retained on any reversed phase HPLC column. Its impurities, however, mostly lack of the partial amino acid structure, thus they can be separated on C18, C8, biphenyl, and CN stationary phases due to their moderate polarity [23-25]. One particular challenge regarding the detection of gabapentin and most of its impurities, is the absence of a suitable chromophore (Table 1) that causes the relatively low sensitivity of the reported UV methods [24, 25]. To improve the sensitivity for the weakly-chromophoric impurities, a HPLC method using in-line UV-CAD detection was developed instead. Reversed phase columns of different hydrophobicity (C18, C8, and Phenyl) were tested for their selectivity towards gabapentin and its impurities. A C8 Agilent Zorbax-SB column was then chosen for the further method development, since it provided the best resolution of all components and appropriate peak shape for the analytes using an ammonium formate buffer in a mixture of DI water and ACN as mobile phase. The pH of the ammonium formate buffer was adjusted to 2.8 to suppress the ionization of the acidic analytes (pKa_{COOH} = 3.7). However, the nitrile group of gabapentin impurity B is likely to hydrolyse in acidic medium, resulting in the formation of impurity E. Thus,

the linearity experiments described below were performed separately for impurity B. Mobile phase A was an aqueous 20 mM ammonium formate buffer pH 2.8, whereas mobile phase B also consisted of a 20 mM ammonium formate buffer pH 2.8 in a mixture of DI water and ACN 10/90 (v/v). To facilitate the quantitation of all compendial impurities in one chromatographic run, a gradient program was applied as stated in section 2.3.2. For the simultaneous detection of all compendial impurities in gabapentin (Table 1), UV and charged aerosol detectors were coupled in-line to cover the weak-chromophoric (B, E, G) as well as the volatile impurities (impurity A). The evaporation temperature setting of the CAD was adjusted to 30 °C to improve the limit of quantitation (LOQ) of the semivolatile impurity B. In contrast to a previously published CAD method [23], impurity A could not be sensitively detected by CAD due to its high volatility. Its chromophore, however, enabled UV detection at 210 nm. The UV-active impurity D was also measured by CAD, since the CAD's baseline was less affected by the applied gradient elution.

4.1.2. Optimization of the PFV

Although the R^2 values of the impurity calibration curves obtained from linear regression at a default PFV of 1.00 suggested a good quality of fit (R^2 >0.995) in the investigated range (0.03% – 0.24%), the residuals plots for each impurity showed a bias. In addition, the relative standard deviation (RSD) of the response factors (peak area/amount) was high across the 6 investigated concentration levels for all impurities (RSD ≥8.2%). As a consequence, the recovery rates of the spiked impurities deviated by more than 10% when using either single-point quantitation relative to a 0.1% solution of the impurity or by the above-described linear regression with greatest deviation at the lower end of the examined range. To address this unsatisfactory result, two independent PFV optimization approaches were evaluated with the objective to improve the accuracy of the method when using external standard quantitation.

4.1.2.1. Empirical approach using the constants a and y

Ahmad et al. [18] introduced an empirically derived equation (Eq. 2) to calculate the CAD's response at any PFV from the response obtained at PFV = 1.00. This approach is based on the assumption that the two constants of the equation modeled by the Excel tool Microsoft Solver™ as stated in section 3.1. follow a consistent trend as a function of PFV. With known values for the PFV-dependent *a* and *y* constants, the response of a particular calibration standard obtained at PFV = 1.00 can be used to predict the standard's response at any PFV. The optimal PFV was then determined by comparing of the RSD of the resulting response factors across the investigated concentration levels. When assuming the universal validity of the proposed equation, the constants derived from a certain analyte should allow for the prediction of the response of all other analytes at any concentration range. Ahmad et al. described excellent correlation between experimental data and calculated results for two

analytes measured at various concentrations on different systems and using different chromatographic methods. In his study, the robustness of this modeling approach to different instrumentation and experimental conditions was further studied on the Vanquish™ Horizon CAD by application to a previously published analytical method for the determination of fatty acids in polysorbate [19] as described in section 2.2.1. The *a* and *y* constants were modeled as depicted in section 3.1 using Microsoft Solver™ for the fatty acids myristic acid, palmitic acid, stearic acid, and oleic acid over a mass range of 10 ng to 1000 ng on column applying PFV between 0.80 and 1.60 based on the original calibration data obtained at PFV 1.00. The *a* constants followed an exponential trend (R^2 >0.98), whereas the trend for the *y* values was linear (R^2 >0.94) (Fig. 2). The two modeled constants of each fatty acid were then used to predict the CAD's response for the gabapentin impurities B, D, E, and G, respectively, at PFV ranging from 0.80 to 1.60 based on the calibration data obtained at PFV 1.00. The quality of fit for calibration at each PFV was evaluated by comparing the RSD of the resulting response factors across the concentration levels in each case (Fig. 3).

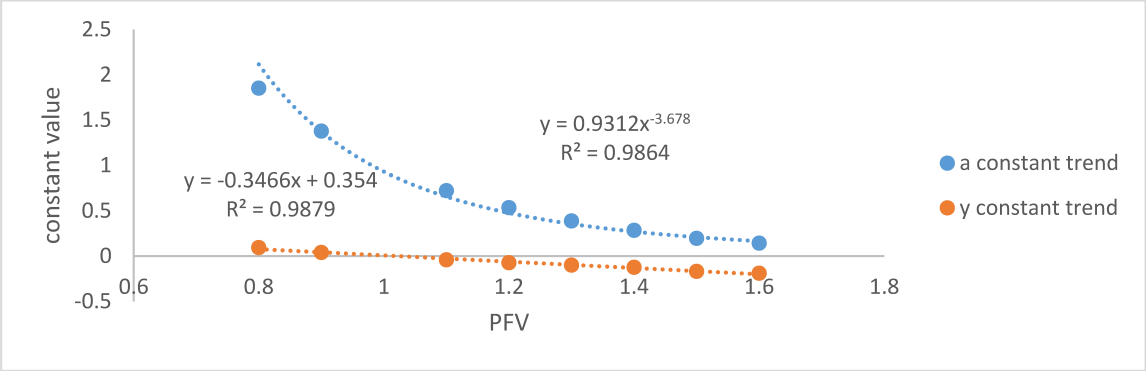

Fig. 2. Trend for the a and y constants modeled for palmitic acid across the investigated PFV range.

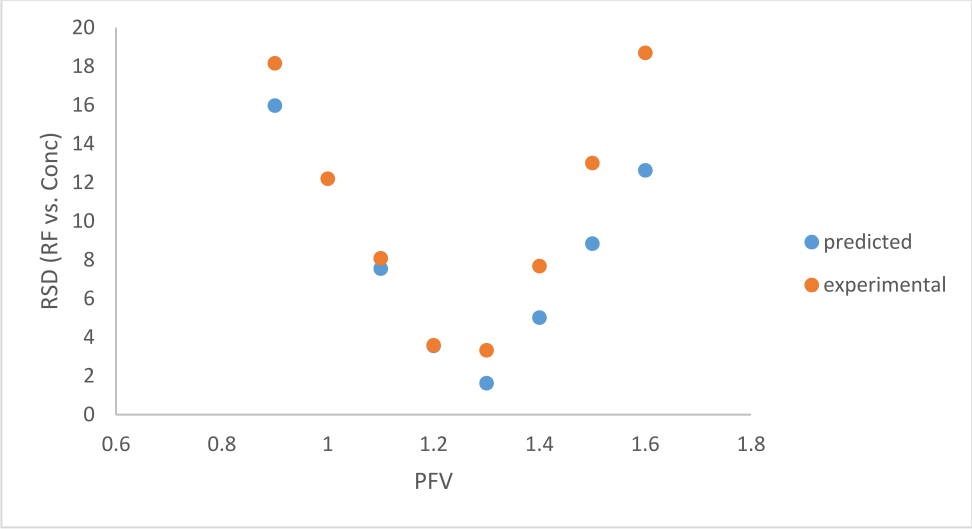

Fig. 3. Comparison of the experimental optimal PFV for gabapentin to the one predicted by the constant modeling of palmitic acid based on the RSD of the response factors across the concentration range.

The predicted optimal PFV were in a narrow range when using the constants obtained from the nonvolatile fatty acids palmitic acid, stearic acid, and oleic acid, respectively (Table 3). For the semivolatile myristic acid, however, the predicted optimal PFV were slightly higher due to the higher values of the slope and y-intercept of the *y* constant's equation. Unlike the sublinear nonvolatile gabapentin impurities (D, E, G), the semivolatile impurity B showed supralinear response in the investigated range. Thus, the predicted optimal PFV was <1 in contrast to the other impurities. To confirm the consistency of the prediction results of this approach, the *a* and *y* constants were also modeled for the gabapentin impurities B, G, and for gabapentin itself over a mass range between 50 ng and 400 ng on column at PFV 0.80 to 1.60. The constants equations followed the same trend as stated above and the gabapentin impurity derived predicted optimal PFV were in good agreement with the fatty acid derived optimal PFV (Table 3).

Table 3. Optimal PFV prediction results for the empirical approach based on the %RSD of the response factors across the concentration range at each PFV.

Constants derived from	Predicted optimal PFV				
Compound	Gabapentin	Impurity B	Impurity D	Impurity E	Impurity G
Palmitic acid	1.28	0.83	1.18	1.23	1.25
Stearic acid	1.27	0.88	1.18	1.22	1.24
Oleic acid	1.26	0.86	1.18	1.21	1.23
Gabapentin	1.23	0.90	1.16	1.19	1.21
Gabapentin impurity G	1.25	0.86	1.17	1.21	1.23
average	1.26	0.87	1.17	1.21	1.23
%RSD	1.37	2.69	0.68	1.09	1.08
experimental[a]	1.25	0.80	n.d.[b]	n.d.	1.22
mathematical approach[a]	1.22	0.77	1.17	1.19	1.20
Semivolatile compounds					
Myristic acid	1.35	0.78	1.23	1.28	1.31
Gabapentin impurity B	1.37	0.83	1.26	1.31	1.33

[a] The optimal PFV were estimated from the %RSD of the response factors across the investigated range at each PFV.

[b] Not determined.

Interestingly, deviations in the predicted optimal PFV observed for the semivolatile myristic acid before in the fatty acid method also occurred for the semivolatile impurity B in the gabapentin method. This result indicates that lower accuracy may be obtained when using the constants derived from a nonvolatile analyte to predict the optimal PFV for a semivolatile analyte and *vice versa*. The higher response curve variability of semivolatile analytes thus limits the general applicability of this approach primarily to analytes that behave as nonvolatiles. The prediction accuracy was excellent (RSD ≤2.69%, n = 5) when comparing the predicted optimal PFV derived from the constants of the nonvolatile fatty acids to those derived from the nonvolatile gabapentin impurities (Table 3). Our studies included experimental generation of response curves for certain gabapentin impurities at different PFV settings

ranging from 0.80 to 1.60. This allowed direct comparison of optimal PFV obtained experimentally to those predicted by the described model (Fig. 3). The predicted and experimentally obtained optimal PFV were in good agreement, further supporting the validity of the predictive model (Table 3). Visual inspection of the resulting residual plots also confirmed the consistency and accuracy of the model, since the indicated optimal PFV was between 1.25 and 1.30 for each nonvolatile analyte when comparing the modeled with the experimental results, while the optimal PFV determined for the semivolatile impurity B between PFV 0.80 and 0.90. The R^2 results tended to support the residual plot observations, however, the global maxima were not always distinguishable and residual plots are generally regarded as a more robust parameter for the assessment of the quality of fit.

4.1.2.2. Mathematical transformation approach using the Chromeleon™ software

For the second approach, the calibration data obtained at PFV = 1.00 for the gabapentin impurities (mass range: 50 – 400 ng on column) were transformed by the Chromeleon™ software applying power factors from 0.80 to 1.40 in 0.05 increments. A new signal channel was generated for each power factor, enabling the parallel assessment of linearity. The resulting chromatograms were evaluated in terms of linearity by plotting the calibration curves and the residual plots. The coefficients of determination (R^2) obtained from linear regression of the calibration curves were then plotted versus the corresponding PFV. The optimal PFV was indicated by the maximum of the resulting graph (Fig. 4).

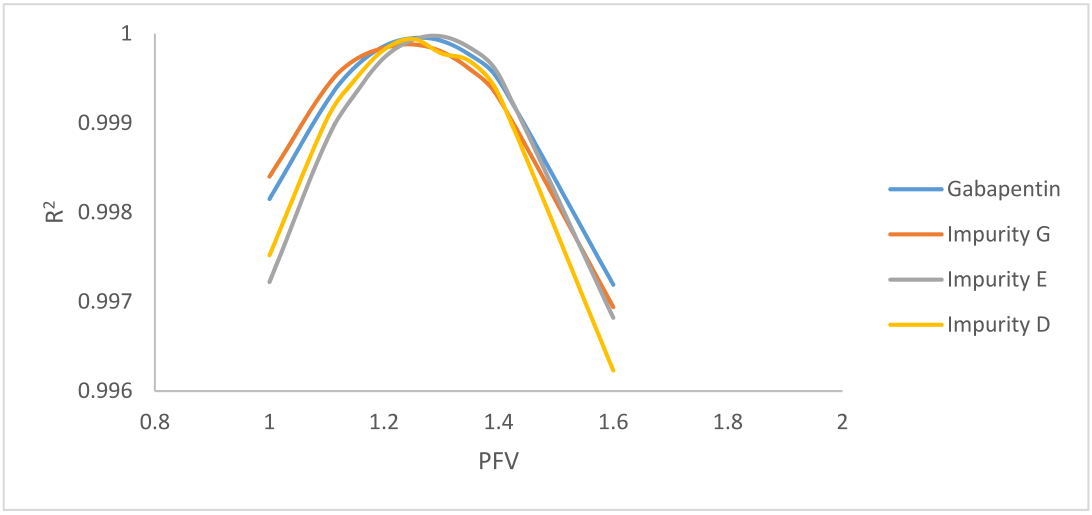

Fig. 4. Prediction of the optimal PFV for gabapentin and its impurities based on the R2 values obtained for the applied power factors.

In addition, the quality of fit was evaluated by visual inspection of the respective residual plot that illustrates the relative deviation (%) of a particular calibration point against the amount of the analyte. At the optimal PFV, the calibration points are expected to be evenly distributed around the 0% error line (Fig. 5).

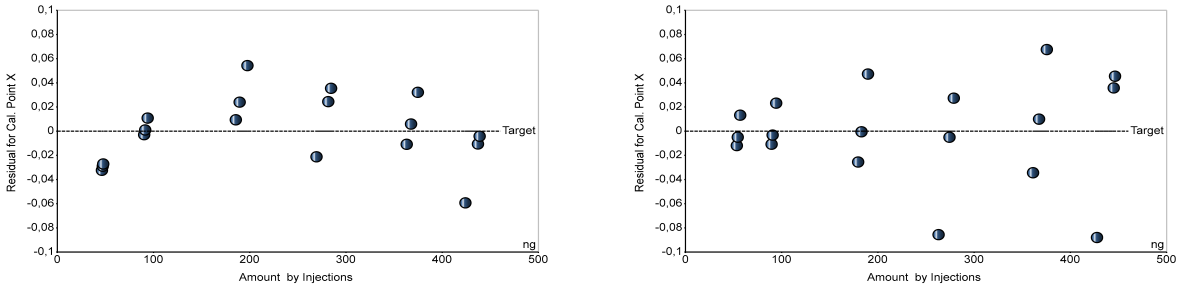

Fig. 5. Residual plot for gabapentin impurity G at PFV = 1.00 (left) and the residual plot with an applied power factor of 1.25 (right).

The indicated optimal PFV were in excellent agreement with the previous approach for all nonvolatile impurities when either applying the residual plots (optimal PFV 1.25 - 1.30), or the RSD of the response factors across the investigated range (Table 3) as parameter for the assessment of the quality of fit. In case of the semivolatile impurity B, the residual plot indicated an optimal PFV of 0.80, also corresponding to the empirical approach, whereas the R^2 optimization did not indicate a distinct maximum.

4.1.3. Comparison of the accuracy of the PFV optimized method to the default method

To demonstrate the benefit of a PFV adjusted method, the accuracy for the quantitation of the gabapentin impurities in the required range (0.03% - 0.24%) was evaluated at PFV = 1.00, 1.20, and 1.30, since the predicted optimal PFV of both approaches were in a range from 1.20 to 1.30 for the majority of the impurities. Sample solutions of gabapentin were spiked with 0.03%, 0.1%, and 0.2% of each impurity with respect to the concentration of the main component to cover the range between the reporting limit and the specification limit of an intended compendial method. The recovery rates of the spiked impurities were determined by means of linear regression of the established calibration curves as well as by using a 0.1% solution of the respective impurity as external standard for single-point calibration. The results of both quantitation procedures are depicted in Table 4.

When a PFV of either 1.20 or 1.30 was applied, the recovery rates of all nonvolatile impurities were substantially improved at the lower level for both quantitation procedures, and at the upper level in case of single-point calibration, compared to the default PFV setting of 1.00. The deviations in the recovery rates of both optimized PFV methods were comparable, however, the method with PFV = 1.20 performed slightly better for single-point calibration, whereas the quantitation by linear regression was more accurate at PFV = 1.30. These results confirm the validity of the prediction approaches, since they are in good agreement with the respective parameter applied for the linearity evaluation.

Table 4. Recovery rates (%) for the gabapentin impurities detected by CAD calculated by either linear regression or single-point calibration at PFV = 1.00, 1.20, and 1.30, respectively (n=3).

Quantitation	Concentration	PFV	Recovery rate [%]			
			Impurity B	Impurity D	Impurity E	Impurity G
Single-point calibration	0.03%	1.00	103 (±5.7)[a]	115 (±2.9)	114 (±2.3)	114 (±2.5)
		1.20	n.d.[b]	89	100	103
		1.30	65 (±8.6)	90 (±1.1)	93 (±4.0)	95 (±2.1)
	0.10%	1.00	101 (±5.8)	100 (±0.6)	100 (±1.1)	101 (±2.0)
		1.20	n.d.	103	104	101
		1.30	101 (±7.2)	101 (±1.8)	101 (±2.3)	99 (±1.0)
	0.20%	1.00	109 (±6.7)	87 (±0.8)	90 (±0.7)	93 (±0.8)
		1.20	n.d.	100	100	95
		1.30	138 (±8.3)	104 (±1.6)	102 (±2.3)	103 (±1.4)
Linear regression	0.03%	1.00	108 (±4.6)	93 (±3.6)	85 (±2.8)	81 (±3.2)
		1.20	n.d.	97	98	91
		1.30	98 (±6.5)	102 (±1.1)	105 (±3.9)	98 (±2.0)
	0.10%	1.00	88 (±4.6)	109 (±0.7)	108 (±1.3)	104 (±2.3)
		1.20	n.d.	103	102	102
		1.30	93 (±5.6)	102 (±1.7)	103 (±2.2)	97 (±1.0)
	0.20%	1.00	90 (±5.3)	99 (±1.0)	103 (±1.0)	103 (±0.9)
		1.20	n.d.	99	99	100
		1.30	112 (±6.3)	102 (±1.5)	101 (±2.2)	99 (±1.3)

[a] The 95% confidence interval for the recovery rates at PFV 1.00 and 1.30 that were subjected to statistical analysis is given in brackets for each level.

[b] Not determined.

The recovery rates of the semivolatile gabapentin impurity B, however, were negatively affected by the application of a PFV >1.00 due to the supralinear response of the analyte in the investigated range. A PFV of 0.80, as indicated by the optimization approaches, also did not improve the recovery rate results compared to a PFV of 1.00. To allow for the simultaneous quantitation of the nonvolatile impurities and impurity B with an applied PFV of 1.30, impurity B should preferentially be quantified by means of linear regression, since the recovery rates obtained from this procedure were satisfactory (93% - 112%). A PFV of 1.30 was finally chosen for the method validation due to the best overall accuracy of the setting with deviations of ≤ ±10% for the recovery rates of the nonvolatile impurities. To test for the statistical significance of the improvement in the recovery rates between the default method (PFV = 1.00) and a method with PFV 1.30, two-tailed F-tests, followed by left-tailed Student's t-tests ($\alpha = 0.05$) with either equal or unequal variances, were performed for the mean absolute errors in the recovery rates. This was done at the 0.03% level for both single-point and linear regression calibration and at the 0.2% level for single-point calibration where differences were most pronounced. With exception of the recovery results for impurity B, the mean absolute error of the PFV = 1.30 method was found to be significantly reduced for each tested level and quantitation procedure with $P(T \leq t) < 0.05$ (data not shown). In case of impurity B, both methods

performed not significantly different for quantitation by linear regression, but the default method performed better for single-point calibration.

4.2. Gabapentin method validation

The final method for the impurity analysis of gabapentin with a PFV setting adjusted to 1.30, as indicated by both optimization approaches, was validated with respect to the requirements outlined in ICH guideline Q2(R1) [20].

The *specificity* of the method was demonstrated by visual inspection of a chromatogram of a gabapentin sample solution (8 mg/mL) spiked with 0.1% of each impurity (Fig. 6). Baseline separation of gabapentin and all of its potential impurities was achieved with resolutions >1.5. The CAD signal was used for the identification of the gabapentin impurities B, D, E, and G, whereas impurity A was detected by UV.

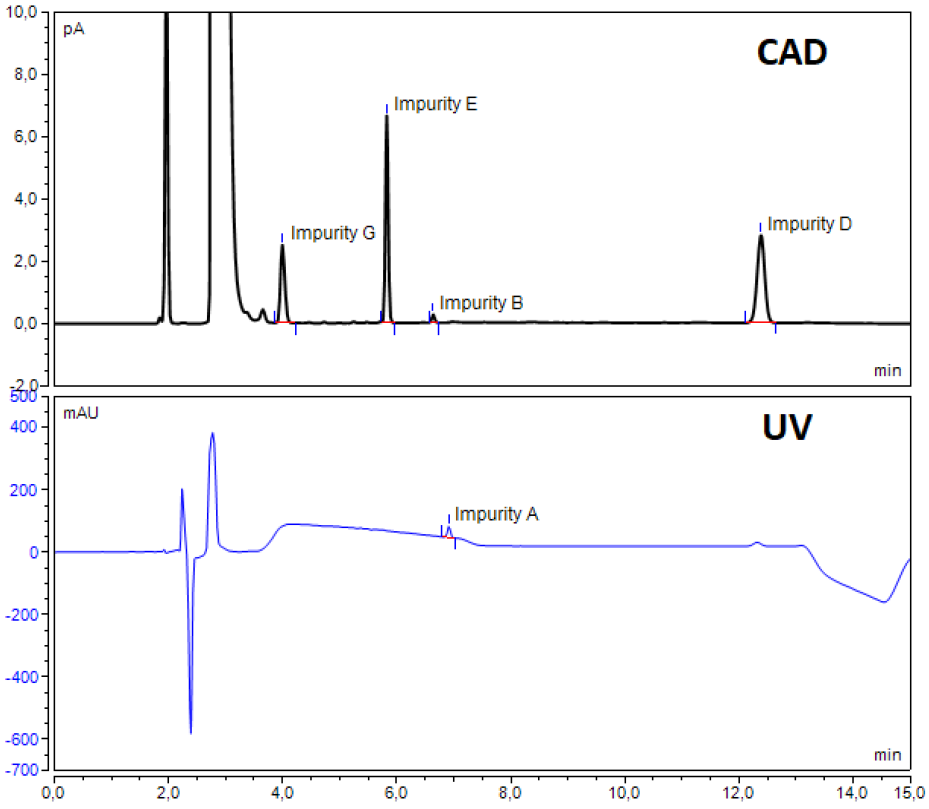

Fig. 6. Chromatogram of a gabapentin sample solution (8 mg/mL) spiked with 0.1% of each impurity. Impurity A is detected by UV.

A *range* between 0.03% and 0.24% with respect to the concentration of the sample solution was chosen for the demonstration of linearity to cover the compendial reporting threshold for a drug with an average daily intake >2 g [26] as the lower limit as well as 120% of the compendial specification limit as the upper limit.

The *linearity* of the method was evaluated across the investigated range by means of linear regression as well as by visual inspection of the residual plots of the calibration points. With R^2 >0.9993 for each impurity (Table 5) and evenly scattered calibration points around the 0% error line in the residual plots, the linearity can be regarded as sufficient for the intended purpose.

Table 5. Validation results of the gabapentin method.

Parameter	Condition	Gaba-pentin	Impurity A[a]	Impurity B	Impurity D	Impurity E	Impurity G
Linearity	Equation[b]	0.0017x	0.0064x	0.00017x	0.0024x	0.0021x	0.0013x
	y = mx + t	- 0.0032	- 0.0145	- 0.0041	- 0.0213	- 0.0164	- 0.0052
	R^2	0.9995	0.9996	0.9993	0.9999	0.9995	0.9996
	SD slope	1.8×10^{-5}	6.5×10^{-5}	2.3×10^{-6}	1.3×10^{-5}	2.4×10^{-5}	1.2×10^{-5}
	SD intercept	0.0048	0.018	0.00057	0.0034	0.0065	0.0033
LOQ	Injected mass (ng)	3	50	50	4	2	3
	S/N (n = 6)	15.5	15.7	15.5	15.5	15.0	14.3
LOD	Injected mass (ng)	1	n.d.[c]	n.d.	2	1	1
	S/N (n = 6)	4.3	-	-	6.6	6.7	3.3
Intra- and (Interday) Repeatability	0.03%, n=6 (2)	n.d.	2.7 (3.8)	8.4 (8.2)	2.1 (1.9)	3.1 (2.8)	2.2 (4.7)
	0.10%, n=6 (2)	n.d.	1.3 (1.1)	7.7 (6.0)	1.2 (1.2)	1.6 (2.0)	1.6 (2.4)
	0.20%, n=6 (2)	n.d.	0.8 (0.9)	5.4 (4.6)	1.0 (1.1)	1.4 (1.5)	1.1 (1.6)

[a] Detected by UV.

[b] Obtained from linear regression of the 6 calibration points.

[c] Not determined.

To evaluate the *accuracy* of the method, the recovery rates of sample solutions spiked with each impurity at 0.03%, 0.1%, and 0.2% concentration levels were determined by means of the calibration curves obtained from linear regression as well as by the single-point calibration procedure using a 0.1% dilution of the respective impurity. The CAD was employed for the quantitation of the gabapentin impurities B, D, E, and G, while the recovery rate of impurity A was determined by UV. The recovery rates for the CAD detected impurities are illustrated in Table 4. With recovery rates ranging from 90% to 105% (n = 3), the accuracy of both quantitation procedures was satisfactory for the nonvolatile impurities. In contrast, linear regression had to be applied to obtain reasonable results for the semivolatile impurity B (93% - 112%, n = 3). The recovery rate of the UV detected impurity A (99%) was solely assessed at the lower limit (0.03%) to stay within the investigated range (0.03% - 0.24%), since the impurity was already present in the gabapentin samples in substantial quantities without spiking (>0.1%).

The *precision* of the method was assessed by replicate injections (n = 6) of spiked sample solutions at concentrations levels of 0.03%, 0.1%, and 0.2% of each impurity with respect to the main component to determine the intraday repeatability (Table 5). Another six replicates were analyzed on the next day to address the interday repeatability of the method. The RSD of the intraday repeatability injections (0.8% – 3.1%, n = 6) were adequate for the nonvolatile impurities D, E, and G detected by CAD and for the volatile impurity A detected by UV. The same held true for the interday repeatability with RSD ranging from 0.9% to 4.7%. The

increased RSD for the intraday and interday repeatability of the semivolatile impurity B (4.6% - 8.4%, n = 6) compared to the nonvolatile impurities can be attributed to the limitations of detection principle. The accuracy results, however, were not too much impaired by the relatively high RSD.

The *quantitation limits (LOQs)* of the gabapentin impurities were determined according to the S/N approach of ICH guideline Q2(R1). With exception of the UV detected impurity A, all other impurities were detected by CAD. The LOQ results are illustrated in Table 5 and Fig. 7. The LOQs of the nonvolatile impurities compare favorably to a previously published CAD method [23]. A reporting threshold of 0.03% claimed by the Ph. Eur. for drugs with an average daily intake >2 g was achieved for all impurities.

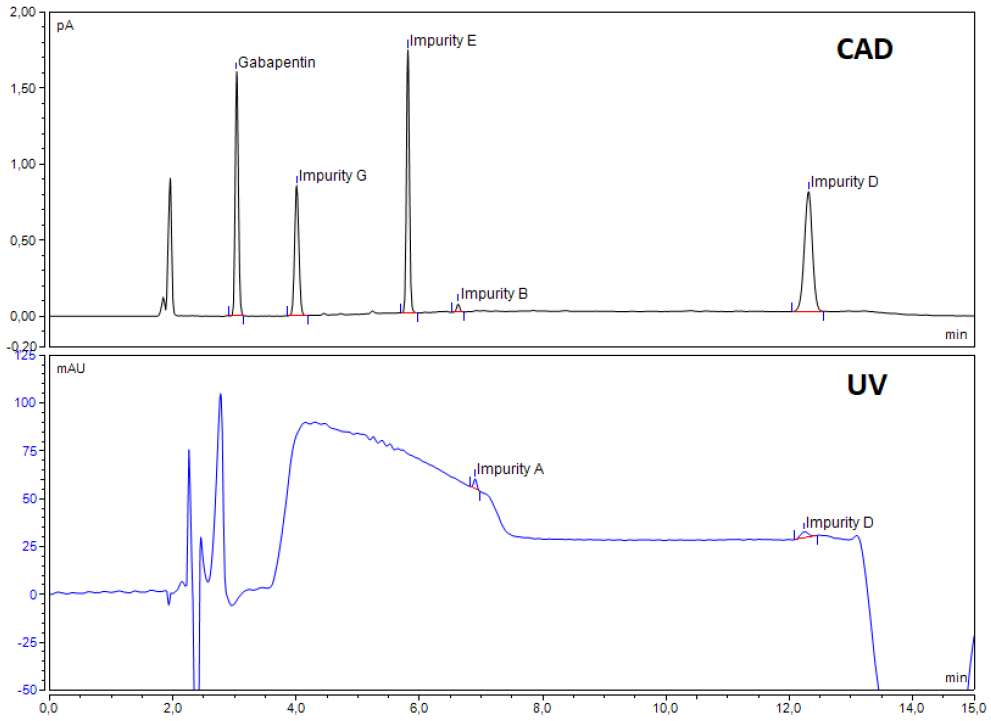

Fig. 7. Chromatogram of a solution of gabapentin and its impurities at 50 ng on column injected mass equivalent to the compendial reporting threshold (0.03%).

For the evaluation of the method's *robustness*, the flow rate (1.1 – 1.3 mL/min) and column temperature (20 °C – 30 °C) were varied as well as the initial percentage of mobile phase B (23% – 27%) and the final percentage (60% – 62%) using a 0.1% solution of gabapentin and its impurities. The resolution was >1.5 for all impurities under each condition and >3 for the peak pair of gabapentin and impurity G. Thus, the method can be regarded as robust against these changes since the system suitability requirement defined below was met.

As a *system suitability* test, a 0.1% solution of gabapentin spiked with 0.1% impurity G was chosen for the demonstration of compliance. The criterion to pass the system suitability test

was a resolution >3 for the peak pair of gabapentin and impurity G determined by the approach described in the Ph. Eur. [16].

5. Conclusion

In this work, two independent approaches for the optimization of the PFV setting in charged aerosol detection were evaluated to improve the accuracy results of a HPLC-UV-CAD method for the impurity analysis of gabapentin. Both approaches solely require the calibration data obtained at PFV = 1.00 to predict the optimal PFV for each analyte. Thus, they greatly simplify the time-consuming experimental optimization of the PFV setting. The comparison of the prediction results of both approaches to the experimentally obtained optimal PFV confirmed the validity of the approaches for the intended purpose. However, more experimental evidence might be required to prove the general validity of the empirical approach, since the analyte's properties also have an impact on the constant modeling as it was shown for the semivolatile analytes exhibiting higher response curve variability. Moreover, a generic method for the establishment of the constants used in this approach is necessary to allow for the prediction of the optimal PFV of other analytes. The mathematical approach, by contrast, is universally applicable, although its utilization being restricted to the Chromeleon software license. The adjusted PFV setting is a valuable tool to improve the accuracy of the detector as was demonstrated by the comparison of the PFV-optimized method for the purity analysis of gabapentin to the default one, though the simultaneous quantitation of semivolatile and nonvolatile analytes in one chromatographic run remains a challenge. A particular advantage of the linearization by means of the PFV setting with regard to the application of the CAD in a GMP regulated environment, is the inherent data integrity of this procedure, since no subsequent data transformation, e.g. double logarithmic transformation, is required.

Conflict of interest statement

None of the authors of this paper does have a financial or personal relationship with other people or organizations that could inappropriately influence or bias the content of the paper.

Acknowledgements

Thanks to Niclas Förtig and Nicolas Scheuplein (both University of Wuerzburg) for their scientific advice regarding the possible reaction and by-products of gabapentin as well as to the Thermo Fisher Scientific team in Germering (Germany) for technical support and scientific feedback and advice.

References

[1] P.H. Gamache, R.S. McCarthy, S.M. Freeto, D.J. Asa, M.J. Woodcock, K. Laws, R.O. Cole, HPLC analysis of nonvolatile analytes using charged aerosol detection, Lc Gc Europe 18(6) (2005) 345.

[2] T.H. Mourey, L.E. Oppenheimer, Principles of operation of an evaporative light-scattering detector for liquid chromatography, Anal. Chem. 56(13) (1984) 2427-2434.

[3] L.B. Allen, J.A. Koropchak, Condensation nucleation light scattering: a new approach to development of high-sensitivity, universal detectors for separations, Anal. Chem. 65(6) (1993) 841-844.

[4] J.P. Hutchinson, J. Li, W. Farrell, E. Groeber, R. Szucs, G. Dicinoski, P.R. Haddad, Comparison of the response of four aerosol detectors used with ultra high pressure liquid chromatography, J. Chromatogr. A 1218(12) (2011) 1646-1655.

[5] N. Vervoort, D. Daemen, G. Török, Performance evaluation of evaporative light scattering Detection and charged aerosol detection in reversed phase liquid chromatography, J. Chromatogr. A 1189 (2008) 92-100.

[6] J. Shaodong, W.J. Lee, J.W. Ee, J.H. Park, S.W. Kwon, J. Lee, Comparison of ultraviolet detection, evaporative light scattering detection and charged aerosol detection methods for liquid-chromatographic determination of anti-diabetic drugs, J. Pharm. Biomed. Anal. 51(4) (2010) 973-978.

[7] H.Y. Eom, S.-Y. Park, M.K. Kim, J.H. Suh, H. Yeom, J.W. Min, U. Kim, J. Lee, J.-R. Youm, S.B. Han, Comparison between evaporative light scattering detection and charged aerosol detection for the analysis of saikosaponins, J. Chromatogr. A 1217(26) (2010) 4347-4354.

[8] K. Schilling, U. Holzgrabe, Recent applications of the Charged Aerosol Detector for liquid chromatography in drug quality control, J. Chromatogr. A (2020) 460911.

[9] S. Almeling, D. Ilko, U. Holzgrabe, Charged aerosol detection in pharmaceutical analysis, J. Pharm. Biomed. Anal. 69 (2012) 50-63.

[10] R. Karongo, T. Ikegami, D.R. Stoll, M. Lämmerhofer, A selective comprehensive reversed-phase × reversed-phase 2D-liquid chromatography approach with multiple complementary detectors as advanced generic method for the quality control of synthetic and therapeutic peptides, J. Chromatogr. A (2020) 461430.

[11] F. Weber, L. Rahnfeld, P. Luciani, Analytical profiling and stability evaluation of liposomal drug delivery systems: a rapid UHPLC-CAD-based approach for phospholipids in research and quality control, Talanta (2020) 121320.

[12] J. Wang, G. Liu, B. Zhu, L. Tang, Universal quantification method of degradation impurities in 16-membered macrolides using HPLC-CAD and study on source of the impurities, J. Pharm. Biomed. Anal. 184 (2020) 113170.

[13] V.K. Ahirrao, V.P. Rane, K.R. Patil, R.A. Jadhav, V.S. Bhamare, D.S. Yadav, R.D. Yeole, Identification of Monomethyl Sulfate and Sulfate Impurities in Zidebactam Using LC–MS and Application of Mixed-Mode Liquid Chromatography with Charged Aerosol Detection and Ion Chromatography for Quantification, Chromatographia 83(2) (2020) 219-228.

[14] Council of Europe, European Pharmacopoeia Online 10.3, EDQM, Strasbourg,France, 2020, Monograph no. 2305. Available from: https://pheur.edqm.eu/app/10-3/. Accessed: September 4th, 2020.

[15] Council of Europe, European Pharmacopoeia Online 10.3, EDQM, Strasbourg,France, 2020, Monograph no. 2616. Available from: https://pheur.edqm.eu/app/10-3/. Accessed: September 4th, 2020.

[16] Council of Europe, European Pharmacopoeia Online 10.3, EDQM, Strasbourg,France, 2020, Chapter 2.2.46. Available from: https://pheur.edqm.eu/app/10-3/. Accessed: October 4th, 2020.

[17] P.H. Gamache, Charged aerosol detection for liquid chromatography and related separation techniques, John Wiley & Sons, 2017.

[18] I.A.H. Ahmad, A. Blasko, J. Tam, N. Variankaval, H.M. Halsey, R. Hartman, E.L. Regalado, Revealing the inner workings of the power function algorithm in Charged Aerosol Detection: A simple and effective approach to optimizing power function value for quantitative analysis, J. Chromatogr. A 1603 (2019) 1-7.

[19] K. Schilling, R. Pawellek, K. Lovejoy, T. Muellner, U. Holzgrabe, Influence of charged aerosol detector instrument settings on the ultra-high-performance liquid chromatography analysis of fatty acids in polysorbate 80, J. Chromatogr. A 1576 (2018) 58-66.

[20] International Council for Harmonization, Guideline Q2 (R1) Validation of Analytical Procedures: Text and Methodology, 2005.

[21] Council of Europe, European Pharmacopoeia Online 10.3, EDQM, Strasbourg,France, 2020, Monograph no. 2173. Available from: https://pheur.edqm.eu/app/10-3/. Accessed: September 4th, 2020.

[22] P. Gamache, T. Muellner, B. Eggart, K. Lovejoy, I. Acworth, Charged aerosol detection – use of the power function and robust calibration practices to achieve the best quantitative results, Thermo Fisher Scientific Technical Note 73299. Available from: https://assets.thermofisher.com/TFS-Assets/CMD/Technical-Notes/tn-73299-lc-cad-calibration-tn73299-en.pdf

[23] P.K. Ragham, K.B. Chandrasekhar, Development and validation of a stability-indicating RP-HPLC-CAD method for gabapentin and its related impurities in presence of degradation products, J. Pharm. Biomed. Anal. 125 (2016) 122-129.

[24] A.B. Ciavarella, A. Gupta, V.A. Sayeed, M.A. Khan, P.J. Faustino, Development and application of a validated HPLC method for the determination of gabapentin and its major degradation impurity in drug products, J. Pharm. Biomed. Anal. 43(5) (2007) 1647-1653.

[25] A. Gupta, A.B. Ciavarella, V.A. Sayeed, M.A. Khan, P.J. Faustino, Development and application of a validated HPLC method for the analysis of dissolution samples of gabapentin drug products, J. Pharm. Biomed. Anal. 46(1) (2008) 181-186.

[26] International Council for Harmonization, Guideline Q3A (R2) Impurities in New Drug Products, 2006.

3.4. Performance evaluation of IPC and HILIC coupled to charged aerosol detection for the analysis of underivatized amino acids

Ruben Pawellek, Ulrike Holzgrabe

Submitted manuscript.

Abstract

The charged aerosol detector (CAD) is frequently employed in liquid chromatography for the analysis of small polar and ionizable compounds such as amino acids and amino sugars, which provide a weak chromophore only. Separation of these compounds is achieved by means of ion pair chromatography (IPC), and, more recently, hydrophilic interaction chromatography (HILIC) techniques. However, as the CAD's response is highly dependent on the mobile phase composition, the substantial differences in the mobile phase composition of IPC and HILIC have a distinct impact on the detector's performance. This study was aimed at systematically comparing the performance of IPC and HILIC when coupled to the CAD. Therefore, the separation techniques characterized by their specific mobile phase compositions were evaluated for their influence on the CAD response and the signal-to-noise ratio (S/N) of the amino acids L-alanine, L-leucine, and L-phenylalanine applying the response surface methodology (RSM). The RSM results derived from flow injection analysis (FIA) indicated that the CAD response and thus the obtainable S/N are significantly higher in HILIC compared to IPC where the S/N decreased with the chain length of the applied ion-pairing reagent.

In addition, an IPC and a HILIC method, respectively, were developed for the impurity profiling of the branched-chain amino acids (BCAAs) L-leucine, L-isoleucine, and L-valine. The beneficial effects of the HILIC conditions on the S/N observed under FIA conditions were partly offset by moderate column bleed effects when using an amide functionalized column, which facilitates the separation in the HILIC method. Satisfactory LOQs (3-10 ng on column) were obtained with both methods; however, the HILIC method was found to be slightly superior in terms of sensitivity and separation efficiency.

1. Introduction

Small polar molecules or molecules carrying charges like amino acids, carbohydrates, and inorganic ions are challenging analytes in many ways, as their detection and separation is often complicated by their physico-chemical properties. The commonly applied reversed phase (RP)-HPLC technique is not appropriate in many cases due to its insufficient separation power toward these mostly hydrophilic compounds. Ion pair chromatography [1, 2] is among the most established separation techniques applied in liquid chromatography for polar ionizable compounds by using ion-pairing reagents of opposite charge under RP conditions. As a relatively new separation technique that has increasingly been used for the analysis of polar compounds over the last decade, hydrophilic interaction chromatography [3-5] comprises polar stationary phases and highly organic, often buffered mobile phases. Besides the challenging separation of polar compounds, their detection also can be a difficult task, when their structures do not contain UV absorbing elements known as chromophores. Thus, the predominantly applied UV detection suffers from poor sensitivity toward these analytes.

Alternatively, the charged aerosol detector [6], which is among the universal aerosol-based detectors, has been proven in numerous applications [7] to be well suited for the analysis of small compounds lacking chromophores such as carbohydrates [8], amino acids [9], lipids [10], or inorganic and organic ions [11]. IPC and HILIC with CAD have been used for multiple purposes, e.g. amino acid analysis [9, 12-14] and the assessment of aminoglycosides [15-17]. However, the low organic, ion-pairing reagent containing mobile phases typically applied in IPC differ significantly from the high organic buffered mobile phases that are commonly used in HILIC. Considering the substantial influence of the mobile phase composition on the CAD response [18], there is no evidence that the assumably beneficial HILIC conditions outperform IPC in terms of sensitivity when applied to the same objective.

In this study, the impact of IPC and HILIC on the CAD response was evaluated for the amino acids L-alanine (Ala), L-leucine (Leu), and L-phenylalanine (Phe) (Table 1) by a response surface methodology (RSM) approach, which aims to describe the functional relationship of input variables on the (systems) response of interest using statistical techniques [19]. Characteristic mobile phase compositions of each separation technique comprising a homologous set of the volatile ion-pairing reagents trifluoroacetic acid (TFA), pentafluoropropionic acid (PFPA), heptafluorobutyric acid (HFBA), and nonafluoropentanoic acid (NFPA) for IPC and the commonly applied ammonium formate and acetate buffers in case of HILIC were subjected to systematic variations of the acetonitrile content (v/v) in the mobile phase (IPC: 0-20%; HILIC: 70-90%) and the CAD's evaporation temperature (35-70 °C). The resulting CAD responses obtained for the amino acids from flow injection analysis (FIA) runs

based on the experimental plan created by RSM were subsequently evaluated statistically to identify the significant input variables.

Table 1. Branched-chain amino acids (Ile, Leu, Val) and their possible impurities with respect to the Ph. Eur. [19-21].

Compound	Structure	logD[a] (pH 5.5)	MW (g/mol)	Impurities
L-Alanine (Ala)	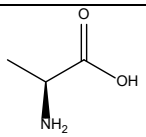	-2.88	89.09	-[b]
L-Proline (Pro)	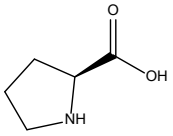	-2.76	115.13	Ala, Val
L-Cysteine (Cys)	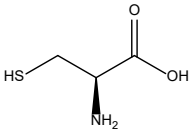	-2.50	121.15	-
L-Valine (Val)	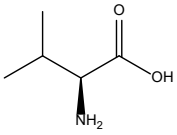	-2.16	117.15	Ala, Ile, Leu
L-Methionine (Met)	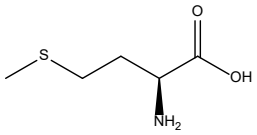	-1.92	149.21	-
L-Isoleucine (Ile)	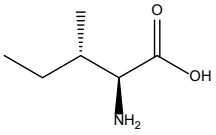	-1.86	131.18	Cys, Leu, Met, Val
L-Leucine (Leu)	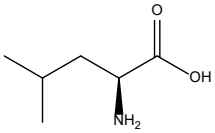	-1.86	131.18	Ile, Met, Phe, Val
L-Phenylalanine (Phe)	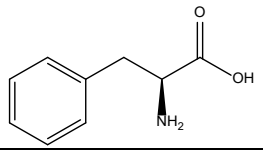	-1.45	165.19	Leu, Met, Tyr, Val

[a] Predicted by ACD labs software version 2020.2.0 (ACD Labs, Toronto, Canada)

[b] Not considered for impurity profiling.

In addition to the theoretical evaluation, an IPC-CAD and a HILIC-CAD method were developed for the impurity profiling of the branched-chain amino acids (BCAAs), i.e. Leu, L-isoleucine (Ile), and L-valine (Val) to compare the performance of the techniques in a more realistic scenario. The impurity profile of the BCAAs as depicted in the European Pharmacopoeia 10 (Ph. Eur.) [20-22] entirely consists of other amino acids mostly showing poor UV absorbance (Table 1). As the Ph. Eur. routinely employs tedious and error-prone derivatization procedures using sophisticated instrumentation for the purity testing of amino acids, called *amino acid analyzer*, which are also limited to the detection of amino group containing compounds, simple and more selective CAD methods could provide a

straightforward alternative and enable simultaneous detection of common impurities like organic acids. The sensitivity of the developed IPC and HILIC methods was then compared to the RSM derived results. The HILIC method was validated exemplarily for Val with respect to the ICH guideline Q2(R1) and compared to an IPC method proposed for compendial implementation [23].

2. Experimental

2.1. Chemicals and reagents

The amino acids Ala, L-cysteine (Cys), Ile, Leu, L-methionine (Met), Phe, L-proline (Pro), L-tyrosine (Tyr) and Val as well as formic acid (FA) 98-100%, acetic acid ≥99.7%, TFA ≥99%, PFPA 97%, HFBA ≥99.5%, NFPA 97%, ammonium acetate ≥99.0%, ammonium formate ≥99.0%, and HPLC grade acetonitrile (ACN) were purchased from Sigma Aldrich (Steinheim, Germany). Ultra-pure deionized (DI) water was delivered by a Milli-Q® system (Merck, Darmstadt, Germany).

2.2. Apparatus

The HPLC experiments were performed on a Vanquish™ Flex modular chromatographic system (Thermo Fisher Scientific, Germering, Germany) consisting of a binary pump with an online degasser, a thermostatted split sampler, a thermostatted column compartment with passive pre-heater, and a variable wavelength detector in-line with a Vanquish™ Horizon CAD. The CAD was supplied with nitrogen gas from an ESA nitrogen generator (Thermo Fisher Scientific) connected to the in-house compressed air system. The instrument was controlled and runs were processed using the Chromeleon® Chromatography Data System Version 7.2.6 software program (Thermo Fisher Scientific).

2.3. Chromatographic procedures

2.3.1. IPC method

For the IPC method, a flow rate of 0.8 mL/min, an injection volume of 10 µL, and a column compartment temperature of 25 °C were applied. Mobile phase A contained a mixture of 11.5 mM HFBA and 6.5 mM TFA in water, mobile phase B was ACN. The gradient program started at 2% B for the first 2 min, followed by a linear increase from 2% B to 14% B between min 2 and 3, which was held constant until min 15. The chromatographic system was returned to the starting conditions from min 15 to 16 and 2% B were then maintained for 4 min to achieve reequilibration resulting in a run time of 20 min. Reequilibration was confirmed by comparing the retention times of multiple injections. The separation of the amino acids was achieved on a polar embedded C18 Acclaim Polar Advantage II column (150 x 4.6 mm i.d., 2.6 µm particle size, Thermo Fisher Scientific). The CAD settings were adjusted to a data collection rate of

10 Hz, a filter constant of 5 s, a power function value of 1.0, and the CAD's evaporation temperature was set at 50 °C.

2.3.2. HILIC method

The HILIC method comprised a flow rate of 0.6 mL/min, an injection volume of 15 µL, and a column compartment temperature of 25 °C. The mobile phase included an aqueous ammonium formate buffer (50 mM) pH 2.8 in a mixture of buffer/ACN 20/80 (v/v). Runs were performed isocratically with a run time of 16 min using an Accucore™ 150 Amide HILIC column (150 x 4.6 mm i.d., 2.6 µm particle size, Thermo Fisher Scientific). The CAD settings were as follows: evaporation temperature 50 °C, filter constant 5 s, data collection rate 10 Hz, power function value 1.0.

2.4. Preparation of solutions

2.4.1. Standard solutions

Standard solutions of the amino acids were prepared by weighing 10.0 mg of the respective substance, which were dissolved in 10.0 mL water. The standard solutions were diluted to the required concentration in a mixture equivalent to the respective mobile phase composition in case of the HILIC method. For the IPC method and the IPC FIA, the standard solutions were diluted with water. Standard solutions of the amino acids Ala, Leu, and Phe used for the FIA under HILIC conditions were prepared by dissolving 50.0 mg of the respective amino acid in water to a concentration of 5 mg/mL, which were then diluted with ACN to achieve a final concentration of 1 mg/mL. All standard solutions were stored at 8 °C.

2.4.2. Sample solutions

Sample solutions of Ile, Leu, Phe, Pro, and Val were prepared daily by weighing of 100 mg of the respective sample, which were dissolved in 10.0 mL water. The samples were injected without further dilution in the IPC method. For the HILIC method, the sample solutions were diluted with a mixture of ACN/water resulting in a sample concentration of 2.5 mg/mL and an ACN proportion of 70% (v/v).

2.5. Flow injection analysis (FIA)

The FIA runs were performed randomly based on the RSM-derived design of experiments (DoE) plans (supplementary material) for IPC and HILIC conditions, respectively, except for the mobile phase additives that were not altered between consecutive runs for practical reasons. To generate sufficient back pressure for operation, the outlet capillary (0.1 x 380 mm) of the Vanquish system's injection valve was linked by a connector (Viper union, Thermo Fisher Scientific) to the inlet capillary (0.1 x 350 mm) of the UV detector (flow cell volume 11 µL) in-line with the CAD. The numeric factors investigated included the CAD's evaporation

temperature (35 °C – 70 °C) and the ACN proportion (v/v) in the mobile phase (IPC: 0 – 20%; HILIC: 70 – 90%), whereas the mobile phase additives (IPC: FA, TFA, PFPA, HFBA, NFPA; HILIC: ammonium formate pH 3, ammonium acetate pH 5) at 10 mM concentration in the mobile phase, respectively, were selected as categoric factors. In total, 23 runs were carried out for each amino acid (Ala, Leu, Phe) at the IPC conditions, and 14 at the HILIC conditions, with a run time of 2 min, an injection volume of 10 µL, and a column compartment temperature of 25 °C. The amino acids were injected at a concentration of 1 mg/mL in water for the IPC experiments, and in a mixture water/ACN 20/80 (v/v) for the HILIC experiments. For determining the response of the amino acids and the background noise, the CAD's instrumental parameters were set to a filter constant of 1s, a power function value of 1.0, and a data collection rate of 10 Hz. When switching between the mobile phase additives, the system was equilibrated for at least 60 min, until a stable baseline was obtained. Prior to each new run, the system was equilibrated for 5 min at the upcoming mobile phase conditions.

2.6. Response surface methodology (RSM)

The separate DoE plans (supplementary material) for conducting the FIA were derived from RSM [19, 24] for both IPC and HILIC conditions using the Design-Expert 12 software (Stat-Ease Inc., MN, US). I-optimal design [25] was applied to describe the experimental domain by minimizing the average prediction variance within the predefined experimental space. The selection of the I-optimality criterion enabled the parallel assessment of numeric and categoric variables with minimal experimentation. A split-plot design had to be chosen as the categoric variable was hard to change between consecutive runs. The input variables evaluated included the evaporation temperature and ACN proportion (v/v) as numeric factors and the mobile phase additives as categoric factors (section 2.5.). The obtained peak area responses and S/N of the amino acids investigated were subjected to restricted maximum likelihood analysis (REML), which is employed to identify the significant factors in split-plot designs. Prior to the statistical analysis, the responses obtained from FIA were either $\log_{10}$ or square root transformed where appropriate to achieve normally distributed data (supplementary material). The validity of the models established was evaluated by visual inspection of the normal plot of residuals, residuals vs. predicted plot, and predicted vs. actual plot in each individual case. The adjusted R^2 were >0.9 and the coefficients of variation <10% for all models established.

3. Results and discussion

3.1. Performance characteristics of IPC and HILIC evaluated by RSM

Though IPC and HILIC can both be employed for the analysis of ionizable compounds, their respective mobile phases usually comprise distinct proportions of organic modifier and divergent mobile phase additives. Considering the response dependency of aerosol-based

detectors on the mobile phase composition [18, 26], significant differences of the CAD response between the IPC and HILIC modes are to be expected. The CAD responsiveness at IPC and HILIC conditions was investigated here for the amino acids Ala, Leu, and Phe. The test compounds represented the minimum, intermediate, and maximum levels in terms of molecular mass and hydrophobicity, respectively, based on the impurity profile of the BCAAs Ile, Leu, and Val (Table 1) analyzed afterwards by two separate IPC and HILIC methods (section 3.2.).

The experimental domain was described by means of RSM (section 2.6.) performing FIA (section 2.5.) for the subsequent evaluation of the CAD response. The organic solvent proportion (v/v) in the mobile phase and the CAD's evaporation temperature were set as numeric factors, while the respective mobile phase additives were selected as categoric variables. The ranges of the organic solvent content in the mobile phase were derived from preliminary experiments on the impurity profiling of the BCAAs and corresponded to the characteristic IPC and HILIC conditions. Volatile perfluorocarboxylic acids (PFCA) have been applied multiple times as ion-pairing reagents in IPC-CAD applications for the analysis of amino acids [9, 12, 14, 27]. Thus, a set of 5 homologous PFCAs ranging from TFA (C2) to NFPA (C5) were investigated here to simulate the IPC conditions and, in addition, FA for comparison purposes. The commonly applied mobile phase additives examined for the HILIC conditions were ammonium formate and ammonium acetate buffers. The evaporation temperature was examined in a range from the default value of 35 °C to a relatively high value of 70 °C, since the analytes investigated were all non-volatile amino acids allowing for higher evaporation temperatures, which reduce the background noise for improved S/N [27]. Moreover, elevated evaporation temperatures can compensate the additional background noise caused by the commercially available ion-pairing reagents of limit purity. Separate IPC and HILIC models were established for Ala, Leu, and Phe, respectively, based on the response data obtained from the FIA. The peak areas and S/N values were subsequently evaluated by REML to identify the significant factors toward the output variables.

3.1.1. Influence of the IPC conditions on the CAD's response and the S/N

The trends for the CAD response obtained at the IPC conditions are illustrated in Fig. 1a for the individual factors. The IPC models were solely based on linear terms as the influence of the numeric factors on CAD response could accurately be described by linear trends (supplementary material). The general trend for the organic modifier was a significant ($p<0.05$) increase in the response of all analytes investigated with increasing ACN proportion. Organic modifiers such as ACN reduce the initial droplet size of the primary aerosol compared to aqueous solvent due to their lower surface tension and viscosity. The resulting aerosol transport process is more efficient as droplets above the d_{cut} are directed to the waste, which

means that a greater fraction of the mobile phase and thus more analyte enters the evaporation tube [18]. The observed trend may be explained to some extent by the selected ranges for the ACN proportion, as it is in good agreement with previously published studies reporting a linear trend of the CAD response for low ACN ranges [28-30]. However, it should be noted that these studies were performed on other CAD models. The influence of the evaporation temperature on the analyte response was inverse compared to the ACN proportion as increasing the evaporation temperature resulted in a decreased response of all analytes ($p<0.05$). At elevated evaporation temperatures, higher proportions of analyte partition to the aerosol's vapor phase during the evaporation step depending on the analyte's volatility, thus lower responses are obtained [28, 31]. Interestingly, the impact of higher evaporation temperatures on the response of Ala was far more pronounced compared to Leu and Phe though being the most polar amino acid. The substantial loss of response at elevated evaporation temperatures for Ala is likely due to the relatively low molecular weight of the compound. A negative correlation between the CAD response and a compound's molecular weight has already been demonstrated [28, 32], which can be attributed to an increased volatility. Thus, it seems reasonable that low molecular compounds are more susceptible to behave as semi-volatiles at higher evaporation temperatures.

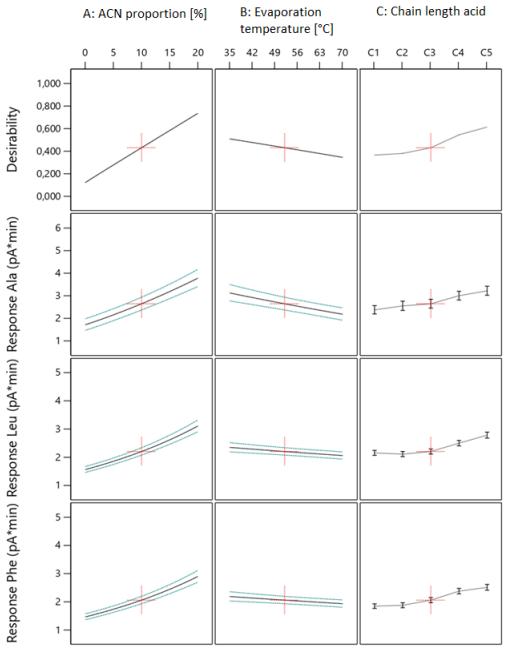

Fig. 1a. Influence of the ACN proportion, the evaporation temperature, and the chain length of the applied ion-pairing reagent on the CAD response of the amino acids Ala, Leu, and Phe at the IPC conditions. The trends are only illustrated for PFPA at the medium factor settings, but they were consistent for all ion-pairing reagents.

The comparison of the influence of the ion-pairing reagents investigated on CAD response revealed the anionic ion-pairing reagents ($pKa_{carboxylic}<1.0$) to increase the response due to salt

formation with the ionized basic moieties of the amino acids (pKa_{amino}>9.0). While the salt formation effect appeared to be rather weak in case of the short-chain ion-pairing reagents TFA and PFPA, the formation of higher molecular mass salts between the longer-chain ion-pairing reagents HFBA and NFPA further enhanced the CAD response resulting in a significant ($p<0.05$) increase.

Since in IPC, the influence of chromatographic parameters on the CAD response could be described by linear terms, the resulting S/N responses followed linear trends as well (Fig. 2a). Though the ACN proportion in the mobile phase had a substantial impact on the CAD response as discussed above, its influence on the S/N of the amino acids was negligible ($p>0.05$), except for the S/N of Leu, which was moderately influenced ($p=0.029$). The enhanced response at higher ACN proportions was compensated by the simultaneously elevated background noise. The increased background noise might be attributed to the impurities being already present in the ACN as well as to the increased mass transport of the mobile phase impurities at higher organic contents. Considering the rather narrow ACN range investigated here (0-20%), it is likely that the other factors were more contributing to the observed S/N.

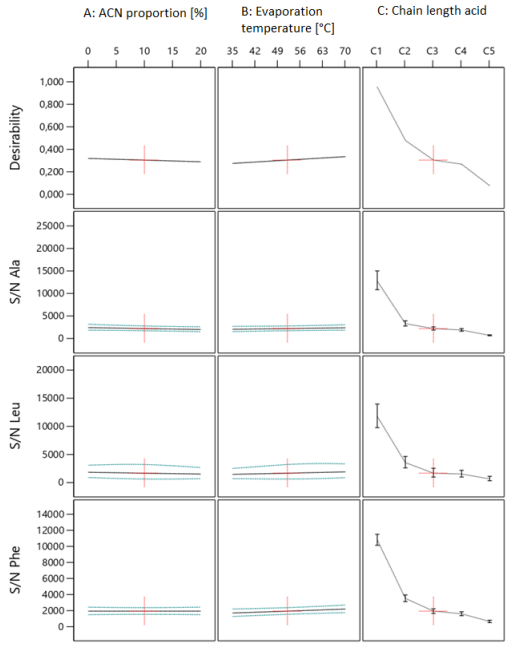

Fig. 2a. Influence of the ACN proportion, the evaporation temperature, and the chain length of the applied ion-pairing reagent on the S/N of the amino acids Ala, Leu, and Phe at the IPC conditions. The trends are only illustrated for PFPA at the medium factor settings, but they were consistent for all ion-pairing reagents.

The evaporation temperature setting of the CAD has a direct impact on the detector's sensitivity toward an analyte as it simultaneously affects the analyte response and the background noise. The optimal evaporation temperature for a specific analyte is then the best compromise between the analyte signal and the background noise. In general, low evaporation

temperatures are recommended [18, 28] since many analyte classes behave as semi-volatiles at elevated temperatures. In this case, the set of analytes entirely consisted of amino acids, which can be classified as non-volatile compounds due their physico-chemical properties, even though the BCAAs belong to the class of non-polar amino acids. Thus, higher S/N of the amino acids were obtained at elevated evaporation temperatures compared to the default setting of 35 °C ($p<0.05$). One exception was the S/N of Ala that did not significantly benefit from higher evaporation temperatures, which can be explained by the substantial loss of response of the compound due to its comparatively high volatility at elevated evaporation temperatures. The effect of the chain length of the ion-pairing reagents on the background noise and thus S/N is evident from Fig. 2a. Though it was previously demonstrated that longer-chain ion-pairing reagents contribute to increased response for the amino acids, their effect on the S/N was inverse due to the simultaneously elevated background noise. The formation of higher molecular mass salts between mobile phase impurities and the long-chain ion-pairing reagents as well as the decreasing volatility of the latter are likely contributing factors to the increased noise levels.

3.1.2. Influence of the HILIC conditions on the CAD's response and the S/N

For the HILIC models (Fig. 1b; Fig. 2b), the inclusion of the quadratic terms for the numeric factors was necessary to establish valid models (supplementary material).

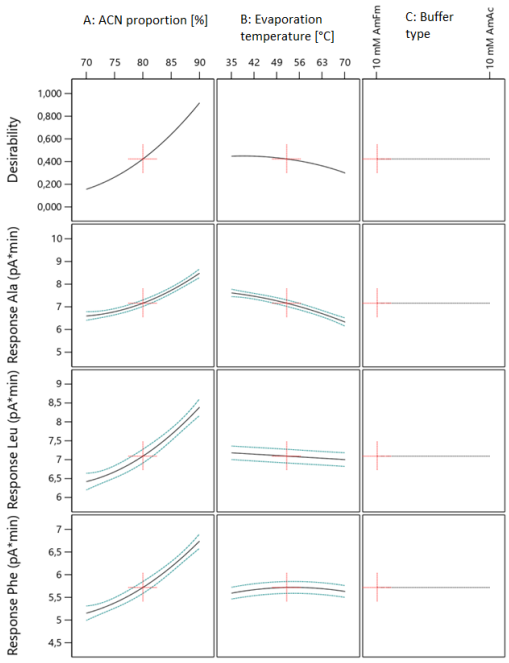

Fig. 1b. Influence of the ACN proportion and the evaporation temperature on the response of the amino acids Ala, Leu, and Phe at the HILIC conditions. The type of buffer used, namely ammonium formate (AmFm) and ammonium acetate (AmAc), was excluded from the models as it was not considered significant ($p>0.05$).

As discussed before, the response of all amino acids increased with the ACN proportion ($p<0.05$) due to the more efficient analyte mass transport. In case of the evaporation temperature, the trend was an analyte specific decrease ($p<0.05$) of the response at elevated temperatures as the salt formation effect is less influential here compared to IPC. No significant difference ($p>0.05$) in the CAD response was observed between the ammonium formate and acetate buffers used as mobile phase additives, which is in good agreement with the results of a previously published study [28] and can be explained by the negligible difference in the counterions of the respective buffers ($MW_{formiate}$: 45.03 g/mol; $MW_{acetate}$: 59.05 g/mol). Consequently, the categoric factor buffer type was excluded from the final models to improve their validity.

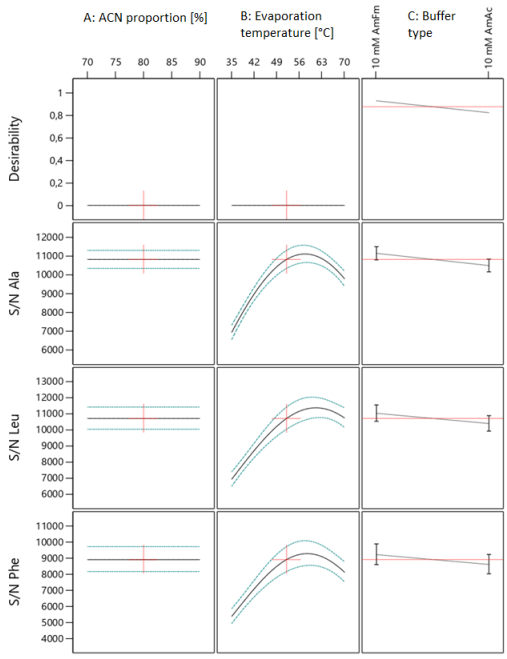

Fig. 2b. Influence of the ACN proportion, the evaporation temperature, and the buffer type on the S/N of the amino acids Ala, Leu, and Phe at the HILIC conditions. The type of buffer used, namely ammonium formate (AmFm) and ammonium acetate (AmAc), was not considered significant, but included in the models.

Regarding the S/N of the amino acids, the ACN proportion in the mobile phase was not considered as influential ($p>0.05$) analogously to the IPC models. In case of the evaporation temperature, however, the HILIC models showed a distinct maximum ranging between 55 and 60 °C (Fig. 2b and 3). In HILIC, the utilized buffers contribute little to additional background noise when applied at a low concentration. Thus, elevated evaporation temperatures are less effective in further reducing the background noise compared to IPC while simultaneously decreasing the analyte response in both techniques. It should be noted that the effect of decreasing analyte response with increasing evaporation temperature is more pronounced for lower analyte levels than were investigated in the FIA. No significant difference ($p>0.05$) was

observed for the impact of the buffer type on the S/N, which is in good agreement with the response models that also indicated no significant difference.

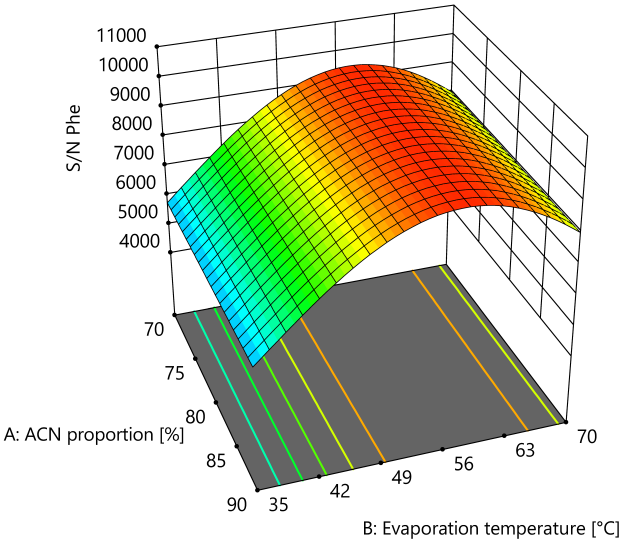

Fig. 3. Response surface plot for the S/N of Phe at the HILIC conditions.

3.1.3. IPC vs. HILIC models

According to a previous study [33], the CAD response is many times higher for HILIC conditions than for RP conditions, which is mainly due to the highly organic mobile phases employed in HILIC. In the present study, the average responses obtained in HILIC mode for both buffer types were 3.9-4.4 times higher compared to FA as mobile phase additive at the IPC conditions in the lowest region of the experimental design space and 2.4-2.8 times in the highest region (Fig. 4).

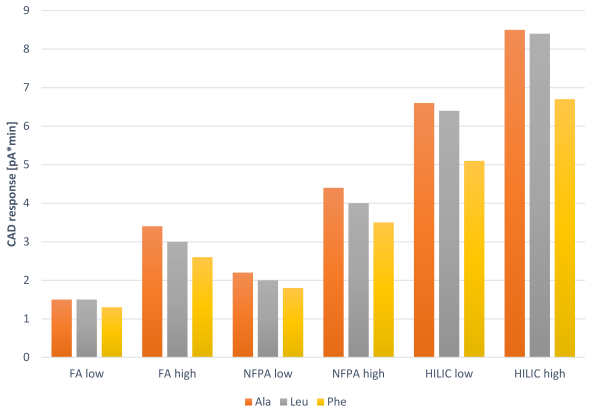

Fig. 4. CAD responses of Ala, Leu, and Phe obtained for FA, NFPA, and the average of the buffers used in HILIC at the lowest (lowest ACN proportion and highest evaporation temperature) and highest (highest ACN proportion and lowest evaporation temperature) regions of the experimental design space.

The differences in the response were least pronounced for NFPA as IPC additive with 2.8-3.2 and 1.9-2.1 times higher response in HILIC mode, for the lowest and highest regions of the experimental design space. A direct comparison of the S/N obtained by FIA between IPC and HILIC should be done with caution as additional effects such as column bleed are not considered but may have a substantial impact on sensitivity as demonstrated in section 3.2. Interestingly, the highest S/N were obtained for FA at IPC conditions concomitant with the lowest levels of background noise. The S/N obtained in HILIC mode were 2-3 times higher compared to IPC using TFA and more than 10 times higher when using NFPA as mobile phase additive. Since the RSM models served as basis for the subsequent method development of separate IPC and HILIC methods for the impurity profiling of BCAAs, two main conclusions could be drawn. For the IPC method, the usage of shorter-chain ion-pairing reagents should be favored as the chain length was the predominant factor toward sensitivity. The HILIC method could be optimized by adjusting the evaporation temperature.

3.2. Comparison of IPC and HILIC for the impurity profiling of BCAAs

3.2.1. Method development

The RSM results clearly indicated that the HILIC conditions are favorable to CAD responsiveness and thus S/N under FIA conditions. However, other factors influencing the sensitivity, such as column bleed and column efficiency, are not considered in the RSM models. Consequently, a HILIC method and a separate IPC method, respectively, was developed to compare the impact of the separation techniques in a more realistic scenario. The aim was to develop generic methods for the impurity profiling of each BCAA (Ile, Leu, Val). Putative impurities that can arise from the production process by fermentation mainly include other amino acids such as Ala, Cys, Met, and Phe (Table 1) with respect to the Ph. Eur. 10 [20-22] and by-products of biosynthesis such as organic acids [34]. LC analysis of these polar substances is challenging as they are poorly separated on RP columns and, for the greater part, are lacking chromophores for UV detection. Thus, IPC and HILIC hyphenated to the CAD are both viable options to solve the detection and separation related issues.

3.2.1.1. IPC method

A polar embedded C18 stationary phase was chosen for its compatibility with low organic mobile phases that are necessary for sufficient retention of the more polar amino acids. Additionally, the column showed good selectivity towards polar amino acids in previous studies when ion-pairing reagents were used to enhance retention [27]. Derived from the results of the RSM models, the initial method development started with TFA, since it was the ion-pairing reagent associated with the highest S/N. The influence of TFA concentrations of 10 mM, 15 mM, 20 mM, and 25 mM, respectively, on the separation of all occurring amino acids (Ala, Cys, Ile, Leu, Met, Phe, Val) in the impurity profile of the BCAAs was investigated under

isocratic conditions at a minimal ACN content of 2% (v/v) in the mobile phase; ACN was necessary to elute the more hydrophobic Phe. Subsequently, the retention factors (k) of the amino acids (Fig. 5a) were determined for each TFA concentration. Additionally, the average responses of the amino acids were investigated, and the background currents were compared (Fig. 5b).

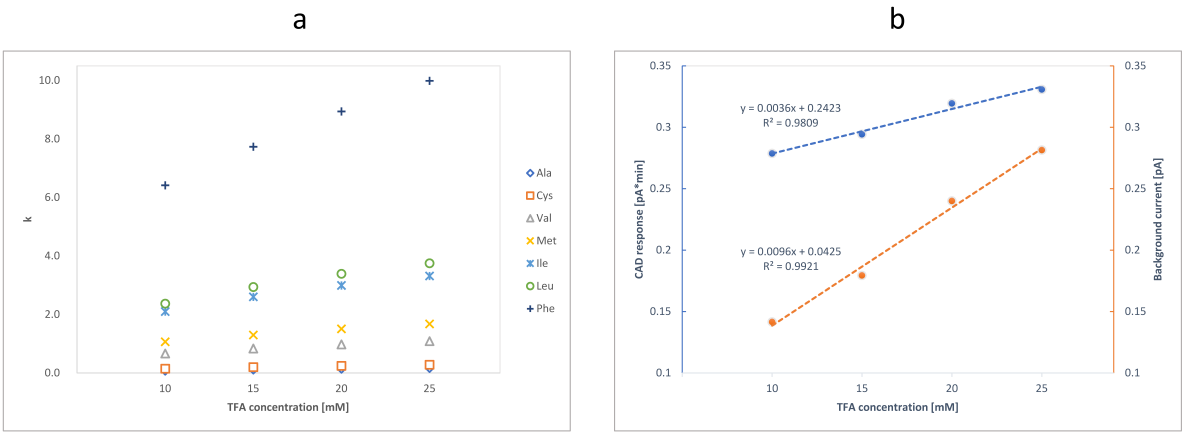

Fig. 5a. Effect of the TFA concentration on the k values of the BCAAs and their impurities. **Fig 5b.** Effect of the TFA concentration on the average CAD response of the amino acids and on the CAD's background current.

Though the k values and the resolution of the amino acids increased from 10 mM to 25 mM TFA, the retention of the more polar amino acids Ala and Cys was still poor resulting in k values close to zero (Fig. S1). Even when applying a concentration of 25 mM TFA, Ala eluted close to the injection peak, which is undesirable for the selectivity of an intended purity analysis method. Moreover, Leu and Ile could not be separated from each other when injecting a spiked sample solution (10 mg/mL) of Ile. The background current and the average response of the amino acids both followed linear trends with increasing TFA concentration in the investigated range. However, when comparing the steepness of the slope of the respective trendlines, the background current was increasing at a higher rate indicating a decline in the S/N at higher TFA concentrations. This observation is in accordance with the RSM models where the increased response generated by the long-chain ion-pairing reagents was overcompensated by the simultaneously elevated background noise. Taking the selectivity and sensitivity observations together, the rationale for the further method development was to use the shortest-chain ion-pairing reagent at the lowest concentration possible that would still achieve sufficient selectivity. However, switching to a longer-chain ion-pairing reagent was inevitable to enhance the retention and separation of the amino acids as the retention of the latter increases with the chain length of the ion-pairing reagent [35]. The best compromise was obtained for a mobile phase comprising a mixture of 11 mM HFBA and 6.5 mM TFA in water as mobile phase A and ACN as mobile phase B. A shallow gradient from 2% to 14% B was

applied to improve the peak shapes of the late eluting Ile, Leu, and Phe and to achieve a reasonable run time of 20 min. Corresponding to the RSM results, the sensitivity of the method was improved at higher evaporation temperatures. However, the S/N decreased at evaporation temperatures higher than 50 °C for the low molecular mass amino acids Ala and Val, which was previously indicated by the RSM model that showed no significant benefit for Ala. Thus, the evaporation temperature was set at 50 °C. All BCAAs and their respective impurities could be separated by one generic method applicable to impurity analysis (Fig. 6). The method was also suitable for the impurity profiling of Phe and Pro due to their comparable impurity profile (Table 1).

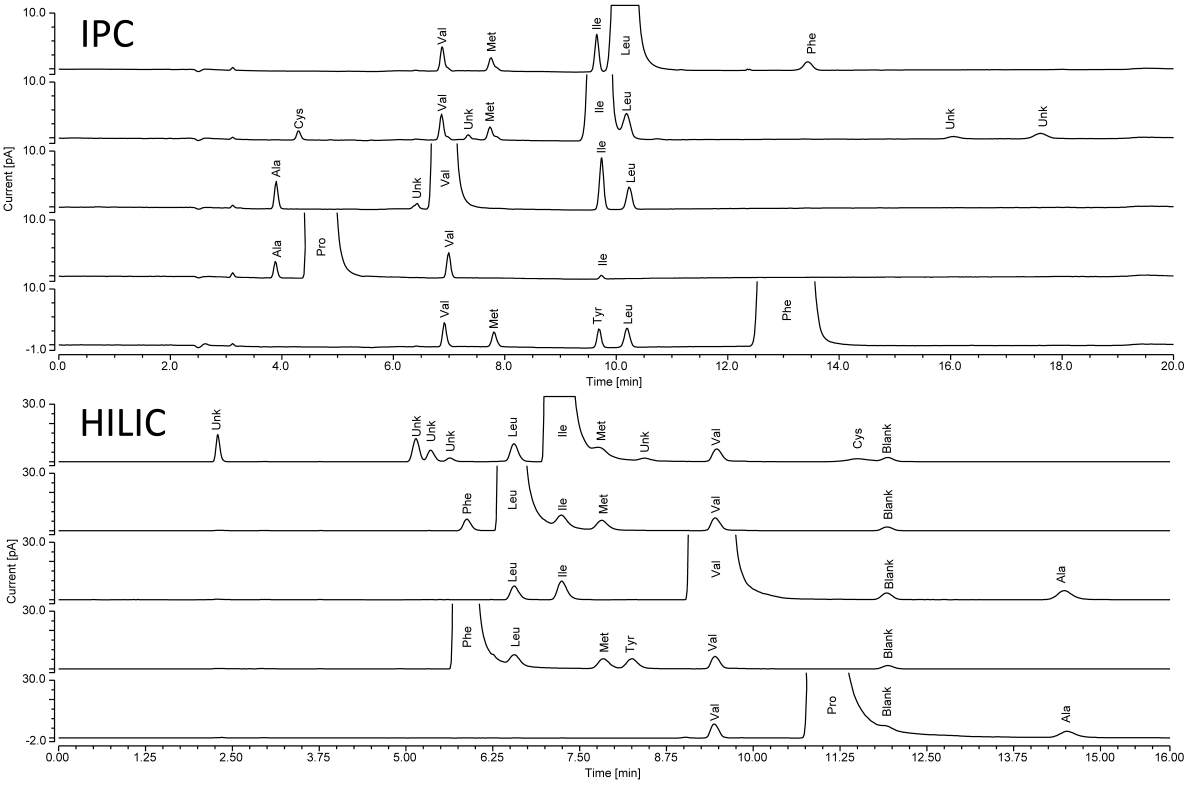

Fig. 6. Zoomed chromatograms of the IPC and HILIC methods for the impurity profiling of BCAAs. The sample concentration is 10 mg/mL for IPC and 2.5 mg/mL for HILIC. The individual impurities are spiked at a concentration of 0.1% (m/m). The chromatographic conditions are depicted in sections 2.3.1. and 2.3.2., respectively. The peak referred to as blank in the HILIC chromatogram is a system peak.

3.2.1.2. HILIC method

The choice of the stationary phase is crucial in HILIC as the column chemistry not only determines the selectivity [36] but may also have a huge impact on the sensitivity of the method due to possible column bleed effects. Comparatively high levels of column bleed have been reported for silica-based HILIC columns in several studies, in particular when coupled to mass spectrometric (MS) detection [37]. Even though the CAD is less sensitive than MS, the universal detection can result in higher levels of background current and noise for relatively

low levels of non-volatile and semivolatile mobile phase impurities. Consequently, column bleed effects must be considered in the CAD method development as well [38-40].

Among the HILIC stationary phases available, amide functionalized columns have been proven to be well suited for the separation of amino acids [13, 41]. Thus, a silica-based column with amide groups bonded to the solid core particles was chosen for the method development. The retention in HILIC is mainly dependent on the percentage of the solvent with the weaker elution power in the mobile phase, i.e. the organic solvent. Previous studies demonstrated that good selectivity is obtained on the selected column using ammonium formate buffered mobile phases at low pH values (2.8-3.0) and ACN proportions between 75-90% (v/v) [13]. Consequently, isocratic runs were performed at ACN proportions of 75%, 80%, and 85% ACN (v/v) in the mobile phase, respectively. The k values of the amino acids (Fig. 7a) as well as the average response and background current (Fig. 7b) were determined analogously to IPC to evaluate the impact of the ACN proportion on selectivity and sensitivity.

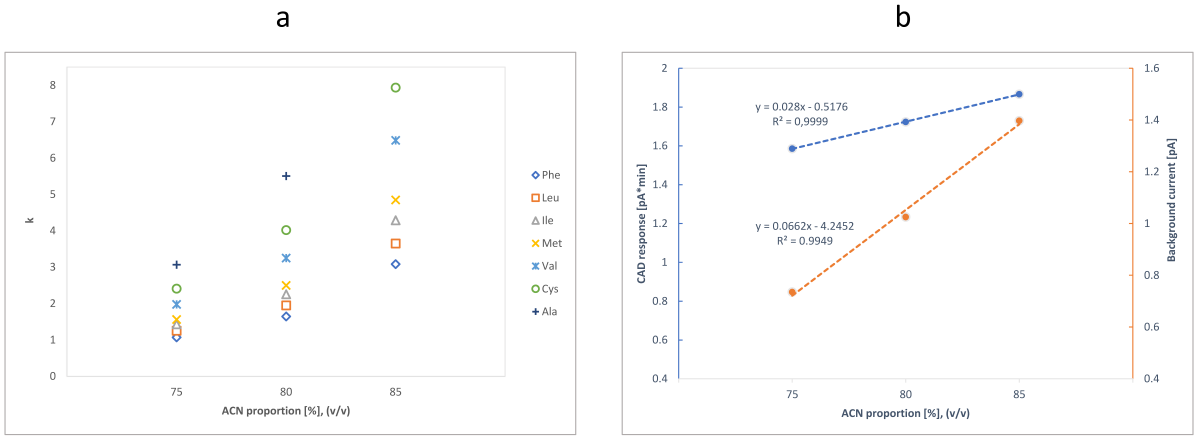

Fig. 7a. Effect of the ACN proportion (v/v) on the k values of the BCAAs and their impurities. **Fig. 7b.** Effect of the ACN proportion (v/v) on the average CAD response of the amino acids and on the CAD's background current.

Sufficient separation of all amino acids investigated was achieved at 80% ACN (v/v) in a run time of less than 20 min (Fig. S2). Higher ACN proportions further increased the resolution, however, they negatively affected the sensitivity as broader peaks and increased levels of background current were obtained. In contrast to the IPC method, the initial levels of background current monitored under flow injection conditions were distinctly lower than the corresponding values when the HILIC column was used with the remaining chromatographic conditions kept constant. Thus, a column bleed effect contributing to the background noise with increasing impact at high ACN proportions could be confirmed for the HILIC method. It should be noted that the levels of background noise were still within an acceptable range, particularly at ACN proportions ≥80%. Considering the RSM model results, evaporation temperatures of 35 °C, 50 °C, and 70 °C were screened for their influence on the S/N. In good

agreement with the RSM models, the highest S/N were obtained for the medium setting of 50 °C as at elevated temperatures the background current was not further reduced. With respect to the IPC method, the HILIC method likewise represents a generic approach for the impurity analysis of the amino acids Ile, Leu, Phe, Pro, and Val (Table 1; Fig. 6).

3.2.2. Performance comparison of the IPC and HILIC methods

The IPC and HILIC methods were compared in terms of selectivity, limits of quantitation (LOQs), and linearity. Both methods achieved sufficient separation of the BCAAs from each other and their putative impurities when spiked sample solutions were injected (Fig. 6). In accordance with the respective retention mechanisms, the amino acids were retained corresponding to their log D values (Table 1), thus the elution order of the IPC method was reversed compared to the HILIC method with the more polar amino acids eluting first. The HILIC method allowed isocratic separation of all amino acids in a run time of 16 min. In contrast, the IPC method required the usage of a gradient program since the low organic percentage initially applied for the separation of the more polar amino acids were not adequate to achieve reasonable peak shapes and appropriate retention times for the late eluting amino acids. The selectivity, however, was slightly better for the IPC method, because in the HILIC method Cys was not entirely separated from a system peak at min 12. Cys and Pro coeluted in the HILIC method, whereas Tyr and Ile coeluted in the IPC method, which was not an issue as their simultaneous occurrence is not expected in the relevant impurity profiles.

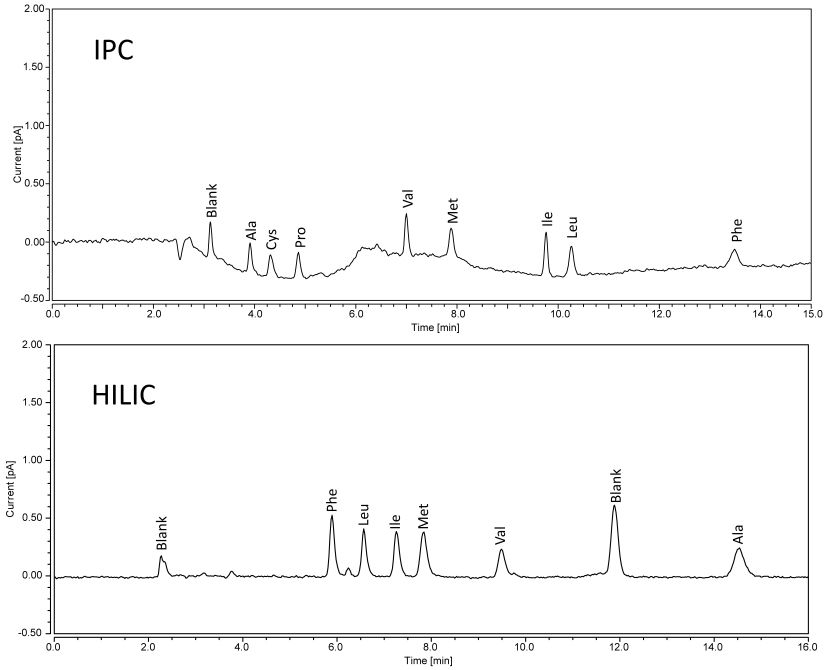

Fig. 8. Chromatograms of a solution of the BCAAs and their impurities at 5 ng injected mass. The chromatographic conditions are depicted in sections 2.3.1. and 2.3.2., respectively. The second peak referred to as blank in the HILIC chromatogram is a system peak.

The sensitivity of both methods was compared by determining the S/N (n=6) and peak area %RSD (n=6) of a solution containing all amino acids at a mass of 5 ng on column (Fig. 8 and Table 2). The noise of the HILIC method was calculated using a blank injection according to the S/N approach depicted in the ICH guideline Q2(R1) [42]. For the noise calculation of the IPC method, a fixed interval at the initially isocratic conditions was chosen, which corresponded to roughly 20 times the peak half width to allow for a meaningful comparison. The S/N of the HILIC method were roughly twice as high for most of the amino acids except for Cys, which was poorly separated from the system peak. The superior sensitivity of the HILIC method was further supported by the %RSD of the peak areas showing an improved precision for all amino acids investigated. However, the differences in sensitivity were not as pronounced as indicated by the previous FIA experiments. The comparatively high column bleed and lower column efficiency of the HILIC method are likely contributing factors to the partial compensation observed. In general, the LOQs obtained with the HILIC method (Table 2) are superior compared to previously published CAD methods for the quantitation of amino acids [9, 12-14].

Table 2. S/N and peak area %RSD of the amino acids obtained at 5 ng on column injected mass. The linearity parameters were determined for a mass range of 10-80 ng (HILIC) and 15-120 ng (IPC), respectively.

	S/N (n=6)		%RSD (n=6)		LOQ[a]		Equation (linear regression)		R^2	
	IPC	HILIC	IPC	HILIC	IPC	HILIC	IPC	HILIC	IPC	HILIC
Ala	9.2	17.5	6.2	2.5	6	3	y=0.005x-0.0131	y=0.016x-0.0266	0.9999	0.9997
Cys	6.7	n.d.[b]	9.7	n.d.	10	10	y=0.0036x-0.0045	y=0.0079x-0.0139	0.9993	0.9994
Ile	14.3	19.8	3.8	1.6	5	3	y=0.0079x+0.0058	y=0.018x-0.0489	0.9990	0.9998
Leu	10.2	19.8	3.1	2.3	5	3	y=0.008x+0.0036	y=0.0181x-0.0522	0.9993	0.9998
Met	9.8	19.7	5.5	2.9	5	3	y=0.0063x+0.0021	y=0.0176x-0.0324	0.9998	0.9996
Phe	5.8	26.9	5.9	1.8	10	3	y=0.0069x-0.0039	y=0.015x+0.0014	0.9999	0.9996
Val	13.7	23.4	6.1	2.7	5	3	y=0.0076x-0.0024	y=0.0203x-0.1225	0.9996	0.9991

[a] Injected ng on column, defined as S/N >10 for n=6.

[b] Not determined due to coelution with a system peak.

For investigation of the methods linearity, calibration curves were established ranging from 10-80 ng (HILIC) and 15-120 ng (IPC), respectively, considering the higher sensitivity of the HILIC method (Table 2). The ranges were chosen to meet the requirements for a compendial application [43] covering impurity concentrations of 0.03-0.24%, with respect to the main substance. With coefficients of determination (R^2) ≥0.9990 and evenly scattered residuals (not shown), both methods can be regarded as sufficiently linear for the intended purpose. Both methods were capable to quantify the impurities at a reporting threshold of 0.03% (Fig. S3).

3.3. Validation of the HILIC method and comparison to a published IPC method

The generic HILIC method was validated exemplarily for the impurity profiling of Val. Val was chosen as test substance for its challenging impurity profile consisting of the isomeric Ile-Leu pair and the most polar amino acid Ala. Moreover, another validated IPC method employing 20 mM HFBA has been published for consideration as a substitute to the compendial derivatization method [23]. Thus, the validation of the HILIC method would allow a direct comparison of the methods performance.

With respect to the ICH guideline Q2(R1) [42], *specificity*, *range*, *linearity*, *accuracy*, *precision*, and *robustness* were evaluated.

The *specificity* of the method was proven by inspection of a chromatogram obtained from a sample solution (2.5 mg/mL) spiked with 0.1% of the impurities (Fig. S4). All impurities were well separated with resolution values >2.5. A *range* between 10-80 ng was chosen for the demonstration of linearity to cover the reporting threshold of 0.03% with respect to the main component (lower limit) as well as 120% of the specification limit (upper limit).

Sufficient *linearity* can be assumed as indicated in Table 2.

The *accuracy* and *precision* of the method were assessed on samples already containing all impurities at relevant levels, and on samples spiked with 0.03%, 0.1% or 0.2% of each impurity, respectively. The recovery rates of the impurities and the %RSD of the peak areas are illustrated in Table 3. As the recovery rates did not exceed ±10% and the peak area %RSD was <5% in each case, the method can be regarded as appropriate for the intended purpose.

Table 3. %Recovery rates of the Val impurities ±RSD (n=3) calculated by linear regression and peak area %RSD determined for the intraday repeatability and interday repeatability.

	%Recovery rate (n=3)			%RSD (n=6;n=2)		
Concentration[a]	0.03%	0.1%	0.2%	0[b]	0.1%	0.2%
Ala	94.1±2.0	100.8±0.8	105.6±0.6	1.7(2.3)[c]	0.7(1.1)	1.0(1.4)
Ile	100.1±4.3	99.8±1.7	96.7±0.6	1.0(1.4)	0.5(0.9)	0.7(1.5)
Leu	101.0±3.0	103.4±0.3	100.9±0.6	2.2(3.8)	0.3(1.0)	1.0(1.6)

[a] With respect to the concentration of the Val sample solution (2.5 mg/mL).

[b] The sample solution was injected without spiked impurities since it already contained relevant amounts of each impurity.

[c] For determining the interday repeatability, sample solutions were injected in sextuple on two consecutive days.

To evaluate the method's *robustness*, systematic variations of the column compartment temperature (20-30 °C), the flow rate (0.5-0.7 mL/min), the ACN proportion in the mobile phase (78-82%), and the concentration of the ammonium formate buffer (8-12 mM) were investigated. The method can be regarded as robust against these variations as the resolution of the critical peak pair Ile-Leu was >2.5 in each case (Table S1) and the peak shapes were not impaired.

The validated method was compared to a published IPC method with the same objective [23]. The proposed IPC method employed a mobile phase consisting of 20 mM HFBA in water/ACN (90/10, v/v). The initially poor sensitivity of the method was improved by the usage of a post-column solution consisting of ACN, thereby increasing the analyte mass transport, and simultaneously decreasing the background noise. However, this required the usage of a second pump and likely impairs the reproducibility of the method. Assuming a roughly linear CAD response, the extrapolated LOQs of the method were ranging between 13 and 67 ng on column. In contrast, the HILIC method yielded LOQs of 3 ng on column without the need for a post-column solution. The recovery rates (101.1-108.4%, n=3) and repeatability (%RSD <2.0, n=3) of the IPC method were comparable to the HILIC method (94.1-105.6%, n=3; %RSD <2.0 at the corresponding level using 6 replicates). Consequently, the concentration of the sample solution was 4 times higher in the IPC method to achieve comparable performance due to the lower sensitivity.

4. Conclusions

IPC and HILIC are both commonly applied in liquid chromatography for the analysis of ionizable compounds lacking chromophores. Representative mobile phase compositions of the separation techniques were investigated here for their impact on the CAD response of amino acids, and, consequently, their influence on the S/N. The HILIC responses obtained at FIA conditions were more than twice as high compared to the IPC values, consequently the resulting S/N were greater as well. The comparison of the IPC method and the HILIC method developed for the impurity analysis of BCAAs demonstrated that column effects must also be considered as the relatively high column bleed of the HILIC column partly thwarted the increased response obtained by the HILIC method. Column bleed is a HILIC related issue of increasing relevance for the development of CAD methods as the recent detector models are more sensitive to both analyte and mobile phase impurities. However, LOQs of 3 ng on column were obtained for most of the amino acids with the HILIC method, which compared favorably to previously published methods. Thus, the HILIC method outperformed an IPC method proposed for compendial implementation and can be regarded as superior to the compendial applied derivatization methods as it is more selective and straightforward.

Conflict of interest statement

None of the authors of this paper does have a financial or personal relationship with other people or organizations that could inappropriately influence or bias the content of the paper.

Acknowledgements

The authors would like to thank Frank Steiner and Tibor Muellner (Thermo Fisher Scientific, Germering, Germany) and Paul Gamache (Thermo Fisher Scientific, Waltham, MA, USA) for

technical support and scientific feedback and advice and Luisa Emmert (University of Wuerzburg) for experimental assistance.

Supplementary material

Table S1. Chromatographic variations and resulting resolution values for the amino acids.

	Resolution		
variation	Leu-Ile	Ile-Val	Val-Ala
no variation	2.85	8.94	15.89
20 °C column compartment temperature	2.89	9.28	16.49
30 °C column compartment temperature	2.75	8.78	15.39
0.5 ml/min flow rate	2.88	9.15	15.98
0.7 ml/min flow rate	2.66	8.42	15.21
78% ACN proportion (v/v)	2.52	7.52	13.35
82% ACN proportion (v/v)	3.03	11.55	20.38
8 mM ammonium formate pH 2.8	2.64	8.09	14.36
12 mM ammonium formate pH 2.8	2.71	9.13	16.03

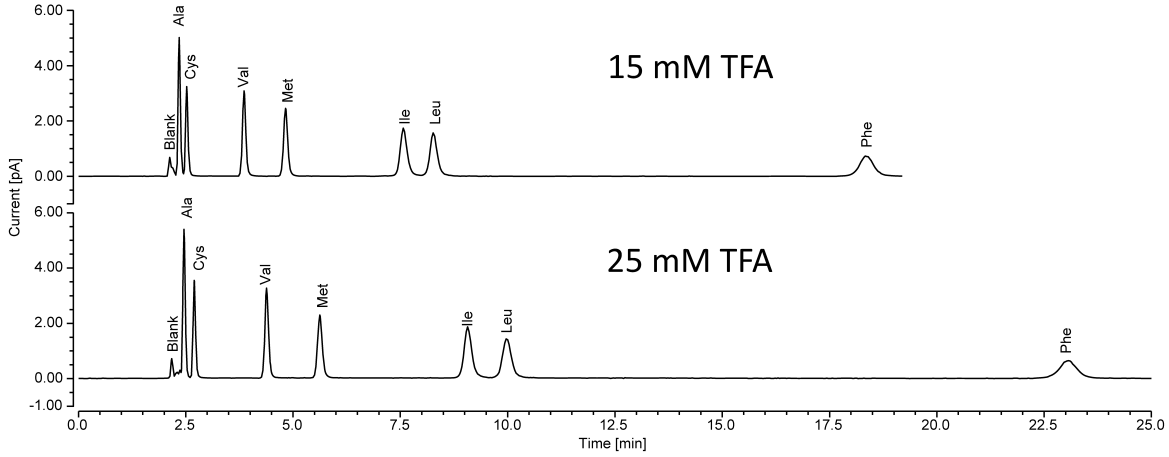

Fig. S1. Chromatograms of a solution of the BCAAs and their impurities (100 ng on column) for TFA concentrations of 15 and 25 mM, respectively. Chromatographic conditions: flow rate 0.8 mL/min, mobile phase water/ACN 98/2 (v/v), isocratic elution mode, evaporation temperature 50 °C.

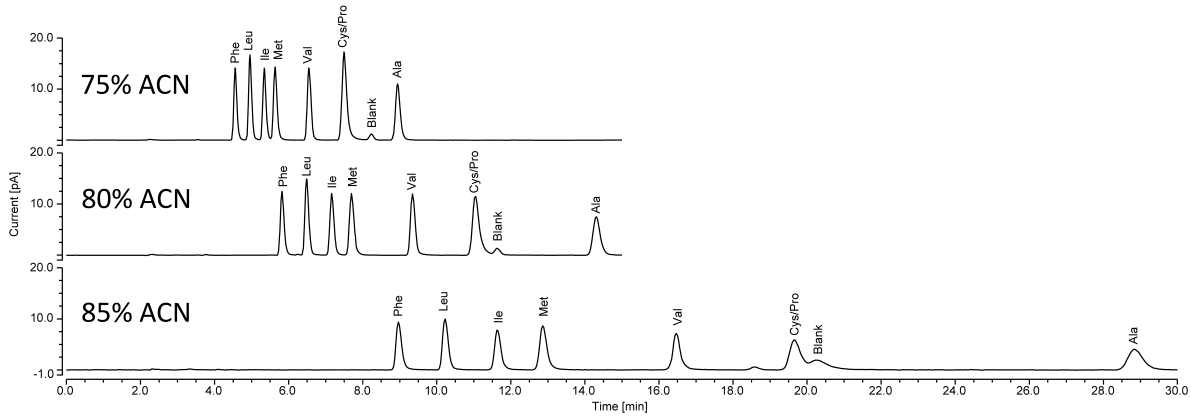

Fig. S2. Chromatograms of a solution of the BCAAs and their impurities (75 ng on column) for ACN proportions of 75,80, and 85% (v/v), respectively. Chromatographic conditions: flow rate 0.6 mL/min, mobile phase 15 mM ammonium formate pH 2.8 in water/ACN, isocratic elution mode, evaporation temperature 50 °C.

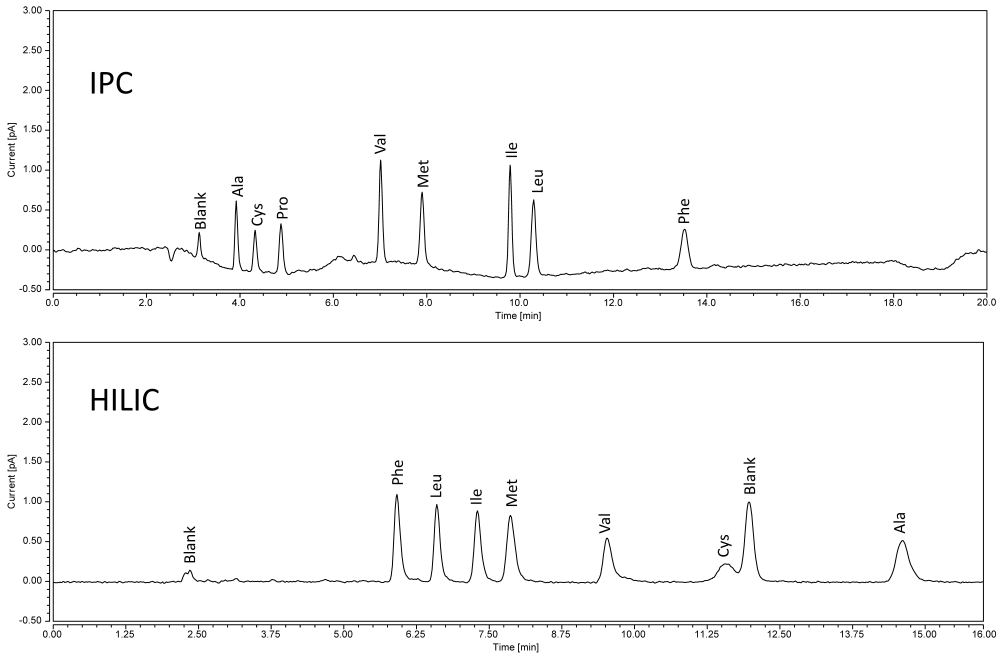

Fig. S3. Chromatograms of a solution of the BCAAs and their impurities at 15 ng (IPC) and 10 ng (HILIC) concentration equivalent to the compendial reporting threshold of 0.03% (m/m). The chromatographic conditions are depicted in section 2.3.1. and 2.3.2.

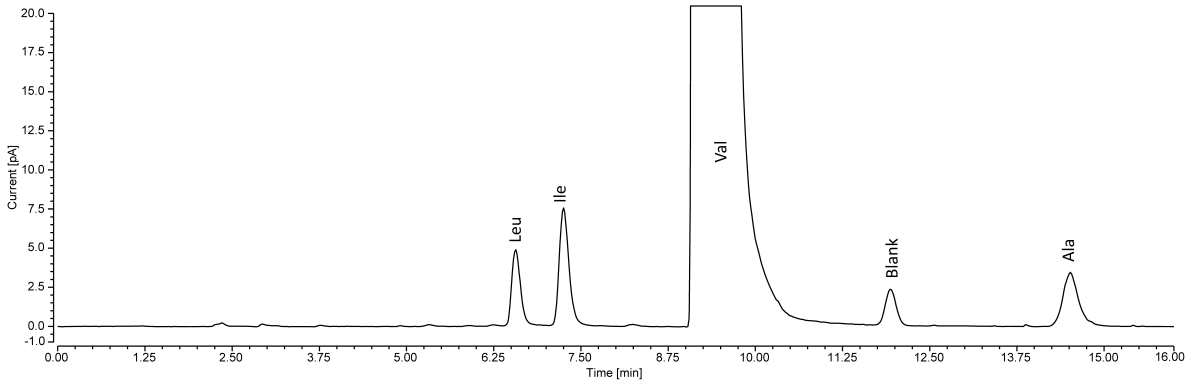

Fig. S4. Chromatogram of a Val sample solution (2.5 mg/mL) spiked with 0.1% of each impurity. The chromatographic conditions are depicted in section 2.3.2.

Table S2. Experimental plan for the IPC response models.

Group	Run	Factor 1 A:ACN %	Factor 2 B:Evaporation °C	Factor 3 c:C atoms	Response 1 R1 Response Ala	Response 2 R2 Response	Response 3 R3 Response Phe
1	1	10	52.5	C5	3.60	3.03	2.75
1	2	0	35	C5	2.24	2.06	1.75
1	3	0	70	C5	1.65	1.69	1.6
2	4	20	52.5	C2	3.78	2.97	2.59
2	5	0	35	C2	1.92	1.55	1.40
2	6	0	70	C2	1.27	1.44	1.27
3	7	10	52.5	C4	3.33	2.63	2.53
3	8	20	70	C4	3.11	3.11	2.92
3	9	0	70	C4	1.51	1.62	1.49

Table S2. (continued)

4	10	0	70	C3	1.46	1.55	1.41
4	11	10	52.5	C3	2.83	2.24	2.05
4	12	20	70	C3	2.88	2.80	2.60
4	13	10	35	C3	3.06	2.25	2.20
5	14	10	70	C1	2.03	2.16	1.82
5	15	20	52.5	C1	3.46	3.05	2.63
5	16	10	35	C1	2.60	2.23	1.89
5	17	0	52.5	C1	1.55	1.45	1.25
6	18	20	70	C5	3.68	3.43	3.16
6	19	20	35	C5	5.07	4.32	3.65
6	20	10	52.5	C5	3.54	2.93	2.75
7	21	10	52.5	C4	3.34	2.60	2.56
7	22	0	35	C4	2.26	1.87	1.76
7	23	20	35	C4	4.89	3.73	3.53

Table S3. Build information of the IPC response models.

File Version	12.0.10.0		
Study Type	Response Surface	**Subtype**	Split-plot
Design Type	I-optimal	Point Exchange	**Runs**	23.00
Design Model	Quadratic	**Blocks**	No Blocks
Groups	7.00	**Build Time (ms)**	249.00

Table S4. Investigated factors and levels of the IPC response models.

Factor	Name	Units	Change	Type	Minimum	Maximum	Coded Low	Coded High	Mean	Std. Dev.
A	ACN proportion	%	Easy	Numeric	0.00	20.00	-1 ↔ 0.00	+1 ↔ 20.00	9.57	8.25
B	Evaporation temperature	°C	Easy	Numeric	3.00	70.00	-1 ↔ 35.00	+1 ↔ 70.00	53.26	14.43
c	C atoms acid		Hard	Categoric	C1	C5			**Levels:**	5.00

Table S5. Obtained responses and applied transformations for the IPC response models.

Response	Name	Units	Observations	Analysis	Minimum	Maximum	Mean	Std. Dev.	Ratio	Transform	Model
R1	R1	Response Ala	23.00	Polynomial	1.27	5.07	2.83	1.05	3.99	Square Root	Linear
R2	R2	Leu	23.00	Polynomial	1.44	4.32	2.47	0.7837	3.00	Base 10 Log	Linear
R3	R3	Response Phe	23.00	Polynomial	1.25	3.65	2.24	0.7124	2.92	Base 10 Log	Linear

Table S6. Experimental plan for the IPC S/N models.

		Factor 1	Factor 2	Factor 3	Response 1	Response 2	Response 3
Group	Run	A:ACN proportion	B:Evaporation temperature	c:C atoms acid	R1	R2	R3
		%	°C		S/N Ala	S/N Leu	S/N Phe
1	1	10	52.5	C5	929.5	654.6	546.5
1	2	0	35	C5	728.9	679.8	736.0
1	3	0	70	C5	720.1	803.7	485.8
2	4	20	52.5	C2	2502.8	3297.4	3391.2
2	5	0	35	C2	4032.2	3527.1	3428.4
2	6	0	70	C2	3701.0	4096.4	3684.8
3	7	10	52.5	C4	2371.5	1779.7	1406.6

Table S6. (continued)

3	8	20	70	C4	1776.7	1597.3	1755.9
3	9	0	70	C4	1782.6	2205.4	2045.6
4	10	0	70	C3	2370.8	2109.9	2585.8
4	11	10	52.5	C3	2322.5	1504.4	1629.1
4	12	20	70	C3	2879.8	2120.5	2765.2
4	13	10	35	C3	1487.8	1249.9	1120.6
5	14	10	70	C1	10356.0	11356.4	10261.5
5	15	20	52.5	C1	11545.8	12333.8	12188.3
5	16	10	35	C1	14122.1	11410.8	10803.4
5	17	0	52.5	C1	14335.0	12117.4	10011.4
6	18	20	70	C5	812.9	640.9	810.2
6	19	20	35	C5	394.4	389.5	429.4
6	20	10	52.5	C5	724.6	765.4	680.2
7	21	10	52.5	C4	1804.7	1276.4	1620.2
7	22	0	35	C4	2012.7	1457.4	1582.7
7	23	20	35	C4	1470.2	947.3	1093.6

Table S7. Build information of the IPC S/N models.

File Version	12.0.10.0			
Study Type	Response Surface		**Subtype**	Split-plot
Design Type	I-optimal	Point Exchange	**Runs**	23.00
Design Model	Quadratic		**Blocks**	No Blocks
Groups	7.00		**Build Time (ms)**	249.00

Table S8. Investigated factors and levels of the IPC S/N models.

Factor	Name	Units	Change	Type	Minimum	Maximum	Coded Low	Coded High	Mean	Std. Dev.
A	ACN proportion	%	Easy	Numeric	0.00	20.00	-1 ↔ 0.00	+1 ↔ 20.00	9.57	8.25
B	Evaporation temperature	°C	Easy	Numeric	35.00	70.00	-1 ↔ 35.00	+1 ↔ 70.00	53.26	14.43
c	C atoms acid		Hard	Categoric	C1	C5			**Levels:**	5.00

Table S9. Obtained responses and applied transformations for the IPC S/N models.

Response	Name	Units	Observations	Analysis	Minimum	Maximum	Mean	Std. Dev.	Ratio	Transform	Model
R1	R1	S/N Ala	23.00	Polynomial	394.4	14335	3703.68	4329.64	36.35	Base 10 Log	Linear
R2	R2	S/N Leu	23.00	Polynomial	389.5	15453	3540.90	4406.68	39.67	Base 10 Log	Linear
R3	R3	S/N Phe	23.00	Polynomial	429.4	12188,3	3263.58	3685.65	28.38	Square Root	Linear

Table S10. Experimental plan for the HILIC response models.

		Factor 1	Factor 2	Factor 3	Response 1	Response 2	Response 3
Group	Run	a:ACN proportion %	B:Evaporation Temperature °C	c:Buffer Type	Ala	Leu	Phe
1	1	70	70	10 mM AmAc pH 5	5.68	6.15	4.96
1	2	70	52.5	10 mM AmAc pH 5	6.45	6.37	5.03
2	3	80	35	10 mM AmAc pH 5	7.50	7.07	5.59
2	4	80	52.5	10 mM AmAc pH 5	7.20	7.12	5.70
3	5	80	35	10 mM AmAc pH 5	7.49	7.06	5.62
3	6	80	70	10 mM AmAc pH 5	6.48	7.01	5.66
4	7	70	70	10 mM AmFm pH 3	5.88	6.47	5.16
4	8	70	35	10 mM AmFm pH 3	7.15	6.63	5.14
5	9	90	70	10 mM AmFm pH 3	7.52	8.25	6.69
5	10	90	35	10 mM AmFm pH 3	9.06	8.55	6.61
6	11	90	70	10 mM AmAc pH 5	7.59	8.30	6.61
6	12	90	52.5	10 mM AmAc pH 5	8.51	8.37	6.75
7	13	80	52.5	10 mM AmFm pH 3	7.15	7.21	5.69
7	14	80	52.5	10 mM AmFm pH 3	7.16	7.18	5.70

Table S11. Build information of the HILIC response models.

File Version	12.0.10.0			
Study Type	Response Surface		**Subtype**	Split-plot
Design Type	I-optimal	Coordinate Exchange	**Runs**	14.00
Design Model	Quadratic		**Blocks**	No Blocks
Groups	7.00		**Build Time (ms)**	24.00

Table S12. Investigated factors and levels of the HILIC response models.

Factor	Name	Units	Change	Type	Minimum	Maximum	Coded Low	Coded High	Mean	Std. Dev.
a	ACN proportion	%	Hard	Numeric	70.00	90.00	-1 ↔ 70.00	+1 ↔ 90.00	80.00	7.84
B	Evaporation Temperature	°C	Easy	Numeric	35.00	70.00	-1 ↔ 35.00	+1 ↔ 70.00	53.75	14.50
c	Buffer Type		Hard	Categoric	10 mM AmFm pH 3	10 mM AmAc pH 5			**Levels:**	2.00

Table S13. Obtained responses and applied transformations for the HILIC response models.

Response	Name	Units	Observations	Analysis	Minimum	Maximum	Mean	Std. Dev.	Ratio	Transform	Model
R1	Ala		14.00	Polynomial	5.68	9.06	7.20	0.9091	1.60	None	Reduced Quadratic
R2	Leu		14.00	Polynomial	6.15	8.55	7.27	0.7927	1.39	None	Reduced Quadratic
R3	Phe		14.00	Polynomial	4.96	6.75	5.78	0.6369	1.36	None	Reduced Quadratic

Table S14. Experimental plan for the HILIC S/N models.

		Factor 1	Factor 2	Factor 3	Response 1	Response 2	Response 3
Group	Run	a:ACN proportion %	B:Evaporation Temperature °C	c:Buffer Type	Ala	Leu	Phe
1	1	70	70	10 mM AmAc pH 5	9682.4	10947.2	7643.9
1	2	70	52.5	10 mM AmAc pH 5	9966.1	9812.7	8288.2
2	3	80	35	10 mM AmAc pH 5	6343.8	6593.8	5402.9
2	4	80	52.5	10 mM AmAc pH 5	10963.2	10551.4	9673.8
3	5	80	35	10 mM AmAc pH 5	6884.9	6624.3	4770.8
3	6	80	70	10 mM AmAc pH 5	9831.1	10927.9	8068.4
4	7	70	70	10 mM AmFm pH 3	9335.6	9934.3	7465.3
4	8	70	35	10 mM AmFm pH 3	7118.0	6839.0	5740.6
5	9	90	70	10 mM AmFm pH 3	10249.1	11411.6	8947.5
5	10	90	35	10 mM AmFm pH 3	7532.4	7717.4	5989.9
6	11	90	70	10 mM AmAc pH 5	9586.0	10325.2	8115.4
6	12	90	52.5	10 mM AmAc pH 5	10410.7	10805.4	8367.8
7	13	80	52.5	10 mM AmFm pH 3	11340.2	10900.6	9381.0
7	14	80	52.5	10 mM AmFm pH 3	11308.8	11679.0	8492.0

Table S15. Build information of the HILIC S/N models.

File Version	12.0.10.0			
Study Type	Response Surface		**Subtype**	Split-plot
Design Type	I-optimal	Coordinate Exchange	**Runs**	14.00
Design Model	Quadratic		**Blocks**	No Blocks
Groups	7.00		**Build Time (ms)**	24.00

Table S16. Investigated factors and levels of the HILIC S/N models.

Factor	**Name**	**Units**	**Change**	**Type**	**Minimum**	**Maximum**	**Coded Low**	**Coded High**	**Mean**	**Std. Dev.**
a	ACN proportion	%	Hard	Numeric	70.00	90.00	-1 ↔ 70.00	+1 ↔ 90.00	80.00	7.84
B	Evaporation Temperature	°C	Easy	Numeric	35.00	70.00	-1 ↔ 35.00	+1 ↔ 70.00	53.75	14.50
c	Buffer Type		Hard	Categoric	10 mM AmFm pH 3	10 mM AmAc pH 5			**Levels:**	2.00

Table S17. Obtained responses and applied transformations for the HILIC S/N models.

Response	**Name**	**Units**	**Observations**	**Analysis**	**Minimum**	**Maximum**	**Mean**	**Std. Dev.**	**Ratio**	**Transform**		**Model**
R1	Ala		14.00	Polynomial	6343.8	11340.2	9325.16	1675,66	1.79	Square Root		Reduced Quadratic
R2	Leu		14.00	Polynomial	6593.8	11679.0	9647.84	1859,33	1.77	Base Log	10	Reduced Quadratic
R3	Phe		14.00	Polynomial	4770.8	9673.8	7596.25	1532,56	2.03	Base Log	10	Reduced Quadratic

References

[1] T. Cecchi, Ion pairing chromatography, Crit. Rev. Anal. Chem. 38(3) (2008) 161-213.

[2] T. Cecchi, Theoretical models of ion pair chromatography: a close up of recent literature production, J. Liq. Chromatogr. Relat. Technol. 38(3) (2015) 404-414.

[3] B. Buszewski, S. Noga, Hydrophilic interaction liquid chromatography (HILIC)—a powerful separation technique, Anal. Bioanal. Chem. 402(1) (2012) 231-247.

[4] B. Dejaegher, Y. Vander Heyden, HILIC methods in pharmaceutical analysis, J. Sep. Sci. 33(6-7) (2010) 698-715.

[5] P. Jandera, Stationary and mobile phases in hydrophilic interaction chromatography: a review, Anal. Chim. Acta 692(1-2) (2011) 1-25.

[6] T. Vehovec, A. Obreza, Review of operating principle and applications of the charged aerosol detector, J. Chromatogr. A 1217(10) (2010) 1549-1556.

[7] S. Almeling, D. Ilko, U. Holzgrabe, Charged aerosol detection in pharmaceutical analysis, J. Pharm. Biomed. Anal. 69 (2012) 50-63.

[8] B. Godin, R. Agneessens, P.A. Gerin, J. Delcarte, Composition of structural carbohydrates in biomass: Precision of a liquid chromatography method using a neutral detergent extraction and a charged aerosol detector, Talanta 85(4) (2011) 2014-2026.

[9] U. Holzgrabe, C.-J. Nap, S. Almeling, Control of impurities in l-aspartic acid and l-alanine by high-performance liquid chromatography coupled with a corona charged aerosol detector, J. Chromatogr. A 1217(3) (2010) 294-301.

[10] R.A. Moreau, The analysis of lipids via HPLC with a charged aerosol detector, Lipids 41(7) (2006) 727-734.

[11] K. Zhang, L. Dai, N.P. Chetwyn, Simultaneous determination of positive and negative pharmaceutical counterions using mixed-mode chromatography coupled with charged aerosol detector, J. Chromatogr. A 1217(37) (2010) 5776-5784.

[12] S. Furota, N.O. Ogawa, Y. Takano, T. Yoshimura, N. Ohkouchi, Quantitative analysis of underivatized amino acids in the sub-to several-nanomolar range by ion-pair HPLC using a corona-charged aerosol detector (HPLC–CAD), J. Chromatogr. B 1095 (2018) 191-197.

[13] A. Socia, J.P. Foley, Direct determination of amino acids by hydrophilic interaction liquid chromatography with charged aerosol detection, J. Chromatogr. A 1446 (2016) 41-49.

[14] X. Qiu, L. Zuo, S. Sun, X. Zhao, S. Xu, Z. Zhu, T. Zhao, Z. Sun, J. Yao, G. Shan, Impurity profiling of Compound Amino Acid Injection (6AA) using ion-pair high performance liquid chromatography coupled with corona-charged aerosol detection and high resolution mass spectrometry, J. Pharm. Biomed. Anal. (2021) 114099.

[15] A. Joseph, A. Rustum, Development and validation of a RP-HPLC method for the determination of gentamicin sulfate and its related substances in a pharmaceutical cream using a short pentafluorophenyl column and a charged aerosol detector, J. Pharm. Biomed. Anal. 51(3) (2010) 521-531.

[16] A. Soliven, I.A.H. Ahmad, J. Tam, N. Kadrichu, P. Challoner, R. Markovich, A. Blasko, A simplified guide for charged aerosol detection of non-chromophoric compounds—Analytical method development and validation for the HPLC assay of aerosol particle size distribution for amikacin, J. Pharm. Biomed. Anal. 143 (2017) 68-76.

[17] Z. Long, Z. Guo, X. Liu, Q. Zhang, X. Liu, Y. Jin, L. Liang, H. Li, J. Wei, N. Wu, A sensitive non-derivatization method for apramycin and impurities analysis using hydrophilic interaction liquid chromatography and charged aerosol detection, Talanta 146 (2016) 423-429.

[18] P.H. Gamache, Charged Aerosol Detection for Liquid Chromatography and Related Separation Techniques, John Wiley & Sons, 2017.

[19] A.I. Khuri, S. Mukhopadhyay, Response surface methodology, Wiley Interdiscip. Rev. Comput. Stat. 2 (2) (2010) 128–149.

[20] Council of Europe, European Pharmacopeia Online 10.5, EDQM, Strasbourg, France, 2021, Monograph no. 0796. https://pheur.edqm.eu/app/10-5/content/10-5/0796E.htm.(Accessed 10.05.2021).

[21] Council of Europe, European Pharmacopeia Online 10.5, EDQM, Strasbourg, France, 2021, Monograph no. 0771. https://pheur.edqm.eu/app/10-5/content/10-5/0771E.htm.(Accessed 10.05.2021).

[22] Council of Europe, European Pharmacopeia Online 10.5, EDQM, Strasbourg, France, 2021, Monograph no. 0770. https://pheur.edqm.eu/app/10-5/content/10-5/0770E.htm.(Accessed 10.05.2021).

[23] A. Lodi, M. Angus, C. Nap, G. Skellern, A. Nicolas, Determination of the purity of valine by isocratic liquid chromatography coupled with charged aerosol detection (CAD), Pharmeur. Bio. Sci. Notes 2015 (2015) 11-18.

[24] R.H. Myers, D.C. Montgomery, C.M. Anderson-Cook, Response surface methodology: process and product optimization using designed experiments, John Wiley & Sons, 2016.

[25] B. Jones, P. Goos, I-optimal versus D-optimal split-plot response surface designs, J. Qual. Technol. 44(2) (2012) 85-101.

[26] T. Gorecki, F. Lynen, R. Szucs, P. Sandra, Universal response in liquid chromatography using charged aerosol detection, Anal. Chem. 78(9) (2006) 3186-3192.

[27] R. Pawellek, K. Schilling, U. Holzgrabe, Impurity profiling of l-aspartic acid and glycine using high-performance liquid chromatography coupled with charged aerosol and ultraviolet detection, J. Pharm. Biomed. Anal. 183 (2020) 113149.

[28] J.J. Russell, J.C. Heaton, T. Underwood, R. Boughtflower, D.V. McCalley, Performance of charged aerosol detection with hydrophilic interaction chromatography, J. Chromatogr. A 1405 (2015) 72-84.

[29] J.P. Hutchinson, T. Remenyi, P. Nesterenko, W. Farrell, E. Groeber, R. Szucs, G. Dicinoski, P.R. Haddad, Investigation of polar organic solvents compatible with Corona Charged Aerosol Detection and their use for the determination of sugars by hydrophilic interaction liquid chromatography, Anal. Chim. Acta 750 (2012) 199-206.

[30] J.P. Hutchinson, J. Li, W. Farrell, E. Groeber, R. Szucs, G. Dicinoski, P.R. Haddad, Comparison of the response of four aerosol detectors used with ultra high pressure liquid chromatography, J. Chromatogr. A 1218(12) (2011) 1646-1655.

[31] K. Schilling, R. Pawellek, K. Lovejoy, T. Muellner, U. Holzgrabe, Influence of charged aerosol detector instrument settings on the ultra-high-performance liquid chromatography analysis of fatty acids in polysorbate 80, J. Chromatogr. A 1576 (2018) 58-66.

[32] P.H. Gamache, R.S. McCarthy, S.M. Freeto, D.J. Asa, M.J. Woodcock, K. Laws, R.O. Cole, HPLC analysis of nonvolatile analytes using charged aerosol detection, Lc Gc Europe 18(6) (2005) 345.

[33] C.R. Mitchell, Y. Bao, N.J. Benz, S. Zhang, Comparison of the sensitivity of evaporative universal detectors and LC/MS in the HILIC and the reversed-phase HPLC modes, J. Chromatogr. B 877(32) (2009) 4133-4139.

[34] S. Kopec, U. Holzgrabe, Impurity profile of amino acids?, Pharmeur. Sci. Notes 2005(1) (2005) 39-45.

[35] K. Petritis, P. Chaimbault, C. Elfakir, M. Dreux, Ion-pair reversed-phase liquid chromatography for determination of polar underivatized amino acids using perfluorinated carboxylic acids as ion pairing agent, J. Chromatogr. A 833(2) (1999) 147-155.

[36] P. Jandera, P. Janás, Recent advances in stationary phases and understanding of retention in hydrophilic interaction chromatography. A review, Anal. Chim. Acta 967 (2017) 12-32.

[37] B. Schulze, T. Bader, W. Seitz, R. Winzenbacher, Column bleed in the analysis of highly polar substances: an overlooked aspect in HRMS, Anal. Bioanal. Chem. (2020) 1-11.

[38] Z. Huang, M. Richards, Y. Zha, R. Francis, R. Lozano, J. Ruan, Determination of inorganic pharmaceutical counterions using hydrophilic interaction chromatography coupled with a Corona® CAD detector, J. Pharm. Biomed. Anal. 50(5) (2009) 809-814.

[39] S. Jia, J.H. Park, J. Lee, S.W. Kwon, Comparison of two aerosol-based detectors for the analysis of gabapentin in pharmaceutical formulations by hydrophilic interaction chromatography, Talanta 85(5) (2011) 2301-2306.

[40] G. Kiełbowicz, P. Micek, C. Wawrzeńczyk, A new liquid chromatography method with charge aerosol detector (CAD) for the determination of phospholipid classes. Application to milk phospholipids, Talanta 105 (2013) 28-33.

[41] E. Tsochatzis, M. Papageorgiou, S. Kalogiannis, Validation of a HILIC UHPLC-MS/MS method for amino acid profiling in triticum species wheat flours, Foods 8(10) (2019) 514.

[42] International Council for Harmonization, Guideline Q2 (R1) Validation of Analytical Procedures: Text and Methodology, 2005.

[43] International Council for Harmonization, Guideline Q3A (R2) Impurities in New Drug Products, 2006.

3.5. Influence of the mobile phase composition on hyphenated ultraviolet and charged aerosol detection for the impurity profiling of vigabatrin

Ruben Pawellek, Ulrike Holzgrabe

Reprinted with permission from J. Pharm. Biomed. Anal. 2021, 201, 114110.

Abstract

Recently, charged aerosol detection (CAD), a universal detection technique in liquid chromatography, has been introduced into monographs of the European Pharmacopoeia (Ph. Eur.), which now employs HPLC-UV-CAD for assessing the impurities of the drug vigabatrin. The separation of vigabatrin and its impurities is facilitated by ion pair chromatography (IPC) in the compendial method using tridecafluoroheptanoic acid (TDFHA) as ion-pairing reagent. However, the subsequent detection of the impurities by UV-CAD is considerably impaired due to the substantial amount of ion-pairing reagent applied in the method generating high levels of background noise.

In this study, the influence of the mobile phase composition on the background noise of the CAD was evaluated applying response surface methodology. The model's results indicated that the chain length of the ion-pairing reagent is a predominant factor for noise generation. Thus, an alternative method for the impurity analysis of vigabatrin using mixed-mode chromatography (MMC) instead of IPC was developed. The dual separation mechanism of the MMC column enabled the choice of a mobile phase better suited for the individual requirements of the UV-CAD detectors, while maintaining excellent selectivity. The MMC method does not require the addition of a post-column solution to reduce the TDFHA concentration in the mobile phase, and, therefore, needs less instrumentation. Moreover, the sample concentration could be halved due to the improved LOQs of the impurities (<50 ng on column) and the analysis time could be shortened (30 to 20 min) due to improved separation efficiency. The MMC method was validated with respect to ICH guideline Q2(R1).

1. Introduction

Drugs with a weak chromophore pose a challenge to regulatory authorities, e.g. the European Pharmacopoeia (Ph. Eur.), because their poor UV absorbance characteristics interfere with the development of sensitive impurity profiling methods for routine quality control purposes when solely using the commonly applied HPLC-UV detection. Alternatively, the UV detector can be coupled with a so-called universal detector, e.g. charged aerosol detector (CAD) [1, 2], to expand the detection scope and to obtain complementary information on the actual impurity profile of the drug [3-6]. The hyphenation of detectors, however, imposes further requirements on the mobile phase composition as each detector is limited to certain organic modifiers and additives. Polar drugs showing poor UV absorbance, e.g. amino acid derived active pharmaceutical ingredients (APIs) like vigabatrin, represent an even more challenging substance class, because the separation of the main substance from its impurities cannot be accomplished by the normally applied reversed phase (RP)-HPLC analysis. To address the unsatisfactory selectivity of RP-HPLC for polar drugs, the Ph. Eur. frequently applies ion pair chromatography (IPC) [7] instead to improve the separation of the analytes investigated. However, the use of long-chain ion-pairing reagents is poorly suited for the impurity profiling of chromophore-deficient polar drugs when detection is achieved by means of coupled detection techniques, such as UV-CAD, because the ion-pairing reagent can impair low wavelength (<220 nm) UV detection and simultaneously elevate the CAD's background noise [8]. In addition, there are some renowned general drawbacks in IPC, such as extensive column equilibration times and strong adsorption of the ion-pairing reagent on the surface of the stationary phase [9, 10]. Over the last decade, mixed-mode chromatography (MMC) [11, 12] as well as hydrophilic interaction chromatography (HILIC) [13, 14] have been established as alternative separation techniques for the analysis of polar substances, thereby offering comparable selectivity without the need for ion-pairing reagents.

This study was aimed at demonstrating the benefit of a MMC method for the impurity profiling of the drug vigabatrin over the compendial applied IPC method when using UV-CAD detection. In the 10th edition of the Ph. Eur., the related substances test of vigabatrin makes use of both detection techniques. The chromophore-deficient impurities (D, E) are quantified by CAD and the UV-active impurities (A, B) by UV (Fig. 1) [15]. The compendial method employs the ion-pairing reagent tridecafluoroheptanoic acid (TDFHA) to facilitate separation of the polar impurities and the drug substance on a phenyl-hexyl column. However, the substantial amount of TDFHA (5.8 mM) used in the method and its relatively low volatility compared to shorter chain perfluorocarboxylic acids [9] is likely to produce elevated background noise in the CAD signal and thwarts low wavelength (<220 nm) UV detection. Therefore, a second pump is required to deliver a separate post-column solution consisting of methanol in order to dilute the

TDFHA-rich mobile phase. This procedure, however, limits the robustness of the method and increases the obtainable limits of quantitation (LOQs) resulting in the need for a higher sample concentration.

Here, the influence of the ion-pairing reagent on the background noise of the CAD was evaluated by response surface methodology (RSM) using a flow injection analysis (FIA) setup for a homologous series of perfluorocarboxylic acids commonly applied with CAD. In addition, the evaporation temperature of the CAD and the acetonitrile (ACN) proportion of the mobile phase were investigated toward their influence on the background noise. Statistical analysis of the flow injection runs by restricted maximum likelihood (REML) indicated that the chain length of the ion-pairing reagent used was the most influential factor toward generating background noise. Alternatively, a MMC method on a reversed-phase/strong cation exchange (RP/SCX) column was developed utilizing TFA as an acidic modifier. The performance of the MMC method was then compared to the compendial IPC method regarding required instrumentation, analysis time, obtainable LOQs, and selectivity. In addition, the MMC method was validated with respect to ICH guideline Q2(R1) [16].

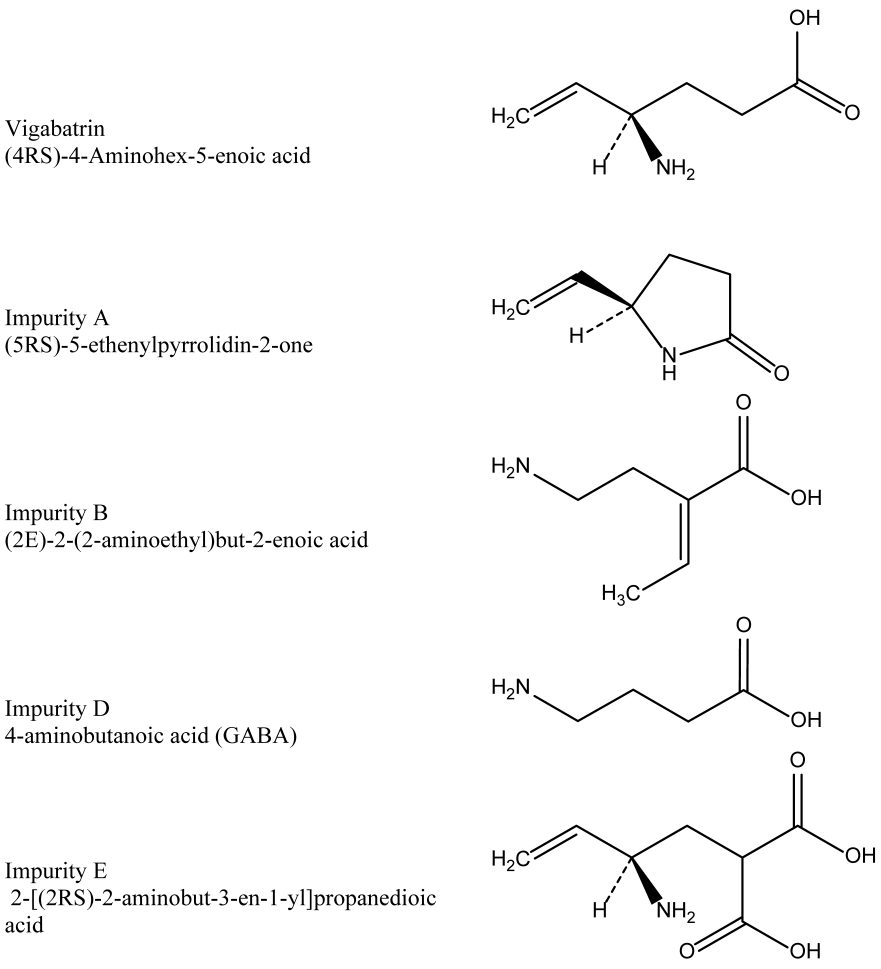

Fig. 1. Impurity profile of vigabatrin as depicted in the Ph. Eur. [15].

1. Experimental

1.1. Chemicals and reagents

Reference standards of the vigabatrin impurities A, B, D, and E as well as the vigabatrin samples were obtained from the European Directorate for the Quality of Medicines & HealthCare (EDQM; Straßbourg, France). Formic acid (FA) 98-100%, trifluoroacetic acid (TFA) ≥99%, pentafluoropropionic acid (PFPA) 97%, heptafluorobutyric acid (HFBA) ≥99.5%, nonafluoropentanoic acid (NFPA) 97%, tridecafluoroheptanoic acid (TDFHA) 99%, and HPLC grade acetonitrile (ACN) were purchased from Sigma Aldrich (Steinheim, Germany). Ultra-pure deionized (DI) water was delivered by a Milli-Q® system (Merck, Darmstadt, Germany).

1.2. Apparatus

The HPLC experiments were performed on a Vanquish™ Flex modular chromatographic system (Thermo Fisher Scientific, Germering, Germany) consisting of a binary pump with online degasser, a thermostatted split sampler, a thermostatted column compartment with passive pre-heater, and a variable wavelength detector in-line with a Vanquish™ Horizon CAD. The CAD was supplied with nitrogen gas from an ESA nitrogen generator (Thermo Fisher Scientific) connected to the in-house compressed air system. The HPLC system was controlled and runs were processed using the Chromeleon® Chromatography Data System Version 7.2.6 software program (Thermo Fisher Scientific).

1.3. Background noise measurement by flow injection analysis (FIA) setup

The outlet capillary of the Vanquish™ system's injection valve was linked to the inlet capillary of the UV detector in-line with a CAD by a connector (Viper™ union, Thermo Fisher Scientific) to perform the FIA at sufficient back pressure (>80 bar). Isocratic runs with a run time of 2 min at a flow rate of 1.0 mL/min and a column compartment temperature of 25 °C were carried out. The mobile phase consisted of either 10 mM FA, or 10 mM perfluorocarboxylic acid (TFA, PFPA, HFBA, and NFPA) respectively, in a mixture of DI water and ACN in various proportions (0 %, 10%, and 20% (v/v) organic modifier) according to the experimental plan (Table S1). Prior to each new run, the system was equilibrated for 10 min at the upcoming mobile phase conditions. When switching to another ion-pairing reagent, the system was flushed for at least 60 min using the upcoming mobile phase conditions, until a stable baseline was obtained. The background noise of the CAD was calculated for a fixed interval between min 1 and 2 of each run by the chromatographic software to prevent any interference of the injected blank solution. A fixed interval of 1 min was considered adequate as the peak half width of the injection peaks was roughly 0.030 min. The CAD's evaporation temperature (35 °C, 52 °C, 70 °C) was altered according to the experimental plan, whereas the filter constant was kept at 1.0 s, and the data collection rate was held constant at 10 Hz.

1.4. Statistical analysis

The experimental plan for conducting the FIA (Table S1) was based on a RSM study design created by the software Design-Expert 12 (Stat-Ease Inc., MN, US). The quadratic model was derived from I-optimal design, consisting of seven groups and 21 runs (Table S2). The choice of the I-optimality criterion enabled the simultaneous evaluation of numeric and categoric factors with minimal required experiments. The ACN proportion (0 – 20%) and evaporation temperature (35 – 70 °C) were chosen as numeric factors, while the number of C-atoms of the (perfluoro)carboxylic acid (C1 – C5) was selected as categoric factor (Table S3). Prior to the statistical analysis, the obtained response values were $\log_{10}$ transformed to obtain normally distributed data. The final model was solely based on linear terms as the inclusion of quadratic terms did not improve the model's validity. The adjusted coefficient of determination (R^2) of the predictive model obtained by restricted maximum likelihood (REML) analysis of the transformed responses was 0.9573 (Table S6). All factors were considered as significantly contributing to the background noise ($p < 0.05$) (Table S5). Further details are given in the supplementary material.

1.5. Chromatographic procedure of the MMC method

The vigabatrin method comprised a flow rate of 1.2 mL/min, a column temperature of 25 °C (run in still air mode), and an injection volume of 30 µL. Runs were performed isocratically on a RP/SCX mixed-mode column, SIELC Primesep® 100 (250 mm × 4.6 mm i.d., with a particle size of 5 µm and pore size of 100 Å, SIELC Technologies, Wheeling IL, USA), with the mobile phase consisting of water/ACN 85/15 (v/v) and 0.1% TFA (v/v). The CAD settings were adjusted to a filter constant of 5s, a data collection rate of 10 Hz, and an evaporation temperature of 70 °C. UV detection was performed at a detection wavelength of 210 nm applying a data collection rate of 20 Hz.

1.6. Preparation of solutions

1.6.1. Standard solutions

Standard solutions of the vigabatrin impurities (A, B, D, and E) were prepared by weighing 1.0 mg of the respective impurity and dissolving in 10.0 mL water. The standard solutions were stored at 8 °C.

1.6.2. Sample solutions

Sample solutions of vigabatrin were prepared daily by weighing 5.0 mg of the substance and dissolving in 1.0 mL water.

3. Results and discussion

3.1. Development of a MMC method as alternative to the compendial IPC method

3.1.1. Influence of the mobile phase composition on UV-CAD detection

In-line coupling of UV-CAD can be applied to extend the detection scope for a set of analytes showing divergent physico-chemical properties [1-4]. A main advantage of hyphenated UV-CAD techniques is that non-volatile analytes with weak chromophores and volatile chromophore-containing analytes can be detected simultaneously in one chromatographic run. However, with the CAD being restricted to volatile mobile phases and the UV detector's dependence on the UV cut-off of the respective mobile phase, the deliberate choice of mobile phase additives and organic modifiers is of paramount importance. With the ion-pairing reagent being the crucial additive in IPC, the obtainable quantitation limits are highly dependent on the concentration and nature of the applied additive.

To evaluate the influence of the ion-pairing reagent on the background noise of the CAD, flow injection analyses (FIA) based on RSM as depicted in section 2.4. were performed for a series of the homologous volatile perfluorocarboxylic acids TFA, PFPA, HFBA, and NFPA, which are frequently used in charged aerosol detection [8, 17, 18], and, for the purpose of comparison, FA at 10 mM concentration, respectively. RSM was chosen for its excellent predictive performance within a predefined experimental domain [19, 20]. I-optimal design aims to minimize the average variance of prediction over the whole experimental design space [21]. Besides the chain length of the ion-pairing reagent, the ACN proportion (0 – 20%) as well as the CAD's evaporation temperature (35 – 70 °C) were varied according to the experimental plan (Table S1) due to their known influence on background noise [8]. The range of the numeric factors investigated was chosen with respect to the estimated extremes of an IPC method. Thus, the maximum ACN proportion of the mobile phase was limited to 20% (v/v), since the organic modifier decreases selectivity and retention for rather polar analytes like the amino acid derived vigabatrin impurities in IPC [7] and was therefore kept at a low level. For the evaporation temperature setting, a range from the default value of 35 °C to 70 °C was selected based on preliminary experiments that showed a benefit of elevated evaporation temperatures for the non-volatile impurities D and E as their response was relatively less decreased compared to the simultaneously decreased background noise. The FIA conditions are detailed in section 2.3. The results of the FIA experiments' statistical analysis by REML are displayed in Fig. 2 and Fig. 3. where the trends for ACN proportion and evaporation temperature are shown for NFPA (C5) as mobile phase additive. It should be noted that these trends were consistent for all additives investigated (not shown).

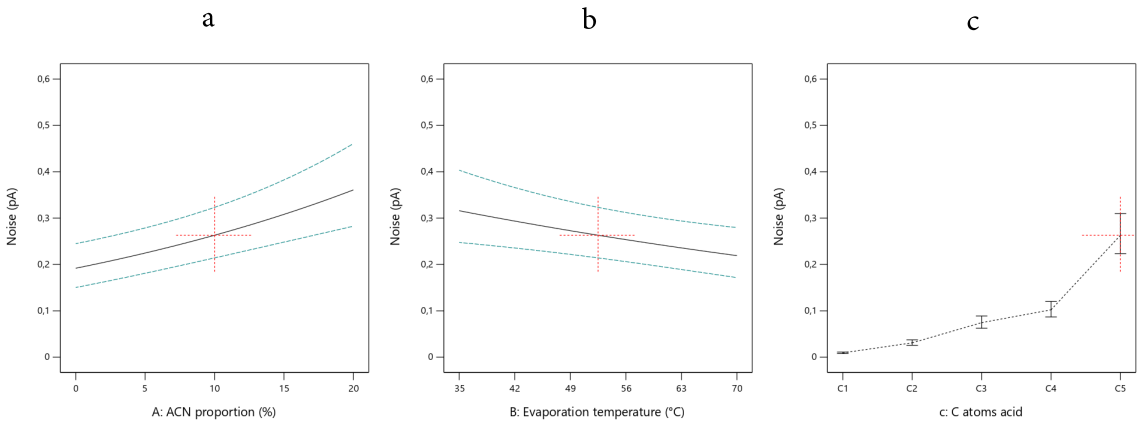

Fig. 2. Influence of (a) ACN proportion (v/v), (b) evaporation temperature on the background noise of the CAD for NFPA as mobile phase additive. One numeric factor was kept constant at a medium value, as indicated by the dotted cross. (c) Influence of the chain length (C1 – C5) of the mobile phase additive on the background noise.

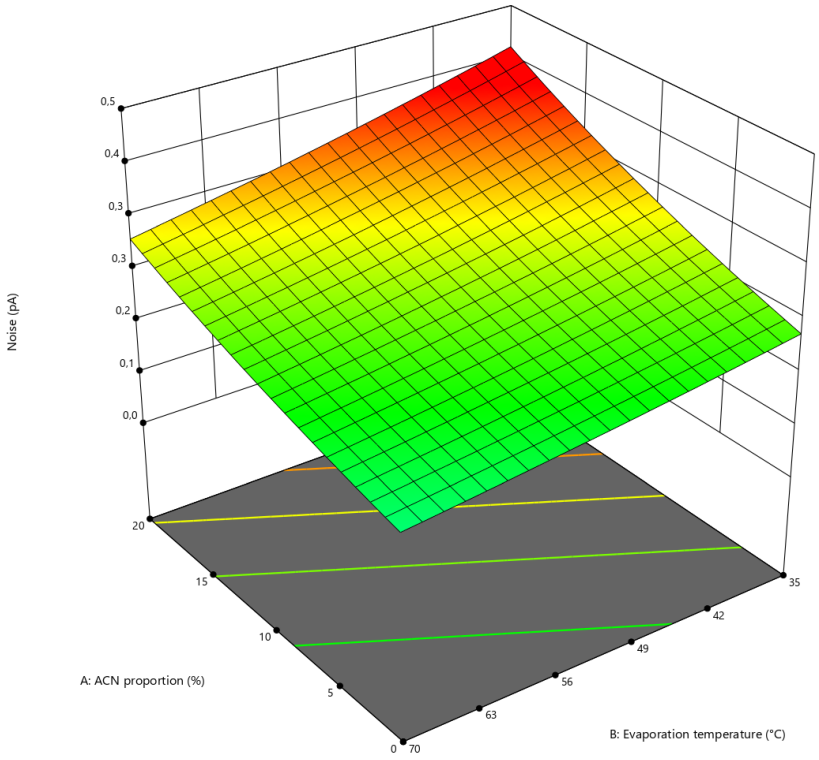

Fig. 3. 3d surface plot showing the influence of the ACN proportion (factor A) and the evaporation temperature (factor B) on the CAD's background noise for NFPA as mobile phase additive.

Increasing the evaporation temperature resulted in a reduction of the background noise, which can be explained by the enhanced evaporation of mobile phase impurities that contribute to the instantaneous background current. By contrast, increasing the ACN proportion led to higher levels of background noise. This effect was more pronounced for the long-chain

perfluorocarboxylic acids and might be attributed to a combination of factors including: increased detector mass transport when spray-drying eluents with a higher proportion of ACN; higher impurity levels being already present in the ACN; and additional factors specifically related to these longer-chain ion pairing reagents as further discussed below. Conclusions on the influence of the ACN proportion toward the S/N of a certain analyte should be drawn with caution considering the FIA results, as the signal height of the analyte also increases with ACN and, in general, organic proportion [22, 23]. The same caveat holds true for the evaporation temperature setting, which likely decreases the response for a certain analyte at elevated temperatures depending on the analyte's volatility [24]. Thus, optimization of these parameters should be based on the individual goal of the application and requires experimental verification. As the ACN content in the mobile phase simultaneously affects the separation of the analytes in most cases, improved sensitivity might be obtained at the cost of decreased selectivity. High evaporation temperatures may improve the sensitivity for non-volatile analytes, but they also reduce the detection scope as semi-volatile analytes are no longer detected.

Although the evaporation temperature and the ACN proportion both significantly influenced the level of background noise ($p < 0.05$, Table S5), the chain length of the ion-pairing reagent was found to be far more influential (Fig. 2c). Going from FA to NFPA, a substantial increase in background noise was observed. This may, in part, be related to the formation of salts between the anionic ion-pairing reagents and cationic impurities in the eluent during the droplet evaporation process [8]. Besides the formation of increasingly stable and higher mass ion-pairing reagent-impurity salts with long-chain ion-pairing reagents, the boiling point of the ion-pairing reagents increases from TFA (72 °C) to NFPA (140 °C). Thus, the formation of higher mass salts with mobile phase impurities as well as decreasing volatility of the ion-pairing reagent can likely be regarded as factors contributing to the enhanced noise generated by the long-chain ion-pairing reagents. Moreover, the purity of commercially available long-chain ion-pairing reagents is limited (97% in case of PFPA and NFPA). A modest increase in response for basic analytes when using anionic ion-pairing reagents has been reported with highest response achieved for long-chain ion-pairing reagents [25]. However, the slight increase is likely to be overcompensated by the simultaneously elevated background noise caused by long-chain ion-pairing reagents, resulting in poor S/N for the analytes. Considering the even longer chain length of the TDFHA (boiling point 175 °C) used in the compendial vigabatrin method, the need for a post-column solution to dilute the noise generating mobile phase seems inevitable to allow for sensitive detection of the impurities. This is further supported by comparing the chromatograms of the background current obtained for a 10 mM solution of TFA and a 2.5 mM solution of TDFHA in water, respectively (Fig. 4). The background current was measured at the experimental conditions showing the lowest observed noise in the RSM model (0% ACN (v/v); 70 °C evaporation temperature). Though the TDFHA concentration

investigated was 4 times lower than the TFA concentration, the observed background current was roughly 12 times higher for TDFHA. In addition, the perfluorocarboxylic acids, in contrast to other commonly applied non-volatile ion-pairing reagents, such as alkylsulfonates, show significant UV absorbance [26], so that the performance of both detectors is impaired by the ion-pairing reagent.

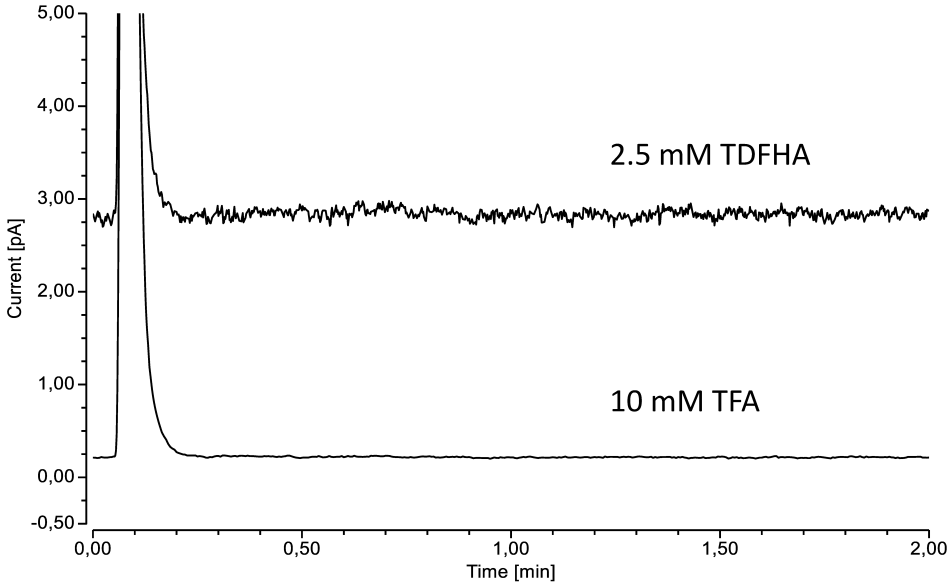

Fig. 4. Chromatograms of the CAD's background current obtained for aqueous solutions of 2.5 mM TDFHA and 10 mM TFA at a flow rate of 1.0 mL/min and an evaporation temperature of 70 °C.

Taking the FIA findings and the UV absorbance requirements together, the avoidance of ion-pairing reagents, or at least, the restriction to shorter-chain ion-pairing reagents, is highly desirable. One possible approach could be to use a higher concentration of a medium-chain ion-pairing reagent available in high purity, such as HFBA, to achieve comparable selectivity to the compendial method without the simultaneously elevated background noise assuming that the chain length is a major factor toward noise generation. However, the other common drawbacks of IPC like time-consuming system equilibration and the possible occurrence of memory effects would persist. Thus, it was aimed to develop a method not impeded by the interaction of the ion-pairing reagent with the column or the chromatographic system. As selectivity in IPC might decrease when switching to short-chain ion-pairing reagents [9], alternative separation techniques are required to maintain the separation of the main substance and its impurities.

3.1.2. Method development on a RP/SCX column

For the replacement of the compendial IPC method, MMC was chosen, since the multiple separation mechanisms in MMC enable the separation of polar and ionic compounds without using long-chain ion-pairing reagents [12]. Reversed-phase columns with embedded weak

cation exchange moiety (Primesep® 200) and strong cation exchange moiety (Primesep® 100) were tested for their selectivity toward vigabatrin and its impurities, since all impurities except the pyrrolidinone impurity A (Fig. 1) contain a primary amino group. The best separation was obtained using the Primesep 100® column; thus, the RP/SCX column was used for the further method development. Due to the dual separation mechanism of the column, selectivity can be adjusted by (I) the ionic strength and pH of the mobile phase and (II) the proportion of organic modifier. For the initial method development, an aqueous ammonium formate buffer was used as pH modifier, however, the lowest accessible pH of 2.8 was not sufficient to achieve full protonation of the dicarboxylic impurity E (pk_a1 propanedioic acid = 2.85), resulting in peak tailing and decreased retention of the latter (Fig. 5a). Moreover, the ionic strength of a 100 mM ammonium formate buffer was not sufficient to promote the elution of the analytes in a reasonable run time and the high buffer concentration already thwarted sensitive low wavelength UV detection at 210 nm. These issues could be overcome by using 0.1% TFA (v/v) instead, which makes pH adjustment to approximately 2 possible (Fig. 5b).

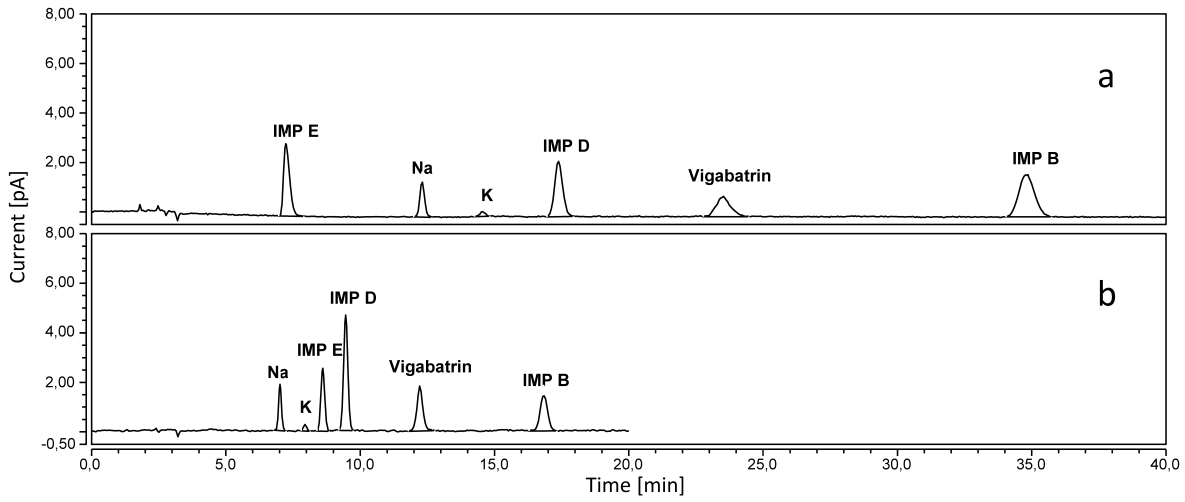

Fig. 5. Chromatograms of a 0.1% solution of vigabatrin and its impurities. Mobile phase conditions: (a) water/ACN 85/15 (v/v), 100 mM ammonium formate pH 2.8. (b) water/ACN 85/15 (v/v), 0.1% TFA (v/v).

Although TFA itself can be regarded as a short-chain ion-pairing reagent, the UV absorbance at the applied concentration (0.1%) was low enough to allow UV detection of the volatile impurity A at 210 nm, while the background noise of the CAD did not substantially increase. Furthermore, TFA does not require an extensive equilibration procedure as is the case for long-chain ion-pairing reagents, because TFA interacts only weakly with the stationary phase [10]. Therefore, using TFA as additive can be considered as the best compromise for achieving the required sensitivity for a compendial application (0.03% with respect to the main component). The ACN proportion was set at 15% (v/v), since the separation of vigabatrin and its impurities was adequate in this case and higher proportions led to increased levels of background noise in the CAD signal. The flow rate was set at 1.2 mL/min to achieve a

reasonable run time of 20 min. The CAD settings were optimized to improve the LOQs of impurities D and E by adjusting the evaporation temperature to 70 °C and the filter constant to 5 s. The data collection rate was maintained at the default value of 10 Hz. The UV detection wavelength was set at 210 nm, allowing for the determination of the volatile impurity A and the UV-active impurity B.

3.2. MMC method validation

The MMC method was validated with respect to the requirements outlined in ICH guideline Q2(R1) [16] assessing *specificity*, *range*, *linearity*, *accuracy*, *precision*, *LOQs*, and *robustness*. In addition, a system suitability test was defined to ensure the reproducibility of the method.

The *specificity* of the method was demonstrated by injection of a sample solution spiked with 0.2% of each impurity (Fig. 6). The obtained resolution was >2.0 for all peak pairs. The impurities A and B were determined by UV, while the CAD was employed for the detection of impurities D and E. Besides vigabatrin and its impurities, sodium and potassium were monitored simultaneously, as they are always present in the chromatographic system originating from the used glassware and are detected by CAD. However, they did not interfere with the analysis, as they were well separated from all other components.

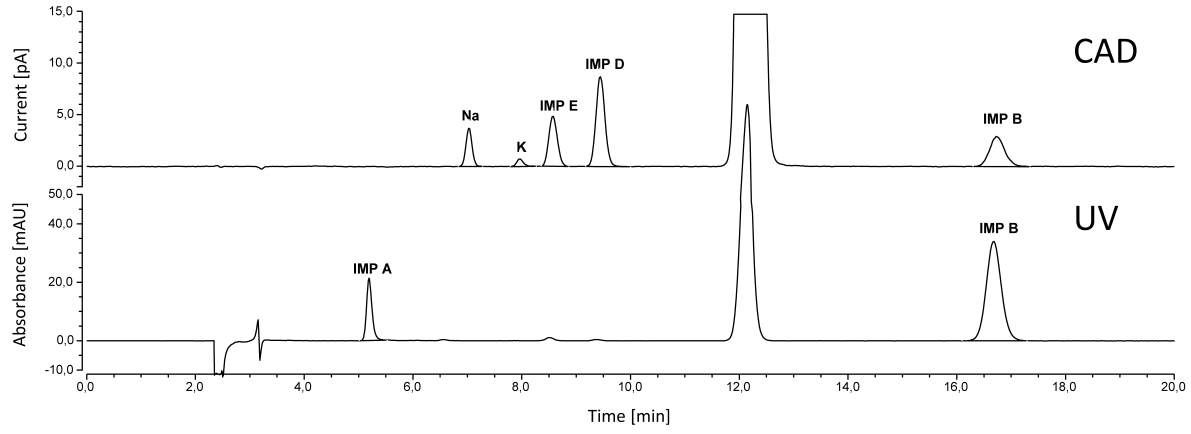

Fig. 6. Chromatograms of a vigabatrin sample solution (5 mg/mL) spiked with 0.2% of each impurity.

A *range* between 45 and 360 ng injected mass equivalent to 0.03 – 0.24% with respect to the concentration of the main substance was assessed for the impurities. The compendial reporting threshold marked the lower limit, while the upper limit was equivalent to 120% of the specification limit.

To demonstrate the method's *linearity* across the predefined range (0.03 – 0.24%), calibration curves for vigabatrin and its impurities were established based on six equally distributed calibration levels. The quality of fit was subsequently evaluated applying linear regression in

each case. With coefficients of determination (R^2) ≥0.999 (Table 1) and evenly scattered residuals (data not shown), the linearity was considered as sufficient for the intended purpose.

Table 1. Validation results for the vigabatrin impurities.

Validation Parameter	Condition	Concentration[a]	Impurity A[b]	Impurity B[b]	Impurity D	Impurity E
Linearity	Equation: y=mx+t	0.03 - 0.24%	y = 0.0074x + 0.0603	y = 0.0364x + 0.0528	y = 0.0053x + 0.0386	y = 0.0028x + 0.0023
	R^2		1	0.9999	0.9996	0.9991
Precision	%RSD Intraday Repeatability (n=6)	0.03%	0.9	0.4	4.0	3.7
		0.1%	0.5	0.2	0.9	0.9
		0.2%	0.4	0.4	1.0	1.0
	%RSD Interday Repeatability (n=2)	0.03%	1.2	0.6	3.0	6.9
		0.1%	0.7	0.2	1.1	2.3
		0.2%	0.5	0.4	1.2	1.6
LOQ	injected mass (ng)		9	6	12	18
	%[a]		0.006	0.004	0.008	0.012

[a] With respect to the concentration of the main substance.

[b] Detected by UV.

The *accuracy* of the method was determined by spiked sample solutions at the 0.03%, 0.1%, and 0.2% concentration level for each impurity. The recovery rates (%) for the individual impurities were calculated by either applying single-point calibration, or linear regression (Table 2). With recovery rates ranging from 89 to 105%, the method's accuracy was appropriate for the intended purpose.

Table 2. Recovery rates (%, n=3) for the vigabatrin impurities at the 0.03%, 0.1%, and 0.2% concentration level calculated by linear regression and single-point calibration.

Impurity	Linear regression concentration[a]			Single-point calibration concentration		
	0.03%	0.1%	0.2%	0.03%	0.1%	0.2%
A[b]	99.3±0.4	100.2±0.8	96.2±0.2	105.3±0.8	99.8±0.4	98.2±0.2
B[b]	95.5±0.5	99.5±0.0	99.8±0.1	98.3±0.6	99.9±0.0	100.2±0.1
D	91.4±2.6	103.1±0.6	102.4±0.2	101.3±0.6	100.0±0.9	97.0±0.2
E	88.8±1.4	100.8±2.5	98.5±1.6	90.7±2.7	101.9±2.3	104.8±2.0

[a] With respect to the concentration of the main substance.

[b] Detected by UV.

For evaluation of the method's *precision*, the intraday repeatability was assessed by injection of spiked sample solutions (n = 6) at the 0.03%, 0.1%, and 0.2% concentration level for each impurity. Another six injections were performed on the next day to determine the interday repeatability. The relative standard deviations (RSDs) were acceptable for both intraday repeatability (0.2 – 4.0%, n = 6) and interday repeatability (0.2 – 6.9%, n = 2) (Table 1).

The *limits of quantitation* (LOQs) for the impurities were calculated according to the S/N approach of ICH guideline Q2(R1). The LOQ was defined as S/N >10 for a threefold determination. With LOQs ranging from 6 to 18 ng (0.004 – 0.012%) injected mass on column (Table 1), the method's sensitivity was sufficient for the quantitation of all compendial impurities at the ICH claimed reporting threshold of 0.03% for drugs with an average daily intake of >2.0 g [27] (Fig. 7) .

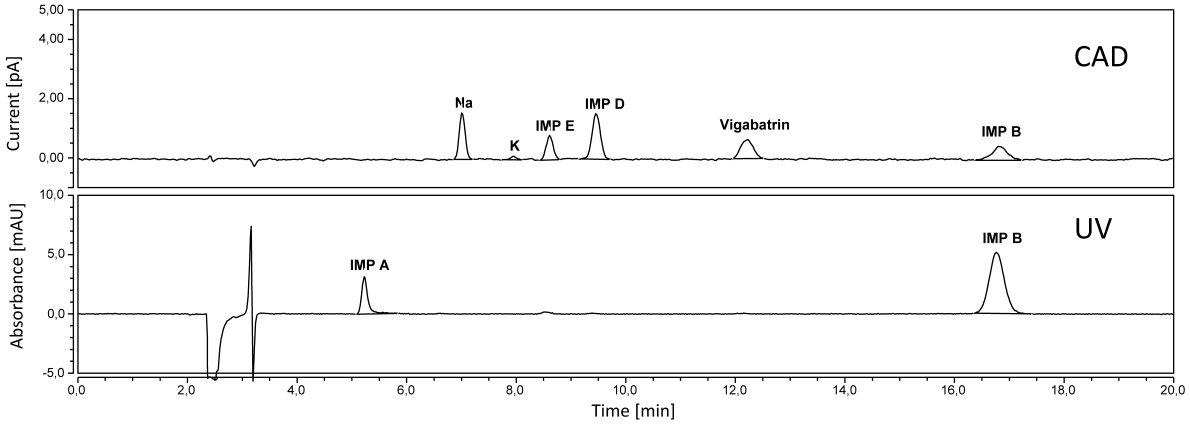

Fig. 7. Chromatograms of a 0.03% solution of vigabatrin and its impurities.

To evaluate the *robustness* of the method, a 0.1% solution of vigabatrin and its impurities was subjected to systematic variations of the chromatographic parameters after injection. The flow rate (1.0 – 1.4), column temperature (20 – 30 °C), ACN proportion (10 – 20%), and TFA proportion (0.08 – 0.12%) were varied. The method can be regarded as robust against these variations, since the resolution for each peak pair was still >1.5 at each variation (Table S7), and the peak shapes were not significantly impaired, either.

A *system suitability test* was defined to ensure the reproducibility of the method. The requirements to pass the test were set to a minimum resolution of 1.5 for the most critical peak pair of potassium – impurity E and to a S/N of ≥10 for impurity E. For evaluation of the method's performance, a 0.03% dilution of impurity E should be assessed.

3.3. MMC and IPC method comparison

The MMC method was compared to the IPC method published in the Ph. Eur. [15, 28] in terms of required instrumentation, obtainable LOQs, and selectivity. The most evident benefit of the MMC method is the avoidance of a post-column solution to dilute the poorly suited mobile phase. Therefore, there is also no need for an additional pump to deliver the flow for the post-column solution. Moreover, the complexity of the chromatographic system is effectively reduced, which could improve the method's robustness. Another advantage of the MMC method is the reduced column equilibration time. The equilibration times for TDFHA on various C18 columns of comparable size (125 x 4 mm) to the phenyl-hexyl column used in the

compendial method (Ascentis Express Phenyl-Hexyl, 100 x 4.6 mm) varied between 61 and 80 min at a flow rate of 1.0 mL/min according to Petritits et al. [9]. It was also demonstrated that the column equilibration time is independent of the applied TDFHA concentration. In contrast, the column equilibration in MMC can be accelerated by initially using a highly concentrated buffer to replace the counterions of the column. As the MMC column used here is stored in a solution of 0.1% FA (v/v), the counterions must not be replaced when using TFA resulting in a column equilibration time of less than 30 min at the method's flow rate of 1.2 mL/min. Consequently, shorter column equilibration times are to be expected for the MMC method despite the MMC column's greater dimensions (250 x 4.6 mm).

The LOQs obtained by the MMC method of 12 – 18 ng on column are comparable to those commonly reported for the CAD [29, 30], while the IPC method's sensitivity is substantially impaired by the elevated background noise. The improved LOQs are apparent when comparing the minimum required S/N for a 0.05% vigabatrin solution as part of the compendial system suitability test [15] to the S/N of a 0.1% solution of vigabatrin with the same injected mass of 150 ng obtained from the MMC method. While the compendial method demands a S/N of at least 15 for the vigabatrin peak, the MMC method yields a S/N of 40 when calculated by the approach depicted in the Ph. Eur. Further evidence is provided when comparing a chromatogram of a 0.1% solution of impurity E published by the EDQM [28] with the chromatogram of a 0.2% solution of impurity E obtained from the MMC method (Fig. 6). Although the injected mass (300 ng) is the same for the compendial chromatogram, the S/N of impurity E was higher for the MMC method chromatogram due to the smoother baseline when zoomed at the corresponding signal height. As further implication of the improved LOQs, the concentration of the sample solution could be reduced by 50% in the MMC method, while still achieving the required reporting threshold of 0.03% for specified impurities (A, B, D) and 0.05% for unspecified impurities (E) (Fig. 7). In terms of selectivity and elution order, the MMC method performed comparable to the IPC one. However, the peak shape of the main substance vigabatrin obtained by MMC was improved and impurity B was less retained resulting in an analysis time reduction from 30 min to 20 min.

4. Conclusion

The use of hyphenated detection techniques in liquid chromatography for impurity profiling purposes offers numerous advantages, e.g. additional information on the impurity profile of the drug due to the complementary detection modes. However, mobile phase considerations play a crucial role for the development of robust methods as different detectors are restricted to a distinct selection of mobile phase additives and organic modifiers. IPC employing long-chain ion-pairing reagents negatively affects at least one detection process when using UV-CAD as coupled detection technique, as was demonstrated in this work. The performance of the

described MMC method was found to be superior in terms of simplicity (no post-column solution required), sensitivity (LOQs below the compendial claimed 0.03% reporting threshold), and analysis time (20 vs. 30 min). Moreover, the MMC method does not require extensive system equilibration or dedicated equipment as is often the case when using long-chain ion-pairing reagents. With the establishment of MMC and HILIC for the analysis of polar substances, the IPC related shortcomings can be overcome, since the newer separation techniques feature low additive mobile phases suited for hyphenated detector setups. Another advantage of the MMC or HILIC techniques is the straightforward method transfer to LC-MS, which is of particular importance for the identification of unknown impurities.

Conflict of interest statement

None of the authors of this paper does have a financial or personal relationship with other people or organizations that could inappropriately influence or bias the content of the paper.

Acknowledgements

Thanks to the Thermo Fisher Scientific teams in Germering (Germany) and Waltham (MA, US) for technical support and scientific feedback and advice.

Supplementary material

Table S1. Experimental plan obtained from response surface methodology featuring I-optimal design.

Group	Run	Factor 1 A:ACN proportion	Factor 2 B:Evaporation temperature	Factor 3 c:C atoms acid	Response 1 Noise
		%	°C		pA
1	1	10	52.5	C5	0.248
1	2	0	35	C5	0.212
1	3	0	70	C5	0.152
2	4	20	52.5	C2	0.041
2	5	0	35	C2	0.024
2	6	0	70	C2	0.020
3	7	10	52.5	C4	0.109
3	8	20	70	C4	0.137
3	9	0	70	C4	0.041
4	10	0	70	C3	0.057
4	11	10	52.5	C3	0.071
4	12	20	70	C3	0.062
4	13	10	35	C3	0.091
5	14	10	70	C1	0.011
5	15	20	52.5	C1	0.009
5	16	10	35	C1	0.009
5	17	0	52.5	C1	0.007
6	18	20	70	C5	0.219
6	19	20	35	C5	0.570
6	20	10	52.5	C5	0.280
7	21	10	52.5	C4	0.119
7	22	0	35	C4	0.073
7	23	20	35	C4	0.181

Table S2. Overview of the RSM parameters.

File Version	12.0.10.0			
Study Type	Response Surface		**Subtype**	Split-plot
Design Type	I-optimal	Point Exchange	**Runs**	23.00
Design Model	Quadratic		**Blocks**	No Blocks
Groups	7.00		**Build Time (ms)**	249.00

Table S3. Factors investigated.

Factor	**Name**	**Units**	**Change**	**Type**	**Minimum**	**Maximum**	**Coded Low**	**Coded High**	**Mean**	**Std. Dev.**
A	ACN proportion	%	Easy	Numeric	0.00	20.00	-1 ↔ 0.00	+1 ↔ 20.00	9.57	8.25
B	Evaporation temperature	°C	Easy	Numeric	35.00	70.00	-1 ↔ 35.00	+1 ↔ 70.00	53.26	14.43
c	C atoms acid		Hard	Categoric	C1	C5			**Levels:**	5.00

Table S4. Analysis of the response data.

Response	**Name**	**Units**	**Observations**	**Analysis**	**Minimum**	**Maximum**	**Mean**	**Std. Dev.**	**Ratio**	**Transform**	**Model**
R1	Noise	pA	23.00	Polynomial	0.007	0.57	0.1193	0.1282	81.43	Base 10 Log	Linear

Table S5. Factors' influence on the background noise calculated by REML (Restricted Maximum Likelihood) analysis.

Source	**Term df**	**Error df**	**F-value**	**p-value**	
Whole-plot	4	16.00	131.91	< 0.0001	significant
c-C atoms acid	4	16.00	131.91	< 0.0001	
Subplot	2	16.00	17.30	< 0.0001	significant
A-ACN proportion	1	16.00	25.87	0.0001	
B-Evaporation temperature	1	16.00	8.73	0.0093	

Table S6. Fit statistics.

Std. Dev.	0,1034	**R^2**	0,9728
Mean	-1,18	**Adjusted R^2**	0,9573
C.V. %	8,77		

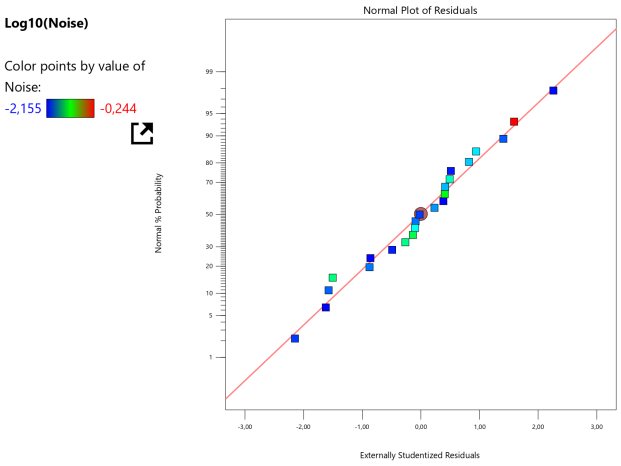

Fig. S1. Normal Plot of Residuals of the background noise.

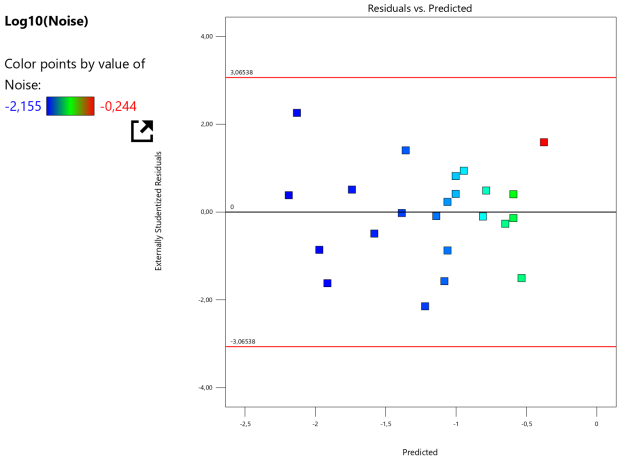

Fig. S2. Residuals vs. predicted plot of the background noise.

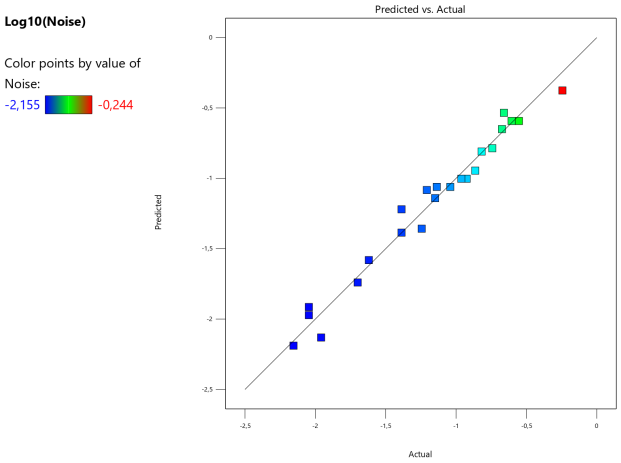

Fig. S3. Predicted vs. actual plot of the background noise.

Table S7. Robustness test and resulting resolution values.

Variation	Resolution				
	Na-Potassium	Potassium-Imp E	Imp E-D	Imp D-Vigabatrin	Vigabatrin-Imp B
no variation	4.25	2.53	2.97	6.33	7.85
20 °C Column	4.36	2.74	3.00	6.37	7.86
30 °C Column	4.16	2.40	3.01	6.25	7.82
1 flow	4.38	2.70	3.05	6.26	8.19
1,4 flow	4.24	2.50	2.91	6.08	7.30
0.08 TFA	4.50	1.50	4.07	6.44	8.26
0.12 TFA	4.04	3.12	2.20	5.86	7.84
10 ACN	4.43	4.20	3.21	5.17	9.84
20 ACN	4.46	1.46	2.74	4.55	4.23

References

[1] T. Vehovec, A. Obreza, Review of operating principle and applications of the charged aerosol detector, J. Chromatogr. A 1217(10) (2010) 1549-1556.

[2] M. Ligor, S. Studzińska, A. Horna, B. Buszewski, Corona-charged aerosol detection: an analytical approach, Crit. Rev. Anal. Chem. 43(2) (2013) 64-78.

[3] P. Sun, X. Wang, L. Alquier, C.A. Maryanoff, Determination of relative response factors of impurities in paclitaxel with high performance liquid chromatography equipped with ultraviolet and charged aerosol detectors, J. Chromatogr. A 1177(1) (2008) 87-91.

[4] A.G. Pereira, F.B. D'Avila, P.C.L. Ferreira, M.G. Holler, R.P. Limberguer, P.E. Froehlich, Method Development and Validation for Determination of Cocaine, its Main Metabolites and Pyrolytic Products by HPLC–UV–CAD, Chromatographia 79(3-4) (2016) 179-187.

[5] C.-E. Zhang, L.-J. Liang, X.-H. Yu, H. Wu, P.-f. Tu, Z.-J. Ma, K.-J. Zhao, Quality assessment of Astragali Radix from different production areas by simultaneous determination of thirteen major compounds using tandem UV/charged aerosol detector, J. Pharm. Biomed. Anal. 165 (2019) 233-241.

[6] O. Wahl, J. Cleynhens, A.M. Verbruggen, U. Holzgrabe, Impurity profiling of N, N′-ethylenebis-l-cysteine diethyl ester (Bicisate), J. Pharm. Biomed. Anal. 150 (2018) 132-136.

[7] T. Cecchi, Ion pairing chromatography, Critical Reviews in Analytical Chemistry 38(3) (2008) 161-213.

[8] P.H. Gamache, Charged aerosol detection for liquid chromatography and related separation techniques, John Wiley & Sons, 2017

[9] K. Petritis, P. Chaimbault, C. Elfakir, M. Dreux, Ion-pair reversed-phase liquid chromatography for determination of polar underivatized amino acids using perfluorinated carboxylic acids as ion pairing agent, J. Chromatogr. A 833(2) (1999) 147-155.

[10] P. Chaimbault, K. Petritis, C. Elfakir, M. Dreux, Ion-pair chromatography on a porous graphitic carbon stationary phase for the analysis of twenty underivatized protein amino acids, J. Chromatogr. A 870(1-2) (2000) 245-254.

[11] Y. Yang, X. Geng, Mixed-mode chromatography and its applications to biopolymers, J. Chromatogr. A 1218(49) (2011) 8813-8825.

[12] K. Zhang, X. Liu, Mixed-mode chromatography in pharmaceutical and biopharmaceutical applications, J. Pharm. Biomed. Anal. 128 (2016) 73-88.

[13] B. Buszewski, S. Noga, Hydrophilic interaction liquid chromatography (HILIC)—a powerful separation technique, Anal. Bioanal. Chem. 402(1) (2012) 231-247.

[14] B. Dejaegher, Y. Vander Heyden, HILIC methods in pharmaceutical analysis, J. Sep. Sci. 33(6-7) (2010) 698-715.

[15] Council of Europe, European Pharmacopeia Online 10.5, EDQM, Strasbourg, France (2021) Monograph no. 2305. https://pheur.edqm.eu/app/10-5/content/10-5/2305E.htm. (Accessed 14.01.2021).

[16] International Council for Harmonization, Guideline Q2 (R1) Validation of Analytical Procedures: Text and Methodology (2005).

[17] S. Furota, N.O. Ogawa, Y. Takano, T. Yoshimura, N. Ohkouchi, Quantitative analysis of underivatized amino acids in the sub-to several-nanomolar range by ion-pair HPLC using a corona-charged aerosol detector (HPLC–CAD), J. Chromatogr. B 1095 (2018) 191-197.

[18] U. Holzgrabe, C.-J. Nap, N. Kunz, S. Almeling, Identification and control of impurities in streptomycin sulfate by high-performance liquid chromatography coupled with mass detection and corona charged-aerosol detection, J. Pharm. Biomed. Anal. 56(2) (2011) 271-279.

[19] A.I. Khuri, S. Mukhopadhyay, Response surface methodology, Wiley Interdiscip. Rev. Comput. Stat. 2(2) (2010) 128-149.

[20] R.H. Myers, D.C. Montgomery, C.M. Anderson-Cook, Response surface methodology: process and product optimization using designed experiments, John Wiley & Sons, 2016.

[21] B. Jones, P. Goos, I-optimal versus D-optimal split-plot response surface designs, J. Qual. Technol. 44(2) (2012) 85-101.

[22] J.P. Hutchinson, T. Remenyi, P. Nesterenko, W. Farrell, E. Groeber, R. Szucs, G. Dicinoski, P.R. Haddad, Investigation of polar organic solvents compatible with Corona Charged Aerosol Detection and their use for the determination of sugars by hydrophilic interaction liquid chromatography, Anal. Chim. Acta 750 (2012) 199-206.

[23] J.P. Hutchinson, J. Li, W. Farrell, E. Groeber, R. Szucs, G. Dicinoski, P.R. Haddad, Universal response model for a corona charged aerosol detector, J. Chromatogr. A 1217(47) (2010) 7418-7427.

[24] K. Schilling, R. Pawellek, K. Lovejoy, T. Muellner, U. Holzgrabe, Influence of charged aerosol detector instrument settings on the ultra-high-performance liquid chromatography analysis of fatty acids in polysorbate 80, J. Chromatogr. A 1576 (2018) 58-66

[25] J.J. Russell, J.C. Heaton, T. Underwood, R. Boughtflower, D.V. McCalley, Performance of charged aerosol detection with hydrophilic interaction chromatography, J. Chromatogr. A 1405 (2015) 72-84.

[26] L. Wójcik, B. Szostek, W. Maruszak, M. Trojanowicz, Separation of perfluorocarboxylic acids using capillary electrophoresis with UV detection, Electrophoresis 26(6) (2005) 1080-1088.

[27] International Council for Harmonization, Guideline Q3A (R2) Impurities in New Drug Products (2006).

[28] Council of Europe, Knowledge Database, EDQM, Strasbourg, France (2021) Search item: Vigabatrin. https://extranet.edqm.eu/4DLink1/4DCGI/Web_View/mono/2305. (Accessed 14.01.2021).

[29] T. Gorecki, F. Lynen, R. Szucs, P. Sandra, Universal response in liquid chromatography using charged aerosol detection, Anal. Chem. 78(9) (2006) 3186-3192.

[30] S. Almeling, D. Ilko, U. Holzgrabe, Charged aerosol detection in pharmaceutical analysis, J. Pharm. Biomed. Anal. 69 (2012) 50-63.

3.6. Impurity profiling of L-aspartic acid and glycine using high-performance liquid chromatography coupled with charged aerosol and ultraviolet detection

Ruben Pawellek, Klaus Schilling, Ulrike Holzgrabe

Reprinted with permission from J. Pharm. Biomed. Anal. 2020, 183, 113149.

Abstract

For the compendial related substances test of L-aspartic acid (Asp) and glycine (Gly), two separate reversed-phase ion-pair high-performance liquid chromatography methods coupled with charged aerosol and ultraviolet detection were developed. Separation of all putative impurities, in particular of the related carboxylic and amino acids, was achieved using volatile perfluorocarboxylic acids as ion-pairing reagents on a polar embedded C18 stationary phase. It was shown that an adjustment of the evaporation temperature of the charged aerosol detector (CAD) was an efficient strategy for meeting the required quantitation limits, when dealing with non-volatile analytes. It was also demonstrated that the usage of a two-detector setup can be beneficial for extending the detection range and providing accurate quantitation of low-level impurities (LOQs from 5 to 50 ng on column). Both methods were validated with accordance to ICH guideline Q2(R1) assessing specificity, linearity, accuracy, precision, and robustness. Several batches of Asp and Gly were tested for related substances using the developed methods. The purity of each sample was higher than 99.7 %. Coupled charged aerosol and UV detection proved to be a more simple, robust and selective alternative to established derivatization procedures such as the Amino-Acid-Analyser (AAA) for the impurity profiling of amino acids and should thus be considered for implementation into pharmacopoeial monographs in the future.

1. Introduction

Amino acids have numerous applications in the pharmaceutical and nutritional field serving as excipients in pharmaceutical and biopharmaceutical formulations, as starting materials for drug and protein synthesis, or directly as active pharmaceutical ingredients e.g. clinical parenteral nutrition solutions and nutritional supplements [1-3]. Since amino acids and amino acid derived substances, such as aspartame, are usually administered with a high daily dose [4], their quality control is of paramount interest because even impurities that are only present in low amounts, are consumed in significant quantities. For drug substances with a daily intake of more than 2 grams per day, the ICH guideline Q3A(R2) requests a reporting threshold of 0.03 % (m/m) for each impurity [5].

The analysis of free amino acids requires the use of sensitive detection techniques. For the detection of underivatized amino acids, liquid chromatography coupled to mass spectrometry [6] or CAD [7, 8] has been frequently used over the last five years. The impurity profiling of amino acids is also predominantly performed by means of HPLC coupled to various detectors, such as UV detector [9], CAD [10], and mass spectrometry [11].

The separation and detection of amino acids is a chromatographic challenge due to their polar nature and lack of a suitable chromophore, which usually prevents the application of RP-HPLC-UV. As an alternative, derivatization procedures, such as the one used by Amino-Acid-Analysers (AAA), were developed for quality control purposes [12]. Derivatization methods may solve some analyte specific challenges but are often prone to errors and are dedicated to the analysis of amino acids or amine-containing structures, making simultaneous detection of structural divergent impurities such as plain organic acids impossible.

The charged aerosol detector (CAD) is an aerosol-based detector that has been used routinely for a wide variety of applications over the last decade [13]. Its detection principle is almost independent of the physicochemical properties of the analyte and therefore suitable for the analysis of the weak-chromophoric amino acids [14]. Analogous to other aerosol-based detectors, namely the evaporative light scattering detector (ELSD) and the condensation nucleation light scattering detector (CNLSD), the detection process starts by the nebulization of the column eluent into droplets, which are subsequently dried into particles. In case of the CAD, the particles are then charged through collision with an ionized gas stream. The aggregate charge is then measured by a highly sensitive electrometer, generating a signal directly proportional to the quantity of analyte present. Compared to the ELSD, the CAD is typically found to be more robust and sensitive [15]. Furthermore, it is cheaper, easier to use and its response is less dependent on analyte properties than the CNLSD [16]. A common drawback for all aerosol-based detectors is the restriction to non-volatile or semi-volatile analytes. The range of analytes measured can be extended by coupling to a complementary

detector, e.g., a UV detector. Another limitation of all aerosol-based detectors is the nonlinear response over extended concentration ranges. However, this is negligible when dealing with small ranges as it is the case with impurity profiling.

Among the proteinogenic amino acids, the more polar ones are the most challenging analytes to measure, since their sole UV-absorbing structure is the carboxylic moiety, and the hydrophilic nature of these compounds causes coelution of many amino acids under RP-HPLC conditions. For this reason, the polar amino acids L-aspartic acid (Asp) and glycine (Gly) were chosen as subjects of this study, as they are currently tested for related substances by two different methods in the European Pharmacopoeia (Ph. Eur.): one being the test for ninhydrin positive substances by means of the AAA, the second covering the remaining impurities that are not accessible by means of the AAA [17, 18].

The impurity profile of a particular amino acid strongly depends on the production process. The main industrial production routes comprise chemical synthesis, hydrolysis of proteins/peptides followed by chromatographic separation, enzyme synthesis and fermentation [19]. For Asp obtained by enzyme catalysis, the main production process according to available information [20], possible impurities are fumaric acid as a starting material, maleic acid as an impurity of fumaric acid, malic acid which may be produced enzymatically from fumaric acid, and L-alanine as a decarboxylation product of Asp (Table 1). In the case of production of Asp by protein hydrolysis, L-glutamic acid (Glu) is also a possible by-product. Since Glu and Asp are acidic amino acids, it is possible that Glu is not completely removed by a chromatographic purification step [10]. For the achiral Gly, the two main processes of production are amination of chloroacetic acid with ammonia [21] and the Strecker amino acid synthesis [20]. The impurity profile of Gly is structurally diverse, consisting of the related amino acids L-serine (Ser), sarcosine (Sar) and beta-alanine (ß-Ala), peptides diglycine (Gly-Gly) and triglycine (Gly-Gly-Gly), carboxylic acids, chloroacetic acid and iminodiacetic acid, and also the apolar substances glycine anhydride and hexamethylentetramine (Urotropine) (Table 1) [18].

The aim of this work was to develop HPLC methods with coupled charged aerosol and UV detection for the related substances test of either Asp or Gly, combining the currently applied separate methods for ninhydrin positive substances and other impurities to one single method. To the best of our knowledge this is the first approach that is capable of separating and quantifying all occurring impurities of both Asp and Gly in one single run at the required concentration level (0.03 %, with respect to the concentration of the sample solution). The presented methods can be considered for implementation into the monographs of the Ph. Eur. as they are less time consuming and are more specific and sensitive compared to the currently applied methods.

Table 1. Impurity profile of L-aspartic acid and glycine, respectively.

L-Aspartic acid (Asp)	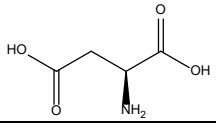	Glycine (Gly)	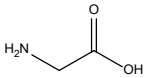
L-Alanine (Ala)	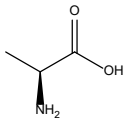	Beta-Alanine (ß-Ala)	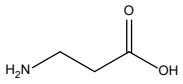
L-Asparagine (Asn)	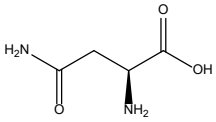	Chloroacetic acid	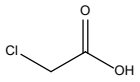
Fumaric acid	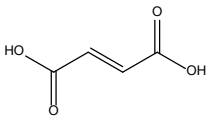	Glycine anhydride	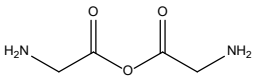
L-Glutamic acid (Glu)	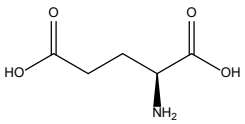	Diglycine (Gly-Gly)	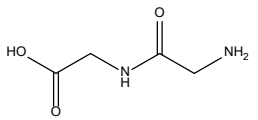
Maleic acid	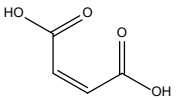	Triglycine (Gly-Gly-Gly)	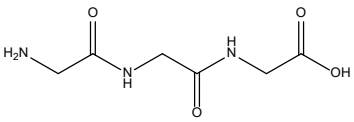
Malic acid	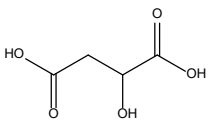	Iminodiacetic acid	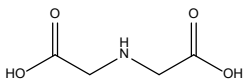
		Sarcosine (Sar)	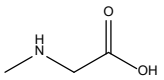
		L-Serine (Ser)	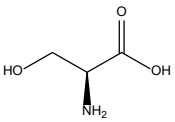
		Hexamethylentetramine (Urotropine)	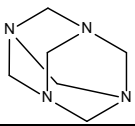

2. Experimental

2.1. Chemicals and reagents

Analytical grade amino acids, carboxylic acids, glycine anhydride and hexamethylentetramine as well as trifluoroacetic acid 99 % (TFA), pentafluoropropionic acid 97 % (PFPA), heptafluorobutyric acid 99 % (HFBA), nonafluoropentanoic acid 97 % (NFPA) and tridecafluoroheptanoic acid 99 % (TDFHA) were purchased from Sigma Aldrich (Steinheim, Germany). The amino acid test samples were obtained from Sigma Aldrich, Fluka (Neu-Ulm, Germany), Merck (Darmstadt, Germany) and Alfa Aesar (Karlsruhe, Germany). Ultra-pure deionized (DI) water was delivered by a Milli-Q® system (Merck). HPLC grade acetonitrile (ACN) was supplied by Sigma Aldrich.

2.2. Apparatus

The HPLC methods were developed and validated on a Thermo Scientific™ Vanquish™ Flex modular chromatographic system consisting of a binary pump with online degasser, a thermostatted split sampler, a thermostatted column compartment with passive pre-heater, and a variable wavelength detector in-line with a Vanquish™ Horizon CAD (Thermo Fisher Scientific, Germering, Germany). The CAD was supplied with nitrogen gas from an ESA nitrogen generator (Thermo Fisher Scientific) connected to the in-house compressed air system. The instrument was controlled and runs were processed using the Chromeleon® Data System Version 7.2.6 software program (Thermo Fisher Scientific).

For both methods, a polar embedded C18 Polar Advantage II (150 x 4.6 mm i.d., 3 µm particle size and 100 Å pore size) column was used as stationary phase (Thermo Fisher Scientific, Runcorn, UK).

2.2.1. Aspartic acid method

The chromatographic conditions used a flow rate of 0.8 mL/min, a column temperature of 25 °C (run in still air mode), and isocratic elution. The mobile phase consisted of 7 mM NFPA and 4 mM TFA in ultrapure water. The injection volume was 20 µL, and the run time was 10 minutes. The detector settings for the CAD were as follows: evaporation temperature 50 °C, filter constant 5 s, data collection rate 10 Hz and a power function value of 1.0. For UV detection, a wavelength of 210 nm and a data collection rate of 20 Hz were used.

2.2.2. Glycine method

In the case of the Gly method, a flow rate of 0.8 mL/min, a column temperature of 25 °C (run in still air mode), and gradient elution were used. Mobile phase A consisted of 1.25 mM TDFHA and 6.5 mM TFA in ultrapure water, mobile phase B was 1.25 mM TDFHA in I. The gradient program started with an isocratic stage of 1% B for the first 8 minutes, followed by a linear

increase from 1 % to 10 % B for the next two minutes, a hold of 10 % B from minutes 10 to 18 and a re-equilibration step between minutes 18 and 20 from 10 % to 1 % B. To ensure complete re-equilibration of the chromatographic system, the column was flushed with the initial mobile phase composition for 15 minutes resulting in a total run time of 35 minutes. The CAD was set to an evaporation temperature of 70 °C, a filter constant of 10 s, a data collection rate of 10 Hz and a power function value of 1.0. UV detection was performed using a detection wavelength of 210 nm and a data collection rate of 20 Hz.

2.2.3. Equilibration, Washing and Retention Time Reproducibility

The observed column equilibration times of the methods varied when switching between the two methods depending on the chain length of the respective ion-pairing reagent. The use of NFPA as ion-pairing reagent led to significantly shorter equilibration times (t_{eq} ~ 25 min), compared to TDFHA (t_{eq} ~ 90 min), due to a lower extent of adsorption on the hydrophobic C18 stationary phase [22]. To prevent irreversible modification of the surface of the stationary phase, the column was flushed with 25 column volumes of I and 15 column volumes of methanol as a regeneration procedure [28] before changing the ion-pairing reagent. Prior to the Gly testing, the column had to be equilibrated at the final gradient conditions of 10 % B to minimize retention time shifts. The retention time reproducibility was satisfactory after injection of three blank runs (RSD < 0.5 %).

2.3. Preparation of solutions

2.3.1. Standard solutions

Stock solutions of each impurity standard were prepared by accurately weighing 10 mg of the impurity and dissolving in 10.0 mL ultrapure water. The stock solutions were used as calibration or external standards and for spiking of the sample solutions by appropriate dilution with mobile phase. The standard solutions were stored at 8 °C and found to be stable for at least one week.

2.3.2. Sample solutions

The sample solutions were freshly prepared on a daily basis by weighing 50 mg of Asp or 100 mg of Gly and dissolving in 10.0 mL mobile phase. Due to low solubility, the sample solution of Asp had to be stirred and heated at 50 °C for about 10 minutes to achieve complete dissolution. No precipitation occurred after cooling to room temperature. The sample solutions were stable for at least one day at room temperature.

3. Results and discussion

3.1. Method development

3.1.1. Separation of the amino acids and other possible impurities

Besides derivatization procedures, ion-pair chromatography [22], ion-exchange chromatography (IEC) [23], hydrophilic interaction chromatography (HILIC) [24] and mixed-mode chromatography [25] have successfully been applied to amino acid analysis. While IEC suffers from limited selectivity, HILIC and mixed-mode chromatography provide good resolution of polar amino acids due to multiple interaction mechanisms. However, the selectivity strongly depends on the nature of the stationary phase and there is a large number of different column chemistries. Even the same column chemistry from two separate manufacturers will result in different selectivity, which makes it impossible to obtain reproducible results, unless the exact same column is used [26, 27]. Moreover, some mixed-mode columns were found to degrade faster than classical RP-HPLC columns [28]. In addition, the sample must be soluble in highly organic mobile phase for HILIC applications, which is not the case for Asp. Ion-pair chromatography on C18 reversed-phase columns coupled to aerosol-based detectors has already been used for the separation and detection of all proteinogenic amino acids as well as for impurity profiling of polar amino acids [10, 22]; thus it was the method of choice. At low concentrations, the common ion-pairing reagents show negligible UV-absorption, which was a prerequisite for the intended two-detector setup using low wavelength UV.

A C18 reversed-phase column with embedded amide groups was chosen as the stationary phase. The amide functionality provides additional selectivity for polar analytes and is compatible even with 100 % aqueous conditions. Since the application of charged aerosol detection requires volatile mobile phase additives, perfluorocarboxylic acids were chosen as ion-pairing reagents. For the impurity testing of Asp (the impurity profile is displayed in Table 1a), TFA, PFPA, HFBA and NFPA were evaluated as mobile phase additives in aqueous solution (Fig. 1). For the retention factor “k” of the analytes, two general tendencies were observed. The retention times of the amino acids could be extended with increasing quantities of the ion-pairing reagent, as well as with their increasing chain length. In contrast, the retention of the organic impurities was reduced upon accumulation of the ion-pairing reagent on the surface of the stationary phase. NFPA was chosen for further development since it provided the best separation for the amino acids. However, the separation of Asn and Asp was impaired by the very broad sample peak of Asp, and fumaric acid coeluted with the late eluting amino acids. By addition of a small amount of the competing ion-pairing reagent TFA, the peak width of the Asp sample peak was significantly decreased and fumaric acid was well separated from Ala and Glu due to a reduced retention of the amino acids.

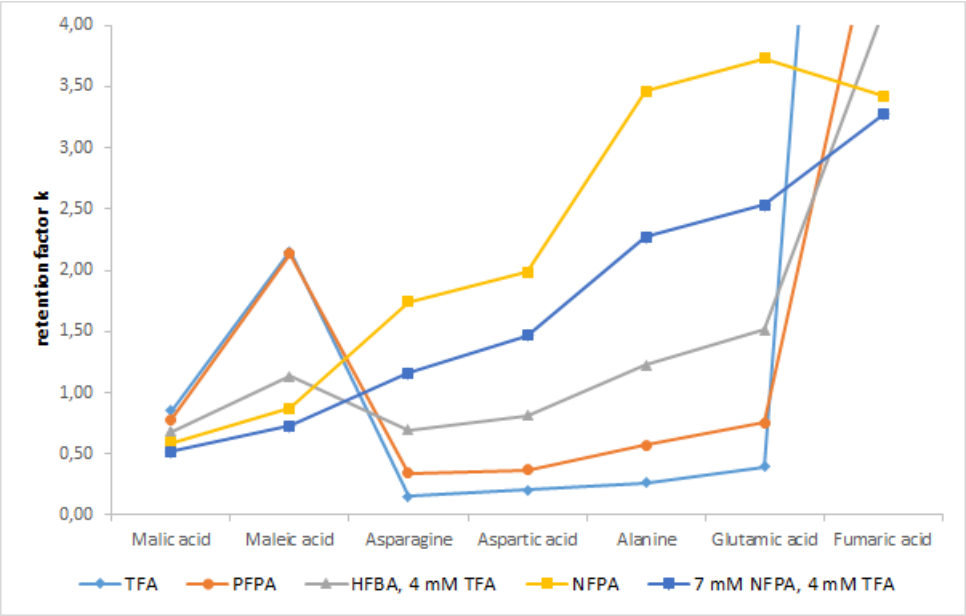

Fig. 1. Retention factor k of the impurities as a function of the mobile phase composition; concentration 10 mM unless otherwise stated. The higher k values for fumaric acid are not shown for better clarity of the graph.

The final ion-pairing reagent composition of 7 mM NFPA and 4 mM TFA represents the best compromise between resolution and sensitivity. NFPA only being commercially available in 97 % purity led to elevated background noise with increasing concentration; thus, a reduction of the amount of the used ion-pairing reagents was necessary. The addition of organic modifier to the mobile phase was also investigated, but not taken into account for the final method conditions, as the selectivity was negatively affected.

The Asp method was also tested for the impurity analysis of Gly, but NFPA was not selective enough to provide separation of the closely related amino acids Ser, Gly and Sar. On a C18 column, the selectivity for amino acids increases with the chain length of the ion-pairing reagent [22], thus TDFHA was chosen instead of NFPA. Variations of the amount of TDFHA under fully aqueous conditions did not significantly affect the separation of the other impurities, therefore, the next method developments concentrated on the separation of the critical peak pairs Ser-Gly and Gly-Sar. At 1 mM TDFHA, the critical peak pairs were all well resolved, the main peak of the Gly-sample, however, coeluted with Sar due to excessive peak fronting. Again, the addition of a small proportion of TFA (6.5 mM) to the mobile phase was necessary to obtain an appropriate peak shape of the main peak. As a consequence, the elution order of the Sar-Gly peak pair was inverted and the retention times of the amino acids decreased. Separation of Gly and all potential impurities was achieved isocratically with 99 % 1.25 mM TDFHA, 6.5 mM TFA in water (A) and a small organic proportion of 1 % 1.25 mM TDFHA in CAN (B). To facilitate a reasonable run time and improve the peak shape of the late eluting impurities, a gradient from 1 % to 10 % B was used. The final method was capable of separating all

impurities in 20 minutes, followed by 15 minutes of re-equilibration to recover the initial chromatographic conditions (the selectivity of the final methods is illustrated in Fig. 5 and Fig. 6).

3.1.2. Optimization of CAD settings and other chromatographic parameters

Among the adjustable CAD settings, the evaporation temperature is by far the most influential parameter regarding the detection performance, i.e., sensitivity limits [29]. As a consequence, optimization procedures become essential in method development, in particular when dealing with volatile perfluorinated ion-pairing reagents, which may produce elevated background noise levels under standard settings. Analyte response and background noise were investigated as a function of evaporation temperature in increments of 5 °C, with the default set point of 35 °C as a starting point (Fig. 2).

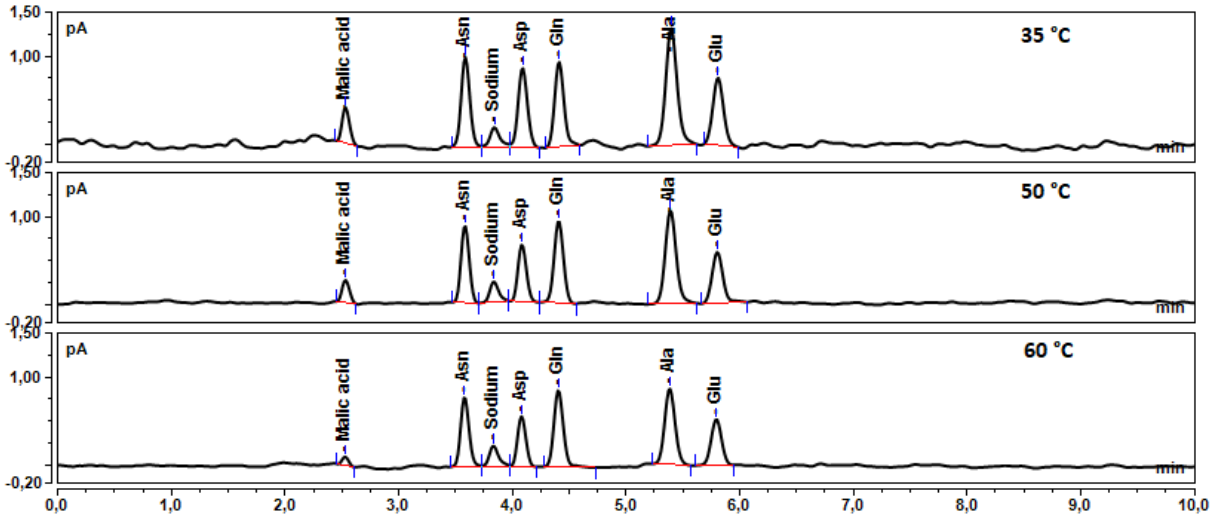

Fig. 2. Influence of the evaporation temperature on the background noise and the response of Asp and potential impurities at a concentration of 0.03 % with respect to the concentration of the sample solution (Gln was not considered to be an impurity of Asp in the following, since it was not found in the investigated batches and it cannot derive from the production process [10]); evaporation temperatures of 35 °C, 50 °C and 60 °C, for further method conditions see section 2.3.1.

It could be shown that sensitivity limits of polar nonvolatile analytes such as amino acids greatly profit from higher evaporation temperatures, since the loss of analyte response is less pronounced compared to the simultaneously reduced background noise. Another reason for the relatively low loss of analyte response is a decrease in volatility of the analyte due to the formation of analyte salts with the ion-pairing reagent. Analytes that do not interact with the ion-pairing reagent and are more volatile, e.g. malic acid, however, had a different evaporation temperature optimum than the non-volatile impurities, which was not relevant for the other organic acids since they were detected by UV. The optimal evaporation temperature for the Asp method was limited to 50 °C due to the more pronounced response drop of malic acid at

higher temperatures, while the response of the non-volatile Gly impurities was stable at even higher temperatures (Fig. 3). For the Gly method, an evaporation temperature of 70 °C was chosen, since it was the best compromise between sensitivity and resolution.

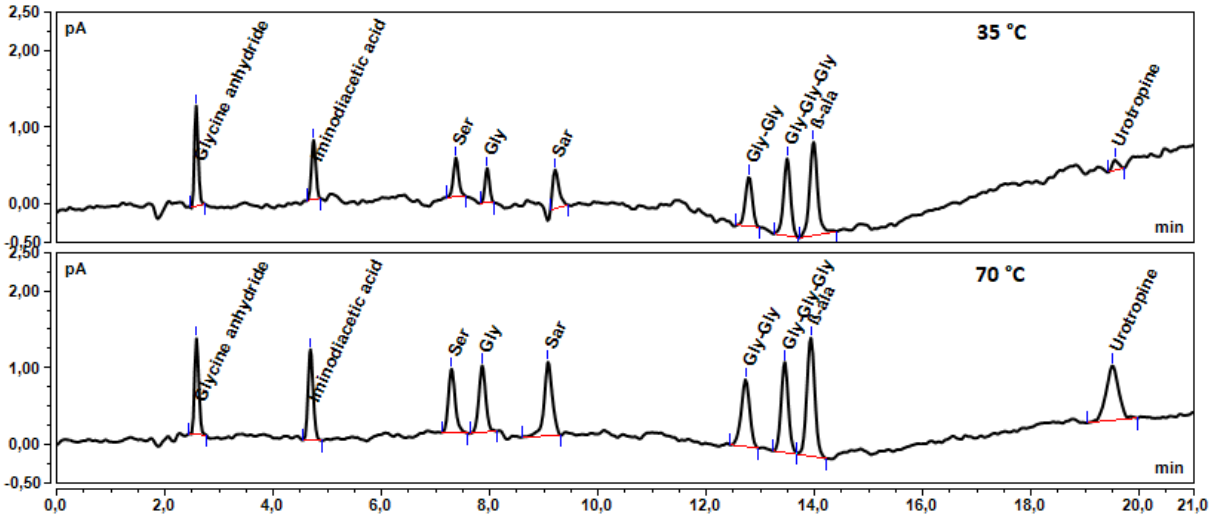

Fig. 3. Influence of the evaporation temperature on the background noise and response of Gly and potential impurities at a concentration of 0.05 % with respect to the concentration of the sample solution; evaporation temperatures of 35 °C and 70 °C, for further method conditions see section 2.3.2.

Another CAD setting influencing the chromatographic and the detection performance simultaneously is the filter constant. A higher filter constant reduces background noise by baseline smoothing, but, conversely, decreases the resolution of the analytes. The chosen filter constant was higher for Gly (10 s) compared to Asp (5 s) due to the elevated background noise of the Gly method. In addition, the power function value setting is primarily used for optimizing the linear range of the detector [29]. In this particular case, the response was demonstrated to be sufficiently linear over the required range (0.03-0.24 %), thus the default value of 1.0 was maintained.

Further parameters that were considered for method development but found to be less influential to chromatographic performance were column temperature and flow rate. For both methods, flow rates of 0.8 mL/min and column temperatures of 25 °C were used.

3.1.3. UV-CAD detection

In-line coupling of UV and CAD can be achieved easily by connecting the outlet of the UV module to the inlet of the CAD module via a capillary. Mobile phase considerations are the most important factor for combined method development, since the CAD is only compatible with volatile mobile phase additives, while the use of low wavelength UV is restricted to mobile phases that allow for the application of a detection wavelength below 220 nm. The use of low concentrations of volatile ion-pairing reagents as mobile phase additives and ACN (UV cutoff 190 nm) as an organic modifier, enabled the application of the coupled detection mode, which

extended the range of analytes detected to include volatile analytes, e.g. chloroacetic acid, and analytes with weak chromophores, e.g. amino acids. Even very low levels of unknown impurities that were not detectable by UV could be detected and quantified using CAD, which underlines the benefit of complementary detection techniques in impurity profiling [1].

The impurity profile of Asp comprises the dicarboxylic acids malic acid, maleic acid and fumaric acid, as well as the polar amino acids Asn, Ala and Glu (Table 1). In general, the organic acids showed a reduced response compared to the amino acids using CAD detection (Fig. 4), which can be explained by their higher volatility and inability to form salts with the ion-pairing reagent. On the other hand, fumaric acid and maleic acid possess a suitable chromophore, making UV detection at 210 nm the method of choice. Malic acid, however, was also quantified with CAD, since its chromophore is too weak for sensitive UV detection.

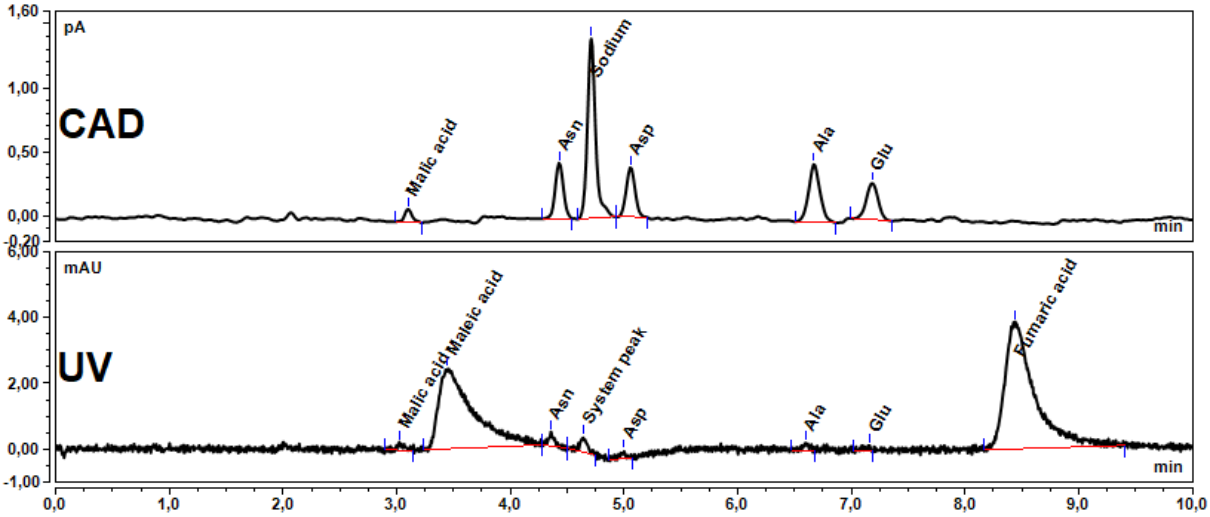

Fig. 4. Chromatogram of Asp and its impurities at 0.01 % concentration with respect to the concentration of the sample solution; for method conditions see section 2.3.1.

The possible impurities of Gly are chemically diverse, ranging from amino acids or small peptides through organic acids to nonpolar substances (Table 1). Except for the volatile chloroacetic acid, all impurities were sufficiently non-volatile at higher evaporation temperatures enabling quantification by the CAD (Fig. 3). The measured response factors were in a relatively narrow range (0.68 – 2.38). Chloroacetic acid was quantified by using low wavelength UV detection at 210 nm. The obtained limits of quantitation for chloroacetic (0.05 %) acid and urotropine (0.05 %) were higher than for the other analytes (0.03 % or less) due to restrictions of the chromatographic system, but still sufficiently low for impurity profiling in routine analysis, since the currently applied methods for Gly have a reporting threshold of 0.05 % [18].

3.2. Method validation

Both methods were validated according to ICH guidline Q2(R1) [30]. Hence, specificity, linearity and range, accuracy, precision, limit of quantitation (LOQ) and robustness of the methods were assessed. In addition, system suitability criteria were established. A summary of the results is provided in the supplementary material.

3.2.1. Aspartic acid

The presented validation parameters refer to CAD for malic acid, Asn, Asp, Ala and Glu. In the case of maleic acid and fumaric acid, UV detection was applied.

Specificity of the method was demonstrated by injection of a sample solution spiked with each impurity at 0.1 % concentration with respect to the concentration of the sample solution (Fig. 5). Baseline separation could be achieved for all impurities and they were well separated from the main peak.

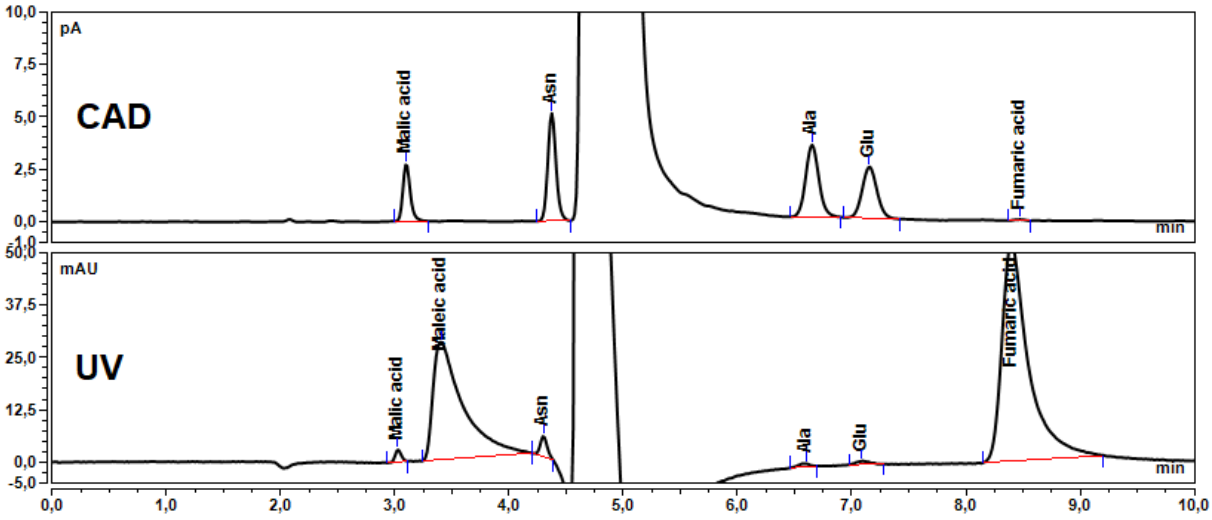

Fig. 5. Sample solution of 5 mg/ml Asp spiked with 0.1 % of each impurity.

The investigated *range* was between 0.03 and 0.24 % of the sample concentration, corresponding to the reporting threshold and 120 % of the specification limit, respectively.

Linearity was determined by means of linear regression with six calibration points (n = 3) distributed equidistantly over the observed range. The obtained coefficients of determination (R^2) were 0.998 or higher (Table 2a).

Table 2a. Linearity and LOQ results of L-aspartic acid (with respect to CAD unless otherwise stated).

Compound	R^2 (linear regression)	LOQ (ng on column)	LOQ[a]	Correction factor
Asp	0.9995	8	0.008 %	1
Ala	0.9987	8	0.008 %	0.56
Asn	0.9982	8	0.008 %	0.81
Fumaric acid	0.9997 (UV)	5 (UV)	0.005 % (UV)	n.d.[b]
Glu	0.9991	10	0.010 %	0.85
Maleic acid	0.9998 (UV)	10 (UV)	0.010 % (UV)	n.d.
Malic acid	0.9991	20	0.020 %	2.20

Table 2b. Linearity and LOQ results of glycine (with respect to CAD unless otherwise stated).

Compound	R^2 (linear regression)	LOQ (ng on column)	LOQ[c]	Correction factor
Gly	0.9997	30	0.030 %	1
ß-Ala	0.9983	30	0.030 %	0.42
Chloroacetic acid	0.9992 (UV)	50 (UV)	0.050 % (UV)	n.d.
Glycine anhydride	0.9984	20	0.020 %	1.47
Gly-Gly	0.9975	30	0.030 %	0.67
Gly-Gly-Gly	0.9962	30	0.030 %	0.64
Iminodiacetic acid	0.9987	25	0.025 %	1.22
Sar	0.9972	30	0.030 %	0.97
Ser	0.9978	30	0.030 %	1.04
Urotropine	0.9967	50	0.050 %	1.47

[a] With respect to an Asp sample solution of 5 mg/mL.

[b] Not determined.

[c] With respect to an Gly sample solution of 10 mg/ml.

For *accuracy* testing, spiked sample solutions were used, covering the previously investigated range with spiked amounts of 0.03, 0.15 and 0.24 % of each impurity, respectively. The peak areas of some spiked impurities had to be corrected by those of blank samples, since all tested batches contained at least one impurity above the reporting threshold. The recovery rates (n = 3) were calculated using either the previously established calibration curves, a 0.1 % dilution of all impurities as external standard, or a 0.1 % dilution of the test substance as external standard, taking into account the correction factors obtained from the slopes of the calibration curves (method of choice of the Ph. Eur.). In case of maleic acid and fumaric acid, a 0.1 % dilution of fumaric acid was chosen as an external standard when using the correction factor approach. The recovery rates, ranging from 84 – 111 %, were satisfactory for the intended purpose, except for the 0.03 % level of malic acid using Asp as external standard (76 %), which can be explained by the relatively low response of malic acid compared to the amino acids. Therefore, a 0.1 % dilution of each impurity as external standard is suggested for quantitation.

Precision was evaluated in terms of intra- and inter-day repeatability. Intra-day repeatability was assessed in sextuple with spiked sample solutions at 0.03, 0.15 and 0.24 % concentration level of each impurity. For the inter-day repeatability, freshly prepared spiked sample solutions were injected on the next day. The obtained relative standard deviation (RSD) values ranged from 0.1 to 7.7 %, which is acceptable for the purpose of this method.

The *quantitation limits (LOQs)* of Asp and its impurities were determined based on the signal-to-noise approach of ICH guideline Q2(R1). A S/N of at least 10, estimated from a 0.03 % dilution and confirmed by appropriate dilution of impurity standards with increments of 5 ng on column above 10 ng, or 1 ng below 10 ng (n = 3), was set as LOQ. All LOQs were below the reporting threshold of 0.03 %, allowing for accurate quantitation (Table 2a).

Robustness was checked by systematic variations of flow rate (0.6 – 1.0 mL/min), column temperature (20 °C – 30 °C), ACN proportion (0 – 1 %), TFA concentration (0.02 – 0.04 %), NFPA concentration (6 – 8 mM), evaporation temperature (45 – 55 °C, CAD) and filter constant (1 s – 10 s, CAD). The resulting resolution and S/N of the impurity was then compared to the original method. The method can be regarded as robust to small changes, as long as the system suitability requirements described below are met.

To ensure the reproducibility of the method, *two system suitability criteria* were defined. Sodium is always present in the chromatographic runs as an impurity because it is dissolved from the utilized glassware and is detected by CAD. The sodium peak eluted between Asn and Asp, leading to the formation of two critical peak pairs of Asn–sodium and sodium–Asp. For both of the critical separations, a minimum resolution requirement of 1.5 was set using a 0.1 % dilution of Asn and Asp as system suitability solution. Changes in the proportion of the ion-pairing reagents also predominantly affected the separation of the critical peak pairs, underlining the importance of the introduced system suitability criteria.

3.2.2. Glycine

The presented validation parameters refer to the CAD, with exception of chloroacetic acid, which was detected by means of UV.

Specificity of the method was demonstrated by injection of a sample solution, spiked with 0.15 % of each impurity (Fig. 6). The impurity peaks were well separated from each other, as the resolution was > 1.5 for all impurities. The incomplete separation of Gly and Sar was controlled by the introduction of a system suitability requirement.

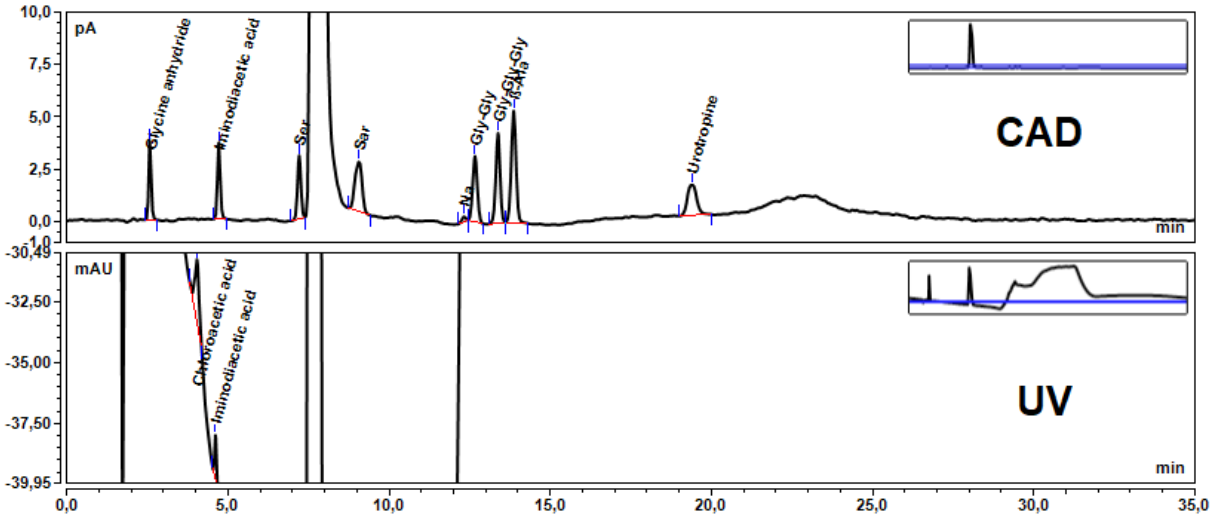

Fig. 6. Sample solution of 10 mg/mL Gly spiked with 0.15 % of each impurity. The overview plots are displayed in the right corner of the chromatogram.

A *range* between 0.03 and 0.24 % of the sample concentration was evaluated. For *linearity* assessment, six-point (n = 3) calibration curves were established over the observed range, except for chloroacetic acid and urotropine (0.05 – 0.24 %). The R^2 values obtained by linear regression were at least 0.996.

Accuracy was demonstrated by determination of the recovery rates (n = 3) of spiked samples at 0.03, 0.15 and 0.24 % concentration level of the impurities. For chloroacetic acid and urotropine, a lower limit of 0.05 % was chosen since it was equivalent to the LOQs of the impurities. Either linear regression or external standard methodology, using a 0.1 % dilution of the impurities, was applied for calculation of the impurity contents. The recovery rates ranged between 82 and 119 % with one exception. For the 0.03 % level of Sar, the recovery rate calculated by linear regression was only 75 % due to insufficient resolution from the main peak. As a consequence, a system suitability criterion for the minimal peak-to-valley ratio was introduced. The recovery was satisfactory for Sar at the 0.03 % level using an external standard for calculation (87 %).

Precision was investigated as described in the previous section. The RSD values for inter- and intra-day repeatability ranged from 0.9 to 8.2 %.

The *LOQs* of Gly and its impurities were again determined with the previously described S/N approach, with exception of chloroacetic acid. For chloroacetic acid a RSD of 5 % or less of the peak area (n = 3) was set as LOQ, since the baseline drift of the method prevented the use of the S/N approach. The LOQs of chloroacetic acid and urotropine did not meet a reporting threshold of 0.03 %, thus a reporting threshold of 0.05 % was set instead, as it is also claimed in the currently applied methods in the Ph. Eur. (Table 2b). However, neither impurity was found in the investigated batches.

Robustness was assessed by systematic variations of flow rate (0.7 – 0.9 mL/min), column temperature (20 – 30 °C) and evaporation temperature (65 – 75 °C, CAD). The composition of the ion-pairing reagents was not changed since the Ph. Eur. does not permit alteration of the pH in gradient methods. The method can be regarded as robust against these small variations.

A system *suitability test* with two requirements was defined. One requirement being a RSD of less than 0.5 % for the retention time of 3 injections of a 0.1 % solution of Gly, which conforms to the United States Pharmacopeia (USP). As a second criterion, a minimum peak-to-valley ratio of 1.5 for the Gly-Sar peak pair was claimed to ensure meaningful integration of the Sar peak.

3.3. Batch analysis

3.3.1. Aspartic acid

Analytical grade batches of four different vendors were tested using the Asp method (Table 3 and Fig. 7). With exception of maleic acid, all specified impurities (Ala, Asn, fumaric acid, Glu, maleic acid, and malic acid) were found in the examined samples at relevant levels. Impurities above the LOQ were quantified using the external standard method with a 0.1 % dilution of Asp as an external standard. One unspecified impurity could be monitored and quantified with the CAD using the same calculation method as for the other impurities. All investigated batches contained at least one specified impurity above the reporting threshold. The compendial requirements, however, were entirely met.

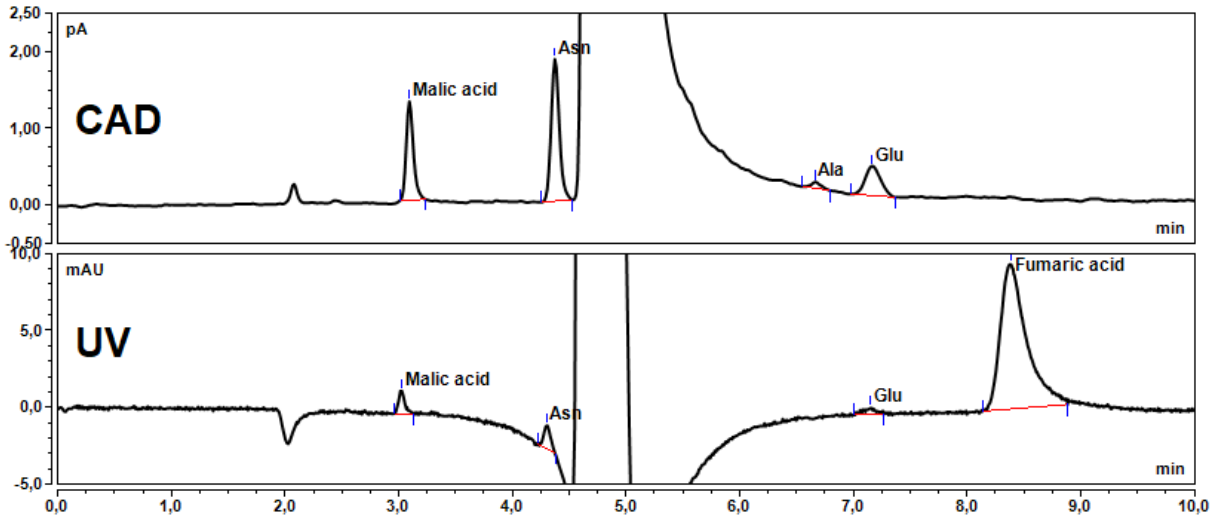

Fig. 7. Sample no. 3 of Asp.

Table 3. Results of the batch testing of L-aspartic acid.

Sample no.	Ala	Asn	Fumaric acid	Glu	Malic acid	Unsp. RRT 1.74	Sum
1	-[a]	0.050 %	0.024 %	0.028 %	0.126 %	-	0.229 %
2	0.010 %	-	0.015 %	0.032 %	-	0.033 %	0.090 %
3	< LOQ	0.060 %	0.053 %	0.021 %	0.098 %	-	0.233 %
4	-	0.011 %	0.024 %	0.116 %	0.069 %	0.014 %	0.235 %

[a] Not detected.

3.3.2. Glycine

Four batches of two different manufacturers were tested applying the Gly method (Table 4 and Fig. 8). Three batches were of analytical grade, one of synthesis grade. The only impurity found at relevant level was Sar, besides small quantities of iminodiacetic acid below the reporting threshold and traces of Gly-Gly and ß-Ala. One unspecified impurity could be detected with CAD and was quantified using an external standard solution of Gly at 0.1 % concentration. All investigated batches were of high purity (> 99.9 %) and met the compendial requirements.

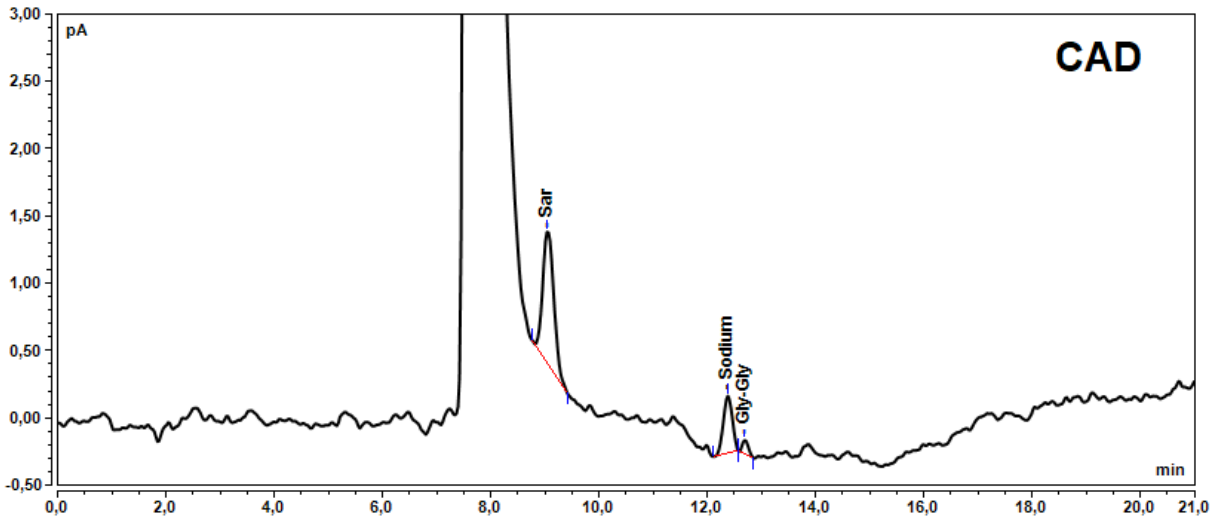

Fig. 8. Sample no. 1 of Gly. Only the CAD signal is shown because no other impurities were detected with UV.

Table 4. Results of the batch testing of glycine.

Sample no.	ß-Ala	Gly-Gly	Iminodiacetic acid	Sar	Unsp. RRT 0.62	Sum
1	-[a]	-	-	0.077 %	-	0.077 %
2	< LOQ	< LOQ	-	0.065 %	-	0.065 %
3	-	-	< LOQ	-	0.012 %	0.012 %
4	-	-	< LOQ	-	0.051 %	0.051 %

[a] Not detected.

4. Conclusion

To obtain meaningful impurity profiles of Asp and Gly with single runs, two separate reversed-phase ion-pair high-performance liquid chromatography methods with charged aerosol and UV detection were successfully developed and validated. Coupled charged aerosol and UV detection proved to be a useful detector setup to obtain complementary information about the actual impurity profile of the respective amino acid. The sensitivity of the CAD could be adjusted by altering the evaporation temperature to meet the required quantitation limits of 0.03 % (relative to the concentration of the respective sample solution) in most cases. An increase of the evaporation temperature worked well for the non-volatile amino acids and other non-volatile impurities, while the more volatile analytes, which suffered from a significant loss of response, e.g. organic acids, were detected by UV, demonstrating another advantage of the two-detector setup. The developed methods represent a versatile alternative to the dedicated derivatization procedures of the AAA used in the Ph. Eur., as they are not restricted to the detection of amino acids. Batches of Asp and Gly from various manufacturers were tested for related substances applying the developed methods. All investigated samples, however, were of high purity (99.7 % or above).

Conflict of interest statement

None of the authors of this paper does have a financial or personal relationship with other people or organizations that could inappropriately influence or bias the content of the paper.

Acknowledgements

Thanks to Oliver Scherf-Clavel for insightful discussions concerning method development and Niclas Förtig for his help concerning the choice of the ion-pairing reagents (both University of Wuerzburg) as well as to the ThermoFisher Scientific teams in Germering (Germany) and Waltham (MA, USA) for technical support and scientific feedback and advice.

Supplementary material

Table S1. Recovery rate (n = 3) of the L-aspartic acid method at 0.03, 0.15 and 0.24 % concentration with respect to a 5 mg/mL sample solution of Asp in %.

Calculation method	Linear regression			External standard 0.1 % dilution of the impurity			External standard 0.1 % dilution of Asp		
Comp./Conc.	0.03%	0.15%	0.24%	0.03%	0.15%	0.24%	0.03%	0.15%	0.24%
Ala	103	104	98	110	103	96	108	97	91
Asn	92	101	94	110	102	94	98	91	84
Fumaric acid	100	100	100	101	101	102	101	101	102
Glu	111	101	98	105	99	96	103	97	94
Maleic acid	104	100	101	99	101	101	97	99	99
Malic acid	104	100	104	76	95	100	94	102	108

Table S2. RSD of the L-aspartic acid method at 0.03, 0.15 and 0.24 % concentration with respect to a 5 mg/mL sample solution of Asp in %.

Repeatability	Intra-day (n = 6)			Inter-day (n = 2)		
Compound/Concentration	0.03 %	0.15 %	0.24 %	0.03 %	0.15 %	0.24 %
Ala	2.6	3.3	3.0	6.2	3.1	2.3
Asn	3.2	1.6	2.6	4.2	2.6	2.5
Fumaric acid	3.5	0.7	0.1	3.1	0.9	0.5
Glu	3.4	3.1	2.4	3.7	3.4	2.1
Maleic acid	2.7	2.3	0.9	2.5	2.3	1.0
Malic acid	4.0	3.7	1.0	7.7	3.2	2.1

Table S3. S/N and resolution of a spiked Asp sample solution at 0.1 % concentration of the impurities in dependence of systematic variations of the chromatographic conditions.

			Flow rate (mL/min)		Column temperature (°C)		ACN (%)	TFA (%)		NFPA (mM)		Evaporation temperature CAD (°C)		Filter constant CAD (s)	
Comp./Variation		No variation	0.6	1.0	20	30	1	0.02	0.04	6	8	45	55	1	10
Ala	S/N	154	144	126	179	204	155	174	136	136	177	132	141	112	164
	Res.	2.19	2.28	2.13	2.51	2.08	1.58	**1.45**	2.46	2.24	1.81	2.31	2.29	2.33	2.15
Asn	S/N	281	225	210	245	294	210	193	265	175	258	191	264	174	210
	Res.	b.s.[a]	b.s.	b.s.	b.s.	b.s.	b.s.	**<b.s.**	b.s.	**<b.s.**	b.s.	b.s.	b.s.	b.s.	b.s.
Fumaric acid (UV)	S/N	302	315	332	302	307	348	304	466	189	124	n.a.[b]	n.a.	n.a.	n.a.
	Res.	n.a.	n.a.	n.a.	n.a.	n.a.	n.a.	n.a.	n.a.	n.a.	n.a.	n.a.	n.a.	n.a.	n.a.
Glu	S/N	110	104	85	120	140	110	121	149	88	126	91	101	78	112
	Res.	6.44	6.25	5.84	7.55	5.98	4.64	3.37	7.23	8.26	4.59	6.87	6.22	6.25	5.42
Maleic acid (UV)	S/N	111	101	115	144	123	217	96	162	103	54	n.a.	n.a.	n.a.	n.a.
	Res.	3.43	3.40	3.60	3.43	3.56	5.75	3.37	4.17	2.81	4.49	n.a.	n.a.	n.a.	n.a.
Malic acid	S/N	81	88	64	80	85	70	81	89	77	92	70	72	61	110
	Res.	10.5	11.2	9.61	10.3	10.5	10.4	10.8	10.3	9.53	11.5	10.4	10.6	11.3	8.36

[a] Baseline separation obtained. The actual resolution value was below 1.5 due to the vast peak width of the main peak used for calculation.

[b] Not applicable.

Table S4. Recovery rate (n = 3) of the glycine method at 0.03 (0.05), 0.15 and 0.24 % concentration with respect to a 10 mg/mL sample solution of Gly in %.

Calculation method	Linear regression			External standard 0.1 % dilution of the impurity		
Comp./Concentration	0.03 %	0.15 %	0.24 %	0.03 %	0.15 %	0.24 %
ß-Ala	112	97	100	91	109	115
Chloroacetic acid	90 (0.05 %)	96	97	82	85	88
Glycine anhydride	98	104	100	119	92	87
Gly-Gly	111	100	100	106	115	116
Gly-Gly-Gly	112	97	100	107	101	104
Iminodiacetic acid	107	103	97	91	92	83
Sar	75	101	91	87	104	93
Ser	111	98	100	109	101	102
Urotropine	97 (0.05 %)	102	88	112	92	82

Table S5. RSD of the glycine method at 0.03 (0.05), 0.15 and 0.24 % concentration with respect to a 10 mg/mL sample solution of Gly in %.

Repeatability	Intra-day (n = 6)			Inter-day (n = 2)		
Comp./Concentration	0.03 %	0.15 %	0.24 %	0.03 %	0.15 %	0.24 %
ß-Ala	4.7	1.5	1.1	4.6	2.8	1.6
Chloroacetic acid	3.9 (0.05 %)	4.0	2.3	5.6	3.1	2.8
Glycine anhydride	5.5	1.5	2.8	5.0	3.7	2.3
Gly-Gly	6.6	2.5	1.5	4.1	0.9	1.3
Gly-Gly-Gly	4.9	1.8	0.9	7.8	3.3	1.3
Iminodiacetic acid	5.2	1.5	3.3	4.9	2.6	1.4
Sar	7.3	3.4	4.3	8.2	0.9	2.8
Ser	3.9	3.4	2.4	6.5	1.7	2.6
Urotropine	4.9 (0.05 %)	2.6	1.7	3.9	1.2	2.4

Table S6. S/N and resolution of a spiked Gly sample solution at 0.1 % concentration of the impurities in dependence of systematic variations of the chromatographic conditions.

			Flow rate (mL/min)		Column temperature (°C)		Evaporation temperature CAD (°C)	
Component		No variation	0.7	0.9	20	30	65	75
ß-Ala	S/N	79	86	64	78	84	103	83
	Res.	14.99	14.58	14.14	13.64	13.94	16.08	13.53
Chloroacetic acid (UV)	S/N	23	20	22	22	23	n.a.[a]	n.a.
	Res.	3.02	3.05	3.79	2.38	4.37	n.a.	n.a.
Glycine anhydride	S/N	56	60	49	50	54	58	69
	Res.	14.39	15.09	13.17	14.19	14.13	14.73	13.42
Gly-Gly	S/N	47	67	25	52	47	53	59
	Res.	2.81	2.46	3.16	2.71	2.67	2.84	2.73
Gly-Gly-Gly	S/N	61	67	41	61	62	69	76
	Res.	1.96	2.18	1.69	1.81	2.01	2.02	1.85
Iminodiacetic acid	S/N	50	50	46	45	50	49	66
	Res.	13.98	14.31	13.26	13.86	13.77	14.61	13.21
Sar	S/N	36	36	35	35	37	44	38
	Res.	9.94	8.83	9.09	9.87	9.35	10.71	9.39
Ser	S/N	45	46	44	41	47	47	62
	Res.	b.s.[b]	b.s.	b.s.	b.s.	b.s.	b.s.	b.s.
Urotropine	S/N	22.6	22	19	20	20	19	62
	Res.	n.a.	n.a.	n.a.	n.a.	n.a.	n.a.	n.a.

[a] Not applicable.

[b] Baseline separation obtained. The actual resolution value was below 1.5 due to the vast peak width of the main peak used for calculation.

References

[1] O. Wahl, U. Holzgrabe, Amino acid analysis for pharmacopoeial purposes. Talanta, 2016. 154: p. 150-163.

[2] G. Wu, Amino acids: metabolism, functions, and nutrition. Amino acids, 2009. 37: p. 1-17.

[3] G. Cardillo, C. Tomasini, Asymmetric synthesis of ß-amino acids and α-substituted β-amino acids. Chem. Soc. Rev., 1996. 25: p. 117-128.

[4] J. Coombes, L. McNaughton, Effects of branched-chain amino acid supplementation on serum creatine kinase and lactate dehydrogenase after prolonged exercise. Journal of sports medicine and physical fitness, 2000. 40: p. 240.

[5] International Council for Harmonization, Guideline Q3A (R2) Impurities in new drug products. 2006.

[6] G. Liyanaarachchi, K. Mahanama, H. Somasiri, P. Punyasiri, Development and validation of a method for direct, underivatized analysis of free amino acids in rice using liquid chromatography–tandem mass spectrometry. J. Chromatogr. A, 2018. 1568: p. 131-139.

[7] A. Socia, J.P. Foley, Direct determination of amino acids by hydrophilic interaction liquid chromatography with charged aerosol detection. J. Chromatogr. A, 2016. 1446: p. 41-49.

[8] S. Furota, N.O. Ogawa, Y. Takano, T. Yoshimura, N. Ohkouchi, Quantitative analysis of underivatized amino acids in the sub-to several-nanomolar range by ion-pair HPLC using a corona-charged aerosol detector (HPLC–CAD). J. Chromatogr. B, 2018. 1095: p. 191-197.

[9] R. Kühnreich, U. Holzgrabe, Impurity profiling of l-methionine by HPLC on a mixed mode column. J. Pharm. Biomed. Anal., 2016. 122: p. 118-125.

[10] U. Holzgrabe, C.-J. Nap, S. Almeling, Control of impurities in l-aspartic acid and l-alanine by high-performance liquid chromatography coupled with a corona charged aerosol detector. J. Chromatogr. A, 2010. 1217: p. 294-301.

[11] S. Schiesel, M. Lämmerhofer, A. Leitner, W. Lindner, Quantitative high-performance liquid chromatography–tandem mass spectrometry impurity profiling methods for the analysis of parenteral infusion solutions for amino acid supplementation containing l-alanyl-l-glutamine. J. Chromatogr. A, 2012. 1259: p. 111-120.

[12] Council of Europe, European Pharmacopoeia Online 9.8; 2019, EDQM, Strasbourg, France. Chapter 2.2.56. Available from: http://online6.edqm.eu/ep908/. Accessed: October 21st, 2019.

[13] S. Almeling, D. Ilko, U. Holzgrabe, Charged aerosol detection in pharmaceutical analysis. J. Pharm. Biomed. Anal., 2012. 69: p. 50-63.

[14] T. Vehovec, A. Obreza, Review of operating principle and applications of the charged aerosol detector. J. Chromatogr. A, 2010. 1217: p. 1549-1556.

[15] N. Vervoort, D. Daemen, G. Török, Performance evaluation of evaporative light scattering detection and charged aerosol detection in reversed phase liquid chromatography. J. Chromatogr. A, 2008. 1189: p. 92-100.

[16] J.P. Hutchinson, J. Li, W. Farrell, E. Groeber, R. Szucs, G. Dicinoski, P.R. Haddad, Comparison of the response of four aerosol detectors used with ultra high pressure liquid chromatography. J. Chromatogr. A, 2011. 1218: p. 1646-1655.

[17] Council of Europe, European Pharmacopoeia Online 9.8; 2019, EDQM, Strasbourg, France. Monograph no. 0797. Available from: http://online6.edqm.eu/ep908/. Accessed: October 21st, 2019.

[18] Council of Europe, European Pharmacopoeia Online 9.8; 2019, EDQM, Strasbourg, France. Monograph no. 0614. Available from: http://online6.edqm.eu/ep908/. Accessed: October 21st, 2019.

[19] S. Kopec, U. Holzgrabe, Impurity profile of amino acids? Pharmeu. Sci. Notes, 2005. 2005(1): p. 39-45.

[20] M. Breuer, K. Ditrich, T. Habicher, B. Hauer, M. Keßeler, R. Stürmer, T. Zelinski, Industrial methods for the production of optically active intermediates. Angew. Chem. Int. Ed., 2004. 43: p. 788-824.

[21] A. Ingersoll, S. Babcock, Hippuric acid. Organic Syntheses, 1943. p. 40.

[22] K. Petritis, P. Chaimbault, C. Elfakir, M. Dreux, Ion-pair reversed-phase liquid chromatography for determination of polar underivatized amino acids using perfluorinated carboxylic acids as ion pairing agent. J. Chromatogr. A, 1999. 833: p. 147-155.

[23] P.B. Hamilton, Ion Exchange Chromatography of Amino Acids. A Single Column, High Resolving, Fully Automatic Procedure. Anal. Chem, 1963. 35: p. 2055-2064.

[24] A.J. Alpert, Hydrophilic-interaction chromatography for the separation of peptides, nucleic acids and other polar compounds. J. Chromatogr. A, 1990. 499: p. 177-196.

[25] A.P. Vilches, S.H. Norström, D. Bylund, Direct analysis of free amino acids by mixed-mode chromatography with tandem mass spectrometry. J. Sep. Sci., 2017. 40: p. 1482-1492.

[26] B. Buszewski, and S. Noga, Hydrophilic interaction liquid chromatography (HILIC)—a powerful separation technique. Anal. Bioanal. Chem., 2012. 402: p. 231-247.

[27] Y. Yang, X. Geng, Mixed-mode chromatography and its applications to biopolymers. J. Chromatogr. A, 2011. 1218: p. 8813-8825.

[28] A.M. Botero-Coy, M. Ibáñez, J. Sancho, F. Hernández, Direct liquid chromatography–tandem mass spectrometry determination of underivatized glyphosate in rice, maize and soybean. J. Chromatogr. A, 2013. 1313: p. 157-165.

[29] P.H. Gamache, Charged aerosol detection for liquid chromatography and related separation techniques, 2017. John Wiley & Sons

[30] International Council for Harmonization, Guideline Q2 (R1) Validation of analytical procedures: text and methodology. 2005.

4. Final discussion

The studies performed in this thesis were aimed at evaluating the influence of recently implemented instrumental settings and various chromatographic separation techniques on the performance of the latest generation charged aerosol detector. The optimization strategies deduced from these insights served as basis for the development of impurity profiling methods for amino acids and amino acid-derived APIs intended for a compendial application. Amino acids lack chromophores in most cases and are poorly retained on conventional RP columns due to their hydrophilic and zwitterionic properties. Thus, the routinely employed HPLC-UV analysis is not feasible, which is also reflected in the compendial employed derivatization procedures [1]. The combination of CAD and modern separation techniques such as HILIC and MMC offers a solution to the detection and separation related issues. However, the optimization of the CAD settings and the chromatographic conditions, e. g. the mobile phase composition, is essential to meet the compendial requirements. Moreover, potential drawbacks of the novel techniques must be considered as well.

4.1. Performance evaluation of the CAD

4.1.1. Uniformity

The main factor towards uniform CAD response is the volatility of the compounds. While volatile compounds are in general not accessible to CAD, the response of semivolatile compounds is influenced by the instrumental and chromatographic parameters.

Among the chromatographic parameters, the mobile phase additive can be considered as the most relevant factor towards nonuniform response at isocratic conditions. It was demonstrated in this thesis that the response of analytes with basic moiety increases with the chain length of the negatively charged perfluorocarboxylic acid applied as ion-pairing reagent. The salt formation between ionized analytes and high molecular mass mobile phase additives of opposing charge thus impedes a uniform response in analyses where uncharged analytes are present as well. For an improved uniformity of response, low molecular mass additives such as formic acid and ammonium formate should be favored.

With respect to the CAD settings, it was shown that the uniformity of response is highest at low evaporation temperatures (<35 °C) for a set of homologous fatty acids (C12-C18) representing semivolatile and nonvolatile compounds. At elevated evaporation temperatures, the apolar fatty acids investigated behaved as semivolatile compounds indicated by a pronounced loss of response. Consequently, the use of higher evaporation temperatures should be restricted to the analysis of polar nonvolatile analytes such as amino acids, which are less affected by a loss of response. Additionally, the highly desirable quantitation of several

compounds by a single calibrant is impaired when some of the analytes behave as semivolatiles at high evaporation temperatures.

The response dependency on the chain length of the fatty acids was further investigated by a machine learning approach to identify the significant molecular properties responsible for the observed differences. Since there are no distinct boundaries between a semivolatile and a nonvolatile compound [2], the development of quantitative structure property relationship (QSPR) models is beneficial for a better understanding of the response determining factors. In the case of the fatty acids investigated, it could be shown that steric factors as well as the molecular weight of the fatty acids contribute to the differences in response. Interestingly, the influence of the molecular descriptor associated with the steric information was more pronounced than the molecular weight of the fatty acids, considering that the molecular weight of a compound is highly correlated to its volatility. A comprehensive model incorporating diverse compound classes and various chromatographic conditions would be highly desirable for a universal quantitation approach. Machine learning algorithms such as artificial neural networks and gradient boosted trees represent powerful tools to accomplish this challenging task.

4.1.2. Sensitivity

In accordance with the prerequisites for a uniform CAD response, the sensitive detection of volatile compounds is not feasible with the CAD and the response is generally reduced for semivolatile compounds. For the CAD's application in the compendial impurity analysis methods, the required sensitivity limits depend on the specifications stated in the ICH guideline Q2(A1) [3]. Thus, the desired limits of quantitation (LOQs) for drugs with a daily intake of less than 2 g should be at least equal to 0.05% (m/m) with respect to the API. In the present thesis, the LOQs obtained for numerous nonvolatile and semivolatile compounds did not exceed 50 ng injected mass on column (equivalent to a sample concentration of 5 mg/mL and an injection volume of 20 µL), which is sufficient for impurity analysis purposes. The LOQs determined with respect to the S/N approach of the ICH guideline Q2(R1) [4] as part of the method validation procedures are summarized Table 1.

Table 1. LOQs of the compounds studied within this thesis and respective applied evaporation temperatures and retention modes.

Compound	LOQ (ng on column)	Evaporation temperature (°C)	Retention mode
alanine	8/6/3	50/50/50	IPC1/IPC2/HILIC
asparagine	8	50	IPC
aspartic acid	8	50	IPC
cysteine	10/10	50/50	IPC/HILIC
diglycine	30	70	IPC
gabapentin	3	30	RPC

Compound	LOQ (ng on column)	Evaporation temperature (°C)	Retention mode
gabapentin impurity B	50	30	RPC
gabapentin impurity D	4	30	RPC
gabapentin impurity E	2	30	RPC
gabapentin impurity G	3	30	RPC
glycine	30	70	IPC
glycine anhydride	20	70	IPC
iminodiacetic acid	25	70	IPC
isoleucine	5/3	50/50	IPC/HILIC
leucine	5/3	50/50	IPC/HILIC
linoleic acid	2	30	RPC
malic acid	20	50	IPC
methionine	5/3	50/50	IPC/HILIC
myristic acid	8	30	RPC
oleic acid	2	30	RPC
palmitic acid	2	30	RPC
petroselinic acid	1	30	RPC
phenylalanine	10/3	50/50	IPC/HILIC
sarcosine	30	70	IPC
serine	30	70	IPC
ß-alanine	30	70	IPC
stearic acid	1	30	RPC
triglycine	30	70	IPC
urotropine	50	70	IPC
valine	5/3	50/50	IPC/HILIC
vigabatrin	25	70	MMC
vigabatrin impurity D (γ-aminobutyric acid)	12	70	MMC
vigabatrin impurity E	18	70	MMC

It was demonstrated that the evaporation temperature setting is an essential tool for the adjustment of a method's sensitivity limits considering the analyte properties as well as the chromatographic conditions. This is illustrated by the broad evaporation temperature ranges (30-70 °C) selected for the individual method optimization. Analyses including semivolatile compounds require low evaporation temperatures, preferentially below the default value of 35 °C. However, mobile phases of high purity are mandatory since the presence of semivolatile mobile impurities gives rise to elevated levels of background noise under these conditions. In contrast, the LOQs of analyses solely containing nonvolatile, evaporation-resistant analytes, e.g. amino acids, can be significantly improved by increasing the evaporation temperature. The benefit of higher evaporation temperatures is most pronounced for methods using additives with known adverse effect on the background noise, e.g. ion-pairing reagents. A potential drawback of higher evaporation temperatures in impurity profiling is the reduced sensitivity for unknown semivolatile impurities which might occur over time.

It should be mentioned that the sensitivity of the recent generation CAD models is superior compared to the legacy CAD models, which is mainly due to the more efficient concentric nebulization process [5]. However, in case of the semivolatile compounds lauric acid and myristic acid, the LOQs obtained for the legacy Corona CAD models were superior compared to the current Vanquish CAD model. This can be explained by the ambient temperature

evaporation which takes place in case of the Corona CAD, whereas comparable low evaporation temperatures are not applicable to the Vanquish CAD due to the more sensitive detection of semivolatile mobile phase impurities. While semivolatile analytes may complicate method transfer between legacy and current CAD models, the sensitivity for nonvolatile compounds should be sufficient for all CAD models when a compendial application is intended.

4.1.3. Linearity

An inherently nonlinear shape of the response curve is characteristic for the CAD due to the involved nonlinear particle generation and subsequent particle charge measurement processes. However, for a compendial application, calibration ranges of less than 2 orders of magnitude (0.03%-0.24%) are sufficient, which complies with the quasi-linear range of the CAD. Consequently, the linearity was acceptable for an accurate quantitation of the impurities without the need for a more complex calibration model in most of the impurity analysis methods developed during the present thesis (Table 2). As the coefficient of determination (R^2) obtained for the calibration curve is not a robust metric for the evaluation of linearity, visual inspection of the residual plot complemented the linearity assessment in each case.

Table 2. Linearity parameters of the developed impurity analysis methods.

Impurity analysis	R^2 range	Calibration range (ng on column)	Calibration type
aspartic acid	0.9982-0.9995	30-240	linear
gabapentin	0.9972-0.9989/0.9993-0.9999	50-400	linear/PFV 1.3
glycine	0.9962-0.9997	50-400	linear
polysorbate	0.9914-0.9988/0.9993-0.9998/0.9970-0.9996	10-1000	linear/log-log/PFV 1.1
valine	0.9991-0.9998	10-80	linear
vigabatrin	0.9991-0.9996	45-360	linear

In case of nonlinear CAD response, data linearization by means of double logarithmic transformation is often adequate to obtain an improved quality of fit. However, the data is modified subsequently to its generation, which impairs the data integrity and can be troublesome in a GMP regulated environment [6]. A more straightforward approach is the use of an optimized PFV to obtain a linear signal without any additional data manipulation. Thereby, the instrumental setting directly alters the CAD's signal output by application of a correction factor to the exponent of the power law equation which describes the nonlinear response. As the experimental determination of the optimal PFV is rather time-consuming and inaccurate, empirical, and mathematical PFV optimization approaches can be applied instead. Table 3 illustrates the characteristics of the individual optimization approaches.

Table 3. PFV optimization approaches.

Parameter	Optimization approach Experimental	Empirical[a]	Mathematical
effort	high	low	low
accuracy	low	high	high
proprietary	no	no	yes
general applicability	nonvolatile and semivolatile analytes	nonvolatile analytes	nonvolatile and semivolatile analytes
preferred metric for linearity assessment	residual plot/%RSD of the response factors	%RSD of the response factors	residual plot/R^2

[a] Based on Ref [7].

Mathematical PFV optimization by the proprietary Chromeleon software represents the most convenient approach and is generally applicable. An empirical approach introduced by Ahmed et al. [7] yields comparable results for nonvolatile analytes but is not generally applicable to semivolatile analytes since it relies on constants which depend on the shape of the response curve. In contrast to the sublinear response, which is obtained for nonvolatile analytes over almost the entire dynamic range of the current detector models [5], semivolatile analytes often produce a supralinear response. This represents a limitation of the PFV linearization method when nonvolatile and semivolatile analytes are to be investigated simultaneously, as PFV of >1 and <1 must be applied, respectively. Although a PFV “gradient” is technically applicable, the resulting chromatogram is questionable, as the PFV directly impacts the baseline noise. Thus, double logarithmic transformation or other mathematical operations such as quadratic fit might be better suited alternatives in this case. For analyses solely comprising nonvolatile analytes, the PFV optimization is a viable option to improve the CAD’s linearity in the range of interest and could thus be employed in the regulated environment. Since the optimal PFV depends on the chromatographic and instrumental conditions, the implementation of guidelines and thresholds is mandatory for a standardized application.

4.2. Influence of IPC, MMC, and HILIC on the CAD performance

The separation technique and, concomitantly, the composition of the mobile phase is an often neglected but crucial aspect toward CAD performance. In many cases, IPC, MMC, and HILIC can be used interchangeably to obtain the desired retention and separation of small polar analytes. Thus, the influence of the respective separation technique on the sensitivity of the CAD and on possible optimization strategies should be considered as well in the method development.

The ion-pairing reagent used in IPC is decisive for the method’s sensitivity limits, because it is a highly contributing factor to additional background noise. While short chain ion-pairing reagents, e.g. TFA, are uncritical when applied in small concentrations, even slightest amounts of the long chain TDFHA acid have a substantial impact on the background noise due to the formation of nonvolatile salts of high molecular mass and the limited volatility of the acid. As a

general rationale for IPC method developed, the shortest chain ion-pairing reagent, which still facilitates sufficient retention and separation of the analytes, should be used. The usage of ion-pairing reagents available in high purity (≥99%) is essential to minimize additional background noise. The evaporation temperature of the CAD is a useful tool to improve the sensitivity in IPC methods, since the additional background noise is effectively reduced at elevated evaporation temperatures. Due to their polar nature and their formation of nonvolatile salts with the ion-pairing reagent, the response of the analytes is typically not impaired too much at higher evaporation temperatures.

MMC and HILIC have comparable mobile phase requirements; thus, the optimization towards optimal CAD performance is similar. Commonly applied mobile phase additives include volatile buffers and pH modifiers. In contrast to IPC, the mobile phase additive can be considered as minor factor towards the generation of additional background noise. Consequently, the beneficial effect of the evaporation temperature on the background noise is less pronounced compared to IPC. A highly relevant factor towards obtainable sensitivity limits is column bleed, e.g. for silica-based columns [8]. Considering the higher sensitivity of the recent generation CAD models, the detection of nonvolatile mobile phase impurities originating from the column material can give rise to elevated levels of background noise. The selection of a column with low column bleed is a prerequisite for methods of adequate sensitivity and may require the screening of multiple columns of comparable selectivity from different manufacturers. Due to the highly organic modifier proportion required for the HILIC separation mode, the aerosol transport is more efficient compared to IPC, resulting in a higher response (Fig. 1). However, as the transport efficiency is likewise increased for mobile phase impurities, the purity of the organic modifier is of major importance.

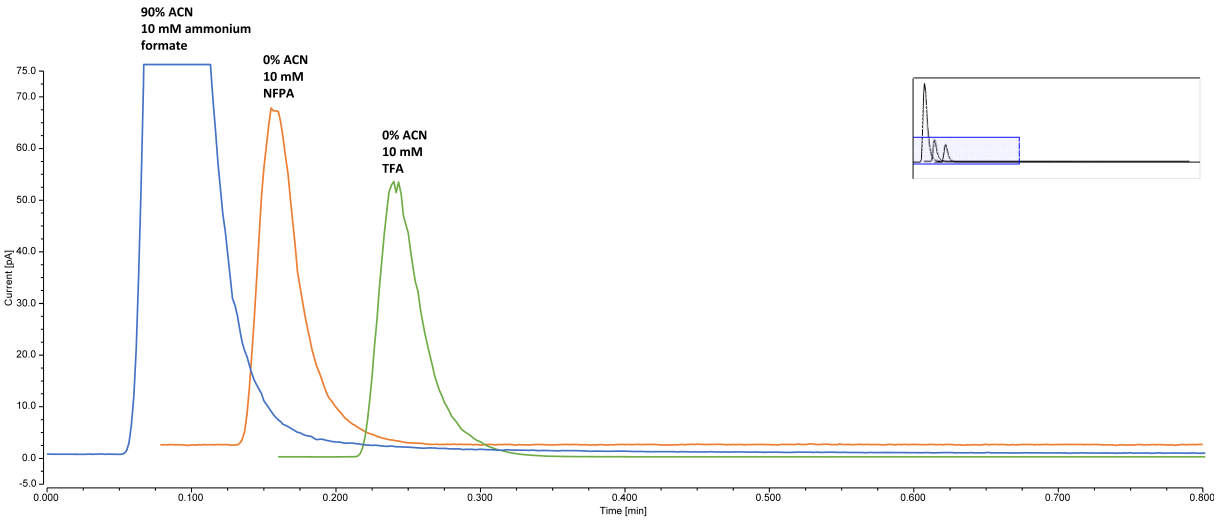

Figure 1. Overlay of chromatograms illustrating the influence of the mobile phase composition on the CAD response of alanine and on the background current. The evaporation temperature is 35 °C and the filter constant 1 s in each case.

4.3. Hyphenated UV-CAD

Hyphenation of UV-CAD was essential for the development of purity analysis methods as part of the present thesis, since the impurity profiles of several APIs investigated comprised weakly-chromophoric compounds as well as volatile compounds. The coupling of both detectors is suited for routine analysis purposes as it requires little additional effort. However, quantitation using a single calibrant is not feasible due to the noncomparable response factors. Thus, the respective UV and CAD chromatograms must be evaluated separately, also applying different calibration models where necessary.

The choice of mobile phase additives and organic modifiers is severely limited when applying the hyphenated detection techniques. While the CAD is restricted to volatile mobile phases, UV detection requires mobile phases of low absorbance at the detection wavelength. When low wavelength UV detection (λ <220 nm) is needed, the requirements are even more strict. Modern separation techniques such as HILIC and MMC represent suitable options to meet these requirements, as they typically comprise mobile phases with low additive concentration (buffer/pH modifier) and ACN (UV_{cutoff} = 190 nm) as organic modifier. Additionally, the usage of isocratic methods is highly desirable due to the distinct effect of the gradient on the baseline of each detector, which complicates the assignment and integration of the analyte peaks and possibly impairs the quantitation results.

In some cases, even hyphenated UV-CAD is not sufficient to assess all possible impurities at the required sensitivity. Volatile compounds, which are also lacking a suitable chromophore, e.g. chloroacetic acid, elude both detection techniques [9]. Thus, the usage of orthogonal detection techniques such as NMR and MS is still indispensable.

4.4. Charged aerosol detection in pharmaceutical analysis

For the CAD's further establishment in the field of pharmaceutical analysis, e.g. compendial monographs, the regulatory requirements must be met and the applicability confirmed by validation procedures. Based on the validation results of the present thesis, it can be stated that the CAD is suited for compendial impurity profiling purposes, with some limitations.

For the general acceptance of a method, the demonstration of accuracy and precision is mandatory [4]. The results from the validation procedures within this thesis for the recovery rate and the intraday repeatability at 0.03% concentration level are depicted in Table 4.

Table 4. Recovery rates (%, n=3) and intraday repeatabilities (%RSD, n=6) of the assessed impurities at 0.03% (m/m) concentration, with respect to the API. Semivolatile impurities are listed separately.

Impurity analysis	Recovery rate[a] (%)	Repeatability (%RSD)	LOQ (%)[b]
aspartic acid	92.2-111.5	2.6-3.4	0.008-0.01
gabapentin	97.8-104.5	2.1-3.1	0.001-0.002
glycine	97.5-112.4[c]	3.9-7.3	0.02-0.05
polysorbate	95.9-99.2	0.6-2.5[d]	n.d.[e]
valine	94.1-101.0	1.0-2.2	0.009
vigabatrin	88.8-91.4	3.7-4.0	0.008-0.01
semivolatile impurities			
gabapentin impurity B	97.8	8.4	0.03
malic acid	103.7	4.0	0.02
myristic acid	90.4	6.6	n.d.

[a] Obtained from linear regression.

[b] With respect to the concentration of the API.

[c] The recovery rate of sarcosine (75%) was not considered since it was impaired by coelution with the main peak.

[d] n=3.

[e] Not determined.

Satisfactory accuracy and precision concomitant with low LOQs were obtained for all methods developed. Considering that the employed separation techniques included RPC, IPC, HILIC, and MMC, it could be confirmed that the CAD is generally applicable to the analysis of nonvolatile small polar compounds. However, the proper adjustment of the CAD settings is essential to achieve optimal performance, e.g. when the sensitivity limits are close to the compendial claimed reporting threshold. As these optimization tools are not available for the legacy CAD models, methods developed and adapted to meet the compendial requirements on a recent CAD model cannot easily be transferred to a legacy model.

The impact of the different CAD models is probably most pronounced for semivolatile analytes. Due to its principle of detection, the CAD's repeatability of response is inherently reduced for semivolatile compounds, which is reflected in a comparatively high %RSD (Table 4). For the semivolatile myristic acid and gabapentin impurity B, it was demonstrated that even a minor alteration of the evaporation temperature (5 °C) has a substantial effect on the analyte response. The evaporation temperature of the legacy CAD models is fixed at ambient temperature; thus, a reliable and reproducible quantitation of semivolatile compounds on different CAD models should be difficult to attain.

To sum up, the CAD's suitability as detector employed in pharmaceutical analysis for routine and quality control purposes is further enhanced by the implementation of new instrumental settings. The sensitivity and linearity of impurity analysis methods can be adjusted by proper selection of the evaporation temperature and PFV, respectively, to meet the requirements of the regulatory authorities. However, due to the novelty of the introduced instrumental parameters, the method development lacks standardization and the transferability between the CAD models can be troublesome. Harmonization and the provision of guidelines for method

development [10] should be addressed in the future to promote the detector's use in the regulated environment.

4.5. Conclusion

Since the CAD's commercial introduction in 2005, the detection technique has been established and stands out among the aerosol-based detectors due to its superior response uniformity [11] and the higher sensitivity compared to the main competitor ELSD [12]. Although the CAD is not as sensitive as the UV and MS detectors in most cases, it is of use in several application areas of pharmaceutical relevance such as the analysis of non-chromophoric APIs and excipients, the relative quantitation of unknown impurities, and polymer screening [13].

The implementation of the evaporation temperature and PFV settings in the recent generation CAD models addressed two main drawbacks of the detection principle, namely the response dependency on the analyte volatility, and the inherently nonlinear response. Hence, the sensitivity and linearity of the CAD can be adjusted to the individual goals and requirements of the intended application, which further extends the scope of the detector. The downside of the additional instrumental parameters is the current lack of standardization. General optimization strategies as they were developed and evaluated within this thesis are essential to facilitate the method development and to increase the acceptance in the regulated environment.

Modern separation techniques such as HILIC and MMC further enhance the CAD capabilities, because their mobile phase conditions are beneficial to the CAD's sensitivity and allow the usage of hyphenated detection techniques, e.g. UV-CAD and CAD-MS. The use of UV-CAD for the impurity analysis of vigabatrin in the Ph. Eur. confirms the applicability of the hyphenated techniques for compendial purposes [14].

The combination of IPC/HILIC/MMC, a parameter adjusted CAD, and a complementary detection technique such as UV enables a sensitive and comprehensive analysis of challenging compounds, e.g. amino acids, which could be experimentally verified in this work. Compared to the compendial applied derivatization procedures and multiple method approaches, the IPC/HILIC/MMC-CAD-UV setup is more straightforward and selective. Moreover, it is less costly and easier-to-use in relation to the more sensitive MS. A soon replacement of the partly outdated compendial methods, however, is thwarted by the monopoly of the CAD manufacturer and the less advanced column standardization compared to RPC.

4.6. References

[1] Council of Europe, European Pharmacopeia Online 10.5, EDQM, Strasbourg, France, 2021.

[2] M.W. Robinson, A.P. Hill, S.A. Readshaw, J.C. Hollerton, R.J. Upton, S.M. Lynn, S.C. Besley, B.J. Boughtflower, Use of calculated physicochemical properties to enhance quantitative response when using charged aerosol detection, Anal. Chem. 89(3) (2017) 1772-1777.

[3] International Council for Harmonization, Guideline Q3A (R2) Impurities in New Drug Products, 2006.

[4] International Council for Harmonization, Guideline Q2 (R1) Validation of Analytical Procedures: Text and Methodology, 2005.

[5] P.H. Gamache, Charged Aerosol Detection for Liquid Chromatography and Related Separation Techniques, John Wiley & Sons, 2017.

[6] A.K. Rattan, Data integrity: history, issues, and remediation of issues, PDA J. Pharm. Sci. Technol. 72(2) (2018) 105-116.

[7] I.A.H. Ahmad, A. Blasko, J. Tam, N. Variankaval, H.M. Halsey, R. Hartman, E.L. Regalado, Revealing the inner workings of the power function algorithm in Charged Aerosol Detection: A simple and effective approach to optimizing power function value for quantitative analysis, J. Chromatogr. A 1603 (2019) 1-7.

[8] K. Qian, Y. Peng, F. Zhang, B. Yang, X. Liang, Preparation of a low bleeding polar stationary phase for hydrophilic interaction liquid chromatography, Talanta 182 (2018) 500-504.

[9] O. Wahl, U. Holzgrabe, Impurity profiling of carbocisteine by HPLC-CAD, qNMR and UV/vis spectroscopy, J. Pharm. Biomed. Anal. 95 (2014) 1-10.

[10] B. Bailey, P. Gamache, I. Acworth, Guidelines for method transfer and optimization - from earlier model Corona detectors to Corona Veo and Vanquish charged aerosol detectors, Thermo Scientific (2017). https://assets.thermofisher.com/TFS-Assets/CMD/Technical-Notes/tn-71290-cad-method-transfer-tn71290-en.pdf. (Accessed 16.06.2021).

[11] L.-E. Magnusson, D.S. Risley, J.A. Koropchak, Aerosol-based detectors for liquid chromatography, J. Chromatogr. A 1421 (2015) 68-81.

[12] N. Vervoort, D. Daemen, G. Török, Performance evaluation of evaporative light scattering detection and charged aerosol detection in reversed phase liquid chromatography, J. Chromatogr. A 1189(1-2) (2008) 92-100.

[13] K. Schilling, U. Holzgrabe, Recent applications of the Charged Aerosol Detector for liquid chromatography in drug quality control, J. Chromatogr. A 1619 (2020) 460911.

[14] Council of Europe, European Pharmacopeia Online 10.5, EDQM, Strasbourg, France, 2021, Monograph no. 2305. https://pheur.edqm.eu/app/10-5/content/10-5/2305E.htm. (Accessed 14.01.2021).

5. Summary

The charged aerosol detector (CAD) is an aerosol-based detector employed in liquid chromatography which has become established in the field of pharmaceutical analysis due to its outstanding performance characteristics, e.g. the almost uniform response for nonvolatile analytes. Owing to its principle of detection, the response of the CAD depends on the volatility of a compound and is inherently nonlinear. However, the newly implemented instrumental settings evaporation temperature and power function value (PFV) are valuable tools to overcome some of these drawbacks and can even enhance the detector's capabilities when adjusted properly.

This thesis aimed to evaluate the impact of the new instrumental settings on the CAD performance. Additionally, the influence of modern separation techniques for small polar compounds on the CAD was assessed and the applicability of hyphenated UV-CAD techniques explored. The optimization strategies derived from the evaluation procedures and the conjunction of the instrumental and chromatographic techniques investigated were utilized for the challenging impurity profiling of amino acids and amino acid-like drugs.

Studies on the uniformity of response were performed for fatty acids of different chain length (C12-C18) representing semivolatile and nonvolatile compounds. It was demonstrated that the CAD's evaporation temperature setting is crucial for the response uniformity, with the highest uniformity being obtained at low evaporation temperatures. The studies on the fatty acids were extended to determine the response determining factors leading to the observed differences associated with the chain length. A mixed quantitative structure property relationship (QSPR) model incorporating chromatographic parameters as well as molecular descriptors was successfully established by means of a gradient boosted trees algorithm. The model could explain 99% of the observed variance in response and identified a steric factor corresponding to the chain length, followed by the molecular weight as most influential molecular descriptors towards response. A comprehensive model suitable of universal quantitation could be obtained by expanding this approach to diverse compound classes of varying physicochemical properties.

Fatty acids also served as test substances to investigate the influence of the CAD parameters filter constant and evaporation temperature on the detector's sensitivity limits. While the optimal evaporation temperature represents the best compromise between analyte signal and background noise, a higher filter constant improves the background noise but likewise reduces the resolution of the analytes. The significance of the separation technique towards the CAD response was illustrated by comparison of representative mobile phase compositions of ion pair chromatography (IPC) and hydrophilic interaction chromatography (HILIC) using a response surface model approach. While the obtainable sensitivity limits in IPC are mainly

dependent on the type of ion-pairing reagent applied, HILIC analyses of nonvolatile amino acids can be optimized by increasing the evaporation temperature. Theoretically, the highly organic mobile phases used in HILIC are beneficial to the sensitivity due to the increased CAD response obtained at these conditions. However, pronounced column bleed of silica based HILIC columns concomitant with high levels of background noise can potentially counteract the higher response.

The PFV setting enables the linearization of nonlinear CAD response without subsequent data manipulation; thus, it is of relevance for the regulated environment. For the simultaneous analysis of semivolatile and nonvolatile analytes, double logarithmic transformation should be preferred to PFV optimization, because semivolatile analytes showing supralinear response require PFV <1, in contrast to nonvolatile analytes, which could be confirmed for the fatty acids investigated. As the experimental PFV optimization is time-consuming, empirical, and mathematical optimization approaches were compared for the response linearization of gabapentin and its impurities. Both optimization approaches yielded comparable results for the nonvolatile analytes, however the proprietary mathematical approach is also applicable to semivolatile analytes. The recovery rates of the gabapentin impurities were significantly improved when an optimized PFV was utilized, further supporting the benefit of the setting for impurity analysis.

The CAD is increasingly used in hyphenated detection techniques for a comprehensive analysis. The consequences of the mobile phase composition on the hyphenated UV-CAD techniques were demonstrated for the impurity analysis of vigabatrin. Mobile phases with low additive concentration and the avoidance of long chain ion-pairing reagents are beneficial to the coupled detection mode as it was exemplified by the comparison of a developed mixed-mode chromatography (MMC) method to a compendial IPC method.

Previously discussed optimization strategies allowed the adaptation to the individual impurity profile and the present mobile phase composition in the development of methods for the impurity profiling of amino acids and their derivatives. Established separation techniques for small polar compounds, e.g. IPC, and modern techniques such as HILIC and MMC were coupled to the CAD and additionally, where applicable, UV detection. The results of the method validation procedures confirmed the broad applicability of the CAD in the pharmaceutical analysis of nonvolatile compounds, supported by satisfactory sensitivity and reproducibility for meeting the regulatory requirements with respect to the ICH guidelines Q2(R1) and Q3A(R2). The limits of applicability include the analysis of semivolatile compounds, and the method transfer between current and legacy CAD models. Further advances in the definition and standardization of allowed ranges for the instrumental settings and the establishment of

general optimization procedures in the method development could lead to a more widespread use of the detection technique in compendial methods.

6. Zusammenfassung

Der “charged aerosol detector” (CAD) ist ein aerosol-basierter Detektor in der Flüssigchromatographie, der sich im Bereich der pharmazeutischen Analytik etabliert hat, da er über herausragende Leistungsmerkmale verfügt, wie das annähernd einheitliche Signal für nichtflüchtige Analyte. Aufgrund des Detektionsprinzips ist das Signal des Detektors abhängig von der Flüchtigkeit einer Verbindung und zudem nichtlinear. Die neu eingeführten Geräteparameter Verdampfungstemperatur und „power function value” (PFV) stellen hierbei wertvolle Werkzeuge dar, um einige der mit dem Detektionsprinzip verbundenen Nachteile auszugleichen und können darüber hinaus die Detektionsmöglichkeiten erweitern, sofern sie auf geeignete Weise eingestellt wurden.

Die vorliegende Arbeit hatte zum Ziel, die Auswirkungen der neuen Geräteparameter auf die Leistungsfähigkeit des Detektors zu untersuchen. Zusätzlich wurde der Einfluss moderner Trenntechniken auf den CAD beurteilt und die Anwendbarkeit gekoppelter UV-CAD Techniken erforscht. Die sich aus den Evaluierungsprozeduren ergebenden Optimierungsstrategien und die Verknüpfung der untersuchten instrumentellen und chromatographischen Techniken wurden anschließend verwendet, um Methoden für die herausfordernde Verunreinigungsanalyse von Aminosäuren und Arzneistoffen mit Aminosäurestruktur zu entwickeln.

Es wurden Studien zur Uniformität des Signals von Fettsäuren (C12-C18) durchgeführt, bei denen es sich um halbflüchtige und nichtflüchtige Verbindungen handelt. Es konnte gezeigt werden, dass die Verdampfungstemperatur entscheidend für die Einheitlichkeit des Signals ist, wobei die größte Einheitlichkeit bei niedrigen Verdampfungstemperaturen erzielt wurde. Die Studien zu den Fettsäuren wurden im Folgenden ausgeweitet, um diejenigen Faktoren zu ermitteln, die entscheidend für die beobachteten Unterschiede in der Signalintensität sind und welche im Zusammenhang mit der Kettenlänge der Fettsäuren stehen. Ein gemischtes „quantitative structure property relationship” (QSPR)-Modell, das sowohl chromatographische Parameter also auch molekulare Deskriptoren beinhaltete, wurde erfolgreich unter Verwendung eines „gradient boosted trees“-Algorithmus konstruiert. Das Modell war in der Lage, 99 % der beobachteten Signalvarianz zu erklären und identifizierte einen sterischen Faktor, der im Zusammenhang zu der Kettenlänge der Fettsäuren steht, gefolgt vom Molekulargewicht, als molekulare Deskriptoren mit dem größten Einfluss auf das Signal. Ein umfassendes Modell, das für eine universelle Quantifizierung geeignet wäre, könnte erhalten werden, indem man diesen Ansatz auf verschiedene Verbindungsklassen mit unterschiedlichen physiko-chemischen Eigenschaften ausdehnt.

Fettsäuren dienten außerdem als Testsubstanzen, um die Auswirkungen der CAD-Einstellungen Filterkonstante und Verdampfungstemperatur auf die Empfindlichkeitsgrenzen des Detektors zu untersuchen. Während die optimale Verdampfungstemperatur den besten Kompromiss aus Analytsignal und Hintergrundrauschen darstellt, verbessert eine hohe Filterkonstante das Hintergrundrauschen bei gleichzeitiger Verschlechterung der Auflösung der Analyte. Der Einfluss der verwendeten Trenntechnik auf das CAD-Signal wurde durch den Vergleich repräsentativer Zusammensetzungen von mobilen Phasen der Ionenpaarchromatographie (IPC) und der hydrophilen Interaktionschromatographie (HILIC) mittels eines „response surface“-Modells aufgezeigt. Während die erreichbaren Empfindlichkeitsgrenzen in der IPC hauptsächlich von der Art des verwendeten Ionenpaarreagenzes abhängen, konnte die Empfindlichkeit von HILIC-Analysen nichtflüchtiger Aminosäuren durch eine Erhöhung der Verdampfungstemperatur optimiert werden. In der Theorie sind die für die HILIC verwendeten mobilen Phasen mit hohem organischem Anteil förderlich für die Empfindlichkeit, da unter diesen Bedingungen ein stärkeres CAD-Signal erhalten wird. Jedoch kann das stärkere Signal potenziell durch ausgeprägtes Säulenbluten von mit Siliziumdioxid gepackten HILIC-Säulen, das mit hohem Grundrauschen einhergeht, konterkariert werden.

Die PFV-Einstellung ermöglicht die Linearisierung eines nichtlinearen CAD-Signals ohne nachträgliche Datenmodifikation. Aus diesem Grund ist sie von Relevanz in einer regulierten Umgebung. Für die gleichzeitige Analyse von halbflüchtigen und nichtflüchtigen Analyten sollte die doppelt-logarithmische Transformation gegenüber der PFV-Optimierung vorgezogen werden, da halbflüchtige Analyte ein supralineares Signal aufweisen und daher, im Gegensatz zu nichtflüchtigen Analyten, PFV < 1 erfordern, was für die untersuchten Fettsäuren bestätigt werden konnte. Da die experimentelle Optimierung des PFV zeitraubend ist, wurden empirische und mathematische Optimierungsansätze verglichen, um das Signal von Gabapentin und möglichen Verunreinigungen zu linearisieren. Beide Optimierungsansätze erzielten vergleichbare Ergebnisse im Falle der nichtflüchtigen Analyten, allerdings ist der firmeneigene mathematische Optimierungsansatz auch auf halbflüchtige Analyte anwendbar. Die Wiederfindungsraten der Verunreinigungen von Gabapentin konnten signifikant verbessert werden, wenn der optimierte PFV genutzt wurde, wodurch der Mehrwert der Einstellung für die pharmazeutische Analytik unterstrichen wurde.

Der CAD findet zunehmend Verwendung in gekoppelten Detektionstechniken für eine umfassende Analyse. Die Auswirkungen der Zusammensetzung der mobilen Phase auf die gekoppelten UV-CAD-Techniken wurden für die Verunreinigungsanalyse von Vigabatrin aufgezeigt. Mobile Phasen mit einer geringen Konzentration an Additiv und die Vermeidung langkettiger Ionenpaarreagenzien sind förderlich für den gekoppelten Detektionsmodus, was

anhand des Vergleichs einer neu entwickelten „mixed-mode“-Chromatographie-Methode mit einer IPC-Methode aus dem Arzneibuch veranschaulicht wurde.

Die zuvor erörterten Optimierungsansätze ermöglichten die Anpassung an das individuelle Verunreinigungsprofil sowie an die vorliegende Zusammensetzung der mobilen Phase in der Methodenentwicklung für die Verunreinigungsanalyse von Aminosäuren und ihrer Derivate. Etablierte Trenntechniken für kleine polare Verbindungen, insbesondere IPC, sowie moderne Trenntechniken wie HILIC und MMC wurden mit dem CAD gekoppelt und zusätzlich, wenn notwendig, mit UV-Detektion. Die Ergebnisse der Validierungsverfahren bestätigten die weitgehende Anwendbarkeit des CAD in der pharmazeutischen Analyse nichtflüchtiger Verbindungen, unterstützt durch zufriedenstellende Empfindlichkeit und Reproduzierbarkeit, wodurch die Vorgaben der ICH-Leitfäden Q2(R1) und Q3A(R2) erfüllt werden konnten. Einschränkungen der Anwendbarkeit bestehen in der Analyse halbflüchtiger Verbindungen, sowie im Methodentransfer zwischen gegenwärtigen und alten CAD-Modellen. Weitere Fortschritte in der Definition und Standardisierung erlaubter Bereiche für die Einstellung der Geräteparameter und die Etablierung allgemeiner Optimierungsverfahren in der Methodenentwicklung könnten zu einer umfassenderen Nutzung der Detektionstechnik für Arzneibuchmethoden führen.

7. Appendix

7.1. List of publications

Resarch papers

- K. Schilling, R. Pawellek, K. Lovejoy, T. Muellner, U. Holzgrabe, Influence of charged aerosol detector instrument settings on the ultra-high-performance liquid chromatography analysis of fatty acids in polysorbate 80, J. Chromatogr. A 1576 (2018) 58-66.
- K. Schilling, J. Krmar, N. Maljurić, R. Pawellek, A. Protić, U. Holzgrabe, Quantitative structure-property relationship modeling of polar analytes lacking UV chromophores to charged aerosol detector response, Anal. Bioanal. Chem. 411(13) (2019) 2945-2959.
- R. Pawellek, K. Schilling, U. Holzgrabe, Impurity profiling of l-aspartic acid and glycine using high-performance liquid chromatography coupled with charged aerosol and ultraviolet detection, J. Pharm. Biomed. Anal. 183 (2020) 113149.
- R. Pawellek, T. Muellner, P. Gamache, U. Holzgrabe, Power function setting in charged aerosol detection for the linearization of detector response–optimization strategies and their application, J. Chromatogr. A 1637 (2021) 461844.
- R. Pawellek, U. Holzgrabe, Influence of the mobile phase composition on hyphenated ultraviolet and charged aerosol detection for the impurity profiling of vigabatrin, J. Pharm. Biomed. Anal. 201 (2021) 114110.
- R. Pawellek, J. Krmar, A. Leistner, N. Djajić, B. Otašević, A. Protić, U. Holzgrabe, Charged Aerosol Detector response modeling for fatty acids based on experimental settings and molecular features: a machine learning approach, [manuscript accepted for publication in J. Cheminformatics].
- R. Pawellek, U. Holzgrabe, Performance evaluation of IPC and HILIC coupled to charged aerosol detection for the analysis of underivatized amino acids, [submitted to J. Chromatogr. A].

Other publications

- K. Schilling, R. Pawellek, O. Wahl, U. Holzgrabe, HPLC-CAD impurity profiling of carbocisteine using SCX RP mixed-mode chromatography, Thermo Scientific Application Note 72706 (2018). https://assets.thermofisher.com/TFS-Assets/CMD/Application-Notes/an-72706-hplc-cad-impurity-carbocisteine-an72706-EN.pdf.

- R. Pawellek, A. Leistner, U. Holzgrabe, Impurity analysis of L-aspartic acid and glycine by HPLC-UV-CAD, Thermo Scientific Customer Application Note 73761 (2020). https://assets.thermofisher.com/TFS-Assets/CMD/Application-Notes/can-73761-lc-uv-cad-impurity-l-aspartic-acid-glycine-can73761-en.pdf.
- R. Pawellek, A. Leistner, U. Holzgrabe, Impurity analysis of gabapentin by HPLC-UV-CAD, Thermo Scientific Customer Application Note 74011 (2021). https://assets.thermofisher.com/TFS-Assets/CMD/Application-Notes/can-74011-hplc-uv-cad-impurity-analysis-gabapentin-can74011-en.pdf.
- U. Holzgrabe, K. Schilling, R. Pawellek, O. Scherf-Clavel, With united forces against impurities, Wiley Anal. Sci. (2021). https://analyticalscience.wiley.com/do/10.1002/was.000600106.
- U. Holzgrabe, K. Schilling, R. Pawellek, C. Theiss, O. Scherf-Clavel, No chromophore-no problem?, Wiley Anal. Sci. (2021). https://analyticalscience.wiley.com/do/10.1002/was.000600107.

7.2. Conference contributions

- K. Schilling, R. Pawellek, K. Lovejoy, T. Muellner, U. Holzgrabe
  UHPLC-CAD analysis of fatty acids in polysorbate 80: Influence of CAD parameters.
  DPhG Annual meeting, 2018, Hamburg.
- R. Pawellek, O. Scherf-Clavel, U. Holzgrabe
  CAD in pharmaceutical analysis.
  Virtual CAD Symposium, 2021, hosted by Thermo Fisher Scientific.

7.3. Documentation of authorship

In this section, the individual contribution for each author to the publications reprinted in this thesis is specified. Unpublished manuscripts are handled, accordingly.

Julius-Maximilians-
UNIVERSITÄT
WÜRZBURG

Fakultät für
CHEMIE UND
PHARMAZIE

Erklärung zur Autorenschaft

Charged Aerosol Detector Performance Evaluation and Development of Optimization Strategies for the Analysis of Amino Acids,
Influence of charged aerosol detector instrument settings on the ultra-high-performance liquid chromatography analysis of fatty acids in polysorbate 80, K. Schilling, R. Pawellek, K. Lovejoy, T. Muellner, U. Holzgrabe, J. Chromatogr. A 1576 (2018) 58-66.

Detaillierte Darstellung der Anteile an der Veröffentlichung (in %)
Angabe Autoren/innen (ggf. Haupt- / Ko- / korrespondierende/r Autor/in) mit Vorname Nachname (Initialen)

Autor/in 1 (KS) Autor/in 2 (RP), Autor/in 3 (KL), Autor/in 4 (TM), Autor/in 5 (UH)

Autor	KS	RP	KL	TM	UH							∑ in Prozent
Studiendesign	2.5	2.5	2.5	2.5	2.5							12.5%
Experimentelle Arbeit	15	15										30%
Datenanalyse und Interpretation	10	10	5	5	5							35%
Verfassen der Veröffentlichung	6.25	6.25										12.5%
Korrektur der Veröffentlichung			2.5	2.5	2.5							7.5%
Koordination der Veröffentlichung					2.5							2.5%
Summe	33.75	33.75	10	10	12.5							100%

Julius-Maximilians-
UNIVERSITÄT
WÜRZBURG

Fakultät für
CHEMIE UND
PHARMAZIE

Die Mitautoren der in dieser (teil-)kumulativen Dissertation verwendeten Manuskripte sind sowohl über die Nutzung als auch über die angegebenen Eigenanteile informiert und stimmen dem zu.

Klaus Schilling	Ruben Pawellek	Katherine Lovejoy
Autor/in 1 (Vorname Nachname)	Autor/in 2 (Vorname Nachname)	Autor/in 3 (Vorname Nachname)
Hauptautor/in	**Hauptautor/in**	**Koautor/in**
☒ Verweis: E-Mail hinterlegt	☒ Verweis: E-Mail hinterlegt	☒ Verweis: E-Mail hinterlegt
Tibor Muellner	Ulrike Holzgrabe	
Autor/in 4 (Vorname Nachname)	Autor/in 5 (Vorname Nachname)	
Koautor/in	**Korrespondenzautor/in**	
☒ Verweis: E-Mail hinterlegt	☒ Verweis: E-Mail hinterlegt	

Würzburg, 02.07.2021
(Datum)

Prof. Dr. Ulrike Holzgrabe (Betreuer/in)

Julius-Maximilians-
UNIVERSITÄT
WÜRZBURG

Fakultät für
CHEMIE UND
PHARMAZIE

Erklärung zur Autorenschaft

Charged Aerosol Detector Performance Evaluation and Development of Optimization Strategies for the Analysis of Amino Acids,
Charged Aerosol Detector response modeling for fatty acids based on experimental settings and molecular features: a machine learning approach, R. Pawellek, J. Krmar, A. Leistner, N. Djajić, B. Otašević, A. Protić, U. Holzgrabe, [manucscript accepted for publication in J. Cheminformatics].

Detaillierte Darstellung der Anteile an der Veröffentlichung (in %)
Angabe Autoren/innen (ggf. Haupt- / Ko- / korrespondierende/r Autor/in) mit Vorname Nachname (Initialen)

Autor/in 1 (RP), Autor/in 2 (JK), Autor/in 3 (AL), Autor/in 4 (ND), Autor/in 5 (BO), Autor/in 6 (AP), Autor/in 7 (UH)

Autor	RP	JK	AL	ND	BO	AP	UH					∑ in Prozent
Studiendesign	1.5	1.5		1.5		1.5	1.5					7.5%
Experimentelle Arbeit: HPLC-Experimente	15		10									25%
Experimentelle Arbeit: Datenmodellierung		15		5								20%
Datenanalyse- und Interpretation	5	5		5	2.5							17.5%
Verfassen der Veröffentlichung	5	5		5								15%
Korrektur der Veröffentlichung			2.5		2.5	2.5	2.5					10%
Koordination der Veröffentlichung						2.5	2.5					5%
Summe	26.5	26.5	12.5	16.5	5	6.5	6.5					100%

Julius-Maximilians-
UNIVERSITÄT
WÜRZBURG

Fakultät für
CHEMIE UND
PHARMAZIE

Die Mitautoren der in dieser (teil-)kumulativen Dissertation verwendeten Manuskripte sind sowohl über die Nutzung als auch über die angegebenen Eigenanteile informiert und stimmen dem zu.

Ruben Pawellek

Autor/in 1 (Vorname Nachname)

Hauptautor/in

☒ Verweis: E-Mail hinterlegt

Jovana Krmar

Autor/in 2 (Vorname Nachname)

Hauptautor/in

☒ Verweis: E-Mail hinterlegt

Adrian Leistner

Autor/in 3 (Vorname Nachname)

Koautor/in

☒ Verweis: E-Mail hinterlegt

Nevena Djajić

Autor/in 4 (Vorname Nachname)

Koautor/in

☒ Verweis: E-Mail hinterlegt

Biljana Otašević

Autor/in 5 (Vorname Nachname)

Koautor/in

☒ Verweis: E-Mail hinterlegt

A. Protić

Autor/in 6 (Vorname Nachname)

Korrespondenzautor/in

☒ Verweis: E-Mail hinterlegt

Ulrike Holzgrabe

Autor/in 7 (Vorname Nachname)

Korrespondenzautor/in

☒ Verweis: E-Mail hinterlegt

Würzburg, 02.07.2021

(Datum)

Prof. Dr. Ulrike Holzgrabe (Betreuer/in)

Julius-Maximilians-
UNIVERSITÄT
WÜRZBURG

Fakultät für
CHEMIE UND
PHARMAZIE

Erklärung zur Autorenschaft

Charged Aerosol Detector Performance Evaluation and Development of Optimization Strategies for the Analysis of Amino Acids,
Power function setting in charged aerosol detection for the linearization of detector response–optimization strategies and their application, R. Pawellek, T. Muellner, P. Gamache, U. Holzgrabe, J. Chromatogr. A 1637 (2021) 461844.

Detaillierte Darstellung der Anteile an der Veröffentlichung (in %)
Angabe Autoren/innen (ggf. Haupt- / Ko- / korrespondierende/r Autor/in) mit Vorname Nachname (Initialen)

Autor/in 1 (RP), Autor/in 2 (TM), Autor/in 3 (PG), Autor/in 4 (UH)

Autor	RP	TM	PG	UH								∑ in Prozent
Studiendesign	2.5	2.5		2.5								7.5%
Experimentelle Arbeit	25											25%
Datenanalyse- und Interpretation	20	5	5	5								35%
Verfassen der Veröffentlichung	15											15%
Korrektur der Veröffentlichung		5	5	5								15%
Koordination der Veröffentlichung				2.5								2.5%
Summe	62.5	12.5	10	15								100%

Julius-Maximilians-
UNIVERSITÄT
WÜRZBURG

Fakultät für
CHEMIE UND
PHARMAZIE

Die Mitautoren der in dieser (teil-)kumulativen Dissertation verwendeten Manuskripte sind sowohl über die Nutzung als auch über die angegebenen Eigenanteile informiert und stimmen dem zu.

Ruben Pawellek

Autor/in 1 (Vorname Nachname)

Hauptautor/in

☒ Verweis: E-Mail hinterlegt

Tibor Muellner

Autor/in 2 (Vorname Nachname)

Koautor/in

☒ Verweis: E-Mail hinterlegt

Paul Gamache

Autor/in 3 (Vorname Nachname)

Koautor/in

☒ Verweis: E-Mail hinterlegt

Ulrike Holzgrabe

Autor/in 4 (Vorname Nachname)

Korrespondenzautor/in

☒ Verweis: E-Mail hinterlegt

Würzburg, 02.07.2021

(Datum)

Prof. Dr. Ulrike Holzgrabe (Betreuer/in)

Julius-Maximilians-
UNIVERSITÄT
WÜRZBURG

Fakultät für
CHEMIE UND
PHARMAZIE

Erklärung zur Autorenschaft

Charged Aerosol Detector Performance Evaluation and Development of Optimization Strategies for the Analysis of Amino Acids,
Performance evaluation of IPC and HILIC coupled to charged aerosol detection for the analysis of underivatized amino acids, R. Pawellek, U. Holzgrabe, [submitted to J. Chromatogr. A].

Detaillierte Darstellung der Anteile an der Veröffentlichung (in %)
Angabe Autoren/innen (ggf. Haupt- / Ko- / korrespondierende/r Autor/in) mit Vorname Nachname (Initialen)

Autor/in 1 (RP), Autor/in 2 (UH)

Autor	RP	UH										∑ in Prozent
Studiendesign	5	5										10%
Experimentelle Arbeit	30											30%
Datenanalyse- und Interpretation	25	5										30%
Verfassen der Veröffentlichung	20											20%
Korrektur der Veröffentlichung		5										5%
Koordination der Veröffentlichung		5										5%
Summe	80	20										100%

Julius-Maximilians-
UNIVERSITÄT
WÜRZBURG

Fakultät für
CHEMIE UND
PHARMAZIE

Die Mitautoren der in dieser (teil-)kumulativen Dissertation verwendeten Manuskripte sind sowohl über die Nutzung als auch über die angegebenen Eigenanteile informiert und stimmen dem zu.

Ruben Pawellek	Ulrike Holzgrabe
Autor/in 1 (Vorname Nachname)	Autor/in 2 (Vorname Nachname)
Hauptautor/in	**Korrespondenzautor/in**
☒ Verweis: E-Mail hinterlegt	☒ Verweis: E-Mail hinterlegt

Würzburg, 02.07.2021
(Datum)

Prof. Dr. Ulrike Holzgrabe (Betreuer/in)

Julius-Maximilians-
UNIVERSITÄT
WÜRZBURG

Fakultät für
CHEMIE UND
PHARMAZIE

Erklärung zur Autorenschaft

Charged Aerosol Detector Performance Evaluation and Development of Optimization Strategies for the Analysis of Amino Acids, Influence of the mobile phase composition on hyphenated ultraviolet and charged aerosol detection for the impurity profiling of vigabatrin, R. Pawellek, U. Holzgrabe, J. Pharm. Biomed. Anal. 201 (2021) 114110.

Detaillierte Darstellung der Anteile an der Veröffentlichung (in %)
Angabe Autoren/innen (ggf. Haupt- / Ko- / korrespondierende/r Autor/in) mit Vorname Nachname (Initialen)

Autor/in 1 (RP), Autor/in 2 (UH)

Autor	RP	UH										∑ in Prozent
Studiendesign	5	5										10%
Experimentelle Arbeit	30											30%
Datenanalyse- und Interpretation	25	5										30%
Verfassen der Veröffentlichung	20											20%
Korrektur der Veröffentlichung		5										5%
Koordination der Veröffentlichung		5										5%
Summe	80	20										100%

Julius-Maximilians-
UNIVERSITÄT
WÜRZBURG

Fakultät für
CHEMIE UND
PHARMAZIE

Die Mitautoren der in dieser (teil-)kumulativen Dissertation verwendeten Manuskripte sind sowohl über die Nutzung als auch über die angegebenen Eigenanteile informiert und stimmen dem zu.

Ruben Pawellek	Ulrike Holzgrabe
Autor/in 1 (Vorname Nachname)	Autor/in 2 (Vorname Nachname)
Hauptautor/in	**Hauptautor/in**
☒ Verweis: E-Mail hinterlegt	☒ Verweis: E-Mail hinterlegt

Würzburg, 02.07.2021
(Datum)

Prof. Dr. Ulrike Holzgrabe (Betreuer/in)

Julius-Maximilians-
UNIVERSITÄT
WÜRZBURG

Fakultät für
CHEMIE UND
PHARMAZIE

Erklärung zur Autorenschaft

Charged Aerosol Detector Performance Evaluation and Development of Optimization Strategies for the Analysis of Amino Acids, Impurity profiling of l-aspartic acid and glycine using high-performance liquid chromatography coupled with charged aerosol and ultraviolet detection, R. Pawellek, K. Schilling, U. Holzgrabe, J. Pharm. Biomed. Anal. 183 (2020) 113149.

Detaillierte Darstellung der Anteile an der Veröffentlichung (in %)
Angabe Autoren/innen (ggf. Haupt- / Ko- / korrespondierende/r Autor/in) mit Vorname Nachname (Initialen)

Autor/in 1 (RP), Autor/in 2 (KS), Autor/in 3 (UH)

Autor	RP	KS	UH									∑ in Prozent
Studiendesign	5		5									10%
Experimentelle Arbeit	30											30%
Datenanalyse und Interpretation	20		5									25%
Verfassen der Veröffentlichung	22.5											22.5%
Korrektur der Veröffentlichung		5	5									10%
Koordination der Veröffentlichung			2.5									2.5%
Summe	77.5	5	17.5									100%

Julius-Maximilians-
UNIVERSITÄT
WÜRZBURG

Fakultät für
CHEMIE UND
PHARMAZIE

Die Mitautoren der in dieser (teil-)kumulativen Dissertation verwendeten Manuskripte sind sowohl über die Nutzung als auch über die angegebenen Eigenanteile informiert und stimmen dem zu.

Ruben Pawellek	Klaus Schilling	Ulrike Holzgrabe
Autor/in 1 (Vorname Nachname)	Autor/in 2 (Vorname Nachname)	Autor/in 3 (Vorname Nachname)
Hauptautor/in	**Koautor/in**	**Korrespondenzautor/in**
☒ Verweis: E-Mail hinterlegt	☒ Verweis: E-Mail hinterlegt	☒ Verweis: E-Mail hinterlegt

Würzburg, 02.07.2021
(Datum)

_____
Prof. Dr. Ulrike Holzgrabe (Betreuer/in)